TABLE OF CONTENTS

Page

LIST OF TABLES

Page

LIST OF FIGURES

Page

LIST OF ABBREVIATIONS AND ACRONYMS

3D	Three-Dimensional
AFP	Automated Fibre Placement
ASTM	American Society for Testing and Materials
BC	Boundary Conditions
BSE	Bad Shape Element
CLT	Classical Lamination Theory
CLPT	Classical Laminated Plate Theory
CMH-17	Composite Material Handbook as referenced by the industry
CNC	Computer Numerical Control
CSM	Chopped Strand Mat
DFEM	Detailed Finite Element Model
DOF	Degree Of Freedom
EKM	Extended Kantorovich Method
ÉTS	École de Technologie Supérieure
FAA	Federal Aviation Administration
FEA	Finite Element Analysis
FEM	Finite Element Model
FPF	First Ply Failure
FRP	Fibres Reinforced Polymers
FSDT	First-order Shear Deformation Theory
GFEM	Global Finite Element Model

GMT	Glass-fibre-Mat-reinforced Thermoplastic
GUI	Graphical User Interface
ILS	InterLaminar Shear
LFRC	Laminated Fibre Reinforced Composite
LFT	Long-Fibre-reinforced Thermoplastic
LPF	Last Ply Failure
PDE	Partial Differential Equation
PEEK	Polyether Ether Ketone
PEKK	Polyether Ketone Ketone
PPS	PolyPhenylene Sulphide
RHBT	Refined Higher-order Beam Theory
RTM	Resin Transfer Moulding
SMC	Sheet-Moulding Compound
SRIM	Structural Reaction Injection Moulding
TFBT	Timoshenko First-order Beam Theory
UCS	Ultimate Compressive Strength
UD	Unidirectional
UTS	Ultimate Tensile Strength
VARTM	Vacuum Assisted Resin Transfer Moulding
WWFE	World Wide Failure Exercise

LIST OF SYMBOLS

Greek:

γ_{12}	In-plane shear strain of UD coupons
γ_{13}	Longitudinal – Through-the-thickness shear strain of UD coupons
γ_{23}	Transverse – Through-the-thickness shear strain of UD coupons
γ_{ij}	Shear strain in the laminate coordinate system
δ_x	Displacement of a node in the axial direction
δ_y	Displacement of a node in the transverse direction
δ_z	Displacement of a node in the through-the-thickness direction
ε_1	Longitudinal strain of UD coupons for tensile tests
ε_2	Transverse strain of UD coupons for tensile tests
ε_3	Through-the-thickness strain of UD coupons for tensile tests
$\varepsilon_{\pm 45°}$	Rosette strains of UD V-notched coupons for shear tests
ε_i	Strain in the lamina coordinate system
ε_{ij}	Strain in the laminate coordinate system
ε_x	Axial strain in a laminate
$\{\varepsilon^0\}$	Vector of the membrane strains
$\{\varepsilon^1\}$	Vector of the bending strains
θ_k	Orientation of the fibres in the layer k
λ	Span-to-depth (or thickness) ratio in three-point bending and pure torsion problems
ν_{12}	Major Poisson's ratio of a ply (or of a UD laminate)
ν_{13}	Longitudinal – Through-the-thickness Poisson's ratio of a ply (or of a UD laminate)
ν_{21}	Minor Poisson's ratio of a ply (or of a UD laminate)
ν_{23}	Transverse – Through-the-thickness Poisson's ratio of a ply (or of a UD laminate)
ν_f	Poisson's ratio of the fibre as an isotropic constituent
ν_m	Poisson's ratio of the matrix as an isotropic constituent
ν_{xy}	In-plane Poisson's ratio of a laminate
ν_{xz}	Through-the-thickness Poisson's ratio of a laminate
σ_i	Stress in the lamina coordinate system
σ_{ij}	Stress in the laminate coordinate system
σ_x	Axial stress in a laminate
τ_{max}	Maximum shear stress in pure torsion problem

Latin:

A	Cross section of the coupon modeled in the FEM
A	Location through-the-thickness where the torsion effect is looked at
A_{ij}	Terms of the matrix of the extensional stiffness
b	Total width of UD coupons for transverse tensile tests Effective width (or thickness) of UD V-notched coupons for shear tests Total width of rectangular bar in pure torsion
B	Location in the width where the torsion effect is looked at
B_{ij}	Terms of the matrix of the bending-extensional coupling stiffness
D_{ij}	Terms of the matrix of the bending stiffness
E_1	Longitudinal Young's modulus of a ply (or of a UD laminate), in the direction of the fibre
E_2	Transverse Young's modulus of a ply (or of a UD laminate)
E_3	Through-the-thickness Young's modulus of a ply (or of a UD laminate)
E_f	Young's modulus of the fibre as an isotropic constituent
E_m	Young's modulus of the matrix as an isotropic constituent
E_x	Young's modulus in the axial direction of a laminate
$E_{xx}^{\ b}$	Equivalent laminate bending stiffness, in the three-point bending beam problem
F	Experimental load in tension and shear Applied load in the FEM
F_0	Midspan linear force, in the three-point bending beam problem
G_{12}	In-plane shear modulus of a ply (or of a UD laminate)
G_{13}	Longitudinal – Through-the-thickness shear modulus of a ply (or of a UD laminate)
G_{23}	Transverse – Through-the-thickness shear modulus of a ply (or of a UD laminate)
G_f	Shear modulus of the fibre as an isotropic constituent
G_m	Shear modulus of the matrix as an isotropic constituent
$G_{xx}^{\ b}$	Equivalent laminate bending-shear stiffness, in the three-point bending beam problem
in	inch
I_{yy}	Moment of inertia in width, in the three-point bending beam problem
J	Constant of torsion
k	Layer identification
k_1	Longitudinal shear correction factor
k_2	Transverse shear correction factor
k_f	Bulk modulus of the fibre as an isotropic constituent
k_m	Bulk modulus of the matrix as an isotropic constituent
K	Shear correction factor (also called k-factor)
K_f	Lateral compression modulus of the fibre as an isotropic constituent
K_l	Lateral compression modulus of a laminate
K_m	Lateral compression modulus of the matrix as an isotropic constituent

L	Span length, in the three-point bending beam problem
	Total length of UD coupons for tensile tests
	Total length of rectangular bar in pure torsion
L_e	Effective length of UD coupons for transverse tensile tests
	Effective length to be used in FEM
mm	millimeter
n	Number of repetitions of a layer or a laminate in a lay-up
N	Total number of layers in a laminate
N_x	Axial applied load on a laminate
$\{N\}$	Vector of the in-plane forces
$\{M\}$	Vector of the in-plane moments
$Q_{ij}^{(k)}$	Plane stress-reduced stiffness, relative to the lamina k
$\overline{Q}_{ij}^{k}$	Plane stress-reduced stiffness of the lamina k, relative to the laminate
Q_x	Longitudinal – Through-the-thickness shear force
Q_y	Transverse – Through-the-thickness shear force
R^2	Coefficient of determination of a linear regression
S	Symbol used, as an index, to identify that a lay-up is symmetric
t	Total thickness of the beam, in the three-point bending beam problem
	Total thickness of UD coupons for tensile and shear tests
	Total thickness of rectangular bar in pure torsion
t_k	Thickness of the layer k
t_p	Average thickness of one cured ply
T	Moment of torsion for rectangular bar in pure torsion
u	Displacement in x, in the three-point bending beam problem
u_0	Initial displacement in x, in the three-point bending beam problem
v	Displacement in y, in the three-point bending beam problem
v_0	Initial displacement in y, in the three-point bending beam problem
V_f	Fibre volume fraction
w	Displacement in z, in the three-point bending beam problem
	Width of UD coupons for longitudinal tensile and shear tests
	Effective width of UD coupons for transverse tensile tests
W	Width of the beam, in the three-point bending beam problem
W_s	Specimen width to be used in FEM
w_0	Initial displacement in z, in the three-point bending beam problem
x	Longitudinal direction in the global coordinate system
	Position in x, in the displacement field
y	Transverse direction in the global coordinate system
	Position in y, in the displacement field
z	Through-the-thickness direction in the global coordinate system
	Position in z, in the displacement field
z_k	Position in z of the layer k

INTRODUCTION

It is now common practice to use composites in very large and thick structures like bridge desks, high pressure vessels, wind turbine blades and aircraft parts, like main landing gear fittings, from 60 to 90 mm thick (Holmes, 2005; Zimmermann and Siemetzki, 2008). Composite materials are being used more and more because of their low weight, adaptable mechanical properties, higher specific strength and stiffness and low cost. The growing trend of having thicker laminates in large structures has raised several questions in the prediction of their mechanical behaviour. Catastrophic events have clearly illustrated that it was the lack of knowledge of materials properties during the design, sizing and manufacturing of thick composite parts.

To avoid these premature failures, it is important to properly understand the behaviour of thick composite structures. Commonly used theories, like classical lamination theory (CTL) or shell elements in finite element analysis (FEA), do not accurately predict the behaviour of thick composite laminates, since they are neglecting through-the-thickness effects. In addition, the influence of the thickness and other manufacturing parameters is not known on the orthotropic elastic mechanical properties. When thick laminates are manufactured, several flaws like residual stresses, voids and fibre misalignments influence the behaviour of parts. To avoid expensive costs related to extensive experimental analysis, solid elements in FEA, with anisotropic material properties, could be used to predict the behaviour of thick composite structures under different load cases. However, nine orthotropic material properties, which may vary with the thickness, are required in this methodology. These nine elastic properties are the three Young's moduli E_1, E_2 and E_3, the three major Poisson's ratios ν_{12}, ν_{13} and ν_{23}, and the three shear moduli G_{12}, G_{13} and G_{23}. In addition to the modeling and the meshing techniques, the application of load and boundary conditions, and the approach to analyse the results, all have an influence on the accuracy of the results.

The main objective of this thesis is to determine the influence of the thickness, if so, on the nine orthotropic elastic mechanical properties (E_1, E_2, E_3, n_{12}, n_{13}, n_{23}, G_{12}, G_{13} and G_{23}) which will be used in lamination theories or FEA, in order to predict accurately the mechanical behaviour of thick laminated structures. With the purpose of measuring the influence of the thickness on nine orthotropic elastic material properties, at least three different thicknesses are required. It is assumed that depending on the structure thickness to be analyzed, the corresponding orthotropic elastic material properties in function of the thickness shall be used in the lamination theories or FEA.

- Chapter 1 presents a literature review on composite materials in terms of manufacturing, analysis methods, material characterization and thickness effects.

- Chapter 2 presents a comparison to determine at which thickness a laminate cannot be considered thin anymore. The comparison is done analyzing the deflection of laminated beams in three points bending using different laminate theories and a FEA model. Within this step, at least three categories of laminate thickness shall be defined.

- In Chapter 3, the influence of the thickness on orthotropic elastic mechanical properties of unidirectional (UD) laminates is measured. To do so, an extensive experimental programme is developed in terms of manufacturing and testing. For three different thicknesses, UD laminated fibreglass/epoxy coupons are prepared and standard experimental procedures are used as basis in order to validate the quality of the manufacturing and to measure each elastic mechanical property of this UD fibreglass composite. In addition, the tensile and shear strengths, at failure, of UD composite material are measured and commented.

- In Chapter 4, the influence of the thickness on the elastic tensile properties of various lay-up configurations is measured. This is done on two different laminate configurations made of the same UD material. The Young's modulus, the in-plane and through-the-thickness Poisson's ratios are measured by tests as well as the ultimate tensile strength. The experimental values are then compared to theoretical (CLT) and numerical (FEA) values computed using the UD experimental elastic properties previously obtained in Chapter 3.

- Chapter 5 presents preliminary works on perspectives of future studies in order to answer some weaknesses of standard test methods highlighted in Chapter 3. This includes a modern inspection method to record displacements and an innovative method to get through-the-thickness shear properties of laminated composite.

Furthermore, since this research evaluates all the facets of a material study: manufacturing, testing and analysis. The influence of the thickness on elastic mechanical properties will be highlighted which is of utmost important for the industry.

CHAPTER 1

LITERATURE REVIEW

In this section, a brief introduction to composite materials is presented as well as their manufacturing processes. It is followed by different studies on the effects of increasing the thickness of a composite laminate during the manufacturing, the characterization, the testing and the analysis: theories and numerical modeling.

1.1 Presentation of Composite Materials

A composite is made of non-soluble constituents, deliberately combined or not to form a heterogeneous structure, with desired or randomly oriented properties. The oldest composites are wood, straw and mud, but the more recent known composites are reinforced concrete, Fibres (glass or carbon) Reinforced Polymers (FRP), which are used to make bridges, boats, sport goods, aircrafts parts and wind turbine blades.

However, the composite domain becomes more complex when other materials and applications are used. As in Figure 1.1, different distributions are used depending of the application (Daniel and Ishai, 1994). The fibres give strength and stiffness to composite materials at a reasonable cost (ASM International, 2002), whereas the matrix is used to hold the fibres together, to transfer the mechanical solicitations to fibres, and to protect the fibres from external damages and environment conditions.

The types of reinforcement (fibres) materials generally used are:

- metallic, e.g. Boron,
- carbon (Graphite),
- glass (E-glass, S-glass),
- ceramic, e.g. Silicon carbide, Alumina,
- organic plastic, e.g. Kevlar (Aramid).

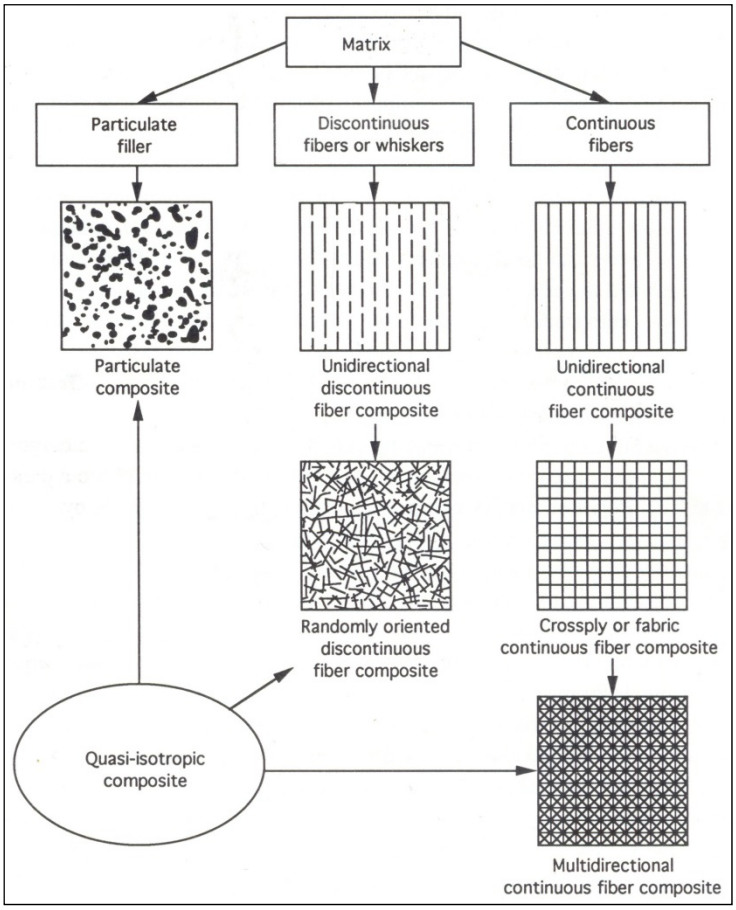

Figure 1.1 Classification of composite material systems
Drawn from Daniel and Ishai (1994)

The types of matrix materials generally used are:

- metallic, e.g. Aluminum, Titanium,
- carbon (Graphite),
- ceramic, e.g. Alumina, Silicon nitride,
- thermoset plastics (Epoxies, polyimide, polyester),
- Thermoplastics (Polysulfone, PolyEtherEtherKetone (PEEK), PolyEtherKetoneKetone (PEKK)).

Metallic matrices are recommended for high temperature applications, up to approximately 800°C (Daniel and Ishai, 1994) and offer a good fatigue resistance (ASM International, 2002). For higher temperature applications, 1000°C to 2600°C, ceramic and carbon matrices are used (ASM International, 2002; Daniel and Ishai, 1994; Gibson, 2007). Thermosets can be exposed to temperature up to 370°C and are used in different applications like commercial products (polyester), aircraft structures (polyimide and some epoxies) and sports equipment. Thermoplastics can be used in applications with temperatures up to 400°C. The main advantage of using thermoplastics as a matrix in laminates is the possibility to recycle them at a low cost compared to other matrix materials (ASM International, 2002).

Laminated composite materials are an important class of composites known as advanced composite materials. Laminated Fibre-Reinforced Composites (LFRC) are formed by sets of lamina (layer or ply of continuous fibre) to give different strength and stiffness in various directions. The fibres used in this research are bundles of continuous unidirectional dry fibres maintained straight and parallel by stitching lines. One layer of this kind of fabric is named a ply or a layer. Then, each ply can be oriented at a desired angle. The thickness of the laminate is driven by the ply thickness and the number of layers. The ply thickness is an average thickness value depending of the fibre and the matrix materials, the manufacturing process and the number of layers in a batch of laminated coupons. The matrix used in this research is thermoset plastics.

Often, lightweight structural cores (honeycomb and foam) are included into thin LFRC sandwich panels to produce extremely stiff and strong structures of minimum weight for bending purposes (ASM International, 2002). An example of a honeycomb sandwich is shown in Figure 1.2. However, this kind of structures cannot be considered thick laminates since they are formed using two thin laminated face sheets and a core.

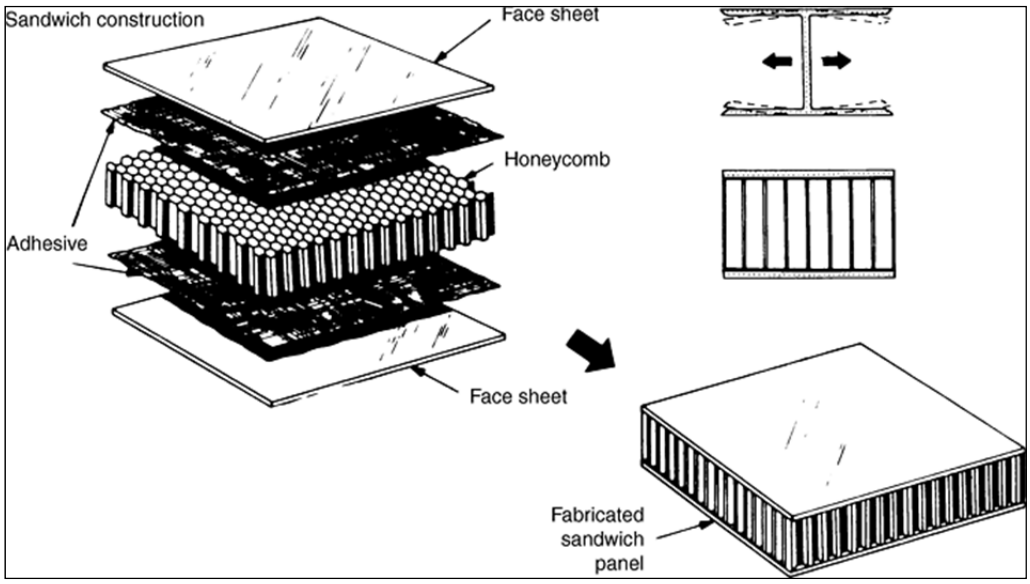

Figure 1.2 Honeycomb sandwich panel components
Drawn from ASM International (2002, Vol. 21: Composites - Lightweight Structural Cores)

1.2 Manufacturing Processes

There are generally 4 steps in the manufacturing process of composite parts: lay-up sequence, impregnation, consolidation and solidification (Mazumdar, 2002). The performance of a composite structure relies heavily on the fibre orientation and lay-up sequence. The impregnation consists of wetting the fibres with a resin. A good advantage of thermoset polymers is that they are less viscous than thermoplastics, and then they require low pressure in the consolidation step (ÉireComposites, 2006). To obtain a good quality composite, the consolidation is an important step where pressure is applied to remove air bubbles. However,

too much pressure could misalign the fibres and create wrinkles. The solidification stage finalises the process and varies in time duration depending on the material used. For example, thermoplastic polymers may take less than a minute to solidify when thermoset resins could take more than two hours due to an exothermic chemical reaction produced during the cure (Mazumdar, 2002).

Several manufacturing processes exist which may influence material properties. An extensive list of manufacturing processes for polymer matrix composites are hereafter presented with their advantages and limitations.

1.2.1 Wet Lay-up

Without any doubt, the oldest process to manufacture laminates is the wet lay-up. This hand lay-up is widely used in the marine industry and to build wind turbine blades (Gibson, 2007; Mazumdar, 2002). In order to make a part, a release agent is applied on the open mould. For a better surface finish, a gel coat can also be applied. Then, a liquid resin is spread on chopped or continuous fibres, unidirectional or woven reinforcements (dry or pre-impregnated). A roller is used for the consolidation. Cure and solidification can be done at room temperature or in an oven. Figure 1.3A shows the set-up for the hand wet lay-up process. This process requires low capital investments and produces very low cost parts. Another advantage of this process is that large structures can be built with no skilled labour. The process is versatile, many types of thermoset resins and fibres can be used, and in any fibre orientations. In counterpart, the wet lay-up process is labour intensive and the part quality is not consistent and is dependent on the operator's skills. This sloppy process can also cause health hazards as it produces a large quantity of volatile emissions. This method does not allow getting high fibre volume fractions. However, the wet lay-up can easily be automated and is called the spray lay-up process (Figure 1.3B). Applications using this method are much more rapid, but the quality of the part is still not uniform through-the-thickness and that across the part. Although thick parts can be made with this process, the parts will contain voids and it is difficult to obtain specific fibre orientations.

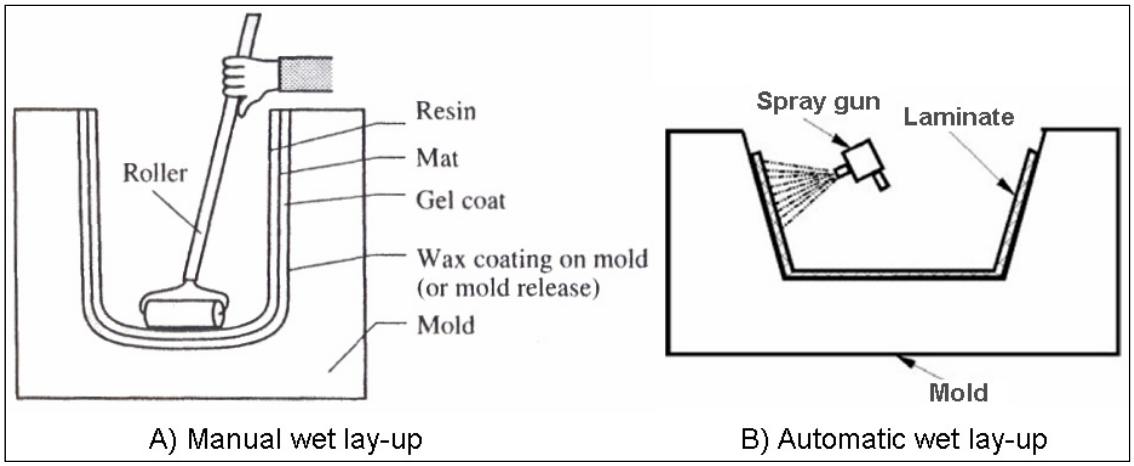

Figure 1.3 Wet lay-up set-ups: A) Manual and B) Automatic spray lay-up
Drawn from Gibson (2007) and Mazumdar (2002)

1.2.2 Vacuum Infusion

The vacuum infusion, or and vacuum assisted resin transfer moulding (VARTM), is a non-expensive manufacturing process since the dry fibre patterns are laid on an open mould at a desired orientation, using or not laser projection (Mazumdar, 2002). Then, the vacuum bagging arrangement is installed to compact the dry preform. When the vacuum is sufficient, the resin is infused into the fibres. The curing of the part can be completed at room temperature or in the oven. Open moulds permit the manufacturing of large and thick laminated parts. Compared to wet lay-up, the compaction process provided by the vacuum allows a better part quality, less voids and higher fibre volume fraction. This process allows a better control of the parameters, produces repeatable and reproducible composite parts, and reduces the quantity of volatile emissions.

1.2.3 Autoclave Curing

The “prepreg” lay-up, also called the autoclave processing or the vacuum bagging, is very common in aerospace (Gibson, 2007; Mazumdar, 2002), especially for wing structures, landing gear doors and flap tracks. “Prepreg” is a short name for pre-impregnated fibres in a resin and it comes in sheets or rollers. The prepreg needs to be kept in a refrigerator. The autoclave process uses mostly thermoset prepreg in open moulds. To manufacture an autoclave part, the prepreg is cut into the desired size. Then, the mould is cleaned and the release agent is applied. The backing paper is removed from the prepreg and the composite piece is laid on the mould. Laser projection can be used to indicate the proper orientation and the correct lay-up sequence. These steps could be automated using narrow rollers which are laid down by robot’s fingers (automated fibre placement (AFP)). The fingers are followed by compaction rollers to carefully remove entrapped air bubbles. After the layup is done, manually or automatically, the next step is the vacuum bagging arrangement. Then, the laminated part is placed in the closed autoclave for the curing cycle. In addition to the vacuum, the autoclave produces an extra pressure on the vacuum bagging and heats the part. The cooling of the cured part may take several hours. Finally, the part is debagged and taken out of the mould. The set-up for the autoclave prepreg process is illustrated in Figure 1.4.

This process permits strong and stiff parts with up to 60% of fibre volume fraction (V_f) to be made (Mazumdar, 2002). It is also used to manufacture complex parts, but there are high capital investments for the autoclave. However, the tooling cost required to produce parts in an autoclave is relatively low compare to closed moulds. The difficulty to have an autoclave available may lead to delays and additional expenses. It is why this process is not retained for this research.

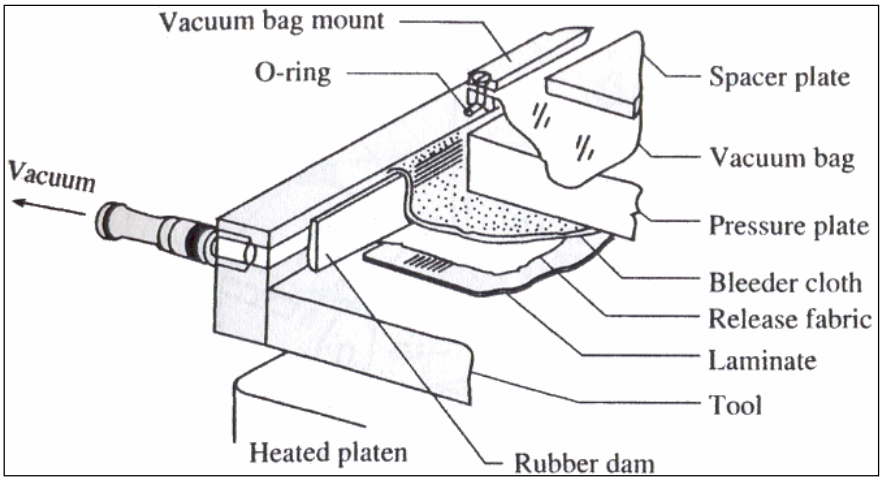

Figure 1.4 Setup autoclave for moulding process
Drawn from Gibson (2007)

1.2.4 Compression Moulding

Sheet-moulding compound (SMC, thermoset) is similar to prepreg tape lay-up but uses thicker chopped fibres. SMC can use randomly reinforced moulding compounds often called glass-fibre-mat-reinforced thermoplastics (GMT) or long-fibre-reinforced thermoplastics (LFT). These sheets are then placed in a compression moulding process like shown in Figure 1.5 (Gibson, 2007; Mazumdar, 2002). More simple and thinner parts can be made with the SMC process.

1.2.5 Filament Winding

The filament winding process is particularly used for pipes, tubing, power transmission shafts and high pressure vessels manufacturing (ASM International, 2002; Mazumdar, 2002). The process consists to wind at specific angle resin-impregnated fibres on a rotating mandrel. The carriage unit moves along the mandrel and it can count up to six axes. The process is schematically represented in Figure 1.6. With this process, it is possible to produce a large volume of composite parts at low-cost. The fibres are laid at a precise angle, but angles less

than 15° are difficult to produce. Only closed and convex structures can be made with a low fibre volume fraction, less than 60%. Thick and thin parts are producible. It is also a challenge to obtain uniform fibre distribution and resin content throughout the thickness.

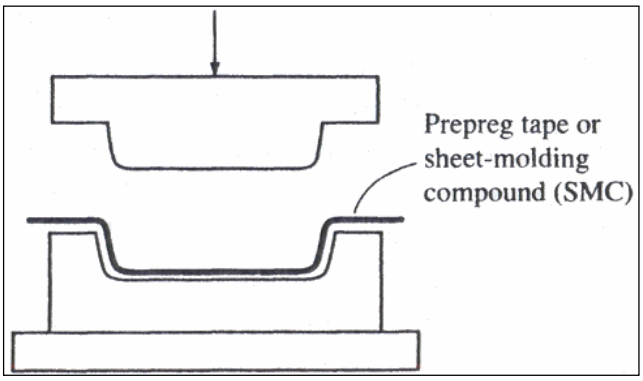

Figure 1.5 Compression moulding process
Drawn from Gibson (2007)

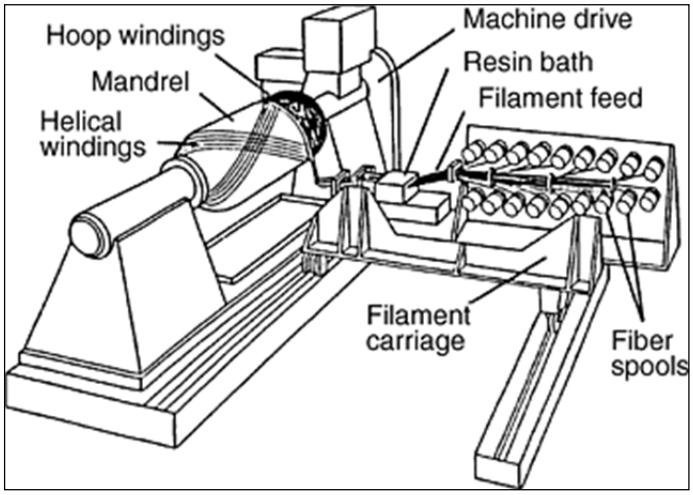

Figure 1.6 Filament winding process
Drawn from ASM International (2002, Vol. 21: Composites – Filament Winding)

1.2.6 Resin Transfer Moulding (RTM)

Another thermoset manufacturing process is the resin transfer moulding (RTM). It is used to manufacture aircraft parts like landing gear doors and wing flaps (ASM International, 2002; Mazumdar, 2002). The first step in this process is to place the resin and the catalyst in its respective thank. Then, a release agent and a gel coat, if required, are applied on the mould surface to obtain a better surface finish. Next, the fibres are placed inside the mould and the mould is clamped. The mould is then heated and filled with the resin mixture by injection. Finally, the part is demoulded after a curing of 6 to 20 minutes, depending of the component size. An illustration of the entire process is shown in Figure 1.7. The initial capital investment of RTM is low compared to compression and injection moulding. The quality of parts is good; geometrical dimensions are closed to dimensional tolerance, the surface finish is good and with a fibre volume fraction up to 65%. In addition, simple and complex parts can be built with low volatile emission due to the closed moulding process. Using closed moulds, the manufacturing of relatively large and thick parts is more expensive than the hand lay-up. Also, the tooling design is complex, requires expert skills and is often done using trial-and-error experimentation.

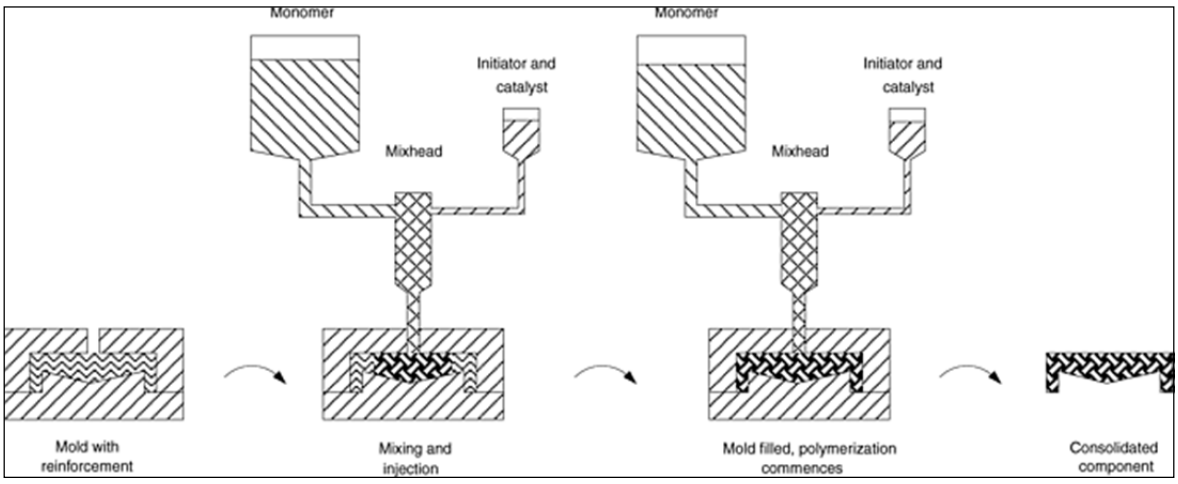

Figure 1.7 Resin transfer moulding (RTM) process
Drawn from ASM International (2002, Vol. 21: Composites - Resin Transfer Molding and Structural Reaction Injection Molding)

1.2.7 Structural Reaction Injection Moulding (SRIM)

The last manufacturing process presented here is the structural reaction injection moulding (SRIM). This manufacturing technique is similar to RTM, the difference being in the resin used and the method of mixing the two resins, at a liquid state, before injection (Mazumdar, 2002). One of the advantages of this process is that very large-sized parts with complex geometry can be made, such as pick-up truck boxes. Also, a high-volume of structural parts can be produced at a lower cost and it is faster than the RTM process. On the other hand, the SRIM requires a large capital investment in equipment and a high tooling cost. In addition, parts contain a low fibre volume fraction of about 40%. The process set-up is schematized in Figure 1.8. Both methods, RTM and SRIM, require very low viscosity matrices to permit a good impregnation of the reinforcements before the polymerization. The resulting part has then a good finish appearance (Gibson, 2007).

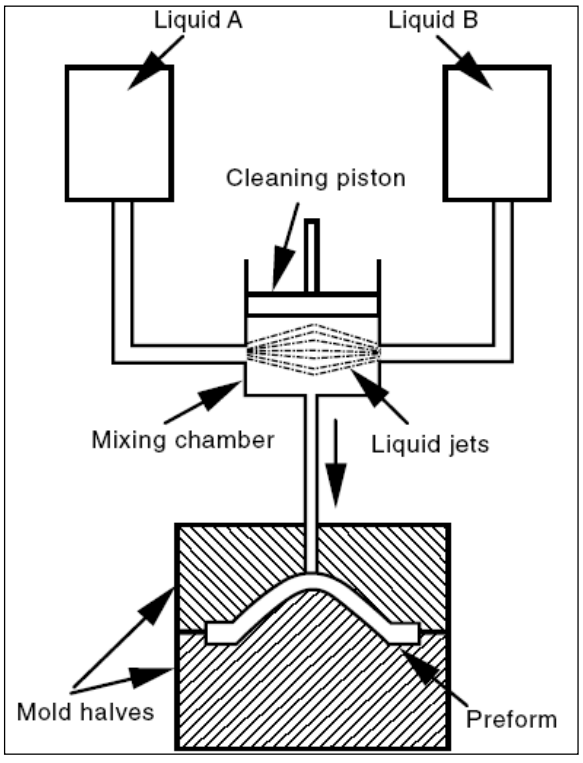

Figure 1.8 Schematic of the SRIM process set-up
Drawn from Mazumdar (2002)

1.3 Analysis Methods

In this section, the analysis methods used in this thesis are exposed. Four of them are compared, the classical lamination theory (CLT), the Timoshenko first-order beam theory (TFBT), the refined higher-order beam theory of Zenkour (RHBT) and the finite element method.

1.3.1 Lamination Theories

All lamination theories (CLT, TFBT and RHBT) are based totally or partially on Kirchhoff's hypothesis (Reddy, 1997). Kirchhoff's hypothesis includes three important assumptions:

- straight lines perpendicular to the mid-surface before deformation, called transverse normal (illustrated by the bold line in Figure 1.9 between points (u_0, w_0) and (u, w)), remain straight after deformation;
- transverse normal do not elongate in bending;
- transverse normal remain perpendicular to the mid-surface.

For the CLT, Kirchhoff's assumptions are integrally considered. This theory does not include the effect of shear deformation which cannot be neglected in thick laminate (Zenkour, 1999). For the TFBT, the perpendicularity of transverse normal with the mid-surface is relaxed to include a constant state of transverse shear strain which requires a shear correction factor. That allows the transverse normal to eventually elongate; in this case only the straightness assumption is enforced. For the RHBT, the straightness assumption is removed but Zenkour has added perpendicularity between the transverse normal and external planes in the development of the RHBT because no shear is found on external faces (Zenkour, 1999). The RHBT includes both transverse shear and transverse normal effects. Theories with higher order are not useful because the gain in accuracy is so little compared to the considerable

effort required to solve the equations. Figure 1.9 illustrates each theory and their assumptions: (A) for CLT, (B) for TFBT, and (C) for RHBT.

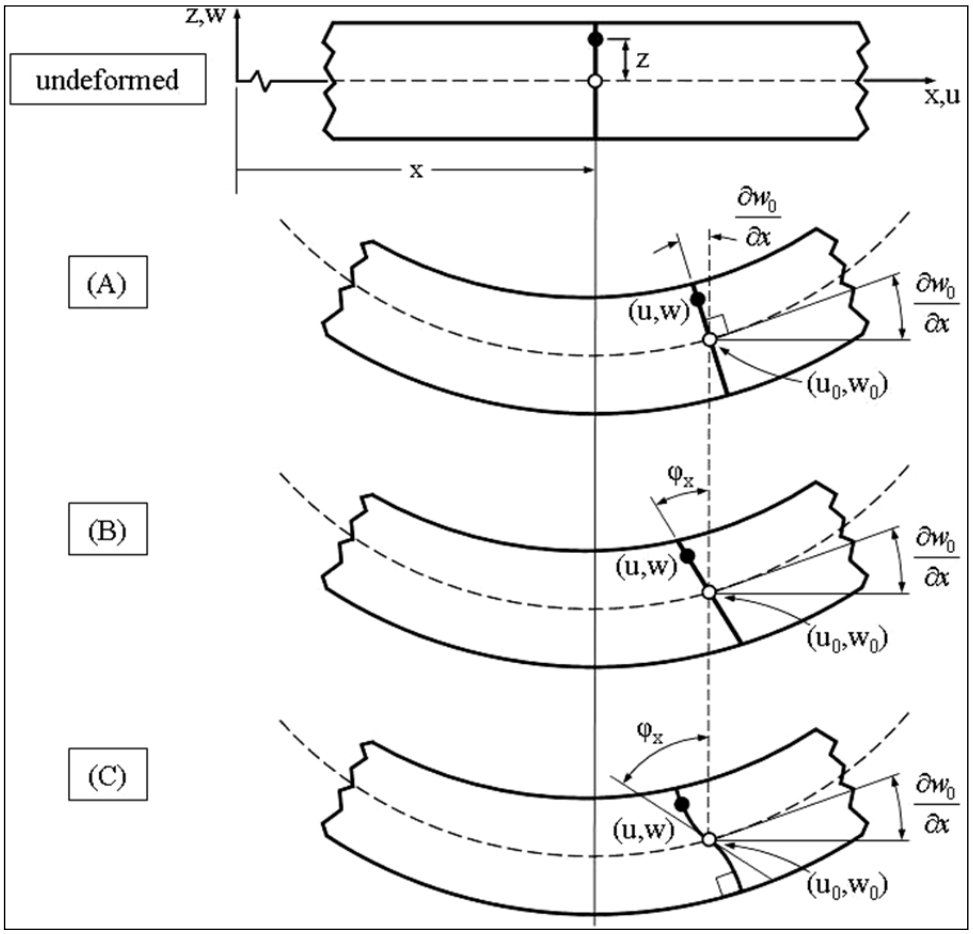

Figure 1.9 Assumption representations for (A) CLT, (B) TFBT, and (C) RHBT

A composite laminated structure is made of a number of layers *N*. Other useful information for future calculation is provided in Figure 1.10. The global coordinate system (*x*, *y*, and *z*) is the coordinate system for a composite laminated structure. Each layer can have an arbitrary orientation θ for its fibres. The orientation of the fibres at layer *k* is identified by θ_k which is an angle taken with respect to the global longitudinal axis, x. The local coordinate system for each individual UD layer is 1 for the fibre direction, 2 for the in-plane transverse direction and 3 for the through-the-thickness direction.

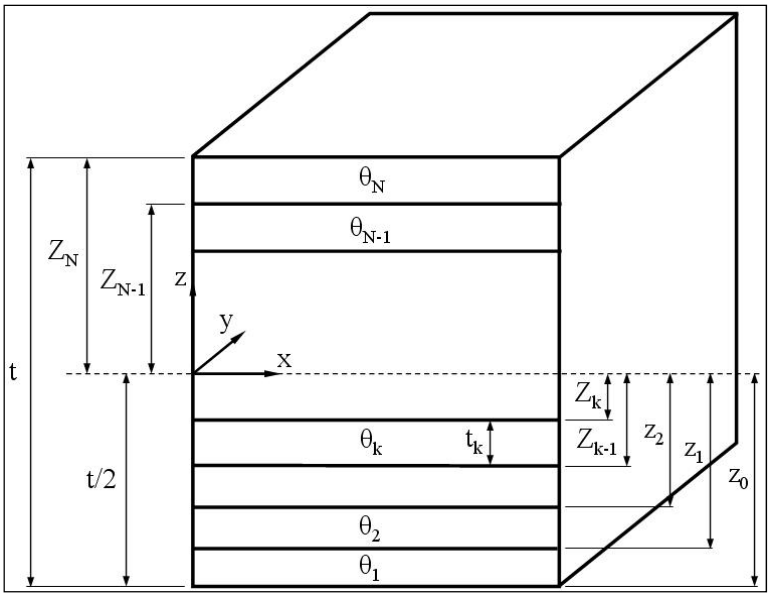

Figure 1.10 Composite laminated structure section with *N* layers in a global coordinate system

t_k is the thickness of the layer k and the total laminate thickness t is the sum of t_k for k equals 1 to N. The location of each layer in the lay-up is also important in order to compute laminate properties. For example, in Figure 1.10, z_k is the position of the top of the layer k, along Z axis.

1.3.1.1 Classical Lamination Theory (CLT)

The classical lamination theory (CLT) for the beam is summarized in this subsection. By respecting precisely the Kirchhoff's hypotheses, the displacement field used in CLT is defined as follows (Daniel and Ishai, 1994; Reddy, 1997):

$$\begin{aligned} u(x,y,z) &= u_0(x,y) - z\frac{\partial w_0}{\partial x} \\ v(x,y,z) &= v_0(x,y) - z\frac{\partial w_0}{\partial y} \\ w(x,y,z) &= w_0(x,y) \end{aligned} \tag{1.1}$$

The constitutive lamina relation or Hooke's law for stress and strain is given by the following equation, as shown in (Reddy, 1997; Lessard, 2004):

$$\begin{Bmatrix} \sigma_1 \\ \sigma_2 \\ \sigma_6 \end{Bmatrix}^{(k)} = \begin{bmatrix} Q_{11} & Q_{12} & 0 \\ Q_{12} & Q_{22} & 0 \\ 0 & 0 & Q_{66} \end{bmatrix}^{(k)} \begin{Bmatrix} \varepsilon_1 \\ \varepsilon_2 \\ \varepsilon_6 \end{Bmatrix}^{(k)} \tag{1.2}$$

where, the $Q_{ij}^{(k)}$ represent the in-plane stress-reduced stiffness matrix components and σ_i and ε_i are the stress and strain components in the local coordinate system of a layer k. In the local coordinate system, the 1 axis is the fibre direction, the 2 axis is the in-pane direction perpendicular to the fibre and 6 is for the in-plane shear. The in-plane stiffness matrix is defined using engineering material properties as (Reddy, 1997; Lessard, 2004):

$$\begin{aligned} Q_{11} &= \left(1 - \frac{\nu_{12}^2 E_2}{E_1}\right)^{-1} E_1 \\ Q_{22} &= \left(1 - \frac{\nu_{12}^2 E_2}{E_1}\right)^{-1} E_2 \\ Q_{12} &= \left(1 - \frac{\nu_{12}^2 E_2}{E_1}\right)^{-1} \nu_{12} E_2 \\ Q_{66} &= G_{12} \end{aligned} \tag{1.3}$$

For a laminate with several layers, the transformed stress-strain relation for each layer k is given by (Reddy, 1997).

$$\begin{Bmatrix} \sigma_{xx} \\ \sigma_{yy} \\ \tau_{xy} \end{Bmatrix}^{(k)} = \begin{bmatrix} \overline{Q}_{11} & \overline{Q}_{12} & \overline{Q}_{16} \\ \overline{Q}_{12} & \overline{Q}_{22} & \overline{Q}_{26} \\ \overline{Q}_{16} & \overline{Q}_{26} & \overline{Q}_{66} \end{bmatrix}^{(k)} \begin{Bmatrix} \varepsilon_{xx} \\ \varepsilon_{yy} \\ \gamma_{xy} \end{Bmatrix} \tag{1.4}$$

where, the $\overline{Q}_{ij}^{k}$ are the in-plane stress-reduced stiffness matrix components in the layer k, relative to the global coordinate system (X axis is the longitudinal direction and Y is the in-plane orthogonal axis) of the composite laminated structure (Details can be found in (Reddy, 1997; Lessard, 2004)):

$$\begin{aligned}
\overline{Q}_{11}^{k} &= \cos^4(\theta)Q_{11} + \sin^4(\theta)Q_{22} + 2\cos^2(\theta)\sin^2(\theta)Q_{12} + 4\cos^2(\theta)\sin^2(\theta)Q_{66} \\
\overline{Q}_{22}^{k} &= \sin^4(\theta)Q_{11} + \cos^4(\theta)Q_{22} + 2\cos^2(\theta)\sin^2(\theta)Q_{12} + 4\cos^2(\theta)\sin^2(\theta)Q_{66} \\
\overline{Q}_{12}^{k} &= \cos^2(\theta)\sin^2(\theta)Q_{11} + \cos^2(\theta)\sin^2(\theta)Q_{22} \\
&\quad + (\cos^4(\theta) + \sin^4(\theta))Q_{12} - 4\cos^2(\theta)\sin^2(\theta)Q_{66} \\
\overline{Q}_{66}^{k} &= \cos^2(\theta)\sin^2(\theta)Q_{11} + \cos^2(\theta)\sin^2(\theta)Q_{22} \\
&\quad - 2\cos^2(\theta)\sin^2(\theta)Q_{12} + (\cos^2(\theta)\sin^2(\theta))^2 Q_{66} \\
\overline{Q}_{16}^{k} &= \cos^3(\theta)\sin(\theta)Q_{11} - \cos(\theta)\sin^3(\theta)Q_{22} \\
&\quad + \left(\cos(\theta)\sin^3(\theta) - \cos^3(\theta)\sin(\theta)\right)Q_{12} + 2\left(\cos(\theta)\sin^3(\theta) - \cos^3(\theta)\sin(\theta)\right)Q_{66} \\
\overline{Q}_{26}^{k} &= \cos(\theta)\sin^3(\theta)Q_{11} - \cos^3(\theta)\sin(\theta)Q_{22} \\
&\quad + \left(\cos^3(\theta)\sin(\theta) - \cos(\theta)\sin^3(\theta)\right)Q_{12} + 2\left(\cos^3(\theta)\sin(\theta) - \cos(\theta)\sin^3(\theta)\right)Q_{66}
\end{aligned} \tag{1.5}$$

After applying equations of motion, the laminate constitutive equations can be written as in Equation 1.6.

$$\begin{Bmatrix} \{N\} \\ \{M\} \end{Bmatrix} = \begin{bmatrix} [A] & [B] \\ [B] & [D] \end{bmatrix} \begin{Bmatrix} \{\varepsilon^0\} \\ \{\varepsilon^1\} \end{Bmatrix} \tag{1.6}$$

The vector $\{N\}$ gives the in-plane force resultants (x, y and xy), while the vector $\{M\}$ gives the in-plane moment resultants. Components of $[A]$ matrix are the extensional stiffness values ($=\int [\bar{Q}] dz$), those of the $[D]$ matrix are the bending stiffness values ($=\int [\bar{Q}] z^2 dz$), and $[B]$ matrix components are the bending-extensional coupling stiffness values ($=\int [\bar{Q}] z\, dz$). The components of the vectors $\{\varepsilon^0\}$ and $\{\varepsilon^1\}$ are the values of the membrane strains and curvatures respectively.

1.3.1.2 Timoshenko First-order Beam Theory (TFBT)

In the Timoshenko first-order beam theory (TFBT), the Kirchhoff's hypothesis is relaxed. The third assumption, i.e. transverse normal remain perpendicular to the mid-surface, is not enforced; thus, a transverse normal is allowed to elongated. With this relaxation, the displacement field for TFBT becomes (Reddy, 1997):

$$\begin{aligned} u(x,y,z) &= u_0(x,y) + z\frac{\partial u(x,y,z)}{\partial z} \\ v(x,y,z) &= v_0(x,y) + z\frac{\partial v(x,y,z)}{\partial z} \\ w(x,y,z) &= w_0(x,y) \end{aligned} \tag{1.7}$$

The basic constitutive laminate equations used in TFBT are the same as those used in CLT, see Equation 1.2 and Equation 1.3. In addition, terms of Equation 1.8 are added to take into account the interlaminar shear (ILS) (Reddy, 1997).

$$\begin{Bmatrix} \tau_{xz} \\ \tau_{yz} \end{Bmatrix}^{(k)} = \begin{bmatrix} \overline{Q}_{44} & \overline{Q}_{45} \\ \overline{Q}_{45} & \overline{Q}_{55} \end{bmatrix}^{(k)} \begin{Bmatrix} \gamma_{xz}^{(0)} \\ \gamma_{yz}^{(0)} \end{Bmatrix} \tag{1.8}$$

where, the $\overline{Q}_{ij}^{k}$ are the out of plane shear stiffness matrix components in the layer *k*, relative to the global coordinate system of the composite laminated structure. The following details can be found in (Reddy, 1997):

$$\begin{aligned} \overline{Q}_{44}^{k} &= \cos^2(\theta)G_{13} + \sin^2(\theta)G_{23} \\ \overline{Q}_{55}^{k} &= \cos^2(\theta)G_{23} + \sin^2(\theta)G_{13} \\ \overline{Q}_{45}^{k} &= \cos(\theta)\sin(\theta)\left(G_{13} - G_{23}\right) \end{aligned} \tag{1.9}$$

After applying the equations of motion to TFBT constitutive equations, Equation 1.10 is added to Equation 1.6 to complete the set of laminate equations for TFBT (Reddy, 1997):

$$\begin{Bmatrix} Q_x \\ Q_y \end{Bmatrix} = K \begin{bmatrix} A_{44} & A_{45} \\ A_{45} & A_{55} \end{bmatrix} \begin{Bmatrix} \gamma_{xz}^{(0)} \\ \gamma_{yz}^{(0)} \end{Bmatrix} \tag{1.10}$$

The terms A_{44}, A_{45}, and A_{55} are the extensional shear stiffness matrix components ($=\int [\overline{Q}] dz$), and Q_x and Q_y are respectively the longitudinal – through-the-thickness and transverse – through-the-thickness shear force resultants as shown in Figure 1.11.

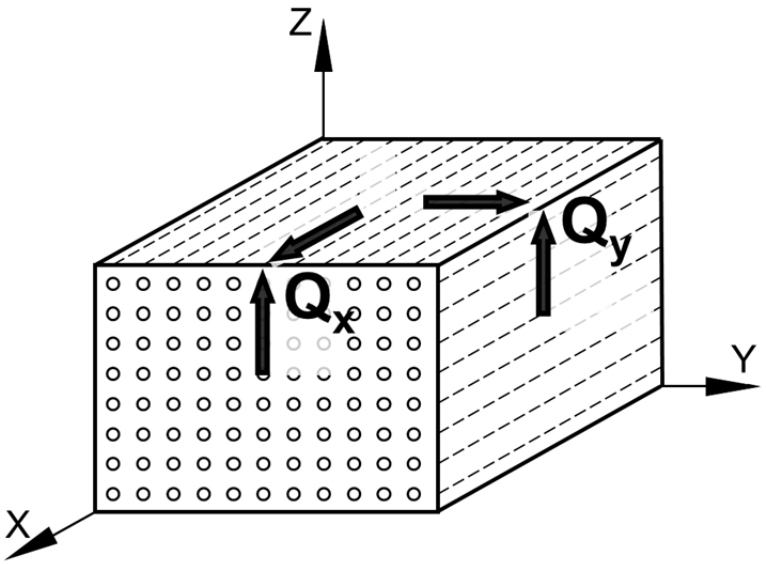

Figure 1.11 Resultant shear forces in the global coordinate system

K, used in Equation 1.10, is the correction shear factor, so-called k-factor. This correction factor accounts for transverse shear stiffness and transverse shear stress. The calculation of this factor is not straight forward for arbitrarily composite laminated plates. It depends on the laminate sequence and the ply orientation (lay-up), the geometric parameters, the loading and the boundary conditions (Madabhusi-Raman and Davalos, 1996; Reddy, 1997).

In this work, two k-factors are compared. One is a constant value of 5/6 as the widely used value for isotropic materials and homogeneous plates (Whitney, 1973; Zenkour, 1999). The second is a lay-up dependent value.

The shear correction factor (*K*) dependent on the lay-up involves calculating it as a function of the laminate geometry. As described in the theory of Madabhusi-Raman and Davalos, Equation 1.10 is then modified and defined as follows for each layer *k* (Madabhusi-Raman and Davalos, 1996):

$$\begin{Bmatrix} Q_x \\ Q_y \end{Bmatrix}^{(k)} = \begin{bmatrix} k_1^2 A_{44} & k_1 k_2 A_{45} \\ k_1 k_2 A_{45} & k_2^2 A_{55} \end{bmatrix}^{(k)} \begin{Bmatrix} \gamma_{xz}^{(0)} \\ \gamma_{yz}^{(0)} \end{Bmatrix} \tag{1.11}$$

Then, k_1^2 is computed using Equation 1.12, Equation 1.13 and Equation 1.14. These equations are obtained by assuming that Q_y is zero in Equation 1.11. And from the constitutive relation for transverse shear stress resultant, the shear strain energy is equated to the transverse shear stress obtained from equilibrium equations. The complete expressions of the extra terms in Equation 1.14 are defined in (Madabhusi-Raman and Davalos, 1996). For k_2, A_{44} and A_{55} are interchanged in Equation 1.12 and in a similar way for $\overline{Q}_{44}^k$ and $\overline{Q}_{55}^k$ in Equation 1.13. This theory can be used for all arbitrary lay-up configurations (Madabhusi-Raman and Davalos, 1996).

$$k_1^{\,2} = \frac{\left[A_{44} - \dfrac{A_{45}^2}{A_{55}}\right]^{-1}}{\left[\sum_{k=1}^{N} S_{k1} Y_k\right]} \tag{1.12}$$

with,

$$S_{k1} = \frac{1}{\left(\overline{Q}_{44}^k - \left(\overline{Q}_{45}^k\right)^2 / \overline{Q}_{55}^k\right)} \tag{1.13}$$

$$\begin{aligned} Y_k = {} & P_k (z_{k+1} - z_k) + \frac{R_k}{2}(z_{k+1}^2 - z_k^2) + \frac{V_k}{3}(z_{k+1}^3 - z_k^3) \\ & + \frac{W_k}{4}(z_{k+1}^4 - z_k^4) + \frac{X_k}{5}(z_{k+1}^5 - z_k^5) \end{aligned} \tag{1.14}$$

1.3.1.3 Refined Higher-order Beam Theory (RHBT)

For the Refined higher-order beam theory (RHBT) developed by Zenkour, the Kirchhoff hypotheses are not at all enforced, but the assumption given by Zenkour assumes transverse normal to be perpendicular to external surfaces because no shear is found on external faces. That assumption leads to the following displacement field (Zenkour, 1999):

$$\begin{aligned} u(x,z) &= u_0(x) + z\,u_1(x) - \frac{z^2}{2}\frac{dw_1}{dx} \\ &\quad - z^3\left[\frac{4}{3t^2}\left(\frac{dw_0}{dx} + u_1(x)\right) + \frac{1}{3}\frac{dw_2}{dx}\right] \\ w(x,z) &= w_0(x) + [z\,w_1(x) + z^2 w_2(x)] \end{aligned} \tag{1.15}$$

where u_0 and w_0 denote the displacement of a point on the mid-plane along the x and z directions respectively, u_1 denotes the rotation of a transverse normal about the y-axis, w_1 and w_2 denote terms in the calculation of the transverse strain. The laminate constitutive equations can be simplified to Equation 1.16 and Equation 1.17. In addition, since the matrix coefficients differ slightly from those in CLT and TFBT, refer to (Zenkour, 1999) for a complete description of all coefficients.

$$\begin{Bmatrix} N_1 \\ N_3 \\ M_1 \\ M_3 \\ P_1 \\ S_1 \end{Bmatrix} = \begin{bmatrix} A_{11} & A_{13} & B_{11} & B_{13} & D_{11} & E_{11} \\ & A_{33} & B_{13} & B_{33} & D_{13} & E_{13} \\ & & D_{11} & D_{13} & E_{11} & F_{11} \\ & & & D_{33} & E_{13} & F_{13} \\ & & & & F_{11} & G_{11} \\ symm. & & & & & H_{11} \end{bmatrix} \begin{Bmatrix} \varepsilon_1^{(0)} \\ \varepsilon_3^{(0)} \\ \varepsilon_1^{(1)} \\ \varepsilon_3^{(1)} \\ \varepsilon_1^{(2)} \\ \varepsilon_1^{(3)} \end{Bmatrix} \tag{1.16}$$

$$and \quad \begin{Bmatrix} Q \\ R \end{Bmatrix} = \begin{bmatrix} A_{55} & D_{55} \\ D_{55} & F_{55} \end{bmatrix} \begin{Bmatrix} \varepsilon_5^{(0)} \\ \varepsilon_5^{(2)} \end{Bmatrix} \tag{1.17}$$

$$
\begin{aligned}
(A_{11}, B_{11}, D_{11}, E_{11}, F_{11}, G_{11}, H_{11}) &= b\sum_{k=1}^{N}\int_{z_{k-1}}^{z_k} \overline{Q}_{11}^{k}\left(1, z, z^2, z^3, z^4, z^5, z^6\right)dz \\
(A_{13}, B_{13}, D_{13}, E_{13}, F_{13}) &= b\sum_{k=1}^{N}\int_{z_{k-1}}^{z_k} \overline{Q}_{13}^{k}\left(1, z, z^2, z^3, z^4\right)dz \\
(A_{33}, B_{33}, D_{33}) &= b\sum_{k=1}^{N}\int_{z_{k-1}}^{z_k} \overline{Q}_{33}^{k}\left(1, z, z^2\right)dz \\
(A_{55}, B_{55}, D_{55}) &= b\sum_{k=1}^{N}\int_{z_{k-1}}^{z_k} \overline{Q}_{55}^{k}\left(1, z^2, z^4\right)dz
\end{aligned}
\tag{1.18}
$$

where, $\overline{Q}_{11}^{k}$ is the in-plane normal stiffness in the layer *k* from Equation 1.5, $\overline{Q}_{13}^{k}$ is the out of plane shear stiffness in the layer *k* as $\overline{Q}_{12}^{k}$ in Equation 1.5, $\overline{Q}_{33}^{k}$ is the out of plane normal stiffness in the layer *k* as $\overline{Q}_{22}^{k}$ in Equation 1.5 and $\overline{Q}_{55}^{k}$ is the out of plane shear stiffness in the layer *k* from Equation 1.8.

Zenkour assumed that the solutions for the deflections u_0, w_0, u_1, w_1 and w_2 are under the form presented in Equation 1.19 and can be obtained by solving the system of equations expressed in Equation 1.20 (Zenkour, 1999). The solution of this system of equations is based on a Navier-like approach and it is only applicable to cross-ply laminated beams.

$$
\boxed{
\begin{aligned}
(u_0, u_1) &= \sum_{m=1}^{\infty} (U_m^{(0)}, U_m^{(1)}) \cos(\mu_m x) \\
(w_0, w_1, w_2) &= \sum_{m=1}^{\infty} (W_m^{(0)}, W_m^{(1)}, W_m^{(2)}) \sin(\mu_m x)
\end{aligned}
}
\tag{1.19}
$$

$$
[C]\begin{Bmatrix} U_m^{(0)} \\ W_m^{(0)} \\ U_m^{(1)} \\ W_m^{(1)} \\ W_m^{(2)} \end{Bmatrix} = Q_m \begin{Bmatrix} 0 \\ 1 \\ 0 \\ -h/2 \\ h^2/4 \end{Bmatrix}
\tag{1.20}
$$

where $\mu_m = m\pi/L$, Q_m is the load and [C] denotes coefficient matrix defined in the appendix of Zenkour's article (Zenkour, 1999). This theory seems to give similar results, within 10%

(±5%) than TFBT for the maximum deflection. For the in-plane longitudinal stress and the out-of-plane shear stress, the difference is more about 30% to 50% respectively.

1.3.2 Finite Element Analysis (FEA)

Finite element analyses (FEA) are widely used to avoid the expensive cost of intensive experimental testing. Several researchers have reproduced their theories or experiments within commercial codes: Aghdam and Falahatgar used ANSYS® (Aghdam and Falahatgar, 2003), Nguyen, Caron and Sab validated their model with a large number of numerical examples in ABAQUS® (Nguyen, Caron and Sab, 2005), Hufenbach *et al.* verified a theoretical analysis using Hashin/Puck failure criterion in I-DEAS® (Hufenbach *et al.*, 2004) and Yildiz and Sarikanat combined ANSYS® and I-DEAS® for their study on thick composite beams and plates (Yildiz and Sarikanat, 2001). Some authors did not identify specific commercial software, as it is the case for Gunnion *et al.* and for Narayana Naik, Krishna Murty and Gopalakrishnan (Gunnion *et al.*, 2004; Narayana Naik, Krishna Murty and Gopalakrishnan, 2005). Rastogi compared a large range of commercial FEA codes: ABAQUS®, ANSYS®, CATIA®, LS-DYNA® and NASTRAN® (ASM International, 2002). In the Rastogi's comparison, all commercial codes support several aspects:

- ply properties based on unidirectional tape or woven fabric architecture;
- ply lay-ups;
- ply orientation in space;
- computation of 3D effective properties;
- computation of **[A]**, **[B]**, and **[D]** stiffness matrices for plate and shell elements using CLT;
- recovery of strains and stresses in various coordinate systems, such as global axis, local element axis, laminate and lamina axes;
- first ply failure based on either point stress/strain (maximum strain/stress) or quadratic failure (Tsai-Wu, Hill, Hashin) criterion.

Some of them provide progressive damage material models for ultimate failure load prediction, such as LS-DYNA® and ABAQUS®. Based on Rastogi's comments, "ESI-SYSPLY (ESI Group, France) is probably the most comprehensive and user-friendly program currently available for composite FEA". However, this last software does not have similar graphic interface capabilities as in ANSYS®, PATRAN® or ABAQUS®.

1.3.2.1 Modeling Methodology

In this section, the aspects of building a composite model in ANSYS® are presented. This commercial software has been chosen, since it is the most widely used in the industry for FEA and it is available at École de Technologie Supérieure (ÉTS).

The first step toward building a FE model starts by selecting the element type that best fits the application (theory assumptions, geometry, computational times, etc.) In ANSYS® three shell element types (SHELL99 – Linear layered structural shell element (250 plies), SHELL91 – Nonlinear layered structural shell element (100 layers) and SHELL181 – Finite strain shell (255 layers)) and two solid elements types (SOLID46 – 3D layered structural solid element (250 plies) and SOLID191 – Layered structural solid element (100 layers)) are available (ANSYS, released 9). The choice between shell and solid elements depends on many factors. Shell elements have 4 nodes of 6 degrees of freedom (DOF), 3 translations and 3 rotations, and solid elements have 8 nodes of 3 DOF, only 3 translations.

For a global FE model (GFEM), like a complete aircraft model, it is preferable to use shell elements to model the composite structure. Shell elements are also dedicated to model thin-walled structures. With shell elements, it is possible to stack two elements on top of each other to model, for example, a flange of a composite frame on a laminated composite skin.

For a detailed FE model (DFEM), like individual components, sub-assemblies or validation of results from experimental coupons, solid elements are recommended. In addition, solid elements are more dedicated to model thick composite laminated structures, particularly to

study the through-the-thickness behaviour. With solid elements, specifically for SOLID46, several elements can be stacked on each another. This characteristic is important, particularly in bending problems when the accuracy of the model is directly proportional to the number of elements through the thickness (Bathe, 1996). Another specification of SOLID46 is that the through-the-thickness shear stiffness is not zero at element interface. Thus interlaminar shear stresses can be computed and analyzed. Furthermore, the method used is based on heuristic findings and numerical experiences rather than on a rigorous theoretical formulation (ANSYS, released 9).

When the choice of the element type is done, the construction of a FE model starts with the geometry. The layered configuration is defined by specifying individual layer properties. There are two ways to input the layer properties in a model. The first one is with real constants (limited to 100 layers using the graphical user interface (GUI)) in which material properties, layer orientation angle and layer thickness are all defined. The second method is by defining the constitutive matrices (unlimited number of plies) computed using the selected theory. It is also possible to define sandwich like and multiple-layered structures and to offset nodes for shell elements. While solving the FEM, different failure criteria (maximum strain, maximum stress, Tsai-Wu, etc.) can be done by specifying in a data table the nonlinear material properties. Up to six other criteria can be programmed via the user interfaced subroutines (USRFC1 through USRFC6). A method to write subroutine in ANSYS® is presented in the thesis of Viens (Viens, 2004). In ANSYS® documentation, additional modeling and post-processing guidelines for composite elements are identified.

1.3.2.2 Orthotropic Material Properties

In order to model an orthotropic material, nine elastic mechanical properties are required. They can be obtained from the literature, experimental data and/or by analytical assumptions. These nine elastic properties are the three Young's moduli E_1, E_2 and E_3, the three major Poisson's ratios ν_{12}, ν_{13} and ν_{23}, and the three shear moduli G_{12}, G_{13} and G_{23}.

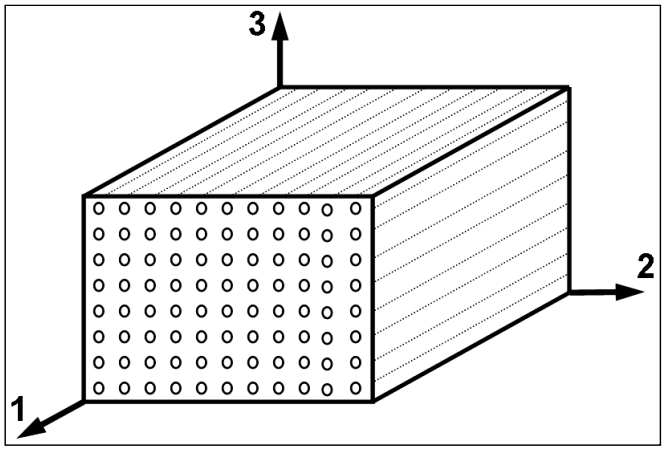

Figure 1.12 Example of a UD laminated section

In reference to Figure 1.12, E_1 is the longitudinal elastic modulus, which is along the fibres. E_2 is the in-plane transverse elastic modulus and it is perpendicular to the fibre direction but not through-the-thickness. E_3 denotes the through-the-thickness elastic modulus, which is perpendicular to the fibre direction and through-the-thickness. ν_{12} is the in-plane major Poisson's ratio, ν_{13} is the longitudinal – through-the-thickness Poisson's ratio and ν_{23} denotes the transverse – through-the-thickness Poisson's ratio. G_{12} is the in-plane shear modulus, G_{13} is the longitudinal – through-the-thickness shear modulus and G_{23} is the transvers – through-the-thickness shear modulus.

Since a total of nine elastic material properties are needed, a minimum of nine relations need to be identified. The relations needed for the longitudinal elastic modulus (E_1) and the major Poisson's ratio (ν_{12}) are based on the fibre volume fraction (V_f) and individual properties of each constituent (f and m denote the fibre the matrix, respectively). The two relations shown in Equation 1.21 and Equation 1.22 are determined by the well-known rule of mixture (Berthelot, 2005; Daniel and Ishai, 1994). They have been developed to express several elastic properties for UD laminates, like the values of E_1 and ν_{12}.

$$E_1 = E_f V_f + E_m (1 - V_f) \tag{1.21}$$

$$\nu_{12} = \nu_f V_f + \nu_m (1 - V_f) \tag{1.22}$$

The longitudinal - transverse shear modulus (G_{12}) and the transverse - through-the-thickness shear modulus (G_{23}) are extracted from an exact solution of a cylindrical problem with two and three phases, respectively (Berthelot, 2005). The two phases are a fibre surrounded by a matrix, where the longitudinal (fibre) direction is 1, the radial direction is 2 and the tangential direction is 3. In the case of three phases, the two phases are surrounded by a homogeneous material made of fibres and matrix.

$$G_{12} = G_m \frac{G_f(1+V_f) + G_m(1-V_f)}{G_f(1-V_f) + G_m(1+V_f)} \tag{1.23}$$

$$G_{23} = G_m \left(1 + \frac{V_f}{\frac{G_m}{G_f - G_m} + \frac{k_m + \frac{7}{3}G_m}{2k_m + \frac{8}{3}G_m}(1-V_f)} \right) \tag{1.24}$$

where k_m is the bulk modulus of the matrix.

The transverse elastic modulus (E_2) is expressed as a function of the lateral compression modulus (K_l), the transverse - through-the-thickness shear modulus (G_{23}), the major Poisson's ratio (ν_{12}) and the longitudinal elastic modulus (E_1), see Equation 1.25. K_l, meaning without longitudinal deformation, is also based on the exact solution of the cylindrical problem and it is presented in Equation 1.26 (Berthelot, 2005).

$$E_2 = \frac{2}{\frac{1}{2K_l} + \frac{1}{2G_{23}} + 2\frac{\nu_{12}^2}{E_1}} \tag{1.25}$$

$$K_l = K_m + \frac{V_f}{\frac{1}{k_f - k_m + \frac{1}{3}(G_f - G_m)} + \frac{1-V_f}{k_m + \frac{4}{3}G_m}} \tag{1.26}$$

To determine the other through-the-thickness properties, it is generally assumed that a UD laminate is considered transversely isotropic in the out of plane perpendicular to the fibres (plane 2-3), as illustrated in Figure 1.12 (Berthelot, 2005; Daniel and Ishai, 1994). In the cross-section of a laminate, fibres are assumed to be equally distributed in the matrix, in the transverse and through-the-thickness directions (2 and 3). This implies that the through-the-thickness elastic modulus (E_3) is equal to the transverse elastic modulus (E_2) (Daniel *et al.*, 2008; Schubel *et al.*, 2006). In the same way, the longitudinal - through-the-thickness shear modulus (G_{13}) and the longitudinal-through-the-thickness Poisson's ratio (ν_{13}) are equal to G_{12} and ν_{12}, respectively (Bogetti *et al.*, 2004a; Daniel and Ishai, 1994; Pervez *et al.*, 2005).

The transverse - through-the-thickness Poisson's ratio (ν_{23}) is computed based on the assumption of a transversely isotropic behaviour of UD laminates, using the relation between the elastic and shear modulus (Berthelot, 2005; Bogetti *et al.*, 2004; Daniel and Ishai, 1994).

$$\nu_{23} = \frac{E_2}{2G_{23}} - 1 \tag{3.7}$$

1.3.2.3 Experimental Characterization

Another method to obtain the nine orthotropic elastic mechanical properties is to measure them by testing specimens. Experimental analysis is a fairly complex problem, fairly labour-intensive and expensive procedure because it requires a large sample of test specimens (Gurvich and Byron Pipes, 1995), even before the issue of size effect (Sutherland *et al.*, 1999a).

1.4 Thick Laminates Opposed to Thin Laminates

This section will present the principal difficulties and differences in term of manufacturing, testing and analyzing thick composite laminates as opposed to thin ones.

1.4.1 Manufacturing: Thin vs Thick Laminates

Many weaknesses can be observed in the manufacturing of composite laminates, as voids, porosities, dry spots, low fibre volume fraction, fibre misalignments, resin shrinkage, residual stresses and heat generation. Several studies prove that the number of voids, porosities and dry zones increases with the specimen thickness creating a weaker composite material (Daniel *et al.*, 2008; Hodgkinson, 2000; Jackson, 1992; Lee and Soutis, 2005). Sutherland *et al.* concluded that the probability of containing several flaws like air bubbles and misalignment of fibres is increased in the manufacturing of larger specimens. As a result, during the flexural test, a loss in strength occurred with an increase in thickness due to a large number of flaws and that led to a premature failure of composite laminates (Sutherland *et al.*, 1999b; 1999c). A judicious choice of time, temperature and pressure will help in the production of fully cured, compacted and high quality composites (White and Hahn, 1992).

According to Shepheard's work, a decrease of 7% of the fibre volume fraction and an increase of 1.5% of the void fraction are observed in thick laminates compared to the ones found in thin coupons (Shepheard *et al.*, 2004). Since fewer fibres are contained in the laminate, the mechanical properties, in compression in this case, are simply lower by about 25% in stiffness and 50% in strength. Shepheard *et al.* used the filament winding process to produce their laminated plates of 25 mm thick with an 89.5° wind angle, considered unidirectional (Shepheard *et al.*, 2004). Furthermore, Broughton and Sims concluded that the interlaminar shear and transverse tensile strengths, matrix dominated properties, diminish dramatically, about 7% for every 1% increase in void content, for void contents in excess of 2% (Broughton and Sims, 1994). The use of an autoclave with prepreg or a RTM process

gives parts with a higher fibre volume fraction (60%) and a lower void content (<1%), then stronger and stiffer parts.

Sutherland *et al.* considered a misalignment angle of 15° to be an appropriate control (Sutherland *et al.*, 1999c). The misalignment of fibres is also studied by Shepheard *et al.* They found that a ±5° misalignment of only half of the fibre content predicted modulus falls by 2.4% and by 9.5% for a ±10° misalignment of half of the fibre content (Shepheard *et al.*, 2004). In addition, if all the misalignment is in the same direction, such as, -10° (in comparison to ±5°), the effect is larger with a reduction of 15% for the compression stiffness (Shepheard *et al.*, 2004). So, particular attention in the consolidation step is essential to keep the fibres in the desired orientation to avoid misalignment problem. In addition, in hand lay-up processes, the operator skills are very helpful. A good solution to misalignment problems is the use of the laser projection, automated fibre placement (AFP) or filament and tape winding, but in large structures with many layers throughout the thickness, the fibre misalignment becomes less problematic.

A real challenge in the manufacturing of thick parts is to build them warp-free and distortion-free. Thick parts are more subject to shrinkage that may lead to residual stresses in the laminated structure. Residual stresses can have a significant effect on engineering properties by inducing warping, fibre buckling, matrix micro-cracking and delamination (Broughton *et al.*, 2001). The pultrusion process for small and medium cross section straight bars tends toward 2-3% of shrinkage (Mazumdar, 2002). Conversely, in thicker structures shrinkage can be over 6% (White and Hahn, 1992). To resolve this problem, a careful selection of the lay-up sequence, using balanced and symmetric lay-ups, will decrease the warping effect. In addition, a cool down at different temperature, particularly in processes using an autoclave, may help (Liu et al., 2010; Luedtke and Brosius, 2009; Schlimbach *et al.*, 2009).

The heat generation and the difficulty to evacuate it, particularly in thicker laminates certainly influence the material properties since that will induce residual stresses (Bogetti *et al.*, 2004a; White and Hahn, 1992). A non-uniform curing can produce poor consolidation,

leading to a lower fibre volume fraction and higher void content (Broughton *et al.*, 2001). Jiang and Hoa developed a technique to reduce internal temperature during the manufacturing of thick composite structures (Jiang and Hoa, 2006). They manufactured coupons of about 30 to 60 mm thick using this method and they showed a reduction of the thermal effect on material properties. Luedtke and Brosius controlled the curing cycle, as well as the exothermal reaction, using a heat transfer fluid in the manufacturing of thick composite parts, up to 50 mm (Luedtke and Brosius, 2009). Schlimbach *et al.* showed by using the Quickstep curing process that they can rapidly manufacture thick laminates of 30 to 50 mm thick, without exothermal effect (Schlimbach *et al.*, 2009). Liu *et al.* manufactured 85 mm thick glass/epoxy laminates using the vacuum infusion manufacturing process (Liu *et al.*, 2010). They observed a large dispersion of the temperature through the thickness and developed cure kinetic equations to optimize the curing stage. Considering the heat generation effect in composites, extensive research would be useful to understand the effect of temperature through-the-thickness on laminated composite mechanical properties.

1.4.2 Characterization and Testing: Thin vs Thick Laminates

Using thin lamina's mechanical properties as assumptions in the calculation of thick laminated structures may be a source of error (Gurvich and Byron Pipes, 1995; Shepheard *et al.*, 2004; Sutherland *et al.*, 1999b). When thick laminates are involved, the experimental analysis becomes more problematic. As already mentioned, it is difficult to fabricate thick laminated specimens of uniform quality. It is also difficult to introduce the loading without stress concentrations at the grips (Broughton *et al.*, 2001; Daniel *et al.*, 2008; Sutherland *et al.*, 1999a; 1999b). In addition, many composites do behave as brittle materials (Sutherland *et al.*, 1999a), which led to premature matrix cracking and ultimately to strain gages failures (Bogetti *et al.*, 2004b; Daniel *et al.*, 2008; Hodgkinson, 2000; Zhou and Davies, 1995a).

This section presents the thickness effect in five categories of mechanical behaviour such as in-plane tension and compression, in-plane shear, bending, through-the-thickness tension and compression and interlaminar shear (ILS).

1.4.2.1 In-plane Tension and Compression

Zhou and Davies characterized E-glass woven-roving fabric impregnated with a polyester resin (Zhou and Davies, 1995a). The manufacturing process is not mentioned; however the authors declared that the laminates contain a high volume fraction of fibres without specifying measured values. They measured the longitudinal and transverse tension and compression properties (E_{11}, E_{22}, ν_{12}, ν_{21}, ν_{13}, ν_{23}, *UTS* and *UCS*) and the in-plane shear properties (G_{12} and τ_{12}) using straight-sided coupons with a thickness of 10 mm.

In tension, it is possible to predict the stiffness values and Poisson's ratios. Zhou and Davies found that their experimental results felt in a range close to theoretical prediction (Zhou and Davies, 1995a). They also observed a significant nonlinear behaviour in tension principally due to a through-the-thickness pressure on the edge, so called "edge effect" (Zhou and Davies, 1995a). This effect creates a compression failure of the matrix on the edge, followed by a delamination advancing from the edge towards the centre. The matrix failure on the edge causes strain gauges breakage, so strain cannot be recorded up to laminate failure. Using the same material as in tension, Zhou and Davies found that the behaviour in compression was linear. The stiffness in compression was about 5% higher than the tensile value. The Poisson's ratios were also much higher in compression than in tension. At the opposite, the compressive strength was lower by about 40% compared to tensile strength (Zhou and Davies, 1995a).

After an extensive literature review on scale effects (Sutherland *et al.*, 1999a), Sutherland *et al.* developed their own methodology and they applied it to unidirectional (Sutherland *et al.*, 1999b) and woven-roving laminates (Sutherland *et al.*, 1999c). For unidirectional laminates, two types of fibres were studied, E-glass and carbon, both in an epoxy resin. The laminated plates were manufactured using a vacuum assisted hand lay-up technique as in marine composite industries, providing a normal fibre volume fraction of 40% (Sutherland *et al.*, 1999b). Three different thicknesses were evaluated, about 1.3, 2.1 and 3.1 mm for tensile tests. The laminate quality has been well controlled since coefficients of variation were

below 5% (Sutherland *et al.*, 1999b). However, it was difficult to find a definite trend in the effect of thickness of tensile strength and stiffness. It was concluded that the manufacturing variation was responsible for the apparent thickness effect (Sutherland *et al.*, 1999b).

For woven-roving laminates, only glass reinforced polyester manufactured by a hand lay-up technique were used. The fibre volume fraction reached 35-40% (Sutherland *et al.*, 1999c). The tested specimens were varying in thicknesses from 3 to 12 mm for tensile tests. The coefficient of variation was around 5% for tensile tests (Sutherland *et al.*, 1999c). This inaccuracy was associated to the calculations of flexural stress and strain. Again, the fabrication method was different between thick and thin laminates since larger panels (for a volume scaling effect) were fabricated and discontinuities were found in thicker panels (Sutherland *et al.*, 1999c).

Lee and Soutis studied the effect of the thickness on open hole compression strength (Lee and Soutis, 2005). The material used was unidirectional tape of carbon fibres pre-impregnated in an epoxy resin. Laminated plates of 2, 3, 4, 6 and 8 mm thick were cured in autoclave They also compared the effect of the thickness on unidirectional (UD) laminate $[0_8]_n$, on a quasi-isotropic lay-up at the ply level ($[45_n/0_n/-45_n/90_n]_S$) and at the sub-laminate level ($[45/0/-45/90]_{nS}$). In all lay-ups, the numerical values are angles of each ply according to the longitudinal axis, *n* corresponds to the laminate thickness since one ply in 0.125 mm thick and *S* means a symmetric laminate. For UD lay-up, the stress-strain behaviour was linear up to a strain of approximately 0.5%, thereafter it was slightly nonlinear (Lee and Soutis, 2005). The axial compression modulus decreased of about 4% with the increase of specimen thickness (Lee and Soutis, 2005). After a catastrophic failure of unidirectional lay-ups, it was shown that the compressive strength and strain dropped by about 35% and 25%, respectively, varying from 2 to 8 mm thick, probably due to stress concentration at the grips (Lee and Soutis, 2005). For both quasi-isotropic lay-ups, the stress-strain behaviour was also linear up to a strain of 0.5% and the nonlinearity was higher than seen in UD. The compressive elastic modulus was similar for both lay-ups and comparable to the one estimated with the CLT (Lee and Soutis, 2005). The ultimate compressive strength was about

5% higher for the sub-laminate level ($[45/0/-45/90]_{nS}$) compared to the ply level ($[45_n/0_n/-45_n/90_n]_S$). In addition, the compressive strength was almost constant regardless of the specimen thickness for sub-laminate level ($[45/0/-45/90]_{nS}$) and ply level ($[45_n/0_n/-45_n/90_n]_S$) scaling up to 4 mm thick. For the 6 mm thick specimen, a drop of about 10% was recorded for the compressive strength (Lee and Soutis, 2005). Contradictory, according to Sutherland *et al.*, the ply level thickness scaling seems not to affect the behaviour during tensile and flexural testing in term of size but more in term of lay-up when for the sub-laminate level scaling, the thickness effect on the strength was significant (Sutherland *et al.*, 1999a). However, Kellas and Morton, and Johnson *et al.* concluded that the strength is little influenced for the ply level scaling when it is not for a sub-laminate level scaling (Johnson *et al.*, 2000; Kellas and Morton, 1993).

Lee and Soutis also verified that the fibre volume fraction was not influenced by the thickness for all lay-up. They also concluded that void content, fibre waviness and the edge effect (through-the-thickness tension and interlaminar shear) were the main parameters inducing the thickness effect on the compressive strength, particularly on UD and ply level lay-ups (Lee and Soutis, 2005). These parameters were not varying with the thickness for the sub-laminate level scaling lay-up (Lee and Soutis, 2005). The same conclusions were reiterated in 2007 by the same authors (Lee and Soutis, 2007).

Lavoie *et al.* studied the scaling effect, on volume and not specifically on thickness, for tensile tests until failure. They manufactured, using autoclave, UD $[0]_{8n}$, cross-ply $[0_{2n}/90_{2n}]_S$ and quasi-isotropic $[45_n/-45_n/0_n/90_n]_S$ laminates of unidirectional carbon/epoxy prepreg with a ply thickness of 0.125 mm (Lavoie *et al.*, 2000). The variation on thickness was from 1 to 4 mm, so *n* was 1, 2, 3 and 4. Six to seven specimens were tested per configurations, for a total of seventy-five specimens tested in tension. For UD and cross-ply lay-ups, about 90% of the specimens failed at the grips, therefore no conclusion on the thickness effect can be drawn using these unacceptable results. However, they blamed the 0° fibres exposed to surfaces which got damaged by the grip due to stress concentration (Lavoie *et al.*, 2000). For the quasi-isotropic lay-ups, the results were acceptable only for the thinner specimens since

failure at the grips was observed for *n* greater than 1, for about half of the specimens (Lavoie *et al.*, 2000). When the failure was on the gauge length, delamination has been observed leading to a loss in stiffness and a nonlinear behaviour prior to fibre failure (Lavoie *et al.*, 2000). This delamination was due to edge effect or a lack of consolidation during the manufacturing.

1.4.2.2 In-plane Shear

For in-plane shear properties, Zhou and Davies performed tensile tests using ±45° straight coupons. A significant nonlinear behaviour was observed enhanced by shear-tension coupling, straightening out of crimped fibres and matrix yielding, caused by the "scissoring" action of the fibres (Zhou and Davies, 1995a).

Melin and Neumeister studied the thickness and the notch angle effects on V-notched beam tests using the modified Iosipescu apparatus (Melin and Neumeister, 2006). They studied two laminated composites, a UD carbon fiber/epoxy prepreg ($[0]_{32}$) with a nominal thickness of 4.35 mm and a E-glass fibre/epoxy ($[0/CSM]_6$) of 5.3 mm thick (CSM means chopped strand mat). The notch angle at 90° as proposed in ASTM standard worked well for anisotropic materials, like composites, to measure shear moduli and strengths using the modified Iosipescu apparatus.

Bernasconi *et al.* tested composite laminates of 9.9 mm thick bonded together using lap joints (Bernasconi *et al.*, 2010). More often, they observed that the failure occurs in the adhesive. In only few specimens, an interlaminar failure was observed between a 45° woven ply and a 0° UD ply in the lap joint area.

1.4.2.3 Bending

Zhou and Davies also measured flexural properties (moduli and strengths) using span-to-depth ratio of 16:1 on 10 and 25 mm thick beams for three- and four-point bending tests (Zhou and Davies, 1995b). The flexural moduli and strengths were much less sensitive to fibre orientation than tensile and compressive properties. A good agreement, about 1.5%, was observed between measured and predicted values for the three-point bending. For the four-point bending, the ILS failure was predominant, so difficult to correlate with the prediction. Zhou and Davies concluded that the flexural behaviour is very dependent on the span-to-depth ratio. In the case of bending, the thickness effect did not affect that much the flexural modulus, but the flexural strength and strain at failure decreased with the increase of thickness (Zhou and Davies, 1995b).

Sutherland *et al.* manufactured two unidirectional laminates, E-glass and carbon, for flexural tests, with thicknesses of 2.2, 4.0 and 6.5 mm. Also during flexural tests, a loss in strength was recorded with increasing thickness, but different trends were observed for carbon and glass reinforced specimens (Sutherland *et al.*, 1999b). It was then concluded that the manufacturing variation was responsible for the apparent thickness effect.

Using woven-roving laminates, as in tension, Sutherland *et al.* found that the coefficient of variation was around 15% for flexural tests (Sutherland *et al.*, 1999c). This inaccuracy was associated to the calculations of flexural stress and strain. Again, larger panels (for a volume scaling effect) were fabricated and discontinuities were found in thicker panels (Sutherland *et al.*, 1999c).

Lavoie *et al.* also tested in three-point bending ninety-three UD ($[0]_{32}$) specimens of the same carbon/epoxy material used in tension. The span-to-depth ratio was greater than 20:1 and the thickness was 4 mm. Just under half of the specimens failed in bearing on the compression side under the loading roller (Lavoie *et al.*, 2000). No strain gauges were used in this investigation, so it was even more difficult to accurately get the maximum stress in bending.

A difference of about 10% was estimated for the valid specimens, which failed in tension showing also evidences of delamination (Lavoie *et al.*, 2000).

1.4.2.4 Through-the-Thickness Tension and Compression

Other significant issues for thick laminated composites are the effects of out-of-plane normal stresses and through-the-thickness transverse shear stresses in the thickness. The differences between a thin and a thick laminate, from a stress point of view, are shown in Figure 1.13, through-the-thickness stresses can be neglected in thin laminates. These 3D stresses put thick laminates in a new category which are difficult to analyse using classical theories. Accurate finite element models (FEM) could be the way forward to avoid expensive costs related to extensive experimental analyses to predict the behaviour of thick laminated structures. However, through-the-thickness properties (stiffness and strength) are essential for reliable and robust design and also accurate analysis of thick structural components under three-dimensional states of stress (Daniel *et al.*, 2008).

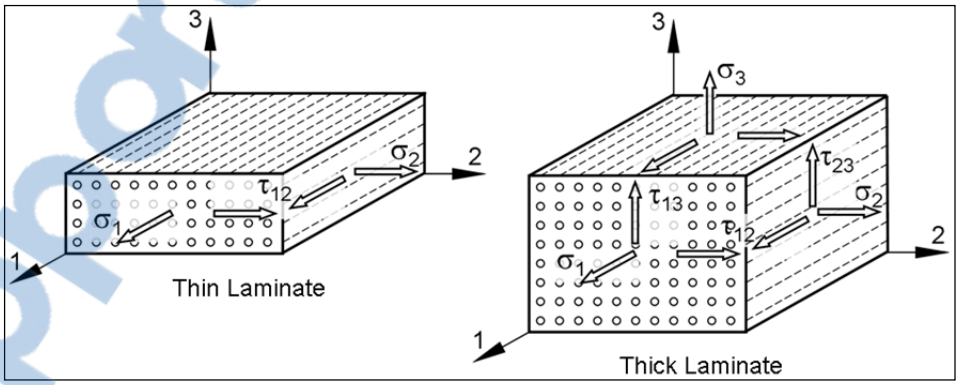

Figure 1.13 Stress representation for a thin and a thick laminate

Through-the-thickness properties of laminated composites are matrix dominated and are significantly lower than in-plane stiffness and strength along the fibre (Broughton *et al.*, 2001). However, as already mentioned, these tensile and compressive values could be

approximated by the stiffness and strength of in-plane transverse tests on unidirectional laminate (Daniel *et al.*, 2008; Schubel *et al.*, 2006).

Broughton *et al.* tested unidirectional carbon fibre reinforced epoxy composite with a fibre volume fraction of 60%. The tested specimens were square blocks with thicknesses ranging from 20 mm and 40 mm to obtain through-the-thickness tensile and compressive properties (Broughton *et al.*, 2001). They concluded that the tensile stiffness and strength are not affected for this range of thicknesses. In compression, the stiffness and strength did not vary with the thickness and the results were quite similar to those obtained on 6 mm thick specimens (Broughton *et al.*, 2001; Broughton and Sims, 1994).

Schubel *et al.* also characterized through-the-thickness composite laminates (Schubel *et al.*, 2006). They used wasted, straight-sided and V-notched specimens of woven-roving carbon fabric/epoxy with a cured thickness of about 23.8 mm (80 plies), to measure respectively the tensile, compressive and shear properties. Typical stress-strain curves were found for these three properties (Schubel *et al.*, 2006). They also performed through-the-thickness off-axis tensile and compression tests. Without any surprises, the stiffness and the strength in tension were higher at an off-axis angle of 45° and at an angle of 0° in compression.

Kim *et al.* studied the effect of the stacking sequence and the geometric shape of thick coupons, 10 mm, on through-the-thickness compression properties (Kim *et al.*, 2010). They concluded that cylindrical specimens should be used for UD lay-ups and hexahedral specimens, with in-plane dimensions (length and width) twice the thickness, should be used for fabric layers.

1.4.2.5 Interlaminar Shear (ILS)

The interlaminar shear (ILS) strength was measured using short beam tests on two different thicknesses, 10 and 20 mm. Zhou and Davies showed a linear ILS behaviour and, again, this

behaviour was very dependent on the span-to-depth ratio. They also concluded that the thickness effect on ILS strength was not significant (Zhou and Davies, 1995a).

Broughton *et al.* compared different test methods to measure the interlaminar shear, short beam, double notch and V-notched beam. They concluded that the V-notched beam test gives the most accurate results for in-plane and through-the-thickness shear moduli and strengths (Broughton *et al.*, 2001; Broughton and Sims, 1994), therefore the V-notched beam shear test will be used in the research.

1.4.2.6 Impact

Sutherland and Guedes Soares studied the effect of the thickness under low and high energy impact tests and compared the behaviour of epoxy and polyester resins (Sutherland and Guedes Soares, 2004). The laminated panels were manufactured by hand-lay of E-glass woven-roving with a fibre volume fraction of 35% as in marine industry. The studied thicknesses varied from 3.2 to 18.8 mm (5 to 30 plies) for the polyester resin and from 3.3 to 9.1 mm (5 to 15 plies) for the epoxy resin. They concluded that thinner coupons, for both resins, and thicker polyester coupons are significantly affected by deflection damages causing delamination by shear. At higher energy impact, only subtle differences were observed between damage modes of epoxy and polyester composites (Sutherland and Guedes Soares, 2004). However, under high energy impact, delamination by shear is still observed on thinner laminates whereas on thicker laminates, the delamination is caused more frequently by indentation (Sutherland and Guedes Soares, 2004).

Nilsson *et al.* analyzed the effect of two thicknesses, 4.16 and 8.32 mm, on the bending strength of composite laminates after impact (Nilsson *et al.*, 2009). Even for relatively thin laminates, they found that the damage area was much larger on thinner coupons. For thicker specimens, they observed an increase of about 20% of the bending strength compared to the compression strength.

1.4.3 Thickness Effect Summary

In the literature review, different research papers on “thick laminates”, so called by their authors, are presented and it was shown some disagreement arise on what can be called a thick laminate. Broughton and Sims wrote an overview on through-the-thickness effects and they concluded that laminates smaller than 6 mm in thickness are considered thin (Broughton and Sims, 1994). For thick laminates, the CMH-17 committee stated that “An example of representative thick-section composite properties … were obtained by a Hercules test program from an 80-ply (t=0.59 in., 15 mm) fiber-placed, autoclave-cured laminate.” (CMH-17, 2012). Therefore, at what thickness shall a laminate be considered thick?

On the manufacturing side, several authors fabricated laminates from 1 to 85 mm thick. The thicker one was specifically to study and control the exothermic reaction (Liu *et al.*, 2010) and this thickness can be considered without ambiguity as thick composite laminates. However, it is difficult and costly to manufacture thick laminates, with thickness greater than 20 mm (Broughton *et al.*, 2001; Broughton and Sims, 1994). Another method to manufacture thick laminated specimens is to stack several thin laminates one over the others and bond them together. That will not represent the real effect of the thickness during the polymerisation. In addition, particular care is required to ensure that the failure will occur in the laminate and not in the bonded joint. It is why, in this research on the thickness effect, the specimens will have a maximum thickness of 20 mm.

Shepheard *et al.* also concluded that the material quality has a greater influence on the decrease in mechanical properties than the thickness of the tested coupons itself (Shepheard *et al.*, 2004). For thick laminated composites, the process offering a better control of composite materials properties seems to be the autoclave process with thermoset and thermoplastic prepreg. This process brings a high fibre volume fraction (strong and stiff parts), fewer voids (when done by an expert in a controlled environment), low misalignment problem (when prepreg are automatically placed or at least laser assisted) and low residual stresses due to shrinkage (when the lay-up is perfectly balanced and symmetric, and a

cooling rate is apply correctly) (Mazumdar, 2002; White and Hahn, 1992). A high fibre volume fraction could be defined with a percentage between 55% (Gurvich and Byron Pipes, 1995) and 65% (Mazumdar, 2002). A low percentage of voids is considered to be below 2-3% (Schmitt, 1974), even less than 1% in typical autoclaved produced material (Shepheard *et al.*, 2004). It is certainly for these reasons that autoclave/prepreg processes are widely used in aerospace industry.

However, the autoclave manufacturing process will not be used in this research due to its higher cost and the specific technical skills required by the process. Oppositely, the hand lay-up manufacturing process is advocated in the fields of composite research since it may lead to greater variation in mechanical properties (Sutherland *et al.*, 1999b). Thus, the vacuum infusion process is chosen for the experiments of this research. This manufacturing process will permit the fabrication of thin to thick laminated specimens using similar parameters. Then, the mechanical properties will not be influenced by the use of two different manufacturing processes, because the mechanical properties are dependent of the manufacturing process, even if a visual inspection could show no difference in material quality (Sutherland *et al.*, 1999a). In addition, the vacuum infusion process is widely used in the manufacturing of wind turbine blades. Furthermore, other industry like aerospace tends to reduce to use of the autoclave in order to reduce their manufacturing cost and time.

From a testing point of view, whatever the experimental test to perform "… the objective is to produce a state of stress in the test specimen which is uniform and will repeatedly measure the true properties with accuracy." (Schube *et al.*, 2006). This condition was not met in many researches where the failure was observed near the grips due to stress concentration (Broughton *et al.*, 2001; Daniel *et al.*, 2008; Lavoie *et al.*, 2000; Sutherland *et al.*, 1999a; 1999b; 1999c). In addition, special care shall be taken to avoid local failure when global strength is studied (Lee and Soutis, 2005; 2007).

Another difficulty in composite material characterization is the inaccuracies in derived mechanical properties such as flexural stress and strain calculations (Sutherland *et al.*, 1999c). This difficulty was also experienced by Zhou and Davies (Zhou and Davies, 1995b) and also by Lavoie *et al.* since they were not using strain gauges in three-point bending (Lavoie *et al.*, 2000). Also, the lack of current standard to test thick laminated specimens is another difficulty (Shepheard *et al.*, 2004). In this research, test methods will be developed based on actual standards.

It was also shown that a tendency of the strength to decrease with increasing the thickness but the failure mechanism was not significantly affected by the material thickness (Gurvich and Byron Pipes, 1995). However, authors are even contradictory in terms of thickness effect (Lee and Soutis, 2005; Sutherland *et al.*, 1999a). Due to these contradictions in the literature, it is clear that an agreement between experimental and theoretical results shall be considered. Nonetheless, it is not valuable to fit the theoretical model to experimental data using the appropriate parameters (Sutherland *et al.*, 1999a), since that would mean that this theoretical model is only good for observing the behaviour of one specific material, manufactured using a specific process and for one specific load case.

Sutherland *et al.* concluded that to perform a complete study on the scale effect of composite: "an efficient experimental programme and statistical analysis techniques in order to separately estimate the effects of each variable, and also to distinguish these effects from the random variation in the experimental data" are required (Sutherland *et al.*, 1999a; 1999b). Zhou and Davies concluded that two to five specimens is not a sufficient number of tests for being conclusive (Zhou and Davies, 1995b). In addition, according to Sutherland *et al.*, four to eight specimens is not enough to significantly identify strength variability in carbon composites (Sutherland *et al.*, 1999a). According to Broughton *et al.*, at least five specimens shall be tested for each test (Broughton *et al.*, 2001). Therefore, in this research, eight specimens will be tested per configuration.

1.5 Originality

Composite materials are relatively new and a broad design base, such as that available for many metals, has not been yet compiled (Sutherland *et al.*, 1999b). That confirms the relevance of this research. In addition, the question "Is there a size effect in composites" was asked by Sutherland *et al.* and still currently studied since no conclusive evidence has yet arisen (Sutherland *et al.*, 1999a). It was also reiterated in the launch of the second edition of the "World Wide Failure Exercise" (WWFE), the effects of thickness on composite laminated structures remain unresolved (Kaddour and Hinton, 2005; Soden *et al.*, 2004). As an industrial experience and Perez's work, the need of the aerospace industry led to development of composite materials and researchers are still trying to understand the behaviour of thick laminated composite (Perez *et al.*, 2005).

Knowing that the behaviour is clearly different for thin and thick composite laminated structures, it is important to categorize composite laminated structures by thicknesses. Moreover, since this research evaluates all the facets of a material study: manufacturing, testing and analysis, it is hoped that the lessons learned and the different observations will help the industry to advance in the developing and the proposing of innovative methods to analyse thick laminated structures.

CHAPTER 2

WHEN A COMPOSITE BEAM GET THICK? - COMPARISON OF LAMINATION THEORIES AND FE MODELS ON THREE-POINT BENDING DEFLECTIONS

As stated previously, some disagreement exists in the literature on what can be called a thick laminate. This chapter aims to answer from which thickness a laminate shall be considered thick. To achieve that objective, the deflections of composite laminated beams under three-point bending loads are calculated and compared using four different methods, lamination theories and finite element (FE) models. The studied composite beams are laminated using unidirectional carbon/epoxy pre-impregnated plies (prepreg) in cross-ply and quasi-isotropic lay-ups for thicknesses varying from 1 to 20 mm. The lamination theories have been presented in the literature review and they are the classical lamination theory (CLT), also called the classical laminated plate theory (CLPT) (Daniel and Ishai, 1994; Reddy, 1997), the first-order shear deformation theory (FSDT), also known as the Timoshenko first-order beam theory (TFBT) (Reddy, 1997; Zenkour, 1999) and a higher-order beam theory developed by Zenkour, called the refined higher-order beam theory (RHBT) (Zenkour, 1999). In TFBT, a shear correction factor (K) is needed and the results from two different ways of calculating the k-factor are also compared, a k-factor from isotropic materials, 5/6, and a k-factor dependent of the lay-up, computed using the method developed by (Madabhusi-Raman and Davalos, 1996). The commercial code ANSYS® is used to build, solve and post-process all FEM used in this comparison.

2.1 Comparison Statement

To study the effect of thickness on composite laminated structures, the comparison of the deflection on a three-point bending composite beam has been chosen. For this type of problem, it is possible to compute the deflection using different lamination theories. Furthermore, in future works, it will also be possible to adapt this three-point bending

problem to an experimental comparison, because it is easier to apply a direct linear load than a distributed load and easier to measure a linear deflection than interlaminar shear (ILS) stresses or other through-the-thickness properties (Lavoie *et al.*, 2000; Sutherland *et al.*, 1999c; Zhou and Davies, 1995b). So, the composite beam is simply supported, it is loaded using a linear force (F_0 in N/mm) applied at the mid-span and the deflection will be computed. The span length (L) is 100 mm and the width of the beam (W) is 20 mm; both are constant values. The beam thickness varies according to the number of layers in the laminate. The composite laminated beam parameters are illustrated in Figure 2.1.

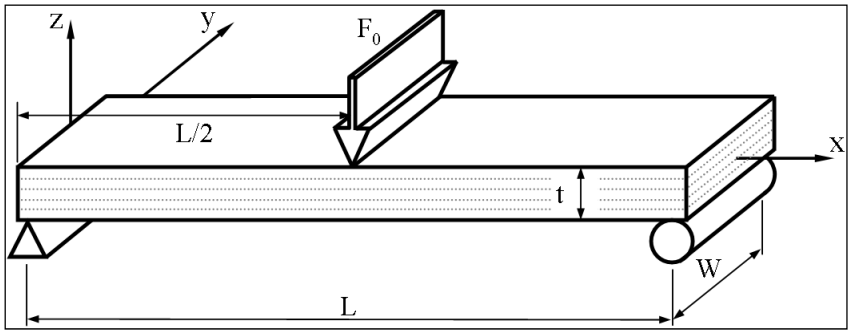

Figure 2.1 Scheme of a composite laminated beam in three-point bending

Two different types of lay-ups are studied in this comparison, a cross-ply symmetric ($[0/90]_{nS}$) and a quasi-isotropic symmetric laminate ($[-45/0/45/90]_{nS}$), both at a sub-laminate level scaling. The numerical values indicate at which angle the unidirectional (UD) ply is aligned in reference to the longitudinal axis, X. S denotes the symmetry of the full laminate and n denotes the number of repetitions of the sub-laminate. The total thickness (t) of a laminated beam is equal to the number of repetitions (n) times the average thickness of one cured ply (t_p). Cross-ply and quasi-isotropic lay-ups are widely used to evaluate the behaviour of composite laminated structures (Lee and Soutis, 2005; Reddy, 1997; Yildiz and Sarikanat, 2001; Zenkour, 1999). In addition, for the RHBT of Zenkour, results can only be computed for cross-ply laminates since the system of differential equations is solely solvable with a Navier-like approach (Zenkour, 1999).

The material used for the laminated beam in this comparison is UD carbon/epoxy prepreg composite, T300/BRT934 since material data are available. The material properties, of one ply of this UD carbon/epoxy prepreg, are defined in Table 2.1. Data are extracted from the course notes (Lessard, 2004) and an article on lamina properties from the "World Wide Failure Exercise" (WWFE) (Soden *et al.*, 1998). As given in Table 2.1, the ply thickness (t_p) is 0.125 mm. Therefore, for the cross-ply lay-up, n will be equal to 1, 2, 4, 8, 10, 16, 20, 26, 30, 36 and 40, for a beam thickness (t) varying from 0.5 to 20 mm. For the quasi-isotropic lay-up, n will be equal to 1, 2, 4, 5, 8, 10, 13, 15, 18 and 20, for the identical value in mm for the total beam thickness (t).

Table 2.1 Material properties of a carbon/epoxy composite, T300/BRT934

Description of the property coefficient, *symbol* (units)	**Value**
Longitudinal Young's modulus, E_1 (GPa)	148
Transverse Young's modulus, E_2 (GPa)	9.65
Through-the-thickness Young's modulus, E_3 (GPa)	9.65[a]
In-plane shear modulus, G_{12} (GPa)	4.55
Transverse – Through-the-thickness shear modulus, G_{23} (GPa)	3.45[b]
Longitudinal – Through-the-thickness shear modulus, G_{13} (GPa)	4.55[c]
Major Poisson's ratio, ν_{12}	0.3
Transverse – Through-the-thickness Poisson's ration, ν_{23}	0.4[d]
Longitudinal – Through-the-thickness Poisson's ration, ν_{13}	0.3[e]
Average cured ply thickness, t_p (mm)	0.125

[a] Assumed to be equal to the transverse Young's modulus.
[b] Computed using Equation 3.7.
[c] Assumed to be equal to the in-plane shear modulus.
[d] Assumed to be equal to the BSL914C epoxy (Bogetti *et al.*, 2004a).
[e] Assumed to be equal to the major Poisson's ratio.

The applied load also varies with the thickness of the beam in order to keep the deflection values in the same range for a better comparison between the studied methods. The load value is computed using CLT. In addition, with various loads, beams are still in an elastic and small strain domain. Therefore, the applied load increases by a cubic factor as the flexural rigidity times the moment of inertia (EI). In comparison studies, dimensionless values are often used. For three-point bending problems, the ASTM proposes a span-to-depth

ratio ($\lambda = L/t$), also called the thickness ratio (ASTM, 2003). For this problem the span-to depth ratio varies from 5:1 to 100:1, and the smallest value represents the thicker beam.

2.2 Evaluation of Beam Deflection

In this section, the equations to compute the beam deflection are presented for each lamination methods, the classical lamination theory (CLT), the Timoshenko first-order beam theory (TFBT) and a refined higher-order beam theory (RHBT) of Zenkour.

2.2.1 Classical Lamination Theory (CLT)

After solving the laminate constitutive Equation 1.6 in Equation 1.1, the beam deflection using CLT is expressed as (Reddy, 1997):

$$\boxed{w(x) = -\frac{F_0 W L^3}{48 E_{xx}^b I_{yy}} \left[3\left(\frac{x}{L}\right) - 4\left(\frac{x}{L}\right)^3 \right]} \tag{2.1}$$

where, F_0 is the linear force, W denotes the beam width, L is the beam span, I_{yy} is the moment of inertia of the laminated beam and E_{xx}^b denotes the effective bending stiffness, as shown in Equation 2.2. The effective bending stiffness utilizes the first term in the flexural compliance matrix [d], which is the inverse of the bending stiffness matrix [D] in Equation 1.6 (Reddy, 1997).

$$E_{xx}^b = \frac{12}{t^3 d_{11}} \tag{2.2}$$

The CLT has been programmed in Matlab® and the script is available in Appendix I.

2.2.2 Timoshenko First-order Beam Theory (TFBT)

To compute the beam deflection using the Timoshenko first-order beam theory (TFBT), the displacement field of Equation 1.7 is solved using the same constitutive equation as with CLT, Equation 1.6 and the addition of Equation 1.10. Then the beam deflection is expressed as in Equation 2.3, where the second part of the equation takes into consideration shear deformations (Reddy, 1997).

$$w(x) = -\frac{F_0 W L^3}{48 E_{xx}^b I_{yy}}\left[3\left(\frac{x}{L}\right) - 4\left(\frac{x}{L}\right)^3\right] - \frac{F_0 L}{2K G_{xx}^b t}\left(\frac{x}{L}\right) \tag{2.3}$$

where all the terms are identical as in CLT, with the addition of K, the shear correction factor as explain in Section 1.3.1.2 and G_{xx}^b, the effective through-the-thickness shear stiffness. Two values of shear correction factor K are compared in this study, a constant value of 5/6 as in isotropic material and another dependent of the laminated beam configuration (Madabhusi-Raman and Davalos, 1996; Reddy, 1997). The effective through-the-thickness shear stiffness is determined using the last term in the inverse of the extensional shear stiffness matrix in Equation 1.10 (Reddy, 1997).

$$G_{xx}^b = \frac{1}{t\ a_{55}} \tag{2.4}$$

The TFBT has been programmed in Matlab® and the scripts are available in Appendix I for a constant shear correction factor and in Appendix II for a shear correction factor dependent on the configuration of the laminated beam.

2.2.3 Refined Higher-order Beam Theory (RHBT)

Using the Refined higher-order beam theory (RHBT) developed by Zenkour, several steps are to be done to get the deflection. First, the linear force F_0 is transformed in accordance of Q_m as defined in (Reddy, 1997) by:

$$Q_m = \frac{2F_0 W}{L} \sin(\mu_m \frac{L}{2}) \tag{2.5}$$

Second, the Equation 1.20 is used to solve the terms $W_m^{(0)}$, $W_m^{(1)}$ and $W_m^{(2)}$. Third, these terms are then summed according to Equation 1.19. Finally, the beam deflection is computed using the Equation 1.15 recalled here in Equation 2.6 (Zenkour, 1999).

$$\boxed{w(x,z) = w_0(x) + [z\, w_1(x) + z^2 w_2(x)]} \tag{2.6}$$

where, z is replaced by the total laminated beam thickness t. The RHBT has also been programmed in Matlab® using twelve terms in Navier-like approach summation and the script is available in Appendix III.

2.2.4 Beam Model Characteristic

For this study, the composite laminated beam is modelled using SOLID46 elements. The model of the beam in three-point bending is illustrated in Figure 2.2.

The beam is modelled with 40 elements lengthwise, 8 elements widthwise, and 10 elements through the thickness. Each element contains 8 layers in the thickness, which can be identified in the enlargement of Figure 2.2. However, short simulations confirmed that the finite element model (FEM) is more accurate when elements contain only one layer (Yildiz and Sarikanat, 2001). A challenge in modelling lies in respecting the aspect ratio, limited to 20:1 by ANSYS®, due to the ratio between the structure dimensions and the ply thickness.

The aspect ratio of an element is the relation between the length, the width and the thickness of the element (ANSYS, released 9). An element that does not respect this limitation is called a bad shape element (BSE). In general, a FEM, with no BSE, will produce more accurate results (Duchaine, 2004).

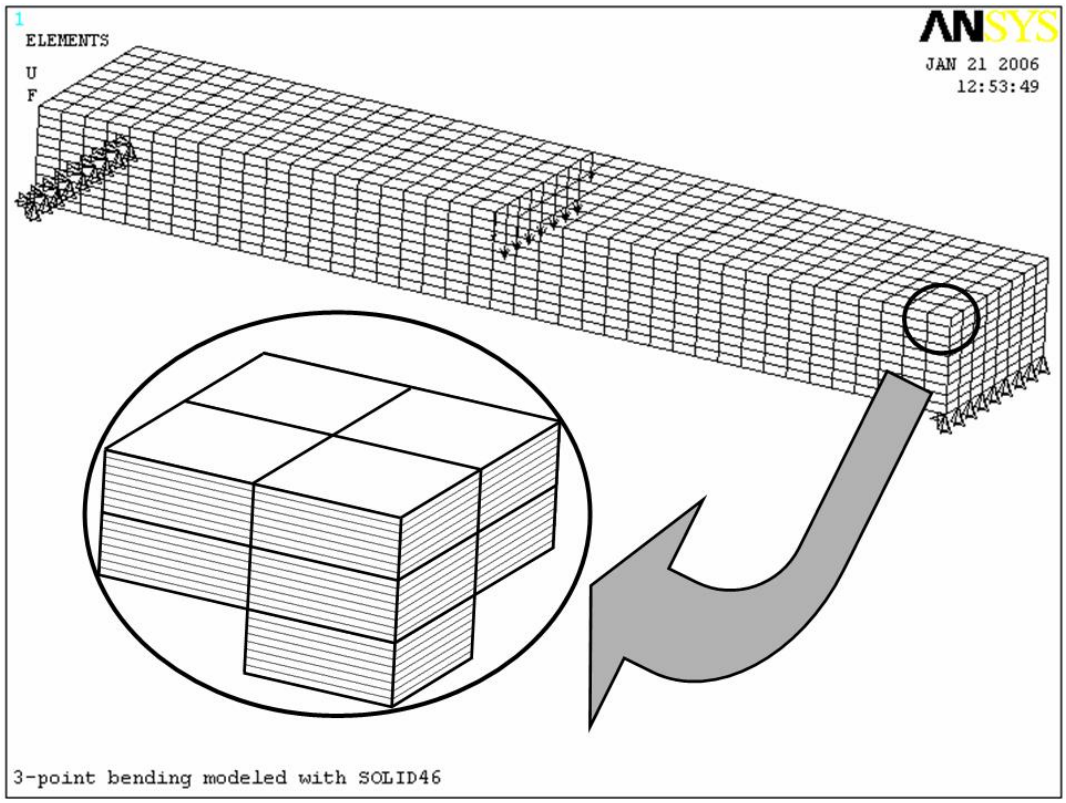

Figure 2.2 Model of a composite laminated beam in three-point bending

For the boundary conditions (BC), the beam is simply supported at both ends, then both rows of bottom nodes at both ends of the model are blocked in the load direction. To complete the equilibrium, bottom nodes on the left end are blocked in the direction of the beam length and two more nodes on the bottom are fixed in the beam width direction. The load is applied on the upper middle nodes of the beam. Note in Figure 2.2 that the load arrows on edges are only the half of the ones in the mid-area, allowing an even distribution of the load on each element. The total load is thus equally split along the width.

In order to compare with analytical methods, only the displacement of nodes on the mid-plane at half distance in the width is considered. Those nodes are at a sufficient distance of BCs and edges, to neglect the stress concentration effect on deflection values.

An example of ANSYS® scripts used in this study is provided in Appendix IV.

2.3 Comparison of Results

In this section, the numerical results for the deflection in three-point bending of a composite laminated beam with thicknesses varying from 1 to 20 mm, are presented and discussed. A total of ninety models are analyzed, considering ten different thicknesses for both laminated beam configurations. For the cross-ply lay-up ($[0/90]_{nS}$), five numerical models are used, one FEM, one for CLT, two for TFBT using the two different shear correction factor and one for RHBT. For the quasi-isotropic lay-up ($[-45/0/45/90]_{nS}$), only four numerical models are used since the RHBT results can only be presented for cross-ply lay-up as a result of the fact that it is not possible to solve the system of differential equations for other arrangements using a Navier-like approach as explained in the theories section,.

For each laminated beam configuration, three kinds of results are illustrated. Firstly, maximum deflection values, *w(L/2)*, at mid-span, are presented as a function of the span-to-depth ratio, λ (L/t), to show the dimensionless behaviour. Secondly, mid-span deflection values, *w(L/2)*, are presented as a function of the total laminated beam thickness, *t*. Finally, all results obtained using the lamination theories are compared to the results of the finite element analysis.

2.3.1 Deflection vs Span-to-Depth Ratio

Here, analytical and numerical deflections are presented and compared as a function of the span-to-depth ratio (λ). In Figure 2.3 and Figure 2.4, mid-span deflections (*w(L/2)*) are

presented as a function of λ for cross-ply and quasi-isotropic lay-ups, respectively. Although results are only given for λ up to 50:1, a significant difference can clearly be identified between CLT and other lamination theories for both lay-ups. In addition, as a reminder, it is observed that the deflection for CLT is always about 1 mm, 1% of the span length, due to the load (F_0) varies with the thickness.

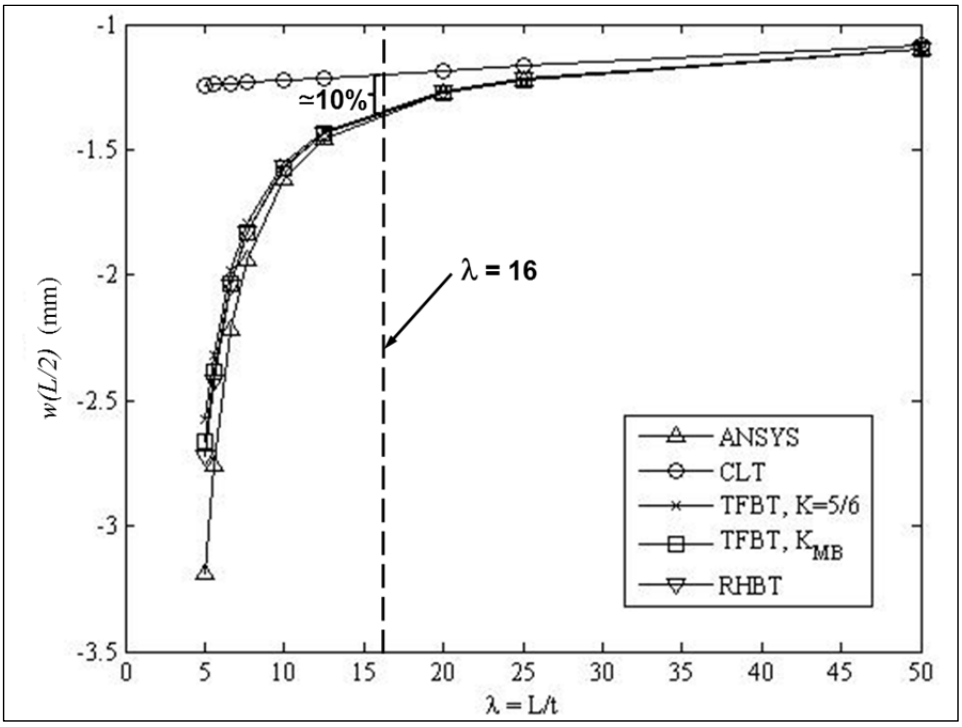

Figure 2.3 Mid-span deflections as a function of λ for cross-ply lay-ups

Since, CLT ignores shear effects in its assumptions and gives comparable results, within about 10%, for span-to-depth ratios above 16:1. These results confirm the assumption of ASTM norms, which state that for a span-to-depth ratio larger than 16:1 shear effects are negligible (ASTM, 2003; Broughton and Sims, 1994). On the other hand, deflection curves obtained with advanced beam theories and FEM look similar for both lay-ups. It is rather difficult to compare them adequately. For a better comparison of these methods, deflections have to be expressed as a function of the thickness.

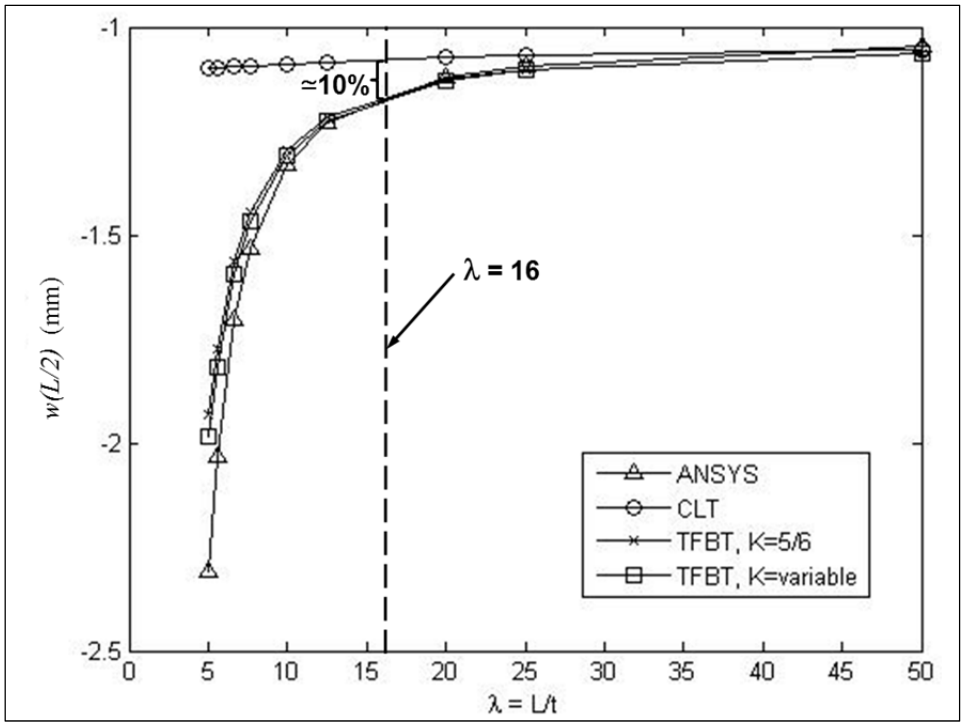

Figure 2.4 Mid-span deflections as a function of λ for quasi-isotropic lay-ups

2.3.2 Deflection vs Thickness

Analytical and numerical deflections are plotted and compared, as a function of the thickness of the beam. Figure 2.5 and Figure 2.6 illustrate the mid-span deflections for both studied lay-ups. The difference between CLT and other methods is still evident for span-to-depth ratios below 16:1, which corresponds to thicknesses over 6.25 mm. At these thicknesses, the deflection given using CLT is at least 10% less than the deflection obtained using other lamination theories and FEM. In addition, greater differences are observable between advanced beam theories and FEM.

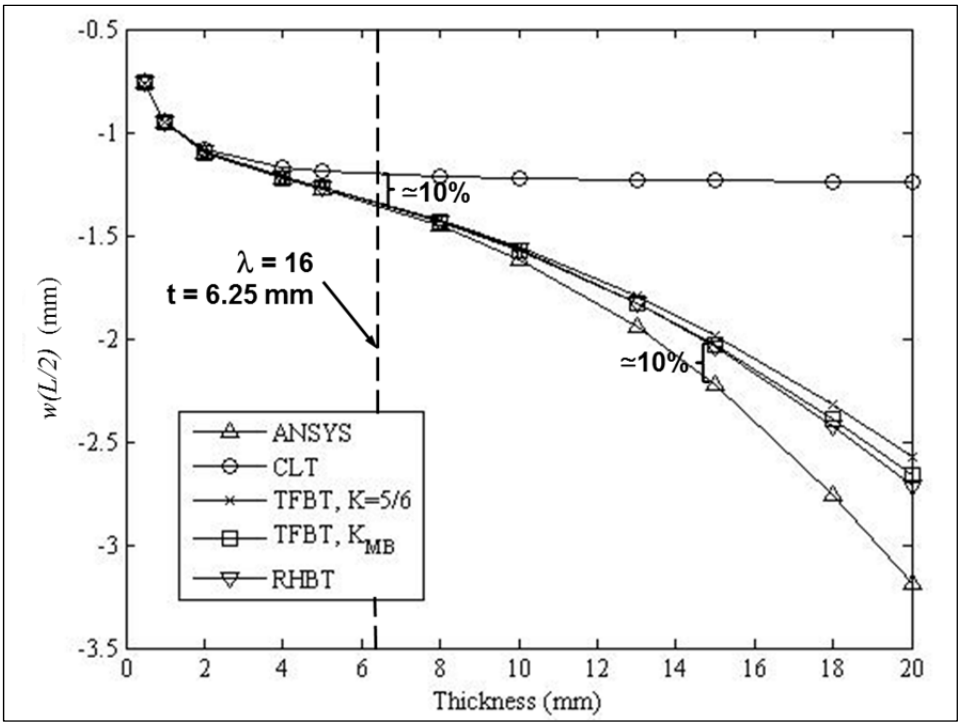

Figure 2.5 Mid-span deflections as a function of the thickness for cross-ply lay-ups

The results of advanced beam theories are not significantly different from each other. The TFBT, with the two alternatives used to compute the shear correction factor and the RHBT, are very similar, in term of deflection, for all thicknesses. Calculating a shear correction factor as a function of the laminated beam specifications, or using a higher order theory does not improve the deflection results significantly as confirmed by (Zenkour, 1999). Differences of only 3% for quasi-isotropic lay-ups and 5.5% for cross-ply lay-ups are observed on the deflection of the laminated beam computed using these analytical methods. To save time and effort, using a constant K-factor of 5/6 in TFBT gives satisfactory results for the mid-span deflection. In the case of a comparison on other measurements, such as stress/strain along the width or through-the-thickness of the beam, the other analytical methods seem to be more accurate as presented by (Zenkour, 1999). But, compared to numerical deflections computed with ANSYS®, a larger difference, above 10%, becomes apparent for thicker beams. So, another comparison on relative differences with ANSYS® results will probably give more information.

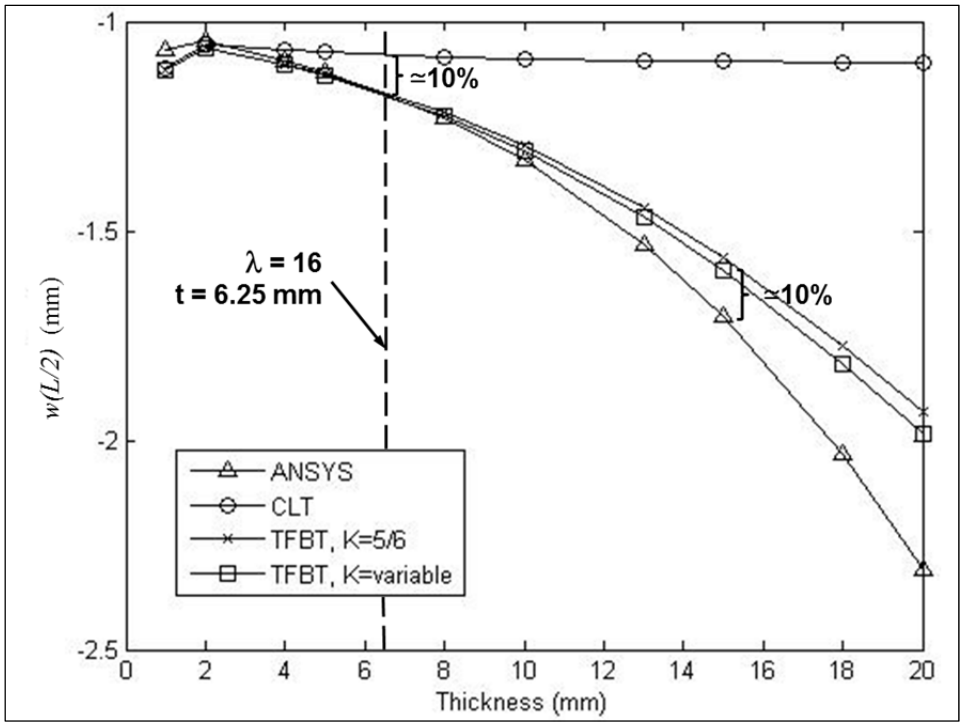

Figure 2.6 Midspan deflections as a function of the thickness for quasi-isotropic lay-ups

2.3.3 Relative Difference with ANSYS®

In this study, only ANSYS® deflections are computed a numerical method, whereas those for theories are obtained analytically. Taking ANSYS® computed deflections as reference, the relative differences between the numerical and analytical solutions are investigated. For cross-ply and quasi-isotropic lay-ups, percentage differences are shown in Figure 2.7 and Figure 2.8, respectively. It should be noted that ANSYS® results are only used as a reference without insinuation that they correspond to real life deflections.

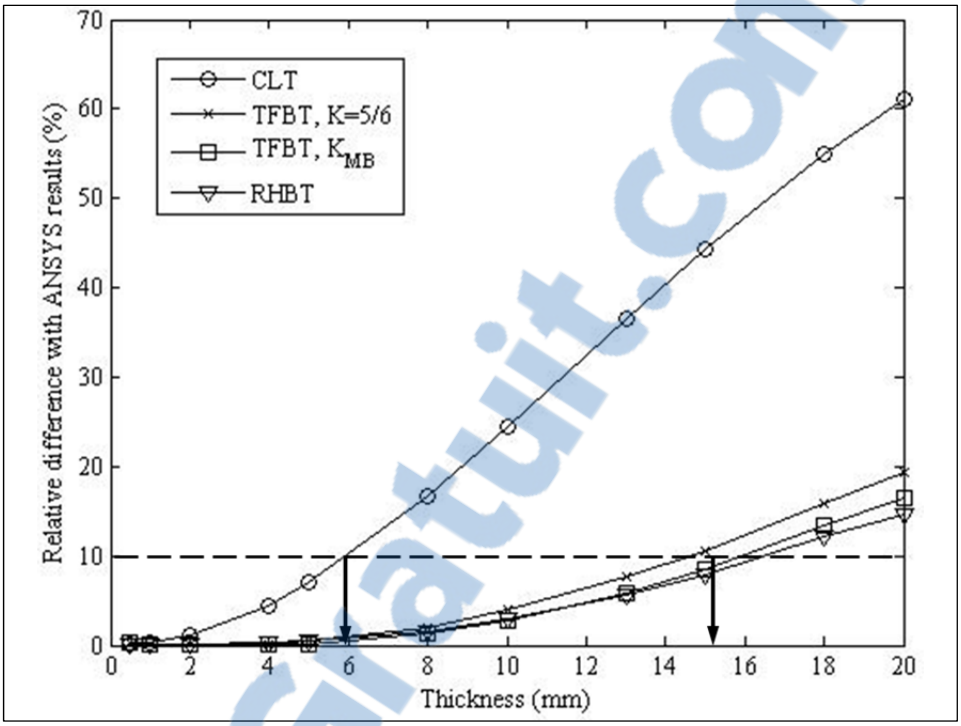

Figure 2.7 Relative difference with ANSYS® as a function of the thickness for cross-ply lay-ups

The relative difference between CLT and ANSYS® results of 10% is considered a reasonable threshold and 10% is widely used to confirm correlation with experimental results. Both studied lay-up configurations of laminated beams showed agreement with ASTM standard for a 6 mm thick laminated beam, a span-to-depth ratio of about 16:1 (ASTM, 2003; Broughton and Sims, 1994). Following this logic, this would mean that a large difference exists between advanced beam theories and ANSYS® results for thicknesses over 16 mm, in both cases analysed here. This threshold is slightly thicker than the 15 mm stated by (CMH-17, 2012). Therefore, three-point bending experiments should be performed for a better understanding of the larger differences between analytical and numerical deflections appearing for thicknesses larger than 16 mm. No information is available in literature about span-to-depth ratio below 16:1 and thicker beams than 16 mm thick.

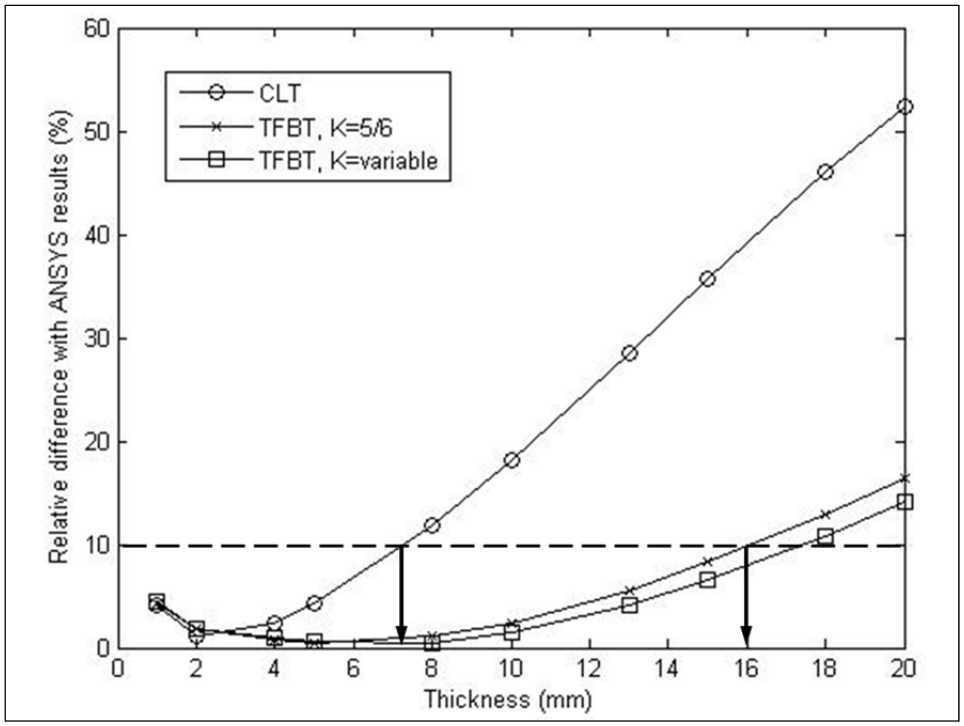

Figure 2.8 Relative difference with ANSYS® as a function of the thickness for quasi-isotropic lay-ups

2.4 Comparison Summary

To summarize, it was shown in this section of the research that it is possible to identify the thickness effect on the deflection of composite laminated beams in three-point bending by comparing three different theories: CLT, TFBT and RHBT; and FEM built in ANSYS®. Significant differences have been observed between studied methods used to calculate the deflection.

As expected, CLT is only applicable for thin laminated beams. A transition thickness has been identified at 6 mm for a span length of 100 mm, as Broughton and Sims concluded as well as the ASTM since this thickness corresponds to a span-to-depth ratio of 16:1 (ASTM, 2003; Broughton and Sims, 1994). In terms of the deflections, close similarities (5% difference) have been observed between advanced beam theories. However, using a constant shear correction factor of 5/6 (in this case) in TFBT gives satisfactory deflections with less

effort and in a shorter computation time. FEM results agreed also well with TFBT and RHBT, but in this studied problem, when the thickness of the beam exceeds 16 mm, advanced beam theories give results significantly different from ANSYS®, more than 10% difference. This thickness is slightly thicker than the 15 mm stated in (CMH-17, 2012). In addition, all lamination theories seem to underestimate deflections compared to FEM. These results show that a simple beam problem is relevant to conclude that a difference in behaviour exists between thin and thick laminates. Then it is determined that three categories of thickness have to be considered: thin laminates (less than 6 mm), moderately thick laminates (between 6 and 16 mm) and thick laminates (more than 16 mm). These conclusions have been presented at the Eighth International Conference on Computational Structures Technology (Duchaine *et al.*, 2006).

The three categories of thickness will be used in the following sections to evaluate the influence of the thickness on unidirectional, cross-ply and quasi-isotropic laminates tensile mechanical properties. In future research, three-point bending tests should be performed on various laminates to validate the influence of the thickness and to correlate with lamination theory and FEM results. These tests should carry out the understanding of the divergence between advanced beam theories themselves and with FEM results for beams thicker than 16 mm. Furthermore, since it is difficult to identify the proper theory to predict the deflection, it will be difficult to predict the behaviour of other properties derived from displacements. Other research could be conducted to evaluate the influence of the thickness on other characteristics, such as the stress on edges, the interlaminar shear stress, the residual stress after impart, etc.

CHAPTER 3

THICKNESS EFFECT ON 3D MATERIAL PROPERTIES

The main objective of this chapter is to study the influence of the thickness on the three-dimensional (3D) mechanical elastic properties (E_1, E_2, E_3, ν_{12}, ν_{13}, ν_{23}, G_{12}, G_{13} and G_{23}) of unidirectional (UD) laminates. The chosen material is a UD E-glass/epoxy laminated composite manufactured using a vacuum infusion process. In order to achieve this objective, a total of eighty-eight specimens of three different thicknesses are tested in tension and shear using mechanical tests based on the American Society for Testing and Materials' methods (ASTM, 2005; 2006). In addition, tensile and shear strengths and strain, at failure, are measured, when possible, and discussed. A detailed description of experimental procedures, specimens manufacturing and testing, is given. Test results are presented and commented, and some suggestions for future works are also proposed.

3.1 Design of Experiments

The material used in this experimentation is an E-glass/epoxy composite. The UD dried glass fibres constituting the laminates are UT-E300-500 provided by Gurit and the epoxy resin holding the fibres together is EPR/EPH 04908 from Hexion. Glass fibres have been chosen opposed to carbon fibres principally due to a lower cost. The properties of both individual constituents are provided by the suppliers and they are listed in Table 3.1. In order to observe the influence of the thickness on mechanical properties, different thicknesses are evaluated. In fact, three different thicknesses are studied in agreement with the three categories found in Chapter 2. The number of plies in each laminate is based on a factor of 8 plies due to future comparisons with symmetric cross-ply and quasi-isotropic lay-ups. In addition, the thickness of each laminate is computed using an average thickness of a single cured ply of 0.185 mm multiplied by the number of layers of its respective lay-up. Then, as a thin laminate, below 6 mm thick, 8 plies of UD dried glass fibres are stacked to form laminate of 1.48 mm thick,

hereafter named 1.5 mm. As a moderately thick laminate, between 6 and 16 mm thick, 56 plies of glass fibres are stacked to form a laminate of about 10 mm thick (10.36 mm). As a thick laminate, 112 plies are stacked to form a laminate of about 20 mm thick (20.72 mm).

Table 3.1 Properties of glass fibres and epoxy matrix

	ρ (g/cm^3)	E (GPa)	ν	k (GPa)	G (GPa)	K (GPa)
Fibres (*f*)	2.63	73	0.22	29.9	43.5	53.4
Matrix (*m*)	1.15	2.9	0.30	1.12	2.42	2.79

An extensive experimental testing programme is necessary to obtain the full set of 3D elastic of unidirectional (UD) E-glass/epoxy laminates for various thicknesses. Table 3.2 presents the design of experiments to characterize this unidirectional material. To measure the longitudinal Young's modulus (E_1), the in-plane Poisson's ratio (ν_{12}) and the longitudinal – through-the-thickness Poisson's ratio (ν_{13}), eight specimens per thickness are tested in tension along the fibres, for a total of twenty-four specimens. Also with this test, the longitudinal ultimate strength and strain in tension, respectively F_{tu1} and ε_{tu1}, are measured when possible. To measure the transvers Young's modulus (E_2) and, the transverse – through-the-thickness Poisson's ratio (ν_{23}), eight specimens per thickness are tested in tension transversely to the fibres, for a total of twenty-four specimens. As a reasonable assumption, the through-the-thickness Young's modulus (E_3) is considered equal to E_2. Also with this test, the transverse ultimate strength and strain in tension, respectively F_{tu2} and ε_{tu2}, are measured when possible. To measure the in-plane shear modulus (G_{12}), eight specimens per thickness are tested, for a total of twenty-four specimens. To measure the longitudinal – through-the-thickness shear modulus (G_{13}), eight specimens are tested. To measure the transverse – through-the-thickness shear modulus (G_{23}), eight specimens are tested. Note that for the last two through-the-thickness shear moduli, the thickness effect cannot be measured due to geometric restrictions, i.e. a standard specimen cannot be cut in the thickness direction because the required standard width is greater than the thickness of thin and moderately thick specimens.

Table 3.2 Design of experiments for UD laminates

Test \ Thickness		8 plies (1.5 mm)	56 plies (10 mm)	112 plies (20 mm)
Tension	Axial (E_1, ν_{12} and ν_{13})	8	8	8
	Transverse (E_2, E_3 and ν_{23})	8	8	8
Shear	G_{12}	8	8	8
	G_{13}	N/A	N/A	8
	G_{23}	N/A	N/A	8
Number of specimens		**24**	**24**	**40**

3.2 Specimens Manufacturing

This section includes a description of all steps of the vacuum infusion manufacturing process. Those steps are the mould preparation, the cutting of the fibres, the bagging setup for thin and thick laminates, the matrix preparation, the injection and the curing.

3.2.1 Mould Plate Preparation

The first step is to prepare the mould plate. The best material for a mould plate is aluminium. The geometry of the mould plate is a function of laminate dimensions. The plate needs to be 10 cm longer and wider than the laminate to provide enough space for the injection setup. It is 15 cm longer for a thick laminate due to the vacuum chamber under the laminate. The thickness of the plate will influence the flatness tolerances; a plate of 10 to 15 mm thick should respect those tolerances.

The mould plate is cleaned with a ScotchBrite and acetone. Any remaining dirt is removed with water and ethanol. Pieces of transparent adhesive tape are applied on all edges where the sealant tape will, in a later stage, be applied. The transparent tape prevents release agent from being applied where the sealant tape needs to stick to the mould. In addition, in manufacturing a thick laminate, transparent tape's bands are applied where the vacuum room under the laminate will be positioned. For the same reason, sealant tape needs to stick to the mould to seal the vacuum room under the laminate with the VAP material. Vacuum room dimensions are in order to fit the laminate inside sealant tape's limits plus a 5-10 cm in the injection direction for the vacuum tube installation (see Figure 3.1a).

Products from WaterWorks are used to prepare the mould plate adequately. FRESH START is recommended to thoroughly clean the mould surface. It is applied directly to the surface from a handy squeeze pouch and worked in with a piece of ScotchBrite; after the plate is well rinsed with water and wipe off. To condition the mould prior to the application of a release coating, the PREFLIGTH is applied with a piece of cloth. It is repeated for four coats separated by a cure of 15 minutes and the last cure is done in an oven at 83°C for 15 minutes or at room temperature for at least 30 minutes. Then a non-hazardous release agent, DEPARTURE, is lightly sprayed on the plate. After 2 minutes, the plate is wiped and 15 minutes later another coating is applied and wiped after 2 minutes, and then left for at least 30 minutes. After that, the transparent tape is removed and replaced by the sealant tape from AeroVac, LTS9OB, (see Figure 3.1b). The backing paper of the sealant tape should be left on until the vacuum bag is positioned.

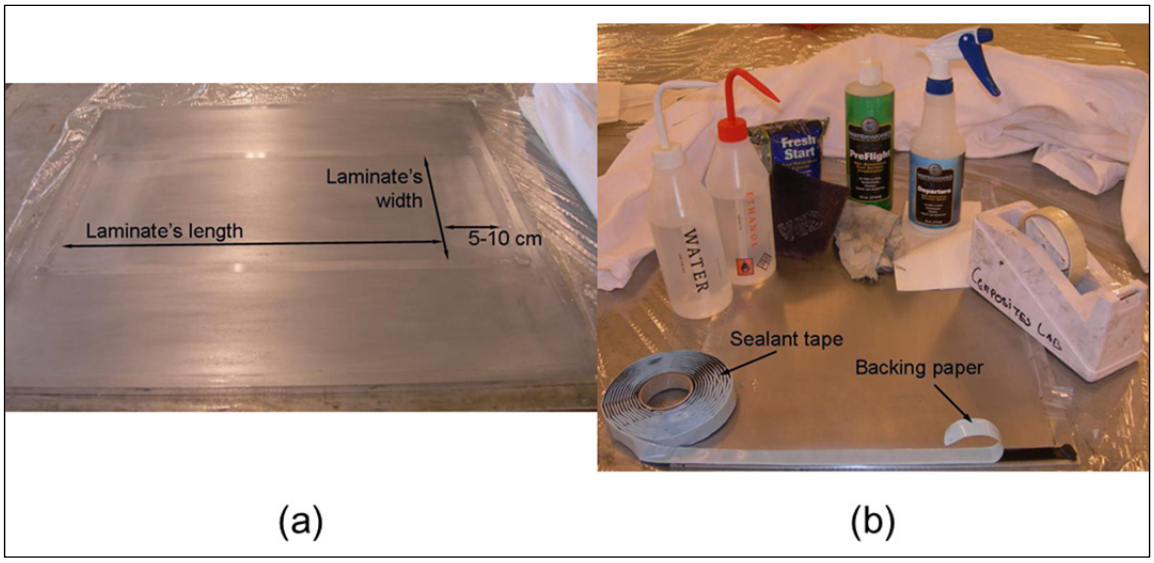

Figure 3.1 Mould preparation: (a) Transparent tape protection for a thick laminate and (b) WaterWorks products and sealant tape installation

3.2.2 Cutting the fibres

During each drying step of the WaterWorks release agent, the fibres may be cut. The fibres are cut with the desired dimensions, laminate's length (L_l) and width (W_l). All around the laminate, about 50 mm should not be used in specimen's geometry; and the cut width is around 3 mm. So, those dimensions have to be taken into account in the laminated plate design. The laminate's thickness (t_l) is determined by the number of plies (n), and the average thickness of one cured ply (t_p). In this study, 8, 56 and 112 plies correspond to laminate thicknesses of about 1.5, 10 and 20 mm respectively. On a cleaned cutting table, the material is unrolled and cut to correct dimensions with a roller cutter (see Figure 3.2). A metal ruler or a rigid template is used to get the desired fibres' shape. A particular attention should be given to the fibres, because they provide the strength and the stiffness of the laminate; a paper envelop can be used to protect them. Also during cutting, a special care should be given to an accurate fibres' alignment.

Figure 3.2 Cutting table and useful tools

3.2.3 Vacuum Bagging Setup

The bagging setup step consists of arranging, in a particular order, different layers of materials. There is the difference between thin and thick laminates, expect for the vacuum pump settings.

3.2.3.1 Thin laminate

A scheme of the bagging setup for a thin laminate is presented in Figure 3.3a. For a thin laminate, the fibres are directly lain down on the release agent coated mould plate (Figure 3.3b). They have to be placed carefully in the desired orientation and held in place using blue tape, Flash tape 2 from AeroVac. Metal ruler, rigid template or laser projection will be useful to obtain the correct fibres' orientation. A long piece of blue tape is also inserted in the laminate, preferably on the top layer, which will show the fibres' direction and

will be helpful in the cutting process later. Peel ply covers the lay-up with 1-3 cm extra around the lay-up (Figure 3.3c). All is maintained in place with blue tape. The white peel ply with red stripes, "stitch ply A" from AirTech, is used because it provides a regular impregnation of the fibres. This will avoid dry fibres in the laminate. A disadvantage of this peel ply is that it is difficult to peel off which can result in cracking and delamination when removed without enough precaution. On the peel ply a flow fabric, green mesh OM70 from DIATEX, is applied to help the resin distribution over the laminate's surface. The flow fabric needs to be shorter, about 3-5 cm as shown in Figure 3.3d, than the laminate and that will provide a good fibres' impregnation.

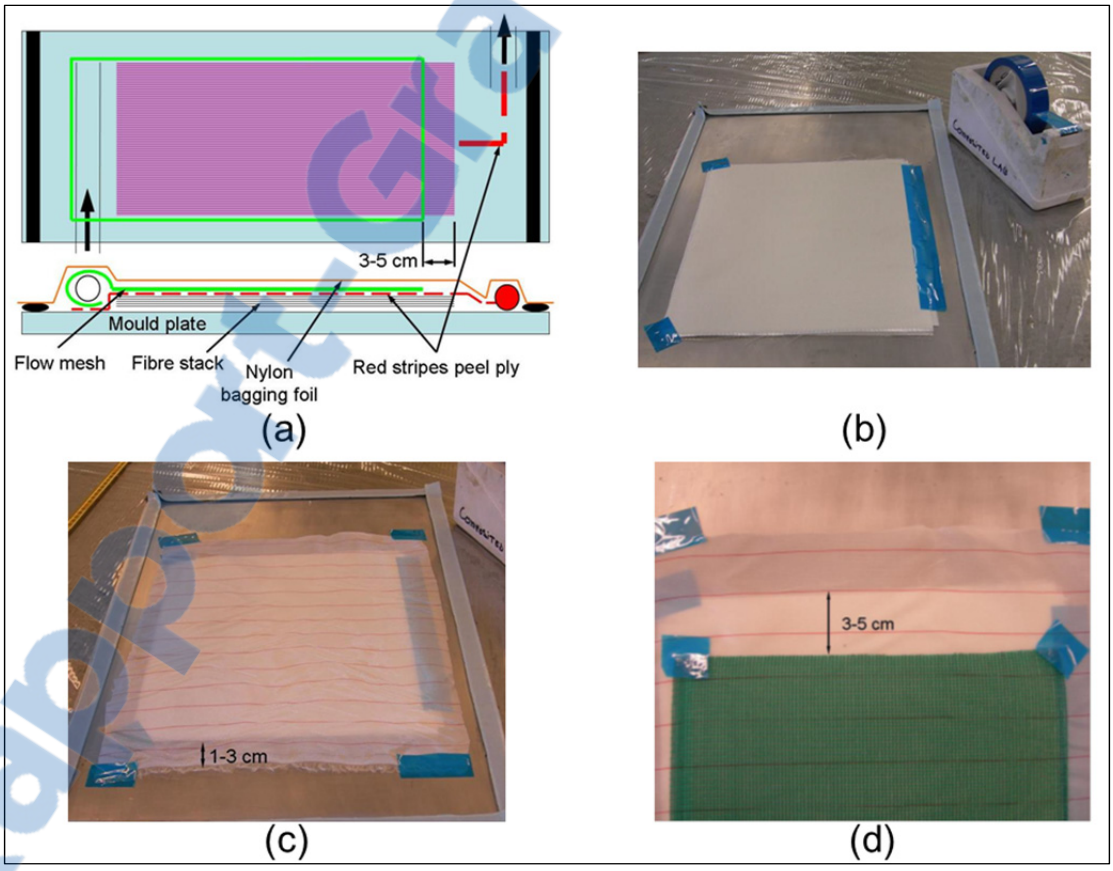

Figure 3.3 Manufacturing setup for thin laminates: (a) Thin laminate setup scheme, (b) Thin lay-up of fibres, (c) Peel ply material and (d) Flow mesh material

The inlet tube is a PVC tube connected to a spiral PVC tube. The spiral tube covers the PVC tube for 2-3 cm long and it is hold by a piece of blue tape (Figure 3.4a). A piece of tape is also applied on the free end (Figure 3.4b) of the spiral tube to stop the resin during injection. Then, it is seated on the green mesh. A piece of sealant tape is applied around the PVC tube to prevent leakage.

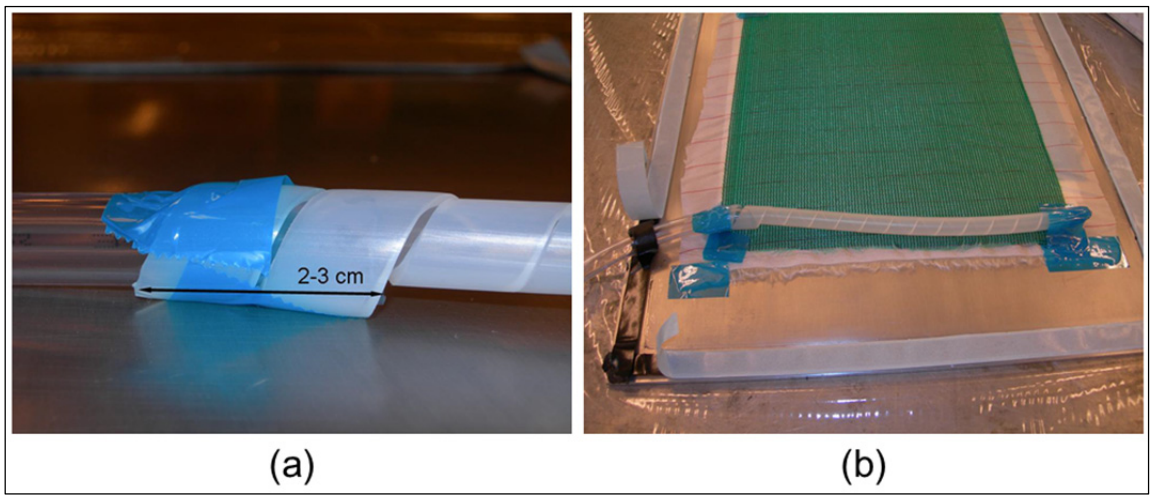

Figure 3.4 Inlet tube setup: (a) Connection with the spiral tube and (b) Installation

On the inlet tube, two clamps are installed as shown on Figure 3.5. These clamps will prevent air suction during vacuum test. It is why the tube is bent in two at the free end. The clamp close to the mould will be also used as a flow controller.

For the exhaust tube, also a PVC tube is used. A small twisted piece of "stitch ply A" under blue tape is used as a connection between laminate's middle-end and the outlet tube (see Figure 3.6a). A piece of cotton is placed over the tube, as shown in Figure 3.6b to prevent vacuum bag sucking or bag perforation. A piece of sealant tape is also used as in the case of the inlet tube.

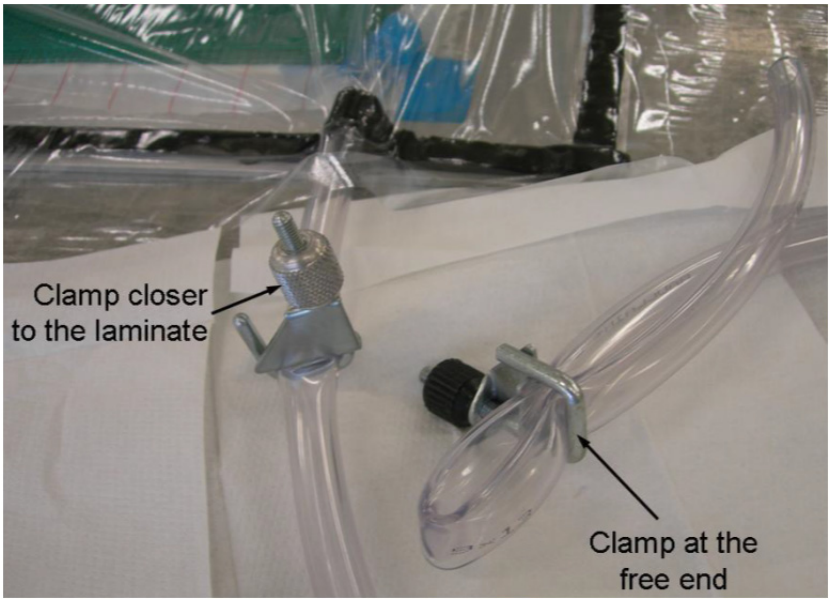

Figure 3.5 Installation of clamps on the inlet tube

Figure 3.6 Outlet tube setup: (a) Twisted peel ply and (b) Piece of cotton

The vacuum bag, a nylon foil, is stretched over the setup, free of ribs, as shown in Figure 3.7a, and attached at the sealant tape. Ribs (see Figure 3.7b) will not seal completely the mould and it will be impossible to get a full vacuum for injection.

Figure 3.7 Vacuum bag over a thin laminate setup: (a) Free of ribs and (b) With ribs

To test if the vacuum bag is sealed correctly, the pump system is installed. First a vacuum pot (Figure 3.8a) is needed to prevent resin or other particles being sucking in the pump. It includes a plastic pot inside and the connection tube (blue tube) should be free of resin. The outlet tube is plugged onto the vacuum pot which is linked to the pump, as in Figure 3.8b with a piece of sealant tape to prevent air sucking. The pump is switched on and the pressure is set progressively to the max vacuum (1-6 mbar). A low vacuum will be helpful at the beginning to adjust the bag around fibres and tubes. When the set pressure is reached, the black valve is closed (see Figure 3.9); if the pressure increases then the vacuum bag leaks. The leak needs to be repaired with sealant tape to continue the manufacturing process. A leak about 1 mbar in 10 seconds is acceptable.

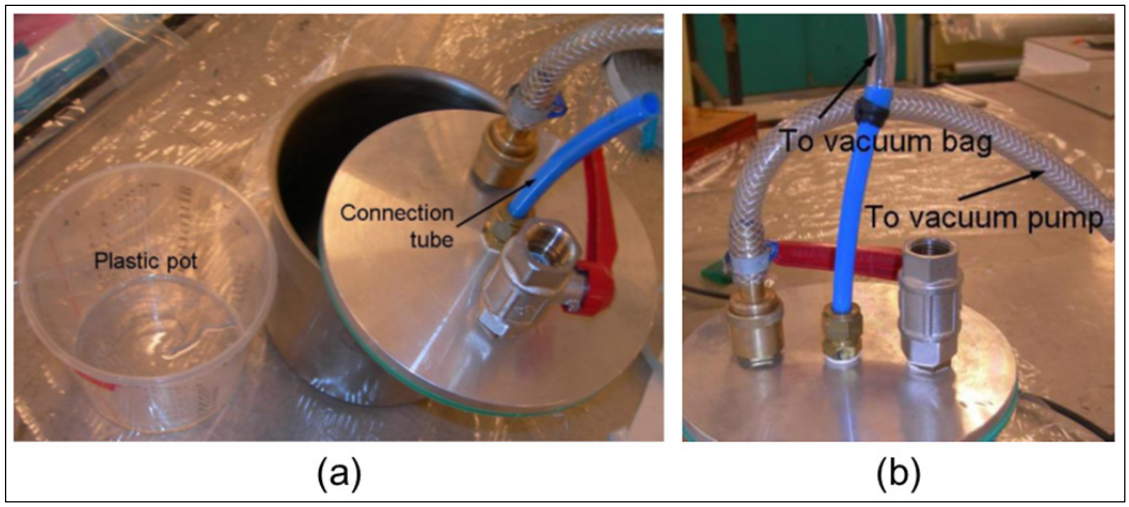

Figure 3.8 Vacuum pot setting: (a) Vacuum pot before connection and (b) Vacuum pot connected

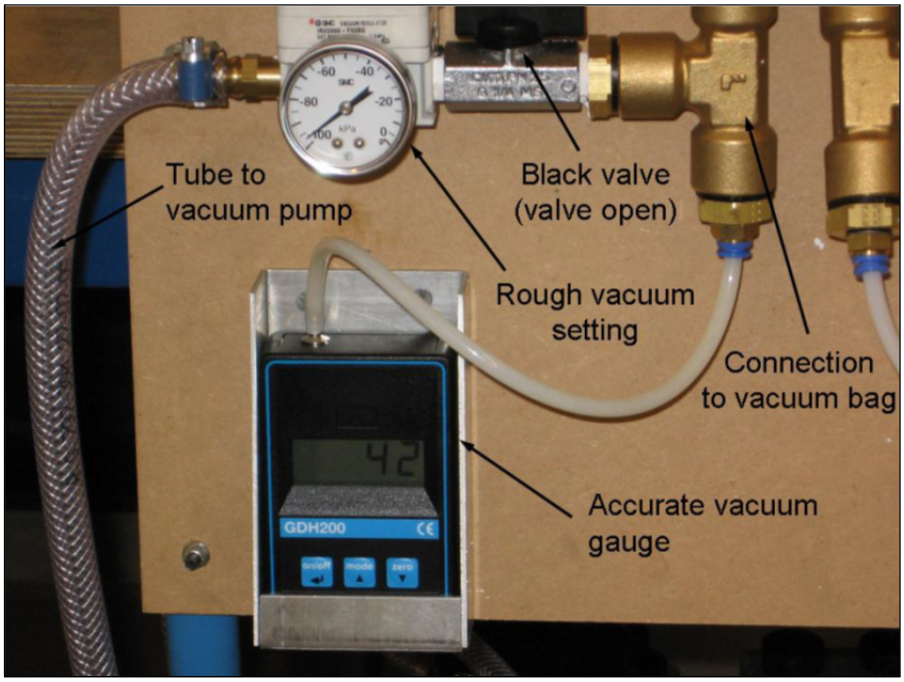

Figure 3.9 Pressure setup and identification of the black valve

3.2.3.2 Thick laminate

A sketch of the total setup for a thick laminated composite is shown in Figure 3.10a. For a thick laminate, the mould has to be prepared in a different way. As written previously in mould plate preparation's section, sealant tape is installed on the edge for the vacuum bag and also where the vacuum room under the laminate needs to be to seal the VAP. To prepare the vacuum room under the laminate, a piece of release foil "stitch ply A" is directly place on the release agent coated plate, the outlet PVC tube is installed, in the reserved space of 5-10 cm, with a piece of the flow fabric and a cotton piece covers the tube's end to do not perforate the breather material (see Figure 3.10b). Then the breather material from VAP seals this vacuum room, it is really important to avoid ribs because they will be imprinted on the laminate. A piece of the pink release foil, WL300P also from AirTech, covers the VAP material before fibres are laid down as in Figure 3.10c. The fibres are place carefully in the desired orientation and held in place by pieces of blue tape. Metal ruler rigid template or laser projection will be useful to be certain of the fibre orientation. Blue tape is also inserted on the top layer of the laminate to indicate the fibres' direction for the cutting process. Another piece of peel ply, "stitch ply A" this time, covers the entire layup. On the release foil a flow fabric, green mesh OM70 from DIATEX, is applied to help the resin distribution along the laminate. The flow fabric needs to cover entirely the laminate; a V-shape is made in the middle, as shown in Figure 3.10d, to provide a good air evacuation. The fibres' impregnation will occur through the thickness.

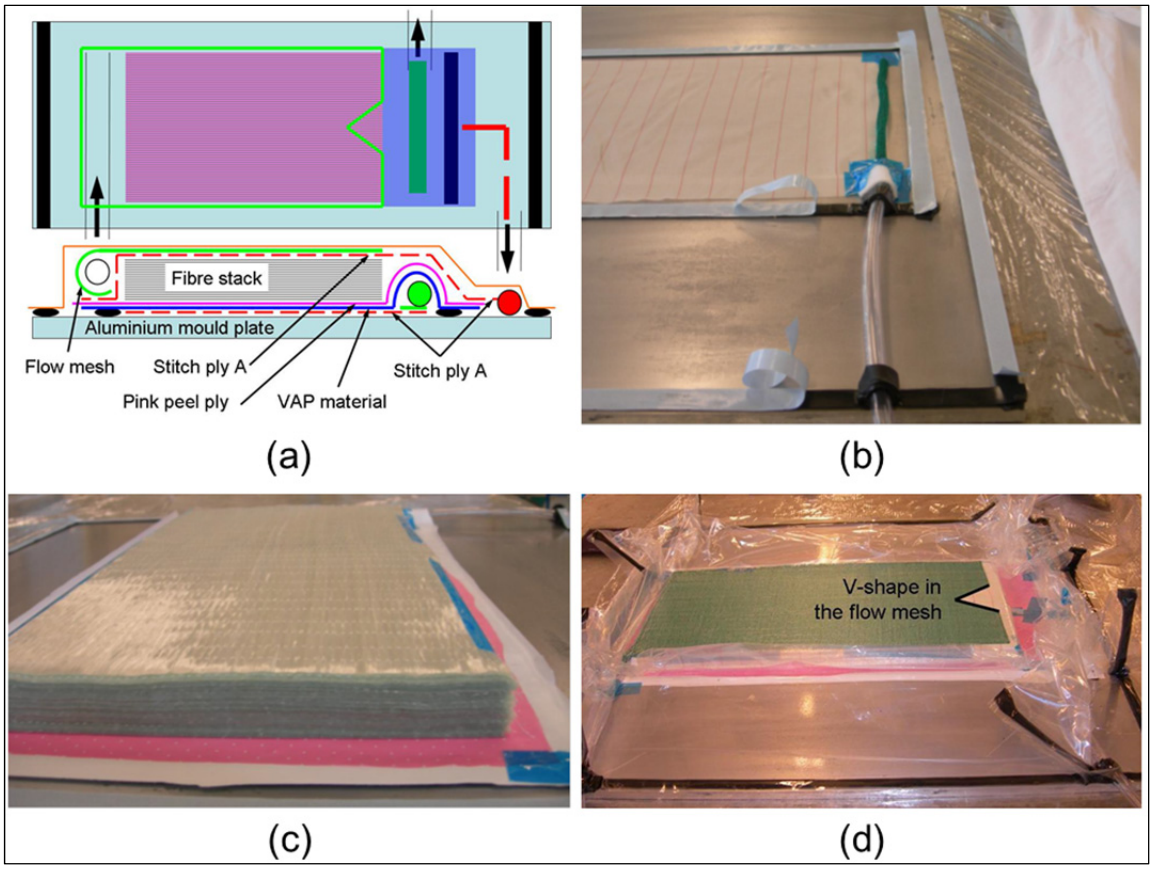

Figure 3.10 Manufacturing setup for thick laminate: (a) Thick laminate setup scheme, (b) Under VAP setup, (c) Thick lay-up of fibres and (d) Thick laminate setup illustration

The outlet tube is installed as explained in the thin laminate's section. Instead to only seat the spiral tube on the flow mesh, the tube is rolled in it and place at the inlet end of the laminate as in Figure 3.11. The nylon foil used for the vacuum bag is also installed differently, to wrap correctly the entire lay-up (see Figure 3.10d). To test if the vacuum bag is sealed correctly, two pump systems are required in that case, one for the normal outlet tube, for the vacuum bag, and another for the vacuum room under the laminate. The inlet tube is obviously clamped to prevent air suction. The pumps are switched on and the pressures are gradually set to a maximum vacuum, a low vacuum at the beginning will permit a better control on the bagging placement. When the set pressure is reached, the vacuum bag is checked for potential leaks as explained in the thin laminate's section.

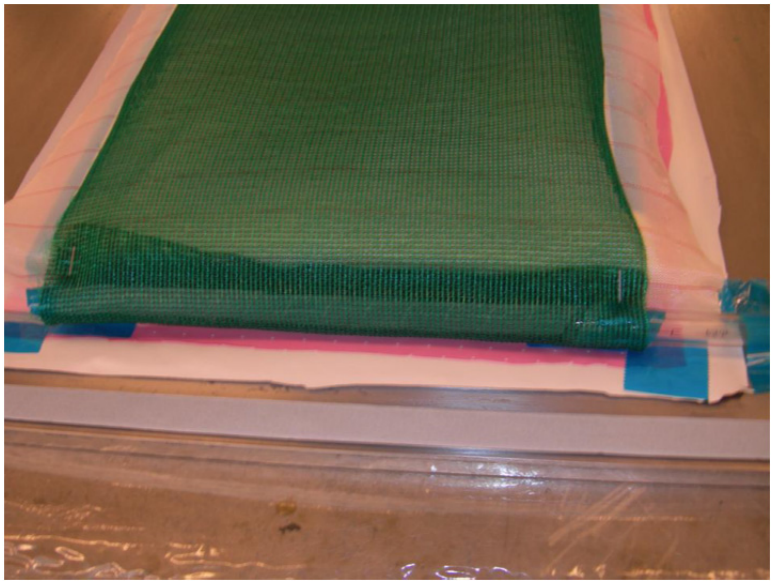

Figure 3.11 Inlet tube installation for a thick laminate

3.2.4 Matrix Preparation

When the bagging is free of leaks, the resin mixture is prepared. To calculate the amount of resin, the volume of the laminate (V_l) has to be known, in cubic millimetres.

$$V_l = L_l \, W_l \, t_l \tag{3.1}$$

In the resin calculation, Equation (3.4), only the half of V_l is considered, the other half is filled by the fibres, so at least a 50 % of fibres volume fraction is expected. An extra amount of resin is added to fill the flow mesh (V_{fm}) which corresponds to a laminate of 1 mm thick.

$$V_{fm} = L_l \, W_l \tag{3.2}$$

The volume of the inlet tube (V_{tube}) is also calculated in the amount of resin, including the length of the tube (L_t) and the length of the spiral tube which is as the width of the laminate. The tubes' inside diameter (ID) has also to be known.

$$V_{tube} = (L_t + W_l)\pi\left(\frac{ID}{2}\right)^2 \tag{3.3}$$

An extra of 10% of the entire volume is necessary to prevent air sucking, which will stay in the pot at the end. Then, the volume of the matrix (V_{matrix}) is expressed in cm^3 as in the following equation:

$$V_{matrix} = 1.1\frac{\left(V_l/2 + V_{fm} + V_{tube}\right)}{1000} \tag{3.4}$$

The entire volume of matrix is multiplied by its density, 1.15 g/cm^3 for the EPR-04908. That amount of the resin is poured and weighed in a cleaned pot (see Figure 3.12a). Thirty percent of the resin mass of the hardener EPH-4908, is added; it is particularly important to observe the recommend mixing ratio as exactly as possible. All ingredients are completely stirred together until no clouding is visible. To degas the matrix, a piece of ScotchBrite is put in the mixture and the pot is placed in the degas oven at least 10 minutes, the vacuum pressure is noted, the ScotchBrite is removed and the resin is degassed a second time for 10 minutes. The vacuum oven is presented in Figure 3.12b. During the degassing a particular attention should be given to prevent matrix foaming out of the plastic cup (Figure 3.12c), using the control knob. If a large quantity of resin is needed, higher than 2 kg, an exothermic reaction may happen. Be very alert, this reaction can produce smoke, high heat, which will cure the resin quickly. To prevent this effect, the resin's pot can be place in a bucket of cold water (see Figure 3.12d) or the total amount of resin is mixed in two separated parts, and the second part will be slowly poured in the first pot during the injection. If the heat is too high, and the plastic pot starts to melt or take in fire, place the plastic pot in a secure bucket presented in Figure 3.13.

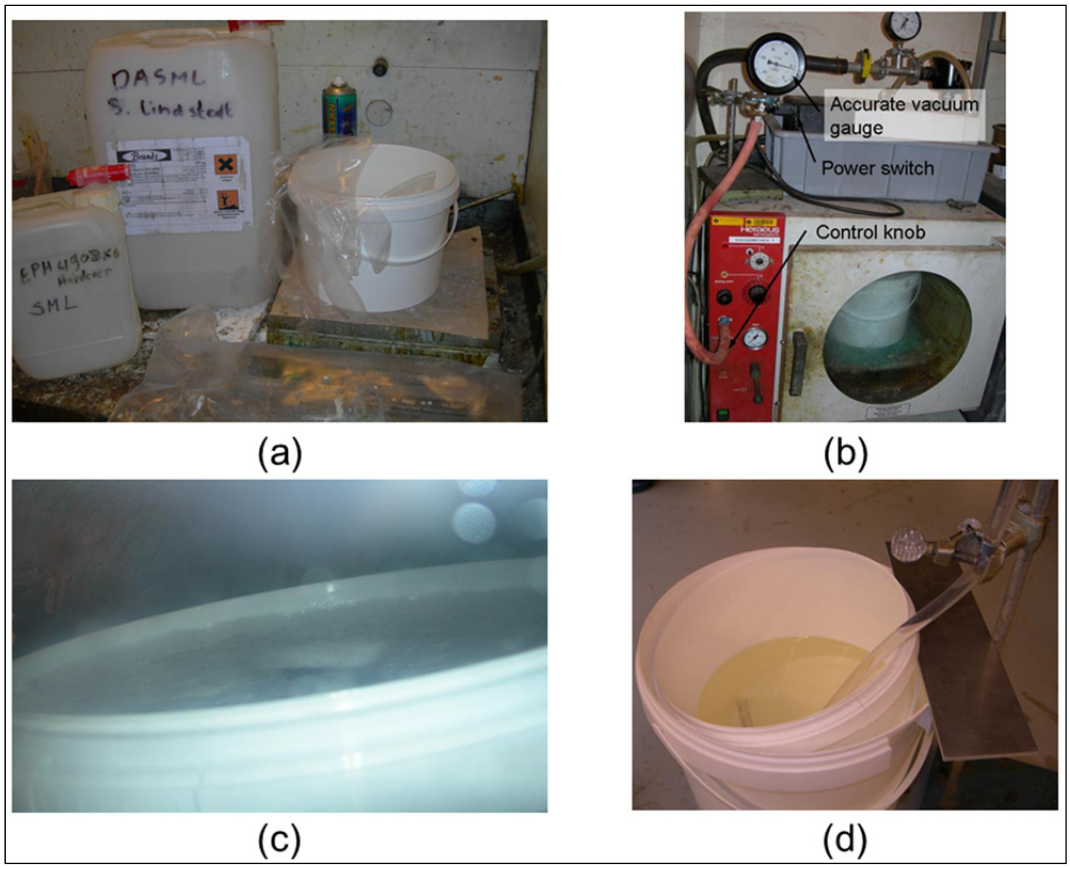

Figure 3.12 Matrix preparation: (a) Weighing of the resin and hardener, (b) Degassing oven, (c) Matrix foaming and (d) Matrix pot installation

Figure 3.13 Emergency “Red Bucket”

3.2.5 Injection and Curing

When the degassing is done properly, the inlet tube is installed in the pot of resin in a way to prevent air sucking (see Figure 3.12d). Also, to prevent that the inlet tube sticks by suction to the pot's sides, the tube's free end can be cut with an angle. As a reminder, the pressure in the vacuum bag was set to the maximum vacuum (1-6 mbar) for leakage testing. The injection can be started with opening slowly the clamp to let the air in the tube be evacuated. When the resin has reached half distance between the clamp and the laminate, the clamp is opened more to fill entirely the spiral tube and then the flow can be controlled to keep a straight front flow. In the case of a thin laminate, the flow is kept as slow as possible for a better impregnation along the fibres, in the longest dimension of the laminated plate. For a thick laminate the valve can be completely open when the flow mesh is completely filled or when the front flow, in the flow mesh, is a great straight line. In thicker laminates, the resin is pulled through the thickness of the laminate using a breather-cloth at the bottom. During the injection, the flow front can be recorded on the vacuum bag, by indicating the time and the impregnated area.

When the entire laminate is full, the vacuum pressure is increased to 500 mbar (the room temperature cure pressure) and the inlet tube is again clamped. The curing at room temperature can take approximately 30 hours or less (when the resin is hard enough), and then the vacuum pump is shut off. The tubes are cut and the laminate with the mould plate are placed at least 6 hours in a preheated oven at 80°C for the final cure. After the complete curing process, the vacuum bag and the peel ply are removed carefully, without damaging the laminate. Unidirectional laminates are particularly brittle along the fibres' direction.

3.2.6 Specimens Preparation

3.2.6.1 Specimens Positioning on the Raw Laminate

After the cure process, before cutting, a visual inspection of the laminated plate is made to identify large defaults as dry spots, cracks and air bubbles region. Those defects are drawn on a raw laminate scheme, as well as the resin inlet, the vacuum outlet and the fibres direction, the 0°. An example of a specimens positioning drawing is presented in Figure 3.14.

In addition to the identification of the visual defects, the position of the first cut is determined. The first cut will have to be perpendicular or parallel to the fibres, to the blue tape. As it is often the case, the specimens' position was already decided before the manufacturing to determine the size of the raw laminated plate. But now, the positioning will permit to trace back each specimen. So the second cut will make the first square corner. From this line, the third cut line is drawn at 160 mm, in this example, what is the total length of specimens for the transverse direction tensile test. Then the next line cut will be placed at a sufficient distance for all specimens. In this example, eight specimens are wanted. The specimens' width is 20 mm, plus the width of the cutting blade, 3 mm; and an extra 10 mm is added to have enough material to clamp the laminate during the cutting of the last specimen. An indication as where the specimen's number will be written on the specimen to test them all in the same way and to track them back for failure reason identification. As an example, if they all fail at the bottom grip on the left. The specimens for the laminate's quality evaluation are also identified. In this example, some sections are reserved for under aluminium tabs material, the use of them will be explained in a following section.

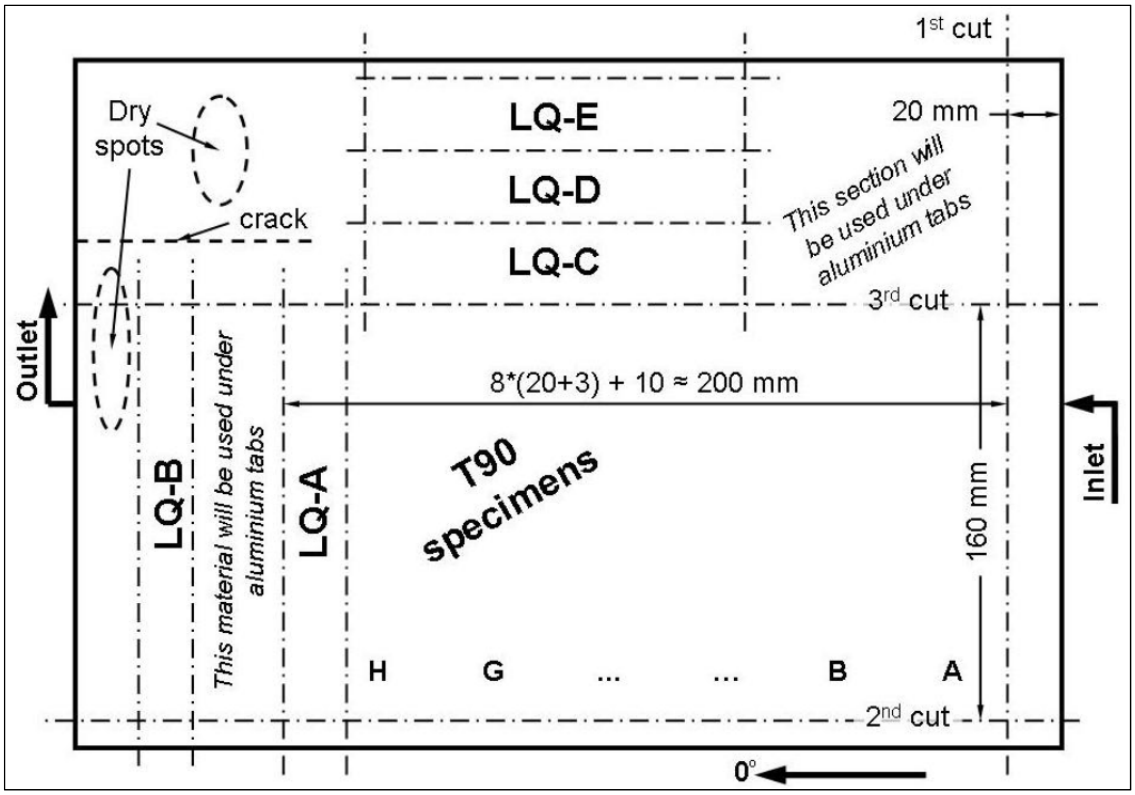

Figure 3.14 Example of specimens' positioning on a raw laminate

3.2.6.2 Specimens Nomenclature Code

To identify adequately each specimen, a nomenclature code is established for the thickness effect study. The specimen identification follows that nomenclature: yyyymmdd-layup code-[scale level]-nb plies-test type-letter. The first term is the date, year, month and day, of the laminate's production. The second term is a lay-up code, which takes the value of "UD" for unidirectional laminate, "ISO" for quasi-isotropic lay-up and "CR" for a cross-ply laminate. The third term is optional and it specifies the scale level through-the-thickness. Two different scale levels are possible, the ply-level and the sub-laminate level. For this optional term, the possible values are "PLY" and "SUB" for the ply and the sub-laminate level respectively. The fourth term is the number of layers in the laminate. The fifth term identifies what type of test the specimen is used for. The code "T0" is for a tensile test in fibre direction; "T90" is for a tensile test in matrix direction; "LQ" is for the laminate quality evaluation; and "G12",

“G21”, “G13” and “G23” are for the V-notched beam tests. The last value is a letter used as a specimen’s number.

3.2.6.3 Cutting and Machining

The specimens are cut with a rotary saw. The laminate is solidly clamped in place on a reference table smooth face down. Only the head of the saw moves which contains the diamond blade, 86EXO - 350x2x35 mm. The blade diameter is then 350 mm, which limits the maximum size of the specimens, as well as the holding table size. The largest plate maintainable in place is around 500 mm long and 250 mm wide. A picture of the rotary saw and a clamped laminate is shown in Figure 3.15. To start cutting the blade is brought close to the laminate surface, the feed is set to 1 mm/s and the start button is pushed. If the cut is not completed due to a too short blade stroke (223 mm), keep the blade in the cut path to stay straight, slide the plate in the necessary direction to get a complete cut. For an accurate cut dimension and a better surface finish, the blade position after the cut is set to “stay in place” in the configuration menu. Other conditions to obtain accurate specimen’s dimensions are to clamp both sides of the laminate, plate and specimen, and avoid a cut less than 5 mm width to prevent that the flexible blade deviate. The log book needs to be filled at each use and the area should be cleaned after use.

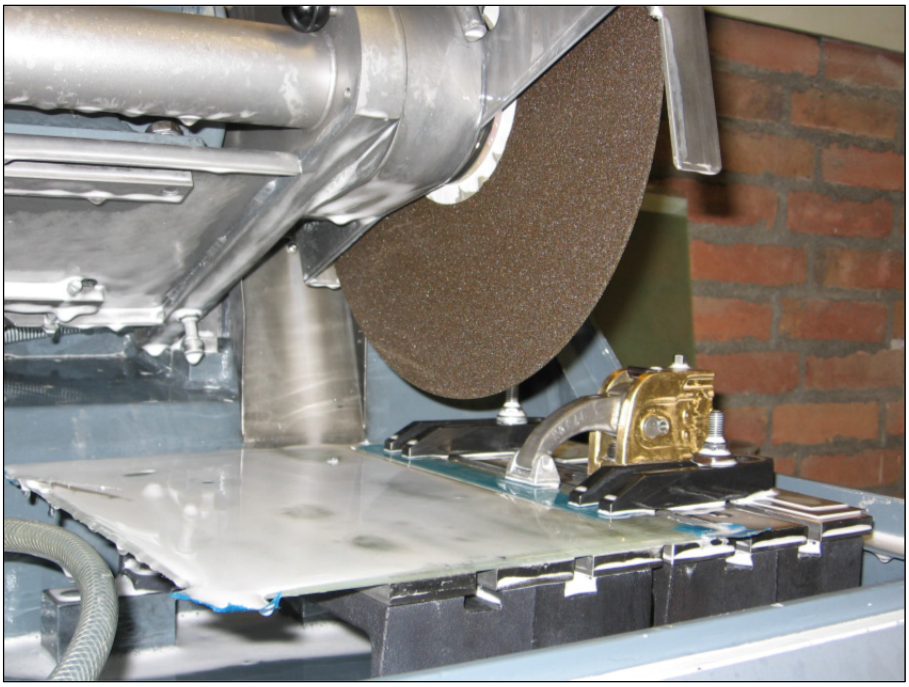

Figure 3.15 Rotary diamond blade cutting machine

The specimens need to be supported in the middle to avoid bending during cutting and get a failed specimen. The final geometry for “dog bone” and V-notched specimens is machined on a CNC milling.

3.2.6.4 Tab Specifications and Installation

For some tests, specimens require tabs. In that case, the tabs are glued as explained in this section, prior to be cut at the final dimensions. It is the case for thin laminates, less than 5 mm, in tension and shear tests, and for thicker ones only in matrix direction tension tests.

The tabs for longitudinal tensile test thin specimens are 2 mm thick [±45] E-glass fabric/epoxy laminates. The length of these tabs is 56 mm. The same material is used for the tabs of V-notched specimens less than 5 mm, but with a length of 32 mm. The tabs’ material is cut at the correct tabs’ length and the length of the tabs’ plate needs to cover at least all specimens. Four tab plates are required for one plate of specimens.

Tabs are bounded with a two parts epoxy, Scotch Weld 9323 B/A provided by 3M. To calculate the amount of glue, the surface to be glued needs to be known in square centimetres. It is known by experience that with 1 g of glue will cover 20 cm2. Then the ratio of the Scotch Weld 9323 B/A is 100 parts of B for 27 parts of A. So the correct amount of part B and part A is poured and weighed in a small recipient. A quantity of glass pearls, diameter of 90 to 150 μm, about five percent of the glue mass, is added to get an uniform thickness of glue. All ingredients are completely stirred together until a nice pink texture is obtained.

Thereafter, the glue is applied on abraded and cleaned specimens and tabs. Specimens and tabs sections were prepared in advance, using sand paper #150 and ethanol, as it shown in Figure 3.16a. Before using, the based plates and holders of the tabs installation fixture were pretreated with WaterWorks release products as explained in the manufacturing report. Figure 3.16b shows that blue or orange tape is applied to facilitate the unmoulding after the curing stage. Then the tabs are squeezed one on the specimens' section with the tabs holders as shown in Figure 3.16c. For maximum shear strength of the glue, it needs to cure one day (24 h) at room temperature, clamped in the fixture, and one hour at 80°C, out of the tabs fixture.

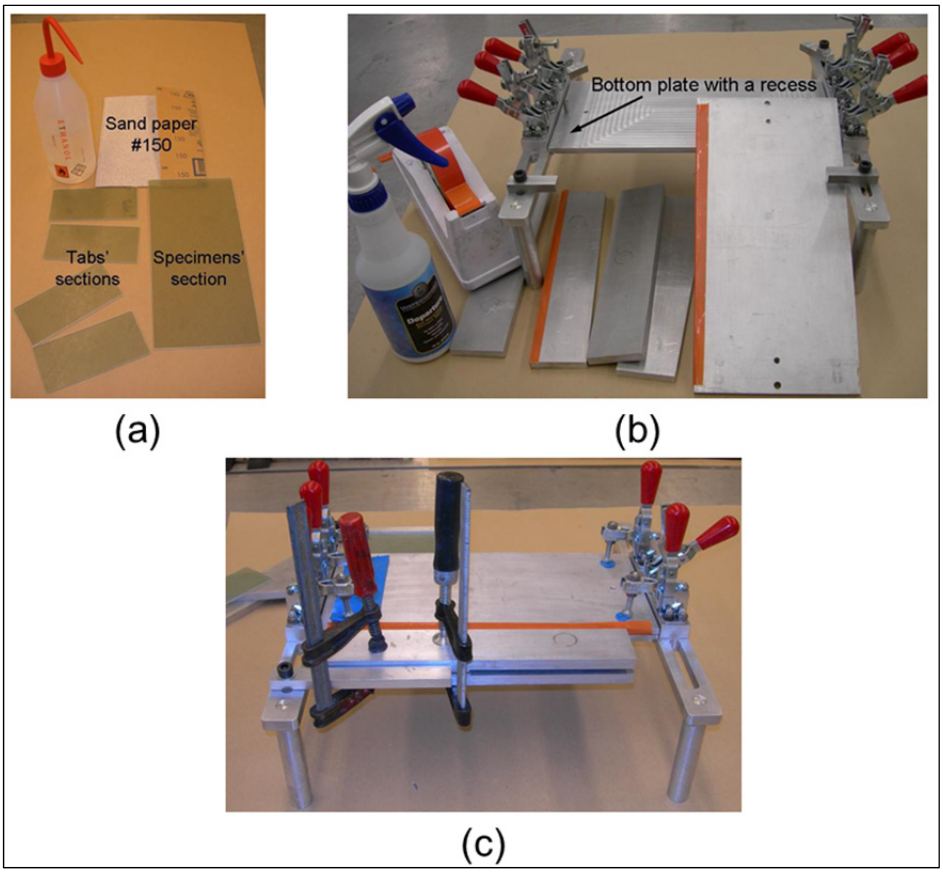

Figure 3.16 Fixture for the assembly of the tabs: (a) Preparation of the tabs material, (b) Preparation of the fixture parts and (c) Gluing the tabs and curing installation

The tabs for the "dog bone" specimens are completely different. The material is thin aluminium sheet, 0,2 mm thick to 1 mm for the thicker specimens, cut in band of 300 mm long, or longer, by 20 mm, the specimens' width. They are bonded on the "dog bone" specimens, at the final geometry, with the strain gauge glue or the pink glue provided by 3M. At both other ends, which will be clamped in the test machine grips, a short piece, about 30 to 50 mm long, of the same material, thickness and width as the specimen, is glued to keep the aluminium tabs parallel, to provide a good load transfer and to prevent peeling of tabs. This material is the one reserved previously in the positioning of the specimens on the raw laminate. Pictures of a "dog bone" specimen and aluminium tabs are presented in Figure 3.17. Another device is installed to hold the tabs on the specimen and then prevent peeling. This device is shown in Figure 3.18.

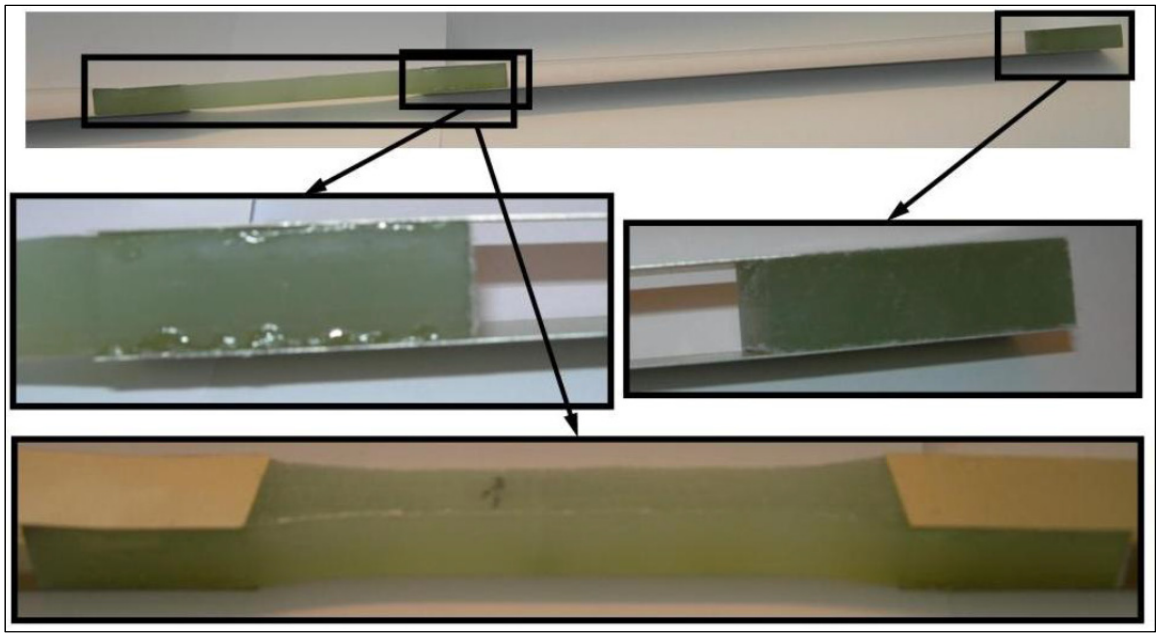

Figure 3.17 Aluminium tabs for tension tests in the matrix direction

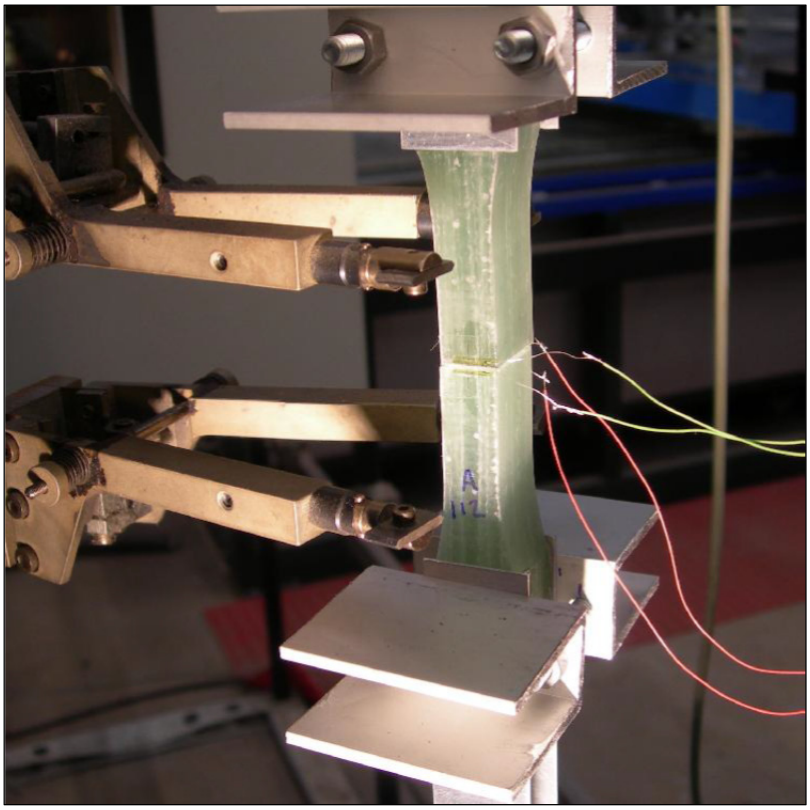

Figure 3.18 Aluminium holder for thicker “dog bone” specimens

The using of tabs aims to protect the first layer against the clamping force and for a better distribution of the load. Nonetheless, when the load becomes too high, as in thick UD laminates, the necessary clamping pressure crushes the specimen and tabs are peeled off causing slippage in the grip as a failure. So a new jig was designed to support through-the-thickness the specimen in the grip to prevent crushing. Figure 3.19 shows a specimen installed in this steel support.

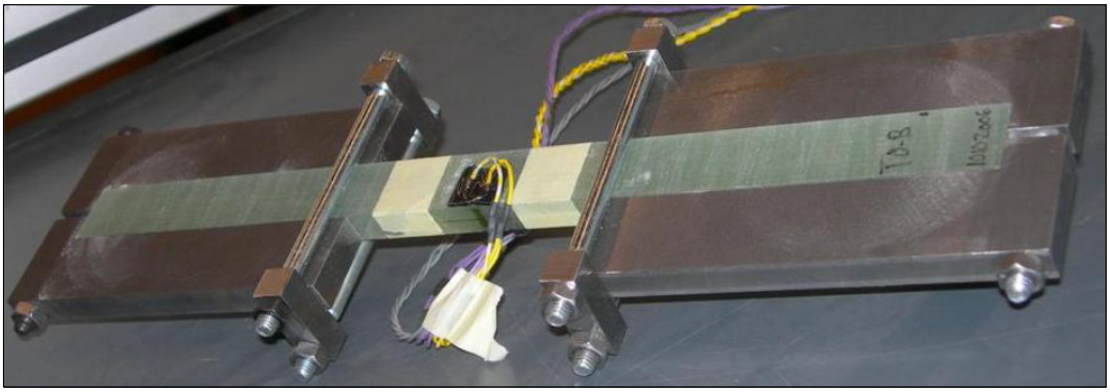

Figure 3.19 Steel jig to prevent crushing in thick specimens

3.2.6.5 Strain Gauges Installation

To measure displacement during testing, strain gauges are used as well as a longitudinal mechanical extensometer. The surface of the specimen is lightly abraded, clean with ethanol and then light pencil marks are made to position strain gauges in good orientations. The gauge length varies from 2 to 5 mm. The 2 mm strain gauges are used to record through-the-thickness deformation on thin specimens and they are mounted on 2 small plastic blocs as shown in Figure 3.20a. They are also used in 45° rosette for V-notched beam shear tests (see Figure 3.20b). In other applications, for all other tensile test specimens, 5 mm strain gauges are used (see Figure 3.20c and d). All strain gauges, supplied by Kyowa, are bonded with precaution with the glue CC 33A also from Kyowa. Just before testing, wires are welded on.

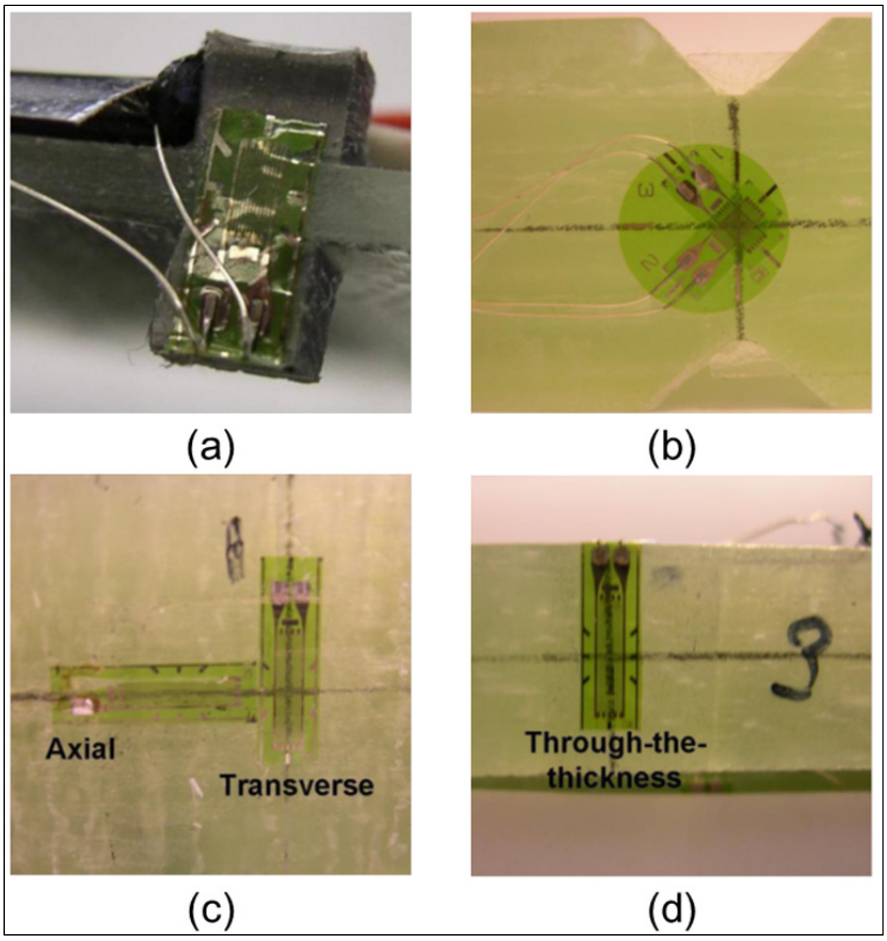

Figure 3.20 Strain gauges installation:
(a) Through-the-thickness strain gauge (2 mm) on thin specimens,
(b) 45° strain gauges rosette on V-notched beam specimens,
(c) Axial and transverse strain gauges (5 mm) for all tensile test specimens
(d) Through-the-thickness strain gauge (5 mm) on thick specimens

3.3 Quality of the Manufacturing Process

The quality of the laminates is controlled using the average of the ply thickness, the density, the fibre volume fraction and the void content measured on each manufactured laminated plate, as described in detail in this section.

All specimen dimensions are recorded. The average of several measurements on each specimen is considered. The specimen's thickness is inspected with a ball micrometre (with

6 mm diameter ball). A flat end micrometre or a digital caliper is used to measure larger dimensions, more than 10 mm, as the specimen's width. The effective length (distance between grips) and the gauge length (distance between extensometer arms) are measured with a ruler and recorded during testing. The average thickness of a cured ply is calculated by dividing the measured thickness by the number of plies in the laminate. This value is significantly affected by the injection pressure and the curing pressure during the laminate production. The average cured ply thickness values for each thickness category are presented in Table 3.3.

The same five specimens are used for the density measurement and the fibre volume content, as identified in the example of Figure 3.14. Those small specimens are cut from leftover. A coupon's volume around 10 mm^3 seems to provide accurate results. Nevertheless, the crucible for the burn-off method accepts as maximum specimen dimensions of 60 mm long by 40 mm wide. According to this, a specimen could be cut again, after the density measurement, in few parts to fit in a crucible for the burn-off test.

The density measurement is done using the principle of the buoyant force. This method is the ASTM D792-00 Standard Test Methods for Density and Specific Gravity (Relative Density) of Plastics by Displacement (ASTM, 2000). Using this method, a metal wire with a hook (an alligator grip in our case) is installed on the electronic scale and which is set to zero. After that, all dried specimens (room's conditions drying only) are weighed with the hook system, to get the mass of the dried specimen (M_{DS}). Specimens are again weighed suspended to the wire, but this time completely immerses, including the hook, in water, to obtain the mass of the wet specimen (M_{WS}). The last needed value is the mass of the hook system in the water (M_{WH}), this value should be below zero. The temperature of the water (T_w) is also recorded. The specific gravity instrumentation is shown in Figure 3.21. The equation of the specimen's density using the specific gravity method is the following one, where ρ_w is the density of the water at T_w given in the Table 3 of the ASTM D 792-00 (ASTM, 2000). The density values for each category of thicknesses are presented in Table 3.3.

$$\rho = \rho_w \frac{1}{\left(1 - \left(M_{WS} - M_{WH}\right) / M_{DS}\right)} \tag{3.5}$$

Figure 3.21 Picture of the specific gravity instrumentation

As a second step, a matrix burn off is done on the same five specimens to obtain more quality information. The matrix burn off is fully explained in the procedure G of the ASTM D3171-99 Standard Test Methods for Constituent Content of Composite Materials (ASTM, 2004). This procedure permits the calculation of the fibre volume fraction and the percentage of void content. The procedure is divided in few steps: wash the crucibles with ethanol and dry them in the oven at 565°C during 30 minutes, take them out with clean tongs, place the crucibles in a desiccator for 1 hour, weigh the empty crucible (M_c), again with a specimen in (M_{cs}), cover it with an aluminium foil, identify each of them and using a drawing retrace the position of each specimen in the oven and in the desiccator. The burn-off time depends of the specimen's size, a maximum of 6 hours should be observed. A good way to apply the burn-off temperature, 565°C, is to reach it gradually, about a rate of 1 to 2°C/min. So it is possible to program the oven for a night running. After the burn-off is completed, place specimens

(dried fibres) and crucibles in a desiccator and allow to cool down to room temperature. Each bundle of reinforcements is weighted in its crucible (M_{cf}). Then it is possible to calculate the fibre volume fraction (V_f), the matrix volume fraction (V_m) and the void content percent (V_v) with the following equations.

$$V_f = 100\frac{(M_{cf} - M_c)}{(M_{cs} - M_c)}\rho_s \Big/ \rho_f \tag{3.6}$$

$$V_m = 100\frac{(M_{cs} - M_{cf})}{(M_{cs} - M_c)}\rho_s \Big/ \rho_m \tag{3.7}$$

$$V_v = 100 - (V_f + V_m) \tag{3.8}$$

where, ρ_s is the density of the specimen, ρ_f and ρ_m are respectively the density of the fibres and the matrix found in Table 3.1. The values for the fibre volume fraction and the void content of each category of thicknesses are presented in Table 3.3.

Table 3.3 Quality evaluation of UD laminates

Measure \ Thickness	**8 plies (1.5 mm)**	**56 plies (10 mm)**	**112 plies (20 mm)**
Average cured ply thickness, mm (standard deviation, %)	0.183 (2.3)	0.187 (1.3)	0.185 (0.4)
Density, g/cm^3 (standard deviation, %)	2.04 (1.0)	2.06 (1.5)	2.06 (1.0)
Fibre volume fraction, % (standard deviation, %)	60.3 (2.3)	60.9 (1.4)	61.5 (2.2)
Void content, %	-0.1	-0.2	-0.4

The measurements show that the density, the average thickness of one ply and the fibre volume fraction are not affected by the thickness of the laminate. The thickness inspection gives an average ply thickness of 0.185 mm with a standard deviation of about 1.1%. High quality UD laminates are produced with a high fibre volume fraction, at an average of more or less 61% and a standard deviation of about 1.6%. The high quality of laminates is also confirmed with a very low percentage of voids of -0.4%. The negative value is due to the superposition of measurement tool tolerances and errors as air bubbles and crucible contamination. Since no large deviations are observed on the average ply thickness, the density and the fibre volume fraction prove the consistency of the vacuum infusion manufacturing process. The void content results also support the theoretical assumptions of the rule of mixture in which a no void composite is considered.

Furthermore, an electronic microscope is also used to make a visual inspection of the laminate quality. The electronic picture (see Figure 3.22) confirms the assumption of a uniform random distribution of fibres in the plane 2-3, across the fibres. In this case, the assumption of a transversely isotropic material is applicable and no through-the-thickness tensile test needs to be performed. The very low percent of voids is once more confirmed with only two black spots in a few resin pockets.

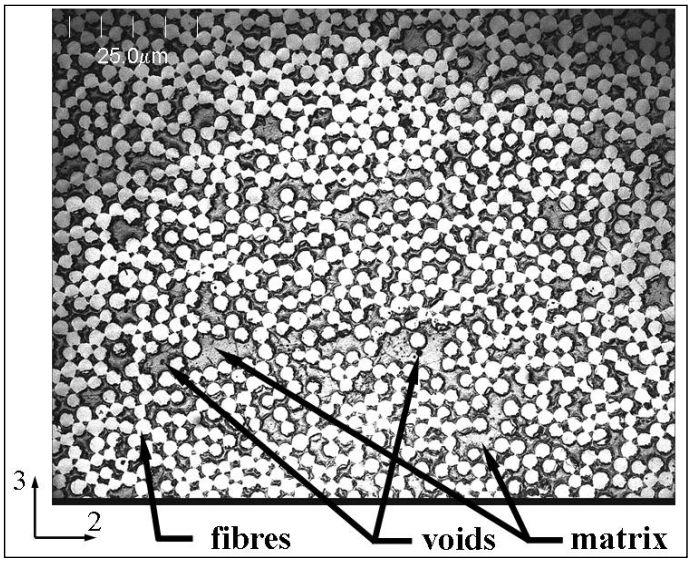

Figure 3.22 Electronic microscope picture of a cross section of a UD laminate

3.4 Theoretical Estimation of Elastic Properties

In this sub-section, the nine elastic properties are estimated using the theory presented in Section 1.3.2.2, from the material properties of each constituent (Table 3.1) and measured fibre volume fraction. The theoretically estimated values of the nine elastic properties are presented in Table 3.4 for each category of thicknesses. The variation in tensile and shear moduli is due to the negligible variation in fibre volume fraction. These values establish a range of values to compare with the experimental ones and to validate this method of estimation for the orthotropic elastic properties.

Table 3.4 Theoretical elastic properties of UD laminates

Thickness / **Elastic properties**	**8 plies (1.5 mm)**	**56 plies (10 mm)**	**112 plies (20 mm)**
Longitudinal Young's modulus, E_1 (GPa)	45.1	45.6	46.0
Transverse Young's moduli, E_2 and E_3 (GPa)	9.33	9.47	9.64
In-plane and longitudinal – through-the-thickness Poisson's ratios, ν_{12} and ν_{13}	0.25	0.25	0.25
Transverse – through-the-thickness Poisson's ratio, ν_{23}	0.37	0.37	0.37
In-plane and longitudinal – through-the-thickness shear moduli, G_{12} and G_{13} (GPa)	3.95	4.01	4.09
Transverse – through-the-thickness shear modulus, G_{23} (GPa)	3.40	3.45	3.52

3.5 Specimens Testing

The main objective of these experiments is to determine several mechanical properties (E, G, ν, F_{tu} and F_{su}) of a UD lamina to be used as an input in structural design and stress analyses. The initial hypothesis is that the lamina elastic and strength properties vary as a function of the thickness. In this section, the experimental tests used to determine the full set of 3D elastic properties and the tensile and the shear strengths are described.

3.5.1 Tension

The tensile properties, the longitudinal and transverse Young's moduli (E_1 and E_2), the three Poisson's ratios (ν_{12}, ν_{13} and ν_{23}), are obtained following a method based on the ASTM D3039/D3039M-00 Standard Test Method for Tensile Properties of Polymer Matrix Composite Material (ASTM, 2006) and other specimen designs presented by Godwin and Hoggart (Hodgkinson, 2000). In addition, the tensile test will be performed until failure, so the mode of failure, the ultimate strength (F_{tu1} and F_{tu2}) and strain (ε_{tu1} and ε_{tu2}) will be recorded, when possible. In order to obtain all tensile properties, eight specimens per thickness are tested in both directions, longitudinal and transverse. In total, forty-eight specimens are tested in tension.

The geometry used in longitudinal tensile testing is a simple straight rectangular bar as shown in Figure 3.23. The length and the width are 300 and 20 mm, respectively. It is well known that testing strong materials such as thick UD laminates for longitudinal tensile properties, without inducing unacceptable stress concentrations, is very difficult (Coguill and Adams, 2000; Kulakov *et al.*, 2004; Schubel *et al.*, 2006). In addition, authors do not agree on the relevance of using tabs nor their geometry, if they are used (Coguill and Adams, 2000; Hodgkinson, 2000). In this investigation, [±45] rectangular tabs of 2 mm thick and 56 mm long are used only on thinner specimens, below 5 mm thick. No tabs are used on thicker specimens.

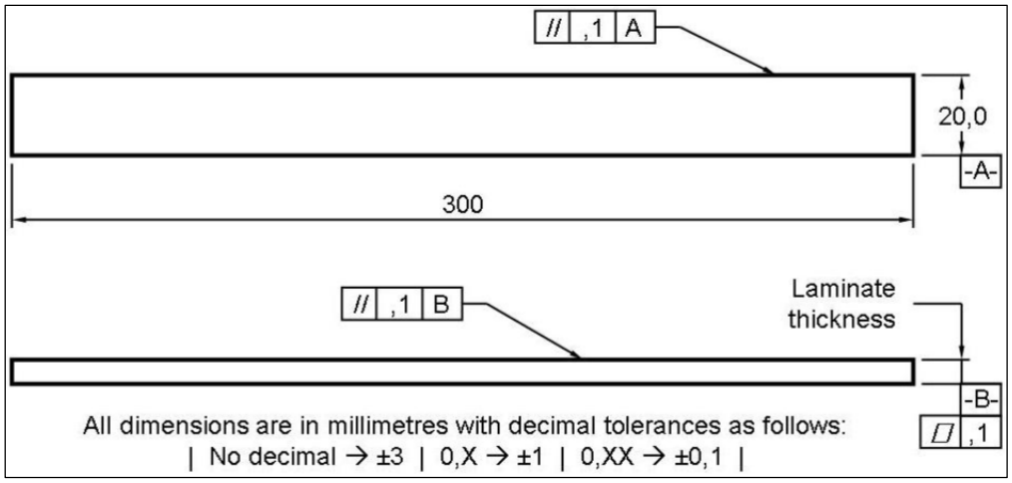

Figure 3.23 Geometry of longitudinal tensile specimen

For thicker specimens, above 5 mm thick, special lateral supports are designed and installed to avoid crushing the specimen in the grip and to reach higher loads before failure (see Figure 3.24). All strains, longitudinal, transverse and through the thickness, are recorded by strain gauges, even on thin specimens. Figure 3.25 shows a scheme of the tensile test in the direction of fibres and the formulas to compute the associated properties. For the through-the-thickness strain on thin coupons, a ratio is computed for the effective length of the strain gauge. As shown in Figure 3.26, the effective thickness is 1.47 mm when the strain gauge has a length of 2 mm.

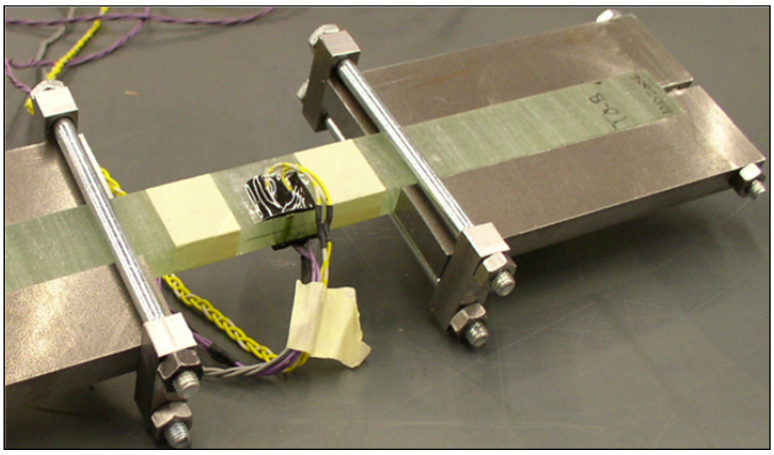

Figure 3.24 Thick specimen for a longitudinal tensile test with lateral supports

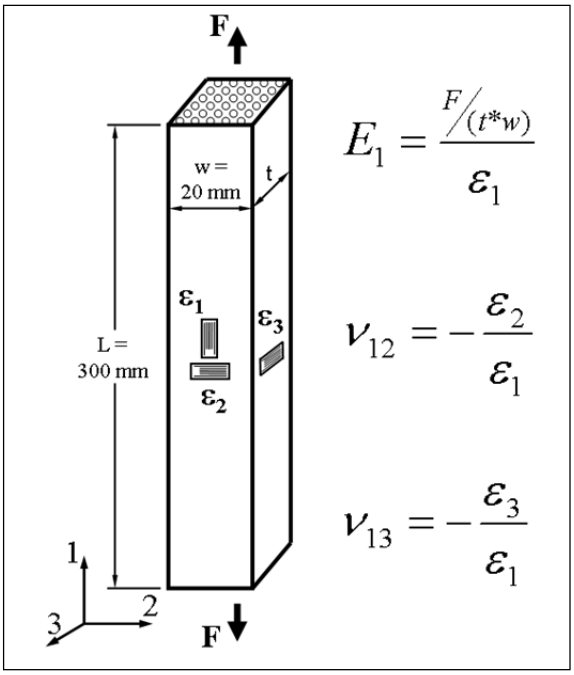

Figure 3.25 Schematic sketch of a tensile test in fibres direction

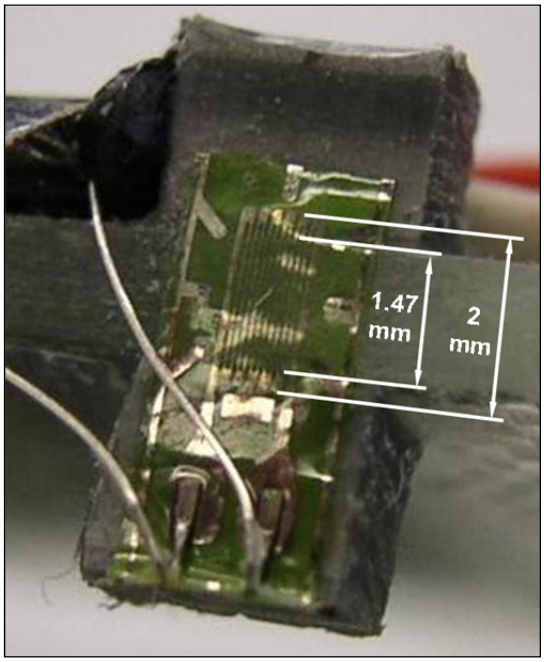

Figure 3.26 Strain gauge installed through-the-thickness of a thin laminate

For the transverse tensile test, the geometry of specimens is based on a Hoggart shape with a gauge length of 50 mm and a cross section of 13 mm in width by the specimen thickness (Hodgkinson, 2000). Figure 3.27 shows the geometry of the specimens used in the transverse tensile test.

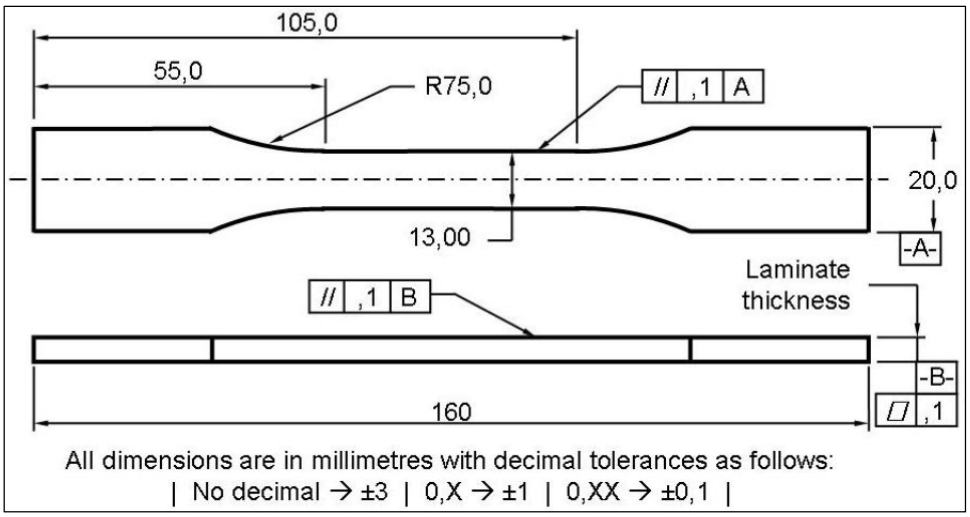

Figure 3.27 Geometry of transverse tensile specimen

The difficulties in testing transverse tensile properties are the brittleness of the material and the randomness of the failure location. To counteract the randomness of the failure location, an axial mechanical extensometer is used to record the deformation in the load direction. Note that the strain gauges are still being used in the transverse and through-the-thickness directions. In addition to the use of an extensometer, the "dog bone" geometry will help to keep the failure in a specific gauge length zone. To prevent an early failure during clamping, long flexible aluminum tabs are used. Long tabs also allow an appropriate tensile load transmission through the specimen, as would the longer specimens of Hoggart (Hodgkinson, 2000). Figure 3.28 presents a thick "dog bone" specimen with long aluminum tabs. The extra clamping devices at both ends of the specimen are installed to prevent the peeling of tabs. Figure 3.28 also shows a typical and desired (right at the strain gauges) failure of a UD specimen in transverse tension. Figure 3.29 shows a scheme of the tensile test in the direction perpendicular to fibres and the formulas to compute the two transverse elastic properties.

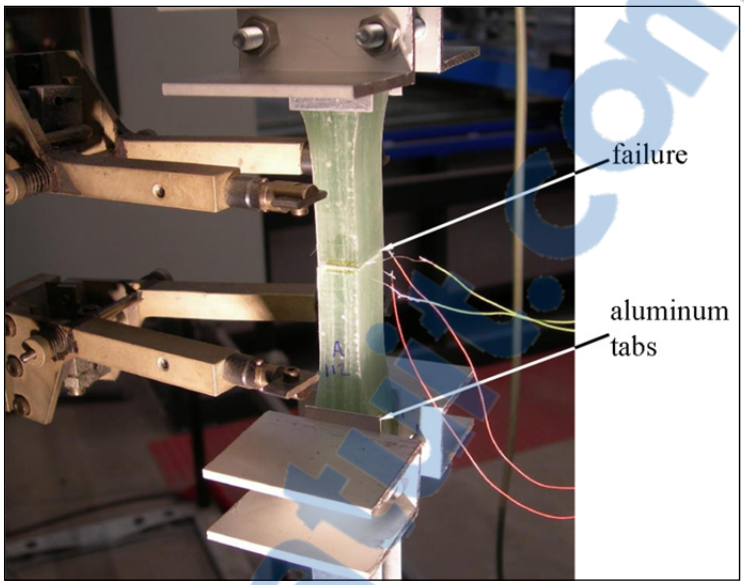

Figure 3.28 Thick "dog bone" specimen for a transverse tensile test with long flexible tabs

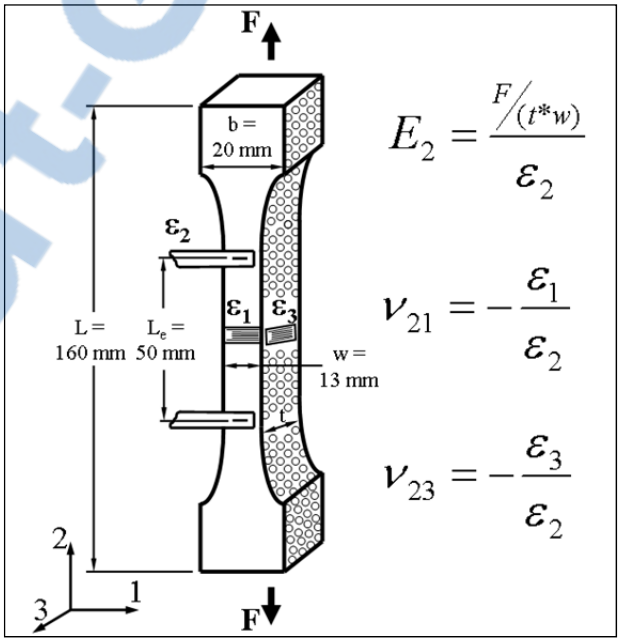

Figure 3.29 Schematic sketch of a tensile test in a direction transverse to fibres

3.5.2 Shear

The elastic shear moduli (G_{12}, G_{13} and G_{23}) and the ultimate shear strengths (F_{su}) are obtained by applying a shear load to a V-notched beam based on the ASTM D5379/D3795M-05 Standard Test Method for Shear properties of Composite Material by the V-Notched Beam Method (ASTM, 2005). This method is also known as the Iosipescu test. The maximum common thickness for this test is about 5 mm, so the existing Iosipescu fixture does not allow specimens thicker than 10 mm to be tested. A new design of a modified Iosipescu fixture is done with deeper jaws to accept thicker specimens. In addition, to reduce the twisting and the bending effect, as specified by Melin and Neumeister, two linear bearings are installed on the mobile jaw. Figure 3.30 shows the modified Iosipescu fixture (Melin and Neumeister, 2006).

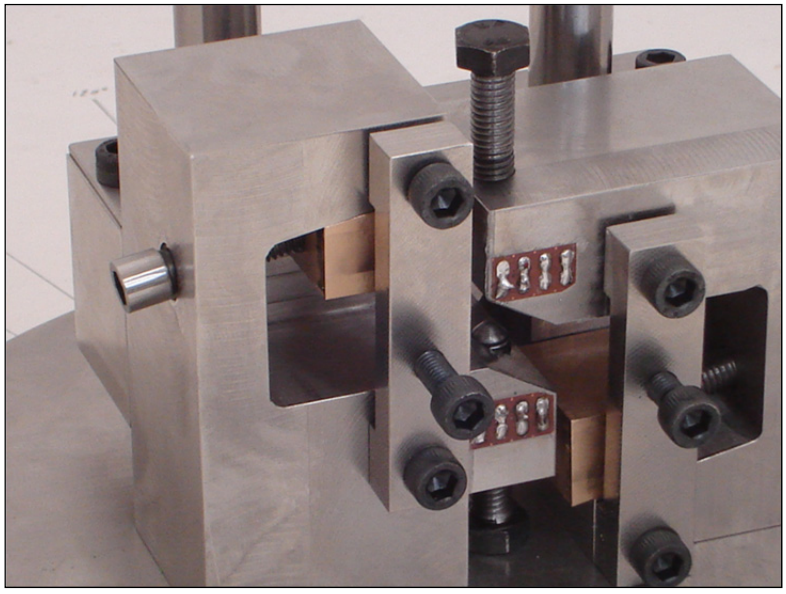

Figure 3.30 Modified Iosipescu fixture

Melin and Neumeister also discussed in their research the optimal notch opening angle determined as a function of the material (Melin and Neumeister, 2006). They concluded that an opening angle of 90° for the V-notch, as in ASTM, is sufficient to give repeatable and reliable results (ASTM, 2005; Melin and Neumeister, 2006). The overall dimensions as

specified by (ASTM, 2005). The geometry with dimensions and tolerances is presented in Figure 3.31. The external dimensions of the v-notched coupon are 76 mm long and 20 mm wide. The thickness is function of the number of layers. However, to obtain the shear properties through-the-thickness, the specimen's thickness is 10 mm and specimens are cut from a 20 mm thick laminate. This restraint is in order to manufacture the V-notches and get a weakest cross-section with a length of 11 mm.

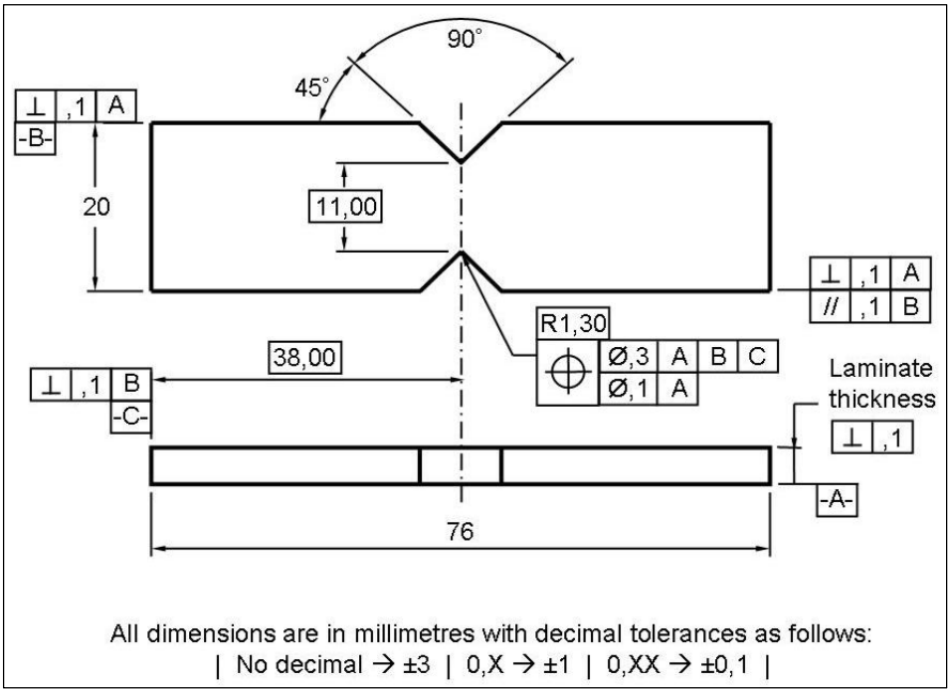

Figure 3.31 Geometry of a V-notched specimen for shear properties

For shear properties, a ±45° strain gauges rosette is used. Eight specimens per thickness are tested for the shear modulus in the plane 1-2. For through-the-thickness shear properties (G_{13} and G_{23}), sixteen V-notched beams are tested. Shear properties in through-the-thickness planes (1-3 and 2-3) are only measured for a laminate of 20 mm thick as specified in (ASTM, 2005), because it is impossible to make the V-notches, respecting the distance between notches of 11 mm, on thinner specimens. Figure 3.32 presents the geometry of V-notched specimens and formulas used to compute the three shear moduli and the ultimate strength and strain whenever possible.

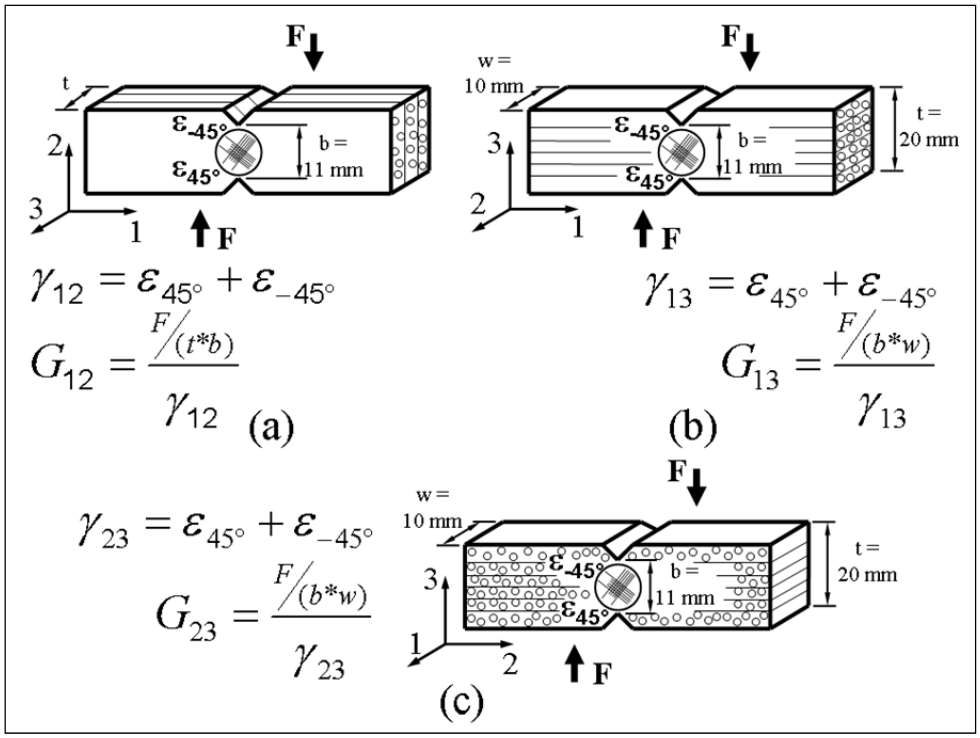

Figure 3.32 Schematic sketch of a shear test in the plane (a) 1-2, (b) 1-3, and (c) 2-3

3.6 Results Analysis

All tests are performed at an average room temperature of 20°C with a relative humidity of 60%. The tensile elastic properties are firstly discussed, followed by the shear elastic properties. At the end, the failure mode and the ultimate strength are presented and discussed for the longitudinal and transverse tensile tests and all the three shear directions.

3.6.1 Tensile Elastic Properties Presentation

Figure 3.33 presents examples of the longitudinal and transverse elastic modulus for thicknesses of 1.5 mm (a) and 20 mm (b), respectively, as well as longitudinal-transverse and longitudinal – through-the-thickness Poisson's ratios for 10 mm thick specimens (c) and (d),

respectively. A linear interpolation is performed on data recorded on all specimens of the same thickness. This method is developed to analyze brittle and unpredictable behaviour such as unidirectional coupons. This random behaviour and the brittleness lead to noisy signals from individual strain gauges, but observing the global signal of all coupons together, it shows a linear behaviour. Each mechanical property for the three studied thicknesses is analyzed using this methodology.

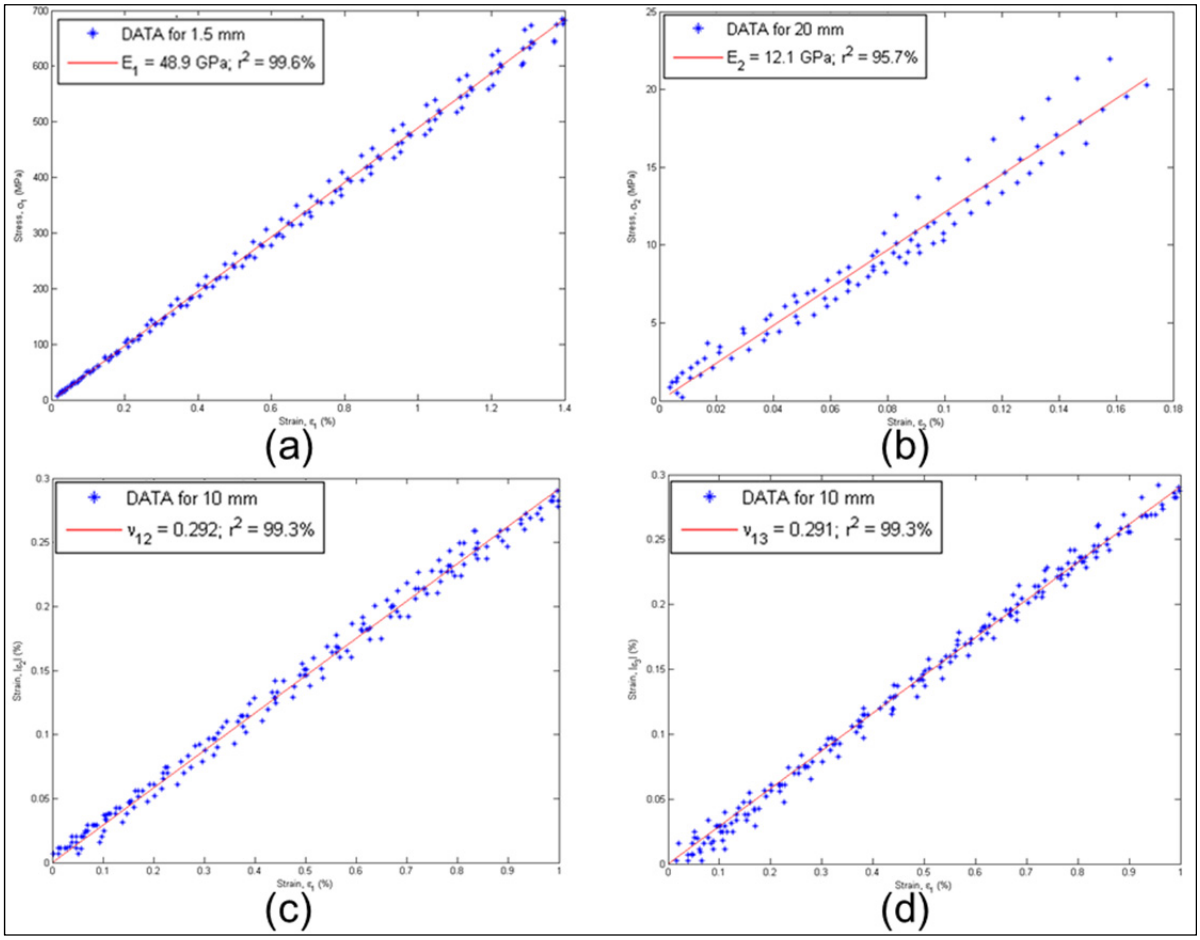

Figure 3.33 Linear interpolation of experimental results:
(a) Longitudinal elastic modulus for the 1.5 mm thick specimens
(b) Transverse elastic modulus for the 20 mm thick specimens
(c) Longitudinal-transverse Poisson's ratio for the 10 mm thick specimens
(d) Longitudinal-through-the-thickness Poisson's ratio for the 10 mm thick specimens

Figure 3.34 presents the longitudinal and the transverse Young's modulus with the distribution of the experimental values for all thicknesses. Focusing on the experimental longitudinal Young's modulus (E_1), this elastic tensile property seems to increase slightly with the thickness, about 7%, but in a comparable magnitude of the theoretical value of 45.6 GPa, a difference of 7%. Furthermore, the coefficient of determination of the linear regression (R^2) is over 99% for all thicknesses, so experimental results are reliable. Even if a larger discrepancy is observed for coupon with a thickness of 1.5 mm, the repeatability in the testing method is not questionable. It is concluded that the thickness does not influence the longitudinal Young's modulus, E_1.

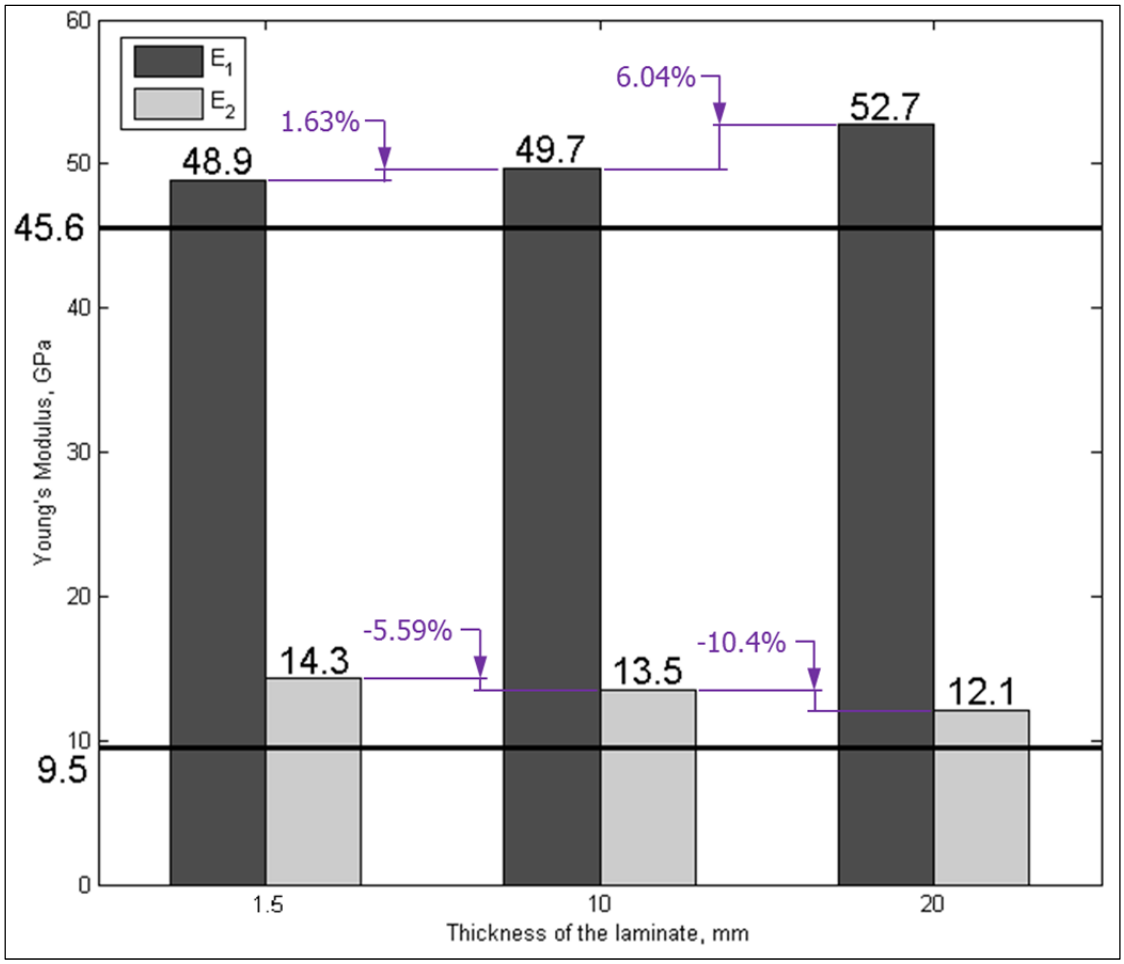

Figure 3.34 Experimental Young's moduli as a function of the thickness in longitudinal (E_1) and transverse (E_2) directions

In the same way, the transverse Young's modulus (E_2) values are higher, by about 30%, than the estimated one of 9.5 GPa. However, the theoretical estimated value seems to be comparable to the experimental values. Unlike the behaviour of E_1, E_2 seems to slightly decrease with the thickness, by about 16%. Even if the R^2 for the transverse Young's modulus of each thickness is only more or less 90%, it can be concluded that E_2 is not influenced by the thickness. The lower R^2 can be explained by the randomness of local deformations and the use of an extensometer instead of an axial strain gauge.

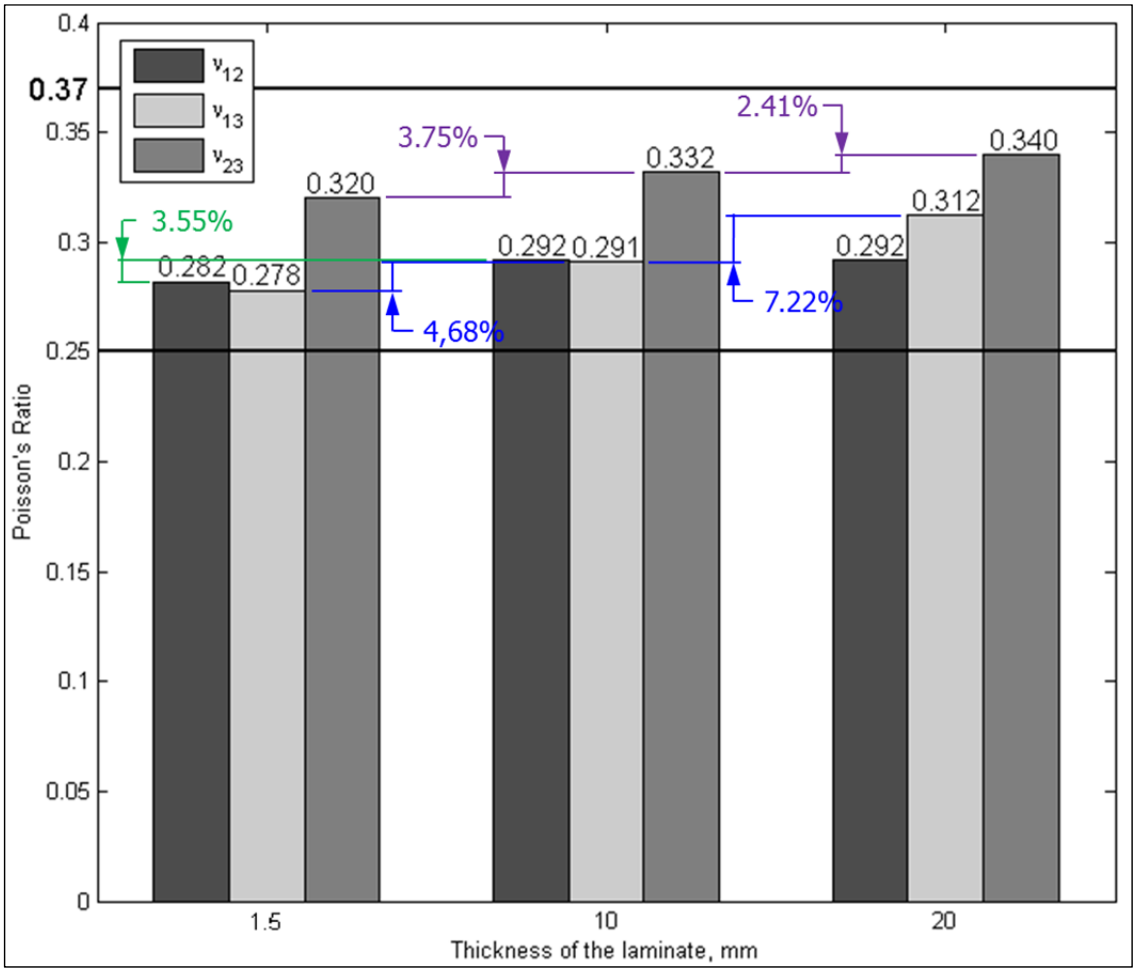

Figure 3.35 Experimental Poisson's ratios as a function of the thickness

The results of linear regression analysis for Poisson's ratios are presented in Figure 3.35. The in-plane Poisson's ratio (ν_{12}) does not change with the thickness. The maximum and solely variation is less than 4% between the first two thicknesses. The experimental values are reliable since the results are in a range of about 13% within the theoretical value of 0.25 and R^2 is over 99%. It is concluded that the in-plane Poisson's ratio is not influenced by the variation of the thickness.

In the case of both out-of-plane Poisson's ratios (ν_{13} and ν_{23}), experimental values slightly increase with the thickness. It is an increase of 12% for the longitudinal – through-the-thickness Poisson's ratio (ν_{13}) and an increase of about 6% for the transverse – through-the-thickness Poisson's ratio (ν_{23}). For ν_{13}, the experimental value is comparable, about 15%, to the theoretical one, which is the same as ν_{12}, i.e. 0.25. It is concluded that the influence of the thickness on the longitudinal – through-the-thickness Poisson's ratio may not be negligible.

The transverse – through-the-thickness Poisson's ratio (ν_{23}) is theoretically evaluated as 0.37 (see Table 3.4). It is the only elastic tensile property where the theoretical approach overestimates the experimental values. However, the theoretical value is in the same order of experimental results, within 12%. In addition, experimentally ν_{23} is greater than ν_{12} like it is the case in theory. As for E_2, the transverse Young's modulus, an extensometer is used to measure the axial displacement due to the brittleness of the material and the randomness of local deformations in the transverse direction. This leads to more dispersed data, particularly for the 20 mm thick specimens, with a coefficient of determination of the linear regression (R^2) of only 82%. Nevertheless, the experimental procedure is satisfactory and because a similar behaviour is observed on ν_{13}, it is concluded that the thickness may have an influence on ν_{23} as well.

3.6.2 Tensile Elastic Properties Analysis

Several reasons could explain the slight thickness effect on out-of-plane Poisson's ratios: the fibre volume fraction variation, the stiffening of the matrix during polymerisation, the misalignment of fibres and the non-uniform fibre/matrix adhesion.

It is computed using the theoretical approach presented in Section 1.3.2.2 that an increase of 1.2% of fibre volume fraction in a laminate increases E_1 by about 2% and E_2 by about 3.3% (see Table 3.3 and Table 3.4). These values are in contradiction with the experimental results where it is observed that E_1 increases and E_2 decreases with the thickness (Figure 3.34). According to theoretical relations, the computed in-plane and transverse – through-the-thickness Poisson's ratio, ν_{12} and ν_{23} respectively, are not influenced by an increase of 1.2% in the fibre volume fraction and these Poisson's ratios experimentally increase (see Table 3.4).

During the polymerization, an extra thermal reaction is observed in thicker plates resulting in an increase of the mechanical properties of the matrix (E_m, ν_m, k_m, G_m and K_m). Using a theoretical approach (Section 1.3.2.2), an increase of 1% of all matrix properties does not influence the longitudinal Young's modulus (E_1) and the in-plane Poisson's ratio (ν_{12}) of a laminate. However, the increase of 1% of all matrix properties increases theoretically the value of E_2 by about 0.9% and this is also in contradiction with experimental results (Figure 3.34).

It is clear that the misalignment of one layer of fibres has a larger effect on a thinner laminate than on a thicker one. Shephard *et al.* also mentioned that "any misalignment would be expected to affect the measured data" (Shepheard *et al.*, 2004). Using CLT formulas, Equation 1.5 and 1.6, it is possible to derive the following engineering constants: axial and transverse Young's moduli (E_x and E_y), in-plane Poisson's ratio (ν_{xy}) and in-plane shear modulus (G_{xy}) (Reddy, 1997).

$$E_x = \frac{\left(A_{11} * A_{22} - A_{12}^2\right)}{\left(t * A_{22}\right)} \tag{3.9}$$

$$E_y = \frac{\left(A_{11} * A_{22} - A_{12}^2\right)}{\left(t * A_{11}\right)} \tag{3.10}$$

$$\nu_{xy} = \frac{A_{12}}{A_{22}} \tag{3.11}$$

$$G_{xy} = \frac{A_{66}}{t} \tag{3.12}$$

Table 3.5 presents the theoretical values, using Equation 3.9 to 3.12, for different misalignment cases. The first example is for a misalignment of the fibre during the lay-up, so 50% of the fibres are properly oriented and the other 50% is equally misaligned with a ±5° angle. The second example is also for a misalignment of the fibre during the lay-up, but this time all the fibres are equally misaligned with a ±5° angle. The third example is for a misalignment during specimen cutting, so all the fibres are misaligned with an angle of +5°. The theoretical results show a decrease of the axial Young's modulus (E_x or E_1) by about 1.5% which is in accordance with experimental results when the thickness decreases (Figure 3.34). On the other hand, a misalignment of fibres does not influence significantly (0.2%) the transverse Young's modulus (E_y or E_2), while the in-plane Poisson's ratio (ν_{xy}) is increased by 10%. These last two observations are also not in agreement with the results obtained experimentally (Figure 3.34 and Figure 3.35).

Table 3.5 Theoretical comparison of misalignment influence on elastic properties of UD laminates

Misalignment / **Elastic properties**	**25% at +5° 25% at -5° 50% at 0°**	**50% at +5° 50% at -5°**	**100% at +5°**
Axial Young's modulus, E_x (GPa)	44.77 (↘0.7%)	44.43 (↘1.5%)	44.43 (↘1.5%)
Transverse Young's modulus, E_y (GPa)	9.32 (↘0.1%)	9.31 (↘0.2%)	9.31 (↘0.2%)
In-plane Poisson's ratio, ν_{12}	0.264 (↗5.4%)	0.277 (↗10.9%)	0.277 (↗10.9%)
In-plane shear modulus, G_{12} (GPa)	4.08 (↗3.3%)	4.21 (↗6.6%)	4.21 (↗6.6%)

Because of a higher number of layers in thicker specimens, it is noticeable that they contain a greater number of stitching lines, made of nylon, in the plane 2-3 (see Figure 3.36). The mix of stitching lines and matrix pockets close to them affect the material properties. To include the weakening effect of these extra materials, the rule of mixture is slightly modified. The modification allows to include terms for constituents with no stiffness as voids and stitching lines. Equation 1.21 is modified into Equation 3.13 by subtracting the void content (V_v) from the matrix volume fraction ($1-V_f$). Equations 1.22 to 1.25 are modified is the same way.

$$E_1 = E_f V_f + E_m (1 - V_f - V_v) \tag{3.13}$$

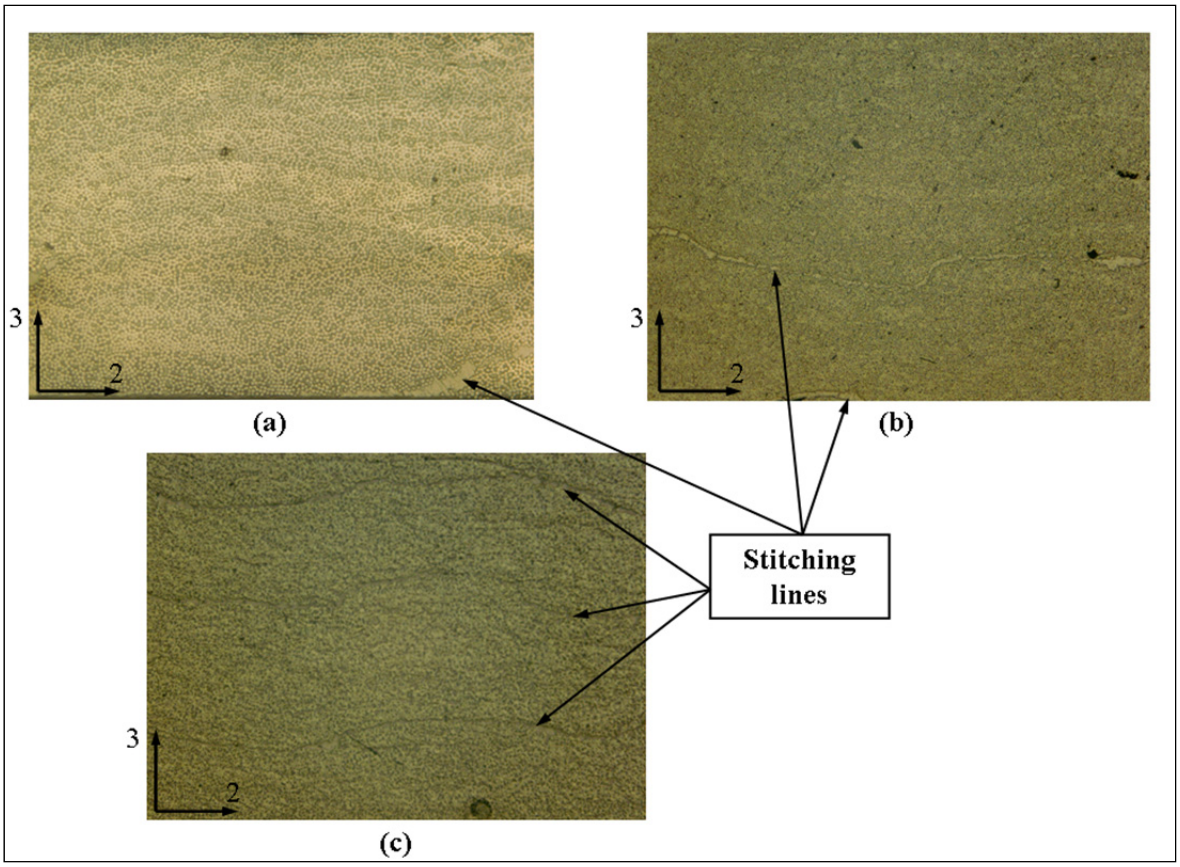

Figure 3.36 Micrographs of cross sections:
(a) Thin laminate, (b) Moderately thick laminate and (c) Thick laminate

According to this modified rule of mixture, sensitivity analyses are performed and results are presented in Table 3.6. The experimental fibre volume fraction (V_f) used, are the one measured and presented in Table 3.3. For the void content (V_v), even though the quality inspection shows no void (see Table 3.3), the values from 1% to 5% are used to represent the void content in thinner to thicker laminates The difference is computed against the material properties of a thin laminate without void (see first column of Table 3.4). The results show that only the longitudinal Young's modulus (E_1) increases as the experimental results do. The results show that the transverse Young's modulus (E_2) increases with the thickness contrary to the experimental results which decrease. For the Poisson's ratios (ν_{12}, ν_{13} and ν_{23}), the computed values obtained using the modified rule of mixture decrease with the thickness which differ from the experimental observations. The rule of mixture seems unable to

characterize the variation observed experimentally for the transverse Young's modulus, the Poisson's ratios and the shear moduli.

Table 3.6 Elastic properties using the modified rules of mixture

Thickness / V_f / V_v / **Elastic properties**	**1.5 mm** **60.3%** **1.0%**	**10 mm** **60.9%** **3.0%**	**20 mm** **61.5%** **5.0%**
Longitudinal Young's modulus, E_1 (GPa)	45.14 (↘0.06%)	45.50 (↗0.74%)	45.87 (↗1.54%)
Transverse Young's moduli, E_2 and E_3 (GPa)	9.48 (↗1.48%)	9.93 (↗6.34%)	10.44 (↗11.84%)
In-plane and longitudinal – through-the-thickness Poisson's ratios, ν_{12} and ν_{13}	0.249 (↘1.19%)	0.242 (↘3.77%)	0.236 (↘6.34%)
Transverse – through-the-thickness Poisson's ratio, ν_{23}	0.371 (↘0.09%)	0.370 (↘0.44%)	0.369 (↘0.84%)
In-plane and longitudinal – through-the-thickness shear moduli, G_{12} and G_{13} (GPa)	4.04 (↗2.21%)	4.30 (↗8.81%)	4.59 (↗16.27%)
Transverse – through-the-thickness shear modulus, G_{23} (GPa)	3.45 (↗1.50%)	3.62 (↗6.47%)	3.82 (↗12.09%)

However, the stitching lines and matrix pockets close to them, more present in thicker specimens, have an influence on adhesion properties which are influencing the elastic mechanical properties. The effect of a weaker matrix-fibre adhesion could be interpreted such that the longitudinal Young's modulus (E_1) will increase to tend to the elastic modulus of fibres and conversely the transverse Young's modulus (E_2) will decrease to reach the elastic modulus of the matrix. In addition, through-the-thickness deformations will be greater in a weaker matrix-fibre adhesion due to the presence of stitching lines. So, both Poisson's ratios in through-the-thickness planes (ν_{13} and ν_{23}) will increase with the thickness. All these assumptions behave exactly as observed experimentally.

3.6.3 Elastic Shear Properties Presentation and Analyses

The experimental results for the in-plane shear properties (G_{12}) are presented in Figure 3.37, Figure 3.38 and Figure 3.39 for specimens with a thickness of 1.5, 10 and 20 mm, respectively. Linear regressions are computed for shear deformation from 0 to 0.6%. With a closer examination of the data, the behaviour of the in-plane shear seems nonlinear. As Bogetti *et al.* did, the shear stress-strain curves could be described by piecewise linear approximations (Bogetti *et al.*, 2004a). In this case, the nonlinearity is approximated by piecewise linear steps of 0.2% of strain based on the ASTM standard for shear properties (ASTM, 2005). The piecewise linear functions representing the stress-strain curves of these material properties could be implemented in FE models as material specifications.

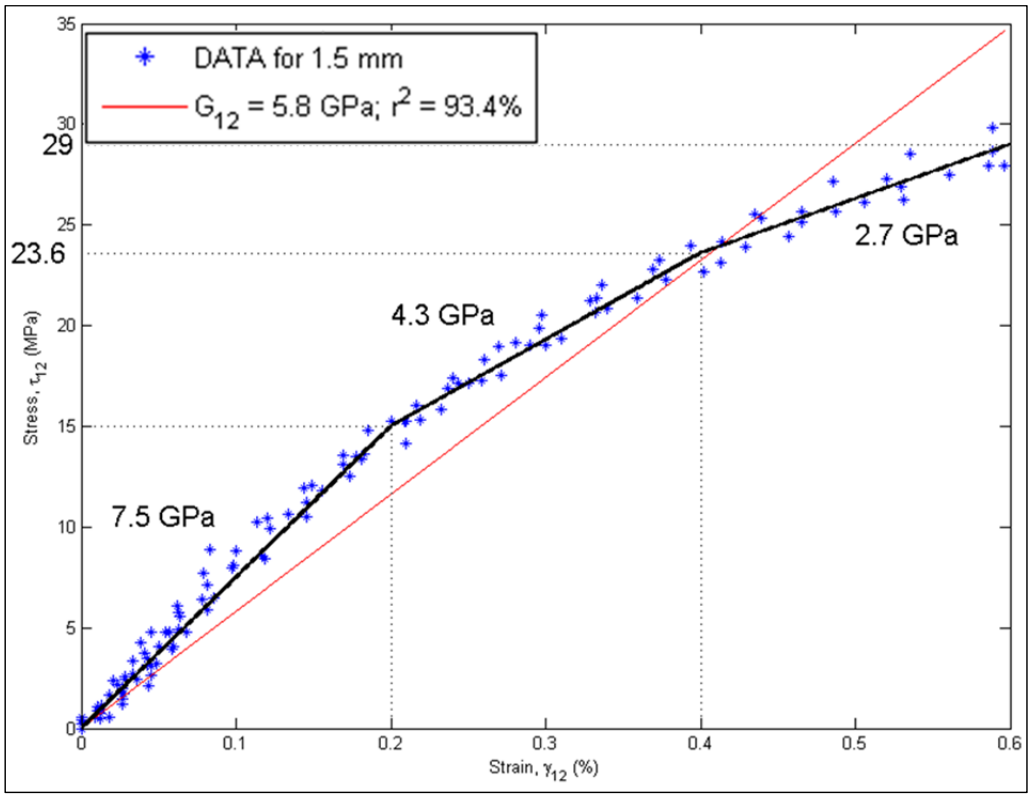

Figure 3.37 In-plane shear modulus (G_{12}) for a thickness of 1.5 mm

The same observation is made in Figure 3.40 for the longitudinal – through-the-thickness shear modulus (G_{13}). The nonlinearity is also observed by Chan *et al.* and it was concluded that the nonlinearity is due to the viscoelastic behaviour of a matrix-dominant property (Chan *et al.*, 2007). Other authors concluded that the nonlinearity is more due to an accumulation of matrix microcracking, which modified the stiffness of the composite material, preceding the eventual ultimate failure (Bogetti *et al.*, 2004b, Daniel *et al*, 2008; Hodgkinson, 2000). The nonlinearity cannot be observable for the transverse-through-the-thickness shear modulus (G_{23}) due to a lack of data because of an early matrix cracking under the strain gauges during tests (Figure 3.41), at a maximum shear deformation of about 0.14%. However, according to Chan *et al.*, G_{23} should be nonlinear too since it corresponds to a matrix-matrix shear property.

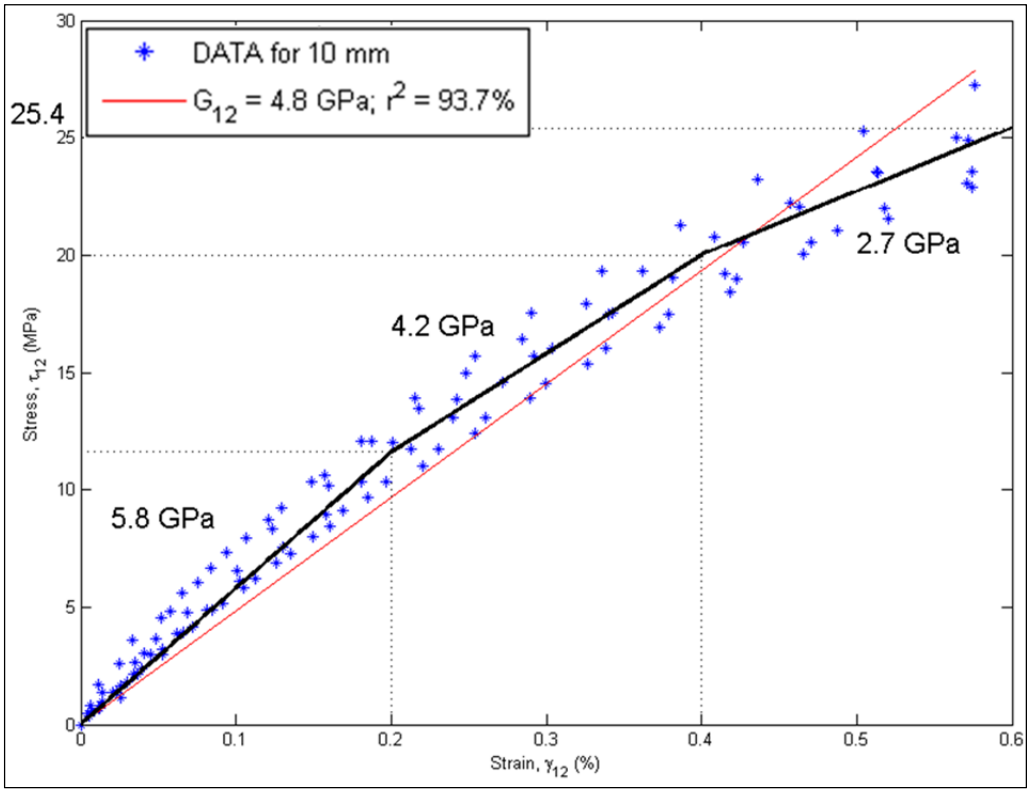

Figure 3.38 In- plane shear modulus (G_{12}) for a thickness of 10 mm

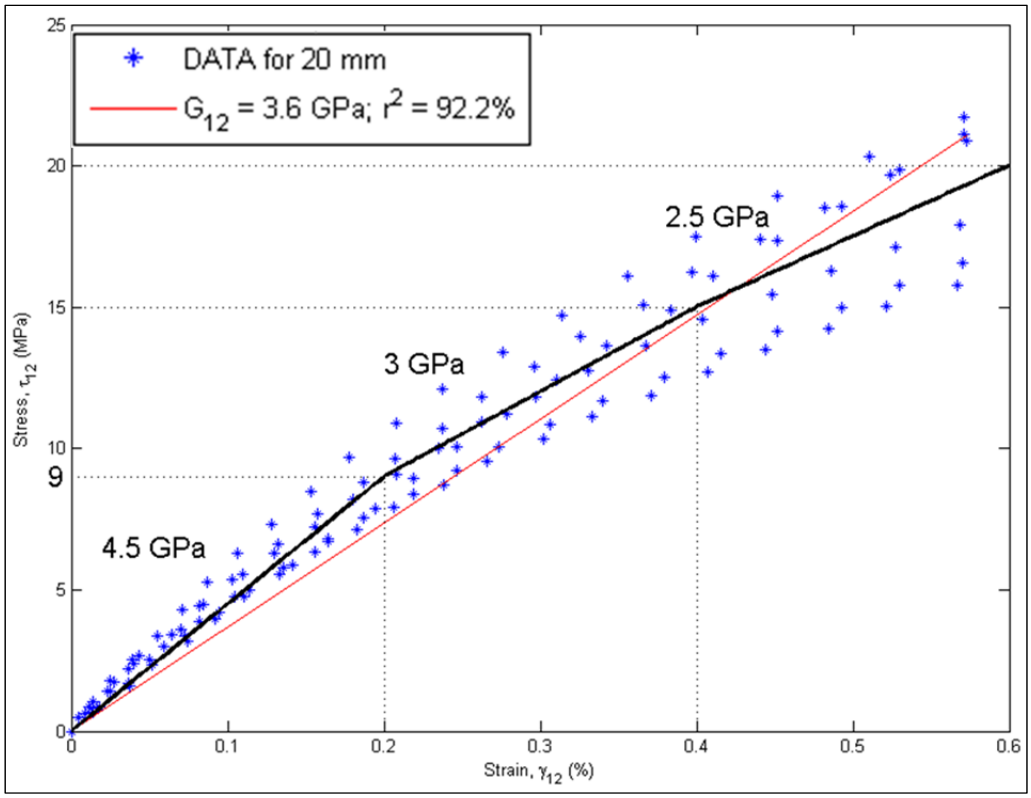

Figure 3.39 In- plane shear modulus (G_{12}) for a thickness of 20 mm

It is clear from Figure 3.37 to Figure 3.39, considering all regression coefficients (R^2) are over 92%, that the in-plane shear modulus is influenced by the thickness. The in-plane shear moduli, obtained from single linear regressions (from 0 to 0.6% of strain), are 5.8, 4.8 and 3.6 GPa for the 1.5, 10 and 20 mm thick specimens, respectively. In addition, although a thickness effect is observed, all values are in an according range with the theoretical value of 4 GPa (see Table 3.4). The experimental procedure is, therefore, suitable even if the thickness effect is exaggerated in the first evaluated step, from 0 to 0.2% of strain. A quick calculation using a range of strain from 0.2 to 0.6%, as proposed in ASTM standards (ASTM, 2005), also shows that the thickness has an effect with in-plane shear moduli of 3.5, 3.45 and 2.75 GPa for thicknesses of 1.5, 10 and 20 mm, respectively (not shown but using data from Figure 3.37 to Figure 3.39). In this case, the theoretical value overestimates the experimental results as in the case of ν_{23}.

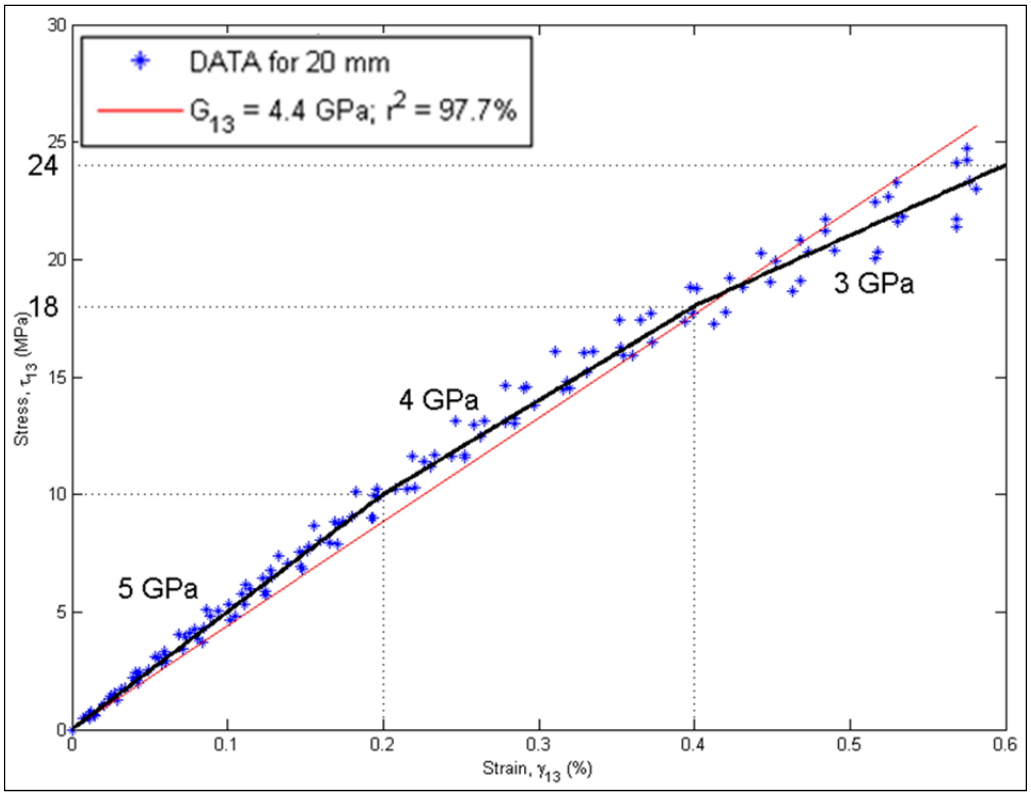

Figure 3.40 Longitudinal – through-the-thickness shear modulus (G_{13})

The influence of the thickness cannot be verified on both through-the-thickness shear moduli (G_{13} and G_{23}), because it is not possible to make the V-notches following the ASTM requirements in geometry on specimens smaller in thickness than 20 mm. However, results are obtained for 20 mm thick specimens with a coefficient of determination greater than 96% (see Figure 3.40 and Figure 3.41). The experimental values for G_{13} and G_{23} are respectively of 4.4 and 4 GPa. These experimental values are analogous, although superior, to theoretical values of 4 and 3.5 GPa, since G_{13} is greater than G_{23}.

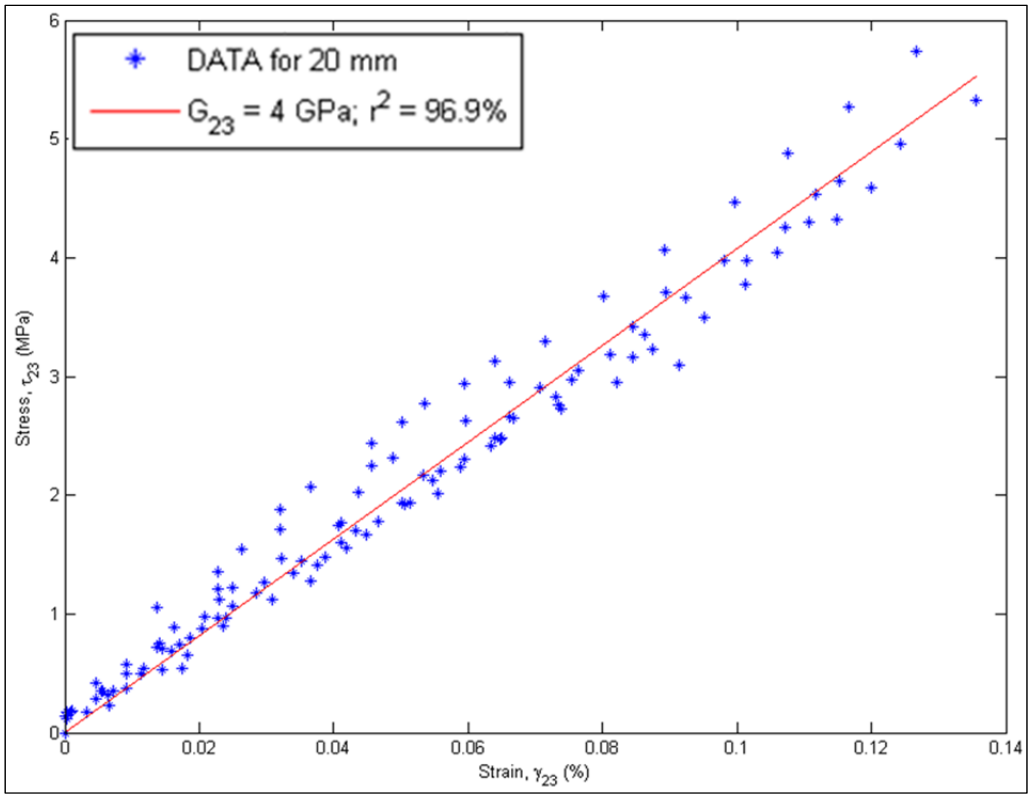

Figure 3.41 Transverse – through-the-thickness shear modulus (G_{23})

3.6.4 Failure Properties Analyses

This section presents the results when these experiments are brought up to failure. So, the effect of the thickness is discussed on the longitudinal and transverse ultimate tensile strengths and on the in-plane shear strength, as well as their modes of failure. In addition, through-the-thickness strengths are also presented with their failure modes.

3.6.4.1 Longitudinal Tensile Strength

In the fibre direction with thin specimens, the mode of failure is “explosive” as expected (see Figure 3.42). The term “explosive” is used to represent the amount of energy accumulated in the fibres and when the failure occurs, this energy projects matrix and fibre fragments as in

an explosion. The measured ultimate tensile stress for specimens of 1.5 mm thick is 1430 MPa with a standard deviation of 1.64%. This value is comparable to the longitudinal ultimate tensile strength of a published unidirectional E-glass/epoxy composite, 1400 MPa (Berthelot, 2005). For the 10 mm thick specimen, the longitudinal ultimate tensile strength measured was 540 MPa with a standard deviation of 27.8% prior of using the lateral support apparatus shown in Figure 3.24. A higher level of longitudinal ultimate tensile strength, 790 MPa, is reached using lateral supports which prevent the crushing in the grips. In addition, the standard deviation is reduced at 7.11%. For thicker specimens, 20 mm thick, the lateral supports were always used. The longitudinal ultimate tensile strength for thicker specimens is 510 MPa with a standard deviation of 13.9%.

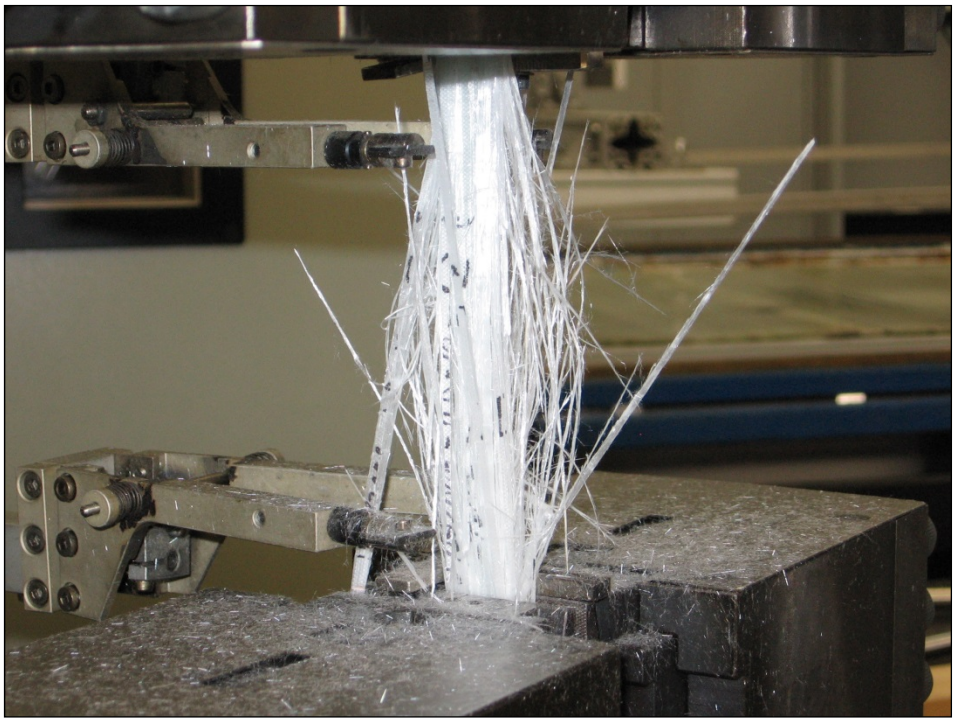

Figure 3.42 Example of a typical mode of failure for a tensile test in the fibre direction of a UD straight specimen

The use of lateral supports permits to obtain a mode of failure which almost looks like an "explosive" one (see Figure 3.43). Nevertheless, experimental results are still far below the reference value of 1400 MPa. This difference is not due to a thickness effect, but could rather be caused by a 3D stress state at the tip of the grips. The strains at ultimate stresses provide additional pertinent information to this observation. The longitudinal ultimate tensile strains are only around 1% for the thicker specimens (10 and 20 mm thick) instead of about 3% reached for specimens with a thickness of 1.5 mm. More investigation should be performed to find a way to apply an appropriate longitudinal tensile load in the gauge length, which will avoid a 3D stress state at the tip of the grips and help to reach an accurate failure stress allowing the evaluation of the thickness effect on properties at failure. Also, instead of using strain gauges, which failed with matrix cracking on surface, a digital extensometer (grid of points painted on specimens with digital cameras) could be used to record displacements and compute stresses, strains, modulus and Poisson's ratios.

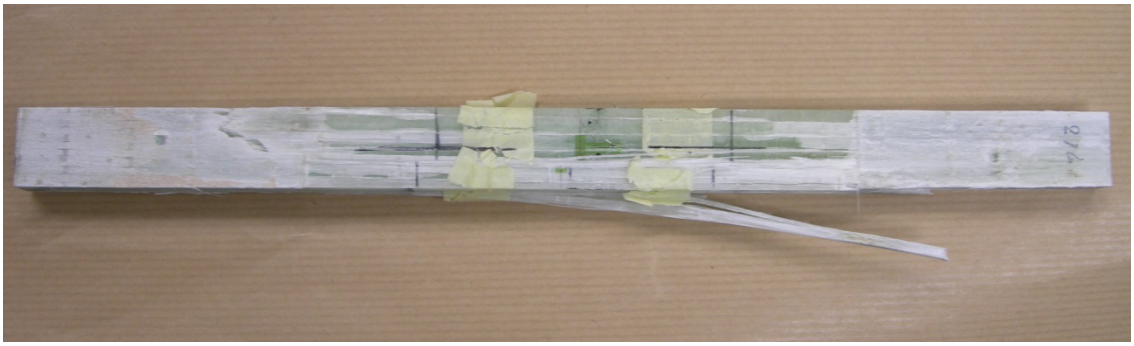

Figure 3.43 Example of the failure for thicker UD specimens under longitudinal tensile load using lateral supports

3.6.4.2 Transverse Tensile Strength

In the direction transverse to the fibres, the typical failure mode is shown in Figure 3.44. The ultimate tensile strengths in the transverse direction are 28, 22 and 23 MPa for specimens of 1.5, 10 and 20 mm thick, respectively. Their standard deviations are respectively 6.28%, 12.6% and 9.08%. Experimental values are all lower than a published transverse ultimate

tensile strength for a similar material, 35 MPa (Daniel and Ishai, 1994). The effect of the thickness on the transverse failure stress is not obvious. The brittleness of this material and the randomness of local deformations in the transverse direction may cause fluctuation in results. In the transverse direction, it is not possible to compare the strains at failure due to the brittleness and the randomness of the failure. In this case particularly, a digital extensometer to measure displacements and compute stresses, strains, modulus and Poisson's ratios would be beneficial.

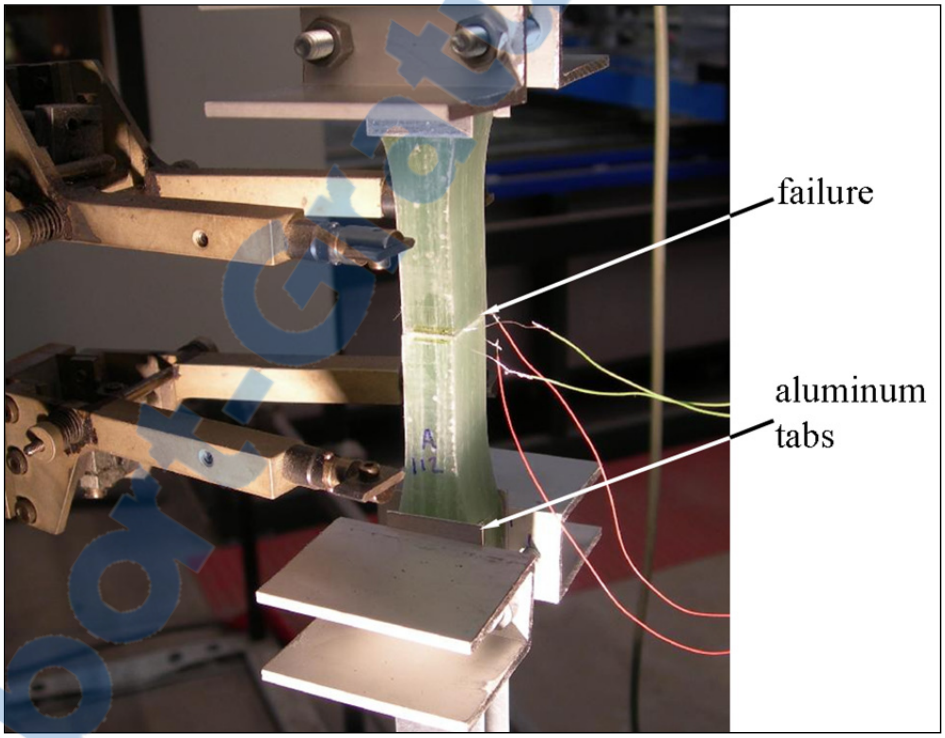

Figure 3.44 Typical failure mode under a tensile load in the direction transverse to the fibres

3.6.4.3 In-plane Shear Strength

Similarly, for the behaviour observed for the in-plane shear modulus, the thickness has an influence on the ultimate in-plane shear stress. A typical failure of the in-plane shear test is presented in Figure 3.45. Other modes of failure for different orientations are shown in Figure 3.46. The asterisk for the plane 2-1 is to identify the crushing caused by the tip of the grips. Experimental results give 73, 65 and 57 MPa from thin to thick specimens. The respective standard deviations are 4.14%, 1.15% and 1.51%. The value of the ultimate in-plane shear strength for the 1.5 mm is really close to the published one for E-glass/epoxy composite, 70 MPa (Berthelot, 2005; Daniel and Ishai, 1994). That similarity in strength, as well as the standard deviation all below 5%, shows the efficiency of the experimental procedure and the values for the other thicknesses must be trustworthy. The decrease in value of the shear strength confirms that the thickness has an effect on shear moduli and strength. To prevent a premature failure of the rosette due to the brittleness of the resin, an inspection method using a digital extensometer to measure displacements and compute stresses, strains, modulus and Poisson's ratios would be essential.

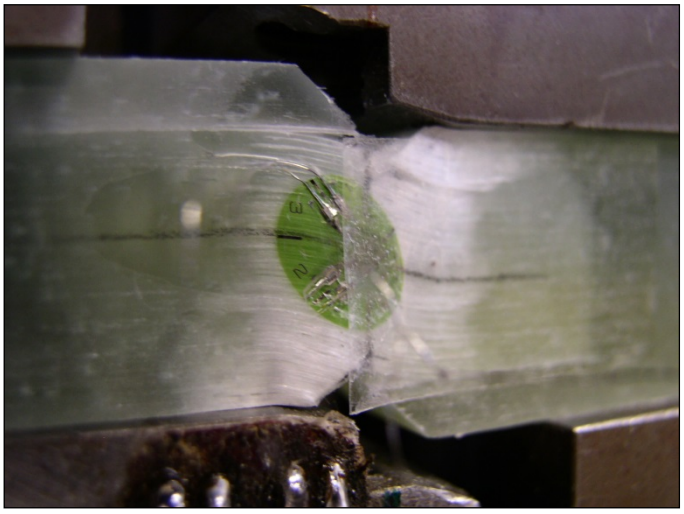

Figure 3.45 Example of a typical failure for an in-plane shear test of a UD V-notched specimen

3.6.4.4 Through-the-thickness Shear Strength

For the ultimate longitudinal – through-the-thickness shear strength (plane 1-3), the experimental value of 58 MPa with a standard deviation of 1.44% is similar to ultimate in-plane shear strength. That proves the isotropy of this material in the plane 2-3. In addition, the mode of failure for in the plane 1-3 is identical to the one in the plane 1-2 (see Figure 3.46). For the ultimate transverse – through-the-thickness shear strength (plane 2-3), the experimental value is only 6.2 MPa with a standard deviation of 9.85%. The failure mode of the transverse – through-the-thickness shear is also shown in Figure 3.46. This strength value and the failure mode have no other reference for unidirectional E-glass/epoxy material. Since the thickness effect cannot be studied on these mechanical properties due to geometric restriction, another shear test shall be developed to allow this evaluation.

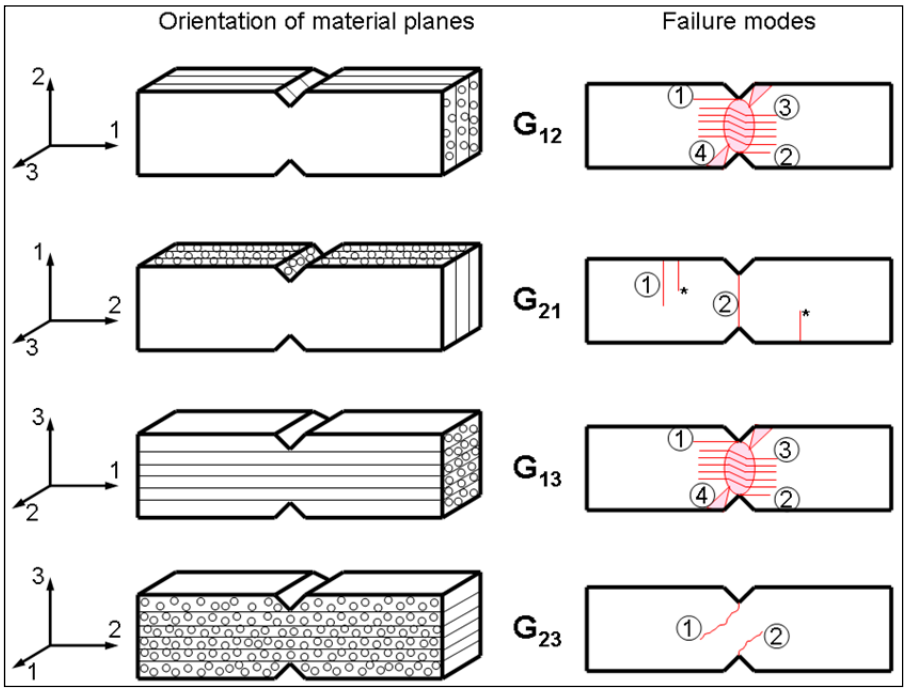

Figure 3.46 Schemes of typical V-notched failure modes for different orientations

3.7 Conclusion and Future Works

In conclusion, the goal of this section of the research was to evaluate the thickness effect on all nine elastic properties of unidirectional composite laminates. The studied composite was a unidirectional E-glass/epoxy laminated composite manufactured using a vacuum infusion process. Experiments showed the repeatability of the manufacturing process and that the production of high quality laminates with a fibre volume fraction greater than 60% was possible.

Tensile tests in the direction of fibres revealed that the longitudinal Young's modulus (E_1) is not significantly influenced by increasing the thickness. The same observation is made for the transverse Young's modulus (E_2). Since the through-the-thickness Young's modulus (E_3) is assumed equal to E_2, it is then considered not to be influenced by the thickness. The thickness does not significantly influence the in-plane Poisson's ratio (ν_{12}). Both through-the-thickness Poisson's ratios (ν_{13} and ν_{23}) seem to be lightly influenced, about 10%, with the increasing thickness due to a weakness adhesion in the direction of the thickness caused by a larger amount of stitching lines in the same cross-section.

Considering the shear properties, it is observed that the longitudinal-transverse shear modulus (G_{12}) is significantly influenced by the thickness, around 38%. It was predictable that the thickness will have an effect on shear properties due to the fact that many theories were developed to include the shear effect for thick composite laminates (Section 1.3.1). In addition, experimental results show that the in-plane shear modulus behaves nonlinearly due to an accumulation of matrix microcracking, which modified the stiffness of the composite material, preceding the eventual ultimate failure. The nonlinear behaviour is also observed on the longitudinal – through-the-thickness shear modulus (G_{13}). However, the nonlinearity was not observed on the transverse-through-the-thickness shear modulus (G_{23}) due to a lack of data cause by premature failure of the strain gauges due to matrix cracking under them. The thickness effect could not been evaluated on G_{13} and G_{23} due to the ASTM requirements of specimen dimensions (ASTM, 2005).

Furthermore, the thickness effect is also examined on longitudinal and transverse tensile strengths and on the in-plane shear strength. A decreasing of the longitudinal strength is observed but it is not clear that the thickness has an influence. The early failure is possibly due to the difficulty to correctly load the specimens in the fibres direction without inducing a 3D state of stress at the tip of the grips. In the transverse direction, no significant thickness effect is observed. In agreement with the in-plane shear modulus, the ultimate in-plane shear stress is subjected to a significant thickness effect, showing a decreasing of 22% when the thicknesses vary from 1.5 to 20 mm. These conclusions have been presented at the Sixth Canadian-International Composites Conference on Development and Commercialization of Composite Materials and Technologies in 2007 (Duchaine *et al.*, 2007).

The next chapter will present the influence of the thickness on tensile properties for different lay-up configurations. The UD elastic properties developed in this part of the research will then be used to correlate the results using CLT and FEM analysis.

Future developments in the experimental procedure should include a method of inspection to reduce oscillations in the signal recorded from the strain gauges. This new inspection method should also avoid the interruption of the signal caused by a premature failure of the strain gauges due to light matrix cracking, particularly observed during shear tests. In addition, another shear test should be advocated to evaluate the thickness effect on through-the-thickness shear mechanical properties such as moduli and ultimate strength. This other shear test will be restricted in using the same material, the same manufacturing process and the same cross sections. Furthermore, to extend the study of the effect of thickness on the longitudinal stress at failure, the load should be properly applied on thick UD specimens without inducing stress concentrations.

CHAPTER 4

THICKNESS AND LAY-UP EFFECT ON ELASTIC AND ULTIMATE TENSILE PROPERTIES

The main objective of this chapter is to study the influence of the thickness on the elastic and failure tensile properties using two different lay-up configurations. The elastic tensile properties are the elastic modulus (E_x), the in-plane Poisson's ratio (ν_{xy}) and the through-the-thickness Poisson's ratio (ν_{xz}). The failure tensile properties are the maximum strain at failure and the ultimate tensile strength. The two studied lay-up configurations are a cross-ply and a quasi-isotropic made of unidirectional (UD) plies of the same E-glass/epoxy material used in Chapter 3. The laminated composite panels are manufactured using the vacuum infusion process described in Chapter 3. In order to achieve this objective, a total of forty-eight specimens with three different thicknesses are tested in tension using the methodology presented in Chapter 3. A detailed description of the experimental procedures is given in the following section. Results and the failure modes are then discussed and compared to analytical values computed using the classical lamination theory (CLT) and those form finite element analyses (FEA).

4.1 Design of Experiments

Two different lay-up configurations are evaluated, a cross-ply and a quasi-isotropic. A cross-ply laminate is made using 0° and 90° layers of unidirectional (UD) dried glass fibres of the same material used in Chapter 3. A common quasi-isotropic laminate, using 4 different orientations, is made of 0°, 90° and ±45° layers of UD or fabric of dried or pre-impregnated fibres. In a quasi-isotropic lay-up, the angles at which the layers of fibres are oriented are related to the number of different orientations in the lay-up (i.e. for 4 different orientations, each angle is at every 180°/4 = 45°). In this study that evaluates the thickness effect, all

configurations are scaled at a sub-laminate level, thus no plies with the same orientation are adjacent.

The three thicknesses of reference (1.5, 10 and 20 mm) are used, assuming an average thickness of a single cured ply of 0.185 mm. The cross-ply lay-up is identified as $[0/90]_{n\mathrm{S}}$ where n is equal to 2, 14 or 28 to achieve the thicknesses of reference. Depending on the value of n, it represents a thin laminate with a thickness of about 1.5 mm, a moderately thick laminate with a thickness of about 10 mm and a thick laminate with a thickness of about 20 mm. The quasi-isotropic lay-up is identified as $[-45/90/45/0]_{n\mathrm{S}}$ where n is equal to 1, 7 or 14, giving a thin, a moderately thick or a thick laminate. In this experiment, eight specimens are tested for each lay-up configuration of each thickness for a total of forty-eight specimens. The design of experiments for this study is presented in Table 4.1.

Table 4.1 Design of experiments for cross-ply and quasi-isotropic laminates

Thickness / **Lay-up configuration**	**8 plies (1.5 mm)**	**56 plies (10 mm)**	**112 plies (20 mm)**
Cross-ply $[0/90]_{nS}$ where n = 2, 14 and 28	8	8	8
Quasi-isotropic $[-45/90/45/0]_{nS}$ where n = 1, 7 and 14	8	8	8
Number of specimens	**16**	**16**	**16**

4.2 Experimental Results

The same E-glass/epoxy composite material which was used to determine the thickness effect on the UD mechanical properties in Chapter 3 is used in the lamination of the cross-ply and quasi-isotropic testing panels. The laminated composite panels are manufactured using the same vacuum infusion process as in Chapter 3. The same parameters used for the UD

laminates are used for this part of the study like the degassing time, the vacuum pressure and the flow rate. The complete methodology for the manufacturing, the preparation and the testing of the specimens is presented in Chapter 3.

4.2.1 Laminates Quality

The pattern of the resin flow is different during the manufacturing of a cross-ply lay-up from a UD lay-up. The time of the resin infusion is slightly faster for a cross-ply laminate. In a cross-ply laminate, the fibres in adjacent layers are not squeezed together, but they are crossed on top of one another allowing more room for the resin to flow freely. The difference in infusing pattern and time is less significant between a quasi-isotropic laminate and a cross-ply laminate.

Since the resin has more room to flow, more resin is trapped in laminates where the fibres are crossed. So, for the same volume, less fibres and more resin are contained in these laminates, in comparison with a UD laminate. It is well known that the material of the fibres is heavier than the one of the resin. Therefore, the density shall be lower for cross-ply and quasi-isotropic lay-ups than for a UD laminate. Since the density is directly related to the fibre volume fraction, the fibre volume fraction shall also be lower in cross-ply and quasi-isotropic lay-ups. The following values prove these assumptions. The average density and the average fibre volume content (with their standard deviation within parentheses) of UD laminates are respectively 2.053 g/cm^3 (1.4%) and 60.9% (1.0%), according to Table 3.3. For the cross-ply laminates, the average density and the average fibre volume content are 2.00 g/cm^3 (0.6%) and 57.7% (1.1%), respectively. For the quasi-isotropic laminates, the average density and the average fibre volume content are respectively 2.00 g/cm^3 (0.7%) and 57.9% (1.0%).

Similarly, the cross-ply and the quasi-isotropic lay-up configurations have an average cured ply thickness larger than the UD laminate one. On UD coupons an average ply thickness of 0.185 mm is measured with a standard deviation of 0.2% (for the next values the standard deviation will be attached within parentheses). For the cross-ply coupons, the average ply

thickness is 0.194 mm (0.6%) and for the quasi-isotropic coupons, the average ply thickness is 0.198 mm (0.7%). The difference comes for the UD when the fibres are well fit one on top of the other and for the other two lay-ups when the fibres are waving and crossing each other. This fact is illustrated in Figure 4.1 for a UD lay-up and a cross-ply lay-up of six layers of fibres.

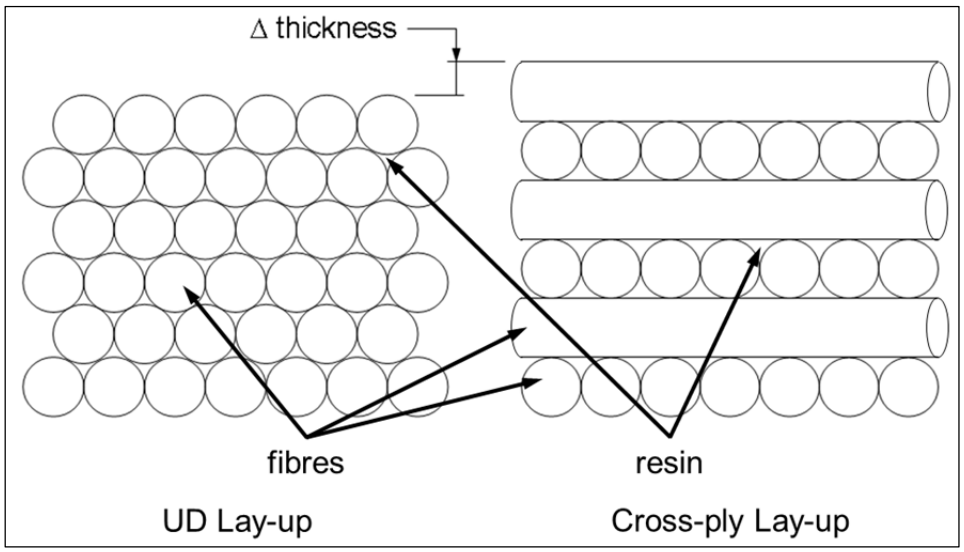

Figure 4.1 Thickness comparison between UD and Cross-ply lay-ups

The consistency of the vacuum infusion manufacturing process and the quality of all laminates are also proven by the very low percentage of voids contained in the coupons. It is -0.4% (0.3%) in UD laminates and it is -0.3% (0.3%) and -0.4% (0.1%) for cross-ply and quasi-isotropic laminates, respectively. As previously explained, the negative values are due to accumulation of tolerances on measurement tools used in the calculation of void content.

4.2.2 Elastic Tensile Properties

Only the tensile test is performed for each lay-up configurations and the three studied thicknesses. The tensile test is chosen due to its simplicity in the geometry of the coupons and the tooling required. Eight coupons are used for each case, forty-eight coupons in total.

The three elastic properties are obtained from this test. They are the Young's modulus in the axial direction (E_x), the Poisson's ratio in the in-plane transverse direction (ν_{xy}) and the Poisson's ratio in the through-the-thickness direction (ν_{xz}). The experimental values for both lay-up configurations and all the thicknesses are presented and discussed in the following paragraphs. For a complete set of elastic properties, transverse tension and V-notch shear tests need to be performed.

4.2.2.1 Elastic Tensile Properties of Cross-ply Lay-up

Regarding the Young's modulus in the axial direction for the cross-ply lay-up, the value of E_x for thinner specimens is 26.9 GPa with a standard deviation of 1.64%. For the moderately thick and the thick specimens, the measured E_x (with their standard deviation) are respectively 26.7 GPa (6.69%) and 28.4 GPa (11.0%). Due to the fact that large deviations are observed within the results for thicker specimens; it is concluded that the thickness does not influence the axial Young's modulus for cross-ply lay-ups. The values of the axial Young's modulus are graphically represented in Figure 4.2.

In Figure 4.2, the values of the in-plane Poisson's ratio (ν_{xy}) are also presented for the cross-ply lay-up. For thinner laminates, ν_{xy} equals 0.122 with a standard deviation of 8.91%. The values for the moderately thick and thick laminates are 0.096 and 0.091, respectively, with scattered data providing standard deviations of 7.67% and 5.57%. The deviations observed are not that large and the values for the three thicknesses are within a range of about 25%, it is concluded that the thickness have an influence the in-plane Poisson's ratio.

The through-the-thickness Poisson's ratio (ν_{xz}) is the third result for the cross-ply lay-up to be presented in Figure 4.2. The values from thinner to thicker laminates are 0.359, 0.341 and 0.358. Scattered data observed on these coupons lead respectively to standard deviations of 4.24%, 7.16% and 5.79% for this mechanical property. Due to large scatters obtained within

coupons, it is again concluded that through-the-thickness Poisson's ratio is not altered by the thickness of cross-ply laminates.

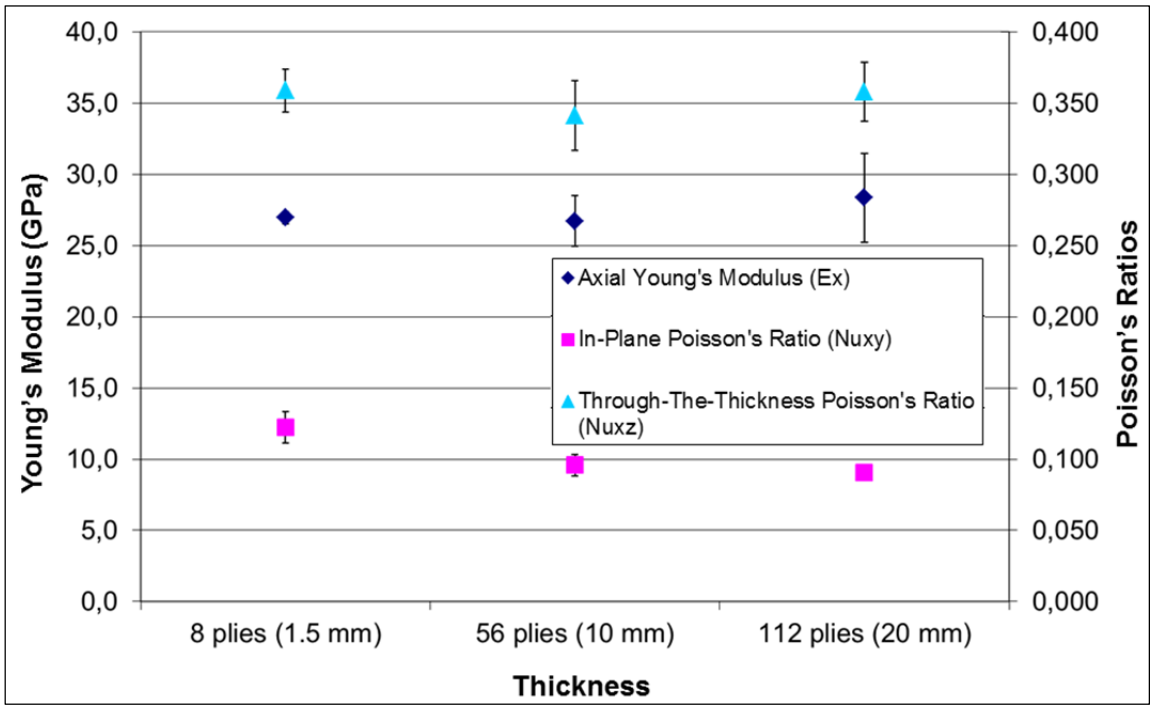

Figure 4.2 Elastic properties of cross-ply lay-ups from a tensile test

4.2.2.2 Elastic Tensile Properties of Quasi-isotropic Lay-up

Figure 4.3 shows the effect of the thickness on the elastic properties for the quasi-isotropic lay-up. The axial Young's Modulus (E_x), for the thinner specimens, is an average value of 20.8 GPa with a standard deviation of 3.00%. A similar value, 20.9 GPa (3.40%), is obtained for the moderately thick laminates. However, the difference is significant for the thicker laminates. The average value for E_x is 23.5 GPa with a standard deviation of 3.79%. Since the interval of results for the thicker laminate is not overlapping with the others; the thickness may influence the axial stiffness of quasi-isotropic laminates. In addition, bringing the results with respect to the same fibre volume fraction of 60%, it makes the trend clearer. However,

additional information from the experiments or other test results is needed to confirm this trend.

Also in Figure 4.3, ν_{xy} are presented with respect to the thickness. For this property, it is the value for the thinner laminates, 0.284 (4.62%), which seems lower than the other two values. The standard deviations of the test give a slight overlap of the data, allowing as a conclusion that the thickness does not have a significant influence on the in-plane Poisson's ratio of quasi-isotropic laminates. The values for the moderately thick and the thicker laminates are respectively, 0.305 (2.83%) and 0.301 (6.16%).

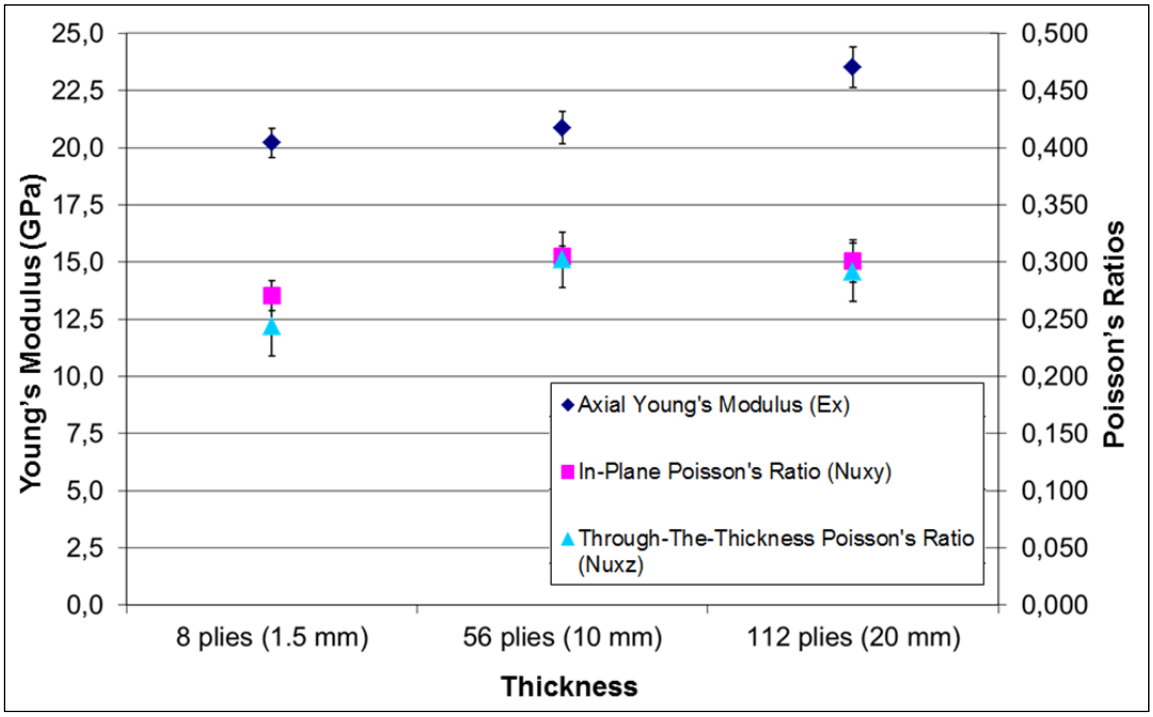

Figure 4.3 Elastic properties of quasi-isotropic lay-ups from a tensile test

The third value to be presented in Figure 4.3 is ν_{xz}. The values from thinner to thicker laminates are 0.269, 0.302 and 0.291. Large scattered data are observed on this mechanical property leading to standard deviations of 9.45, 8.03 and 8.79, respectively to the thicknesses. It is, therefore, concluded that the through-the-thickness Poisson's ratio is not influenced by the thickness of quasi-isotropic laminates due to large scatters obtained within

coupons. In respect to these results, the name of quasi-isotropic laminates seems to be well appropriate since the Poisson's ratios in the two studied planes (xy and xz) are similar as for isotropic materials for which the material properties are identical in all the directions.

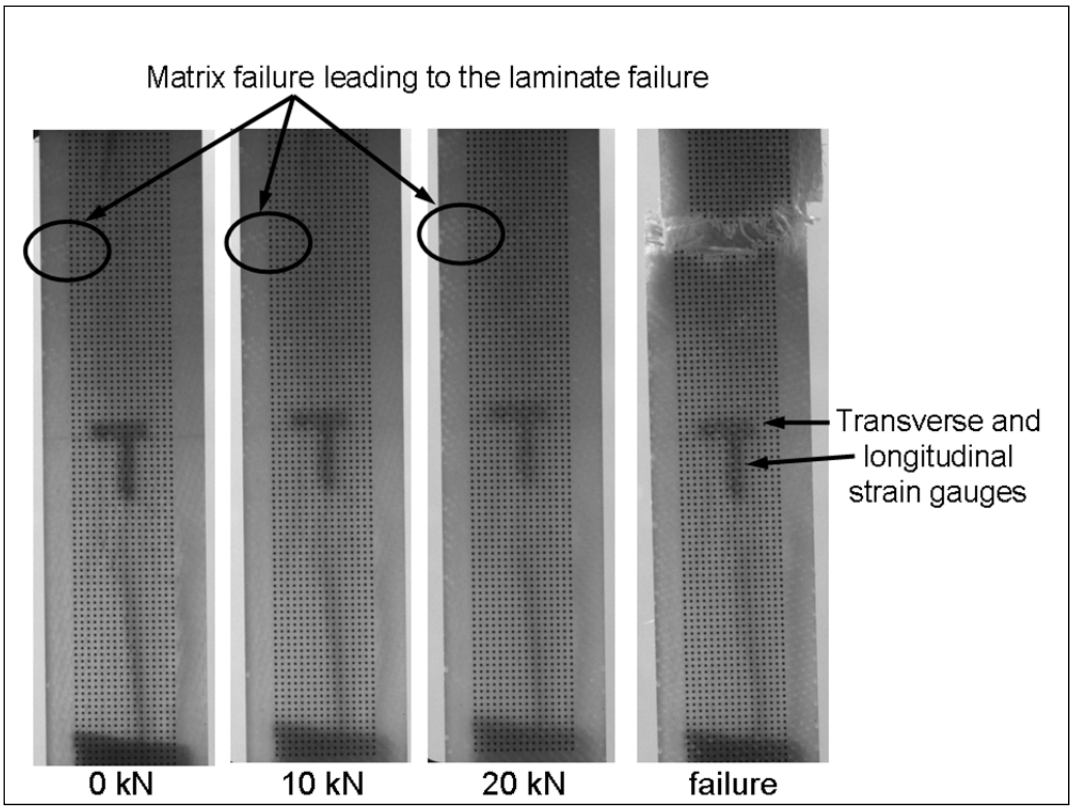

Figure 4.4 Evolution of a random failure with respect to the loading on a thin quasi-isotropic laminate

A trend seems to be suggested that lower standard deviations are observed for thinner laminates. It may be the reason why ASME (ASTM, 2005; 2006) and others (Hodgkinson, 2000) recommend to perform the testing on coupons thinner than 2 mm. As mentioned in the previous chapter, another reason why large standard deviations are observed is the randomness of failure in a fragile material like epoxy. The randomness of failure makes it difficult to properly record the strain using short gauges as shown in Figure 4.4.

4.2.3 Stress and Strain at Failure

In this section, even if it is not the main purpose of this project, the stress and the strain at failure are presented for the three thicknesses and the two lay-ups. Apart a comparison on magnitudes of the stress and strain at failure, differences and similarities about the failure modes are discussed.

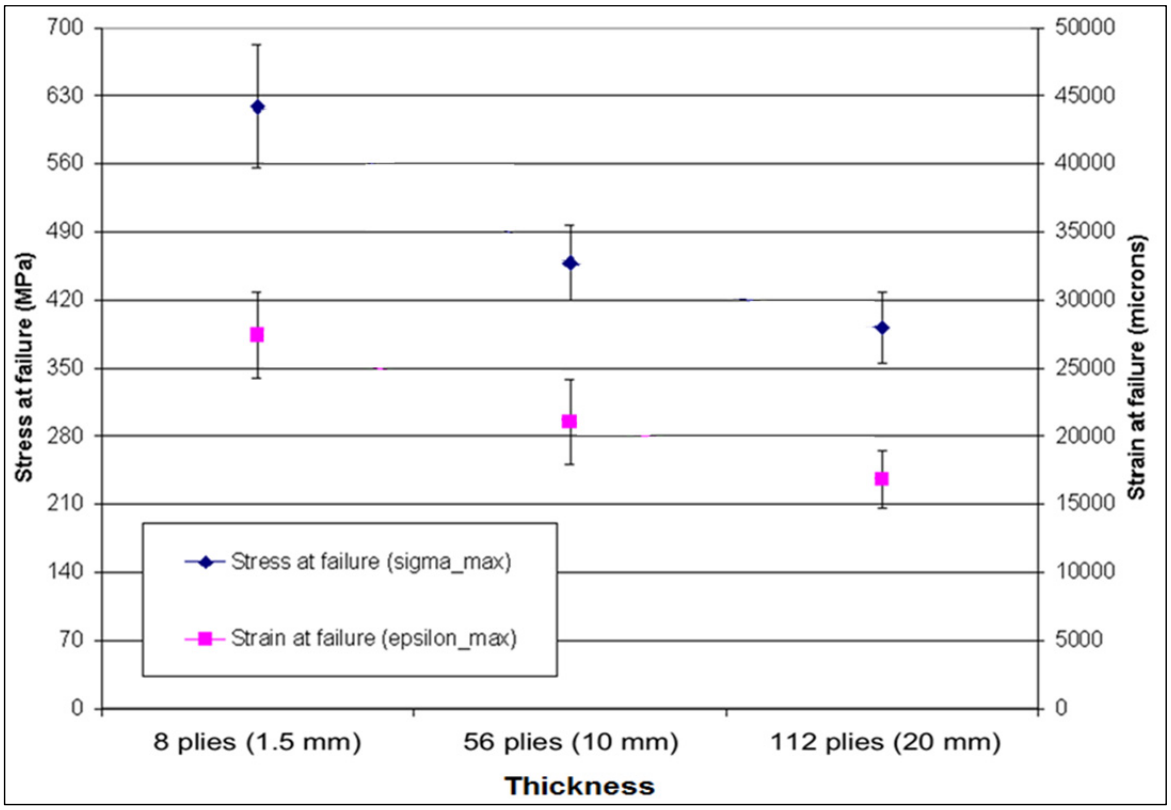

Figure 4.5 Failure properties of cross-ply lay-ups from a tensile test

The results for the cross-ply laminates show a decreasing of ultimate stress and strain. Both failure properties have the same behaviour as shown in Figure 4.5. The values of the stress at failure (and their standard deviation), from thinner to thicker laminates, are respectively 619 MPa (10.3%), 458 MPa (8.4%) and 392 MPa (9.4%). In terms of strain, the corresponding values are 27000μ (11.0%), 21000μ (14.1%) and 17000μ (15.7%). Even with significant scatters in the sampling, the results show a different behaviour at failure for the

thinner laminates compared to the two thicker ones. Photos in Figure 4.6 confirm that the failure mode is different for the thicker laminates, where the failure occurred in the grip region. This failure mode could be an explanation of the lowest values obtained for moderately thick and thicker laminates.

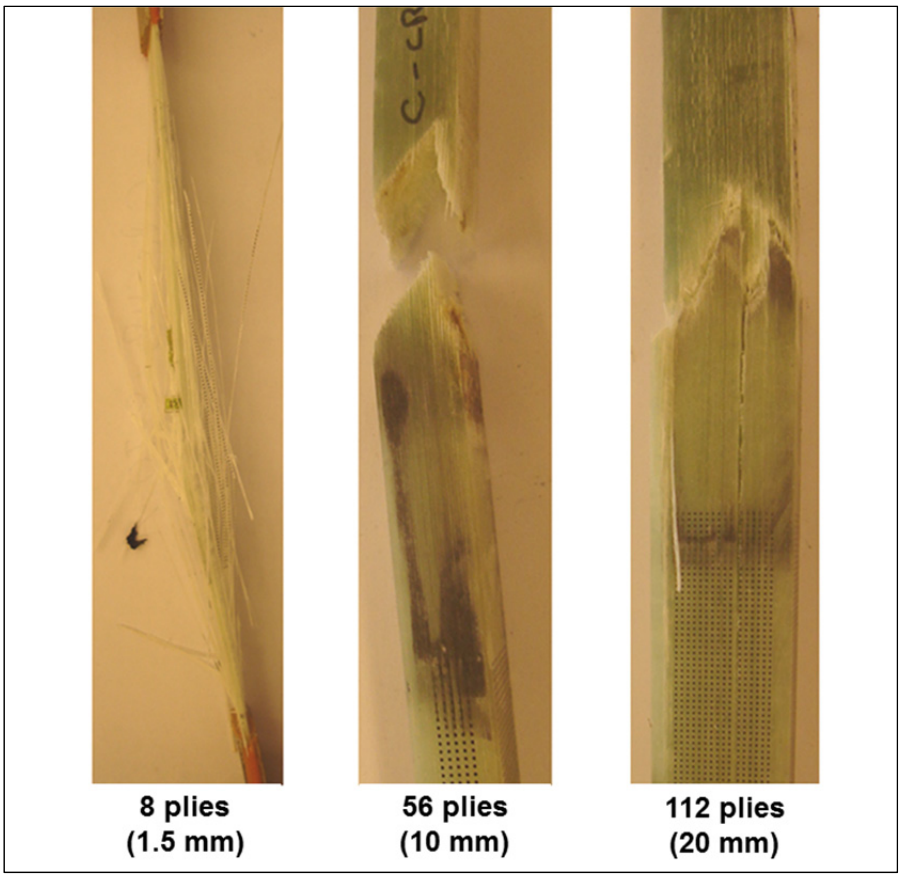

Figure 4.6 Failure modes for the three thicknesses of a cross-ply lay-up

The behaviour for the quasi-isotropic lay-up is different, see Figure 4.7. The stress at failure for the thinner laminates is 334 MPa with a standard deviation of 8.5%. The moderately thick laminates give a stress at failure slightly higher of 411 MPa (7.0%). For the thicker laminates, the stress at failure goes down to 377 MPa with 6.5% of scatters. Due to significant scatters in the sampling, it could only mean that the stress at failure is not influenced by a change in thickness for quasi-isotropic lay-ups. Regardless of the large standard deviations observed, the thickness does not influence the strain at failure. For the

three thicknesses, the values of strain at failure are all around 24000μ with standard deviations of 11.0%, 8.7% and 31.1% from thinner to thicker laminates.

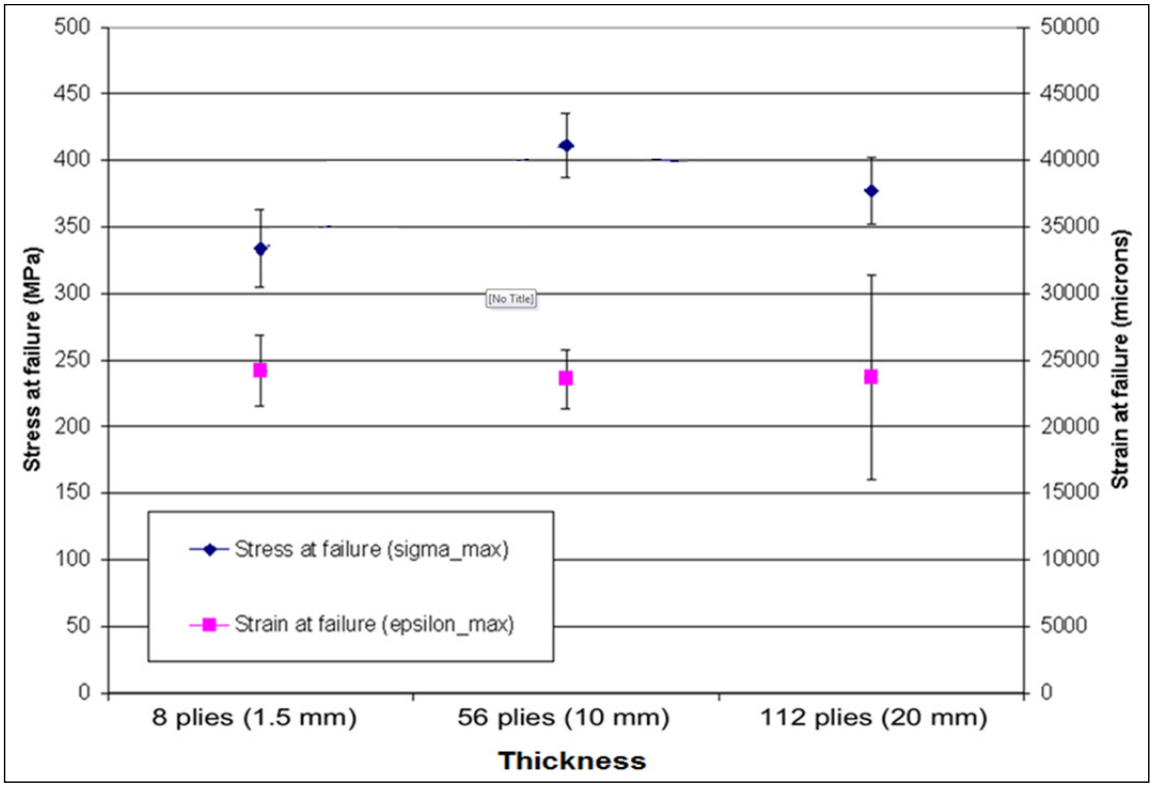

Figure 4.7 Failure properties of quasi-isotropic lay-ups from a tensile test

The failure modes are more similar for the three thicknesses. Photos are presented in Figure 4.8. On the photos, the four different orientations of the fibres are particularly obvious for the thinner specimen. On the photo representing the moderately thick coupons, only the first layer at -45° and the second layer at 90° are noticeable. The failure of the other plies looks more like an “explosion” type, as observed in UD coupons for a large amount of energy. However, even if the failure of the two thicker laminates seems achieved in the gauge length, it is more like a delamination which starts at the external layers in the grip region due to a state of 3D stresses.

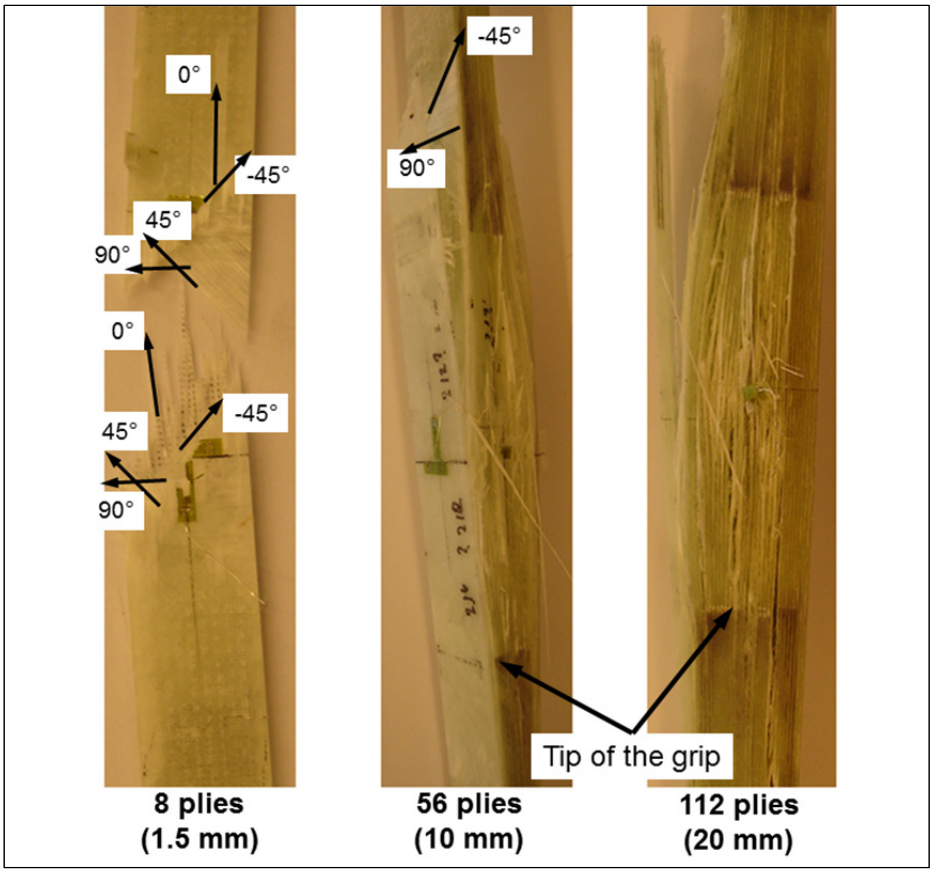

Figure 4.8 Failure modes for the three thicknesses of a quasi-isotropic lay-up

4.3 Evaluation with the Classical Lamination Theory

This section presents a comparison of the values obtained by test (Section 4.2) and the ones computed using the classical lamination theory (CLT) with initial properties coming from the results of the test on UD (Section 3.6). Usually, the material properties of a lamina are used to analyze a laminate. The lamina properties are the ones obtained from ASTM standard tests using thin laminates.

So, using the in-plane properties of the UD laminate of 8 plies from Section 3.6 (E_1=48.9 GPa, E_2=14.3 GPa, ν_{12}=0.282 and G_{12}=5.8 GPa), the equivalent laminate properties are computed using the CLT. The CLT only provides two in-plane properties of the laminates. Equation 4.1 and Equation 4.2 are respectively for the Young's Modulus, E_x, and the in-plane Poisson's ratio, ν_{xy}. The through-the-thickness Poisson's ratio (ν_{xz}) cannot be verified using CLT since no through-the-thickness terms or effects are considered in the CLT.

$$E_x = \frac{\left(A_{11} * A_{22} - A_{12}^2\right)}{\left(t * A_{22}\right)} \tag{4.1}$$

$$E_y = \frac{\left(A_{11} * A_{22} - A_{12}^2\right)}{\left(t * A_{11}\right)} \tag{4.2}$$

$$\nu_{xy} = \frac{A_{12}}{A_{22}} \tag{4.3}$$

$$G_{xy} = \frac{A_{66}}{t} \tag{4.4}$$

Using the CLT, whatever the thickness of the laminate, the mechanical properties are the same. Using these equations, the cross-ply configuration, E_x is evaluated to be equal to 31.8 GPa and ν_{xy} is equal to 0.128. These values are overestimating the test results, where E_x varies between 25 and 30 GPa and ν_{xy} varies between 0.086 and 0.103. For the thinner coupons, the standard deviation is the lowest and the overestimation is about 18%.

One reason for this overestimation could be due to the fibre volume fraction. Since a higher fibre volume fraction of 60.9% is obtained with the UD coupons, it is reasonable to think that stronger properties would be computed using UD properties. The fibre volume fractions of a thin, moderately thick and thick cross-ply laminates are respectively, 58.7%, 57.8% and 56.6%. Even when adding a factor related to the fibre volume fraction (for example 60.9/58.7 for the thinner specimens) for each thickness, the values of E_x stay greater than the

experimental ones (see Table 4.2). The same behaviour is observed for the Poisson's ratio. Though, both properties (elastic modulus and Poisson's ratio) show a slight degradation with the thickness when adjusting with the fibre volume fraction. Their values remain larger than the ones measured experimentally.

Another aspect to observe is the effect of the thickness. As an initial assumption, to compute the mechanical properties of a laminate with a determined thickness, the elastic properties of a UD laminate with the same thickness are needed. The in-plane elastic properties of a UD moderately thick laminate are E_1=49.7 GPa, E_2=13.5 GPa, ν_{12}=0.292 and G_{12}=4.8 GPa. For a thick laminate, the properties are E_1=52.7 GPa, E_2=12.1 GPa, ν_{12}=0.292 and G_{12}=3.6 GPa. The use of the UD properties related to each thickness seems to have a significant influence on the Poisson's ratio. Even with the results of the thickness dependence, presented in the last column in Table 4.2, the values are still over the upper range of the measured properties on cross-ply laminates.

Table 4.2 Summary table of properties computed using CLT for cross-ply laminates

Cross-Ply		Test Results	CLT		
			Thin properties	Thin with Vf factor	Thick. dep. with Vf factor
8 plies	Ex (GPa)	26.9	31.8	30.6	30.6
	νxy	0.122	0.128	0.123	0.123
56 plies	Ex (GPa)	26.7	31.8	30.2	30.2
	νxy	0.096	0.128	0.121	0.118
112 plies	Ex (GPa)	28.4	31.8	29.5	30.3
	νxy	0.091	0.128	0.119	0.101

The same approach is followed for the quasi-isotropic laminates. The results are summarized in Table 4.3. The same UD properties are used and the fibre volume fractions are slightly different for quasi-isotropic lay-up, 58.9%, 57.8% and 57.9% from the thinner to the thicker laminate. The analysis using CLT still overestimates the in-plane elastic properties for the quasi-isotropic lay-up, except E_x for the thicker laminates.

Table 4.3 Summary table of properties computed using CLT for quasi-isotropic laminates

Quasi-Isotropic		Test Results	CLT		
			Thin properties	Thin with Vf factor	Thick. dep. with Vf factor
8 plies	Ex (GPa)	20.8	25.8	24.9	24.9
	νxy	0.284	0.294	0.290	0.290
56 plies	Ex (GPa)	20.9	25.8	24.0	23.2
	νxy	0.305	0.294	0.287	0.308
112 plies	Ex (GPa)	23.5	25.8	24.5	23.2
	νxy	0.301	0.294	0.289	0.329

Another property that can be compared using the CLT is the strain at failure. Applying the axial load, N_x, equivalent to a given experimental stress at failure, it is possible to compute the resulting strain in the laminate. For the thin cross-ply laminate, the experimental failure load is 19.1 kN and the maximum recorded strain is 27442μ. For the same load, the computed strain using CLT is 21051μ. All the computed strains, for both configurations, are much lower, by about 20%, than the ones obtained during the tests. In the tests, it is difficult to identify the first ply to fail due to the small laps of time between the first ply failure and the laminate failure. The first ply failure, in both studied lay-up configurations, occurs in plies at 90° due to a high tension in the matrix direction. During the test, this first failure will increase the strain in the laminate up to the laminate failure. In Figure 4.4, using high performance cameras, it is possible to observe the growth of the amount of white spots when the load increases. These white spots are localized matrix cracks leading to the failure in tension of the 90° plies. The matrix cracking is the reason why the experimental strains at failure are significantly higher than the one computed using the first ply failure (FPF) and CLT. Using an iterative process, it would be possible to compute the ultimate strain using the last ply failure (LPF) method and CLT.

4.4 Evaluation with Finite Element Modeling

This section presents a methodology to compute three elastic tensile properties (E_x, ν_{xy} and ν_{xz}) of two different lay-up configurations of laminated composite using a finite element model (FEM). Then, the computed values using FEM are compared against experimental results presented in Section 4.2. The three properties are: the axial Young's modulus (E_x), the in-plane Poisson's ratio (ν_{xy}) and the axial-through-the-thickness Poisson's ratio (ν_{xz}).

In order to compute the ν_{xz}, solid brick elements is required using, as input material, 3D elastic properties of UD specimens from Chapter 3. The same element type used in Section 2.2.4, SOLID46, is used here due to its numerous advantages mentioned is Section 1.3.2.1. The straight coupon is modeled using symmetric boundaries. Only half of the effective length (L_e = 150 to 191.5 mm) is considered as well as the half of the specimen width (W_s = 20 mm). For the thickness, a comparison of the results will be performed to capture whether a full symmetric lay-up is different than the half of it. To respect the maximum aspect ratio of 20:1 recommended by ANSYS® with a ply thickness (t_p) of 0.185 mm, a minimum of 26 elements in the length direction needs to be used (ANSYS, released 9). Eight elements are used in the width and one element per layer is used through-the-thickness. Examples of the cross-ply and the quasi-isotropic laminate are presented in Figure 4.9. The blue elements are at 0°, the orange at 90°, the green at -45° and the red at 45°.

In order to obtain the most accurate behaviour using FEM, the choice of material properties is important. Like for the CLT and as a common practice, the experimental elastic properties of thinner UD specimens are used (E_1=48.9 GPa, E_2= 14.3 GPa, ν_{12}=0.282 and G_{12}=5.8 GPa) from Figure 3.34, Figure 3.35 and Figure 3.37. In addition, with solid elements, a set of full 3D properties are needed (E_3=E_2=14.3 GPa, ν_{13}=0.278, ν_{23}=0.320, G_{13}=4.4 GPa and G_{23}=4.0 GPa) from Figure 3.34, Figure 3.35, Figure 3.40 and Figure 3.41. Through-the-thickness shear properties were obtained from thick coupons, since it is not possible to achieve the coupon geometry with a laminate less than 20 mm thick.

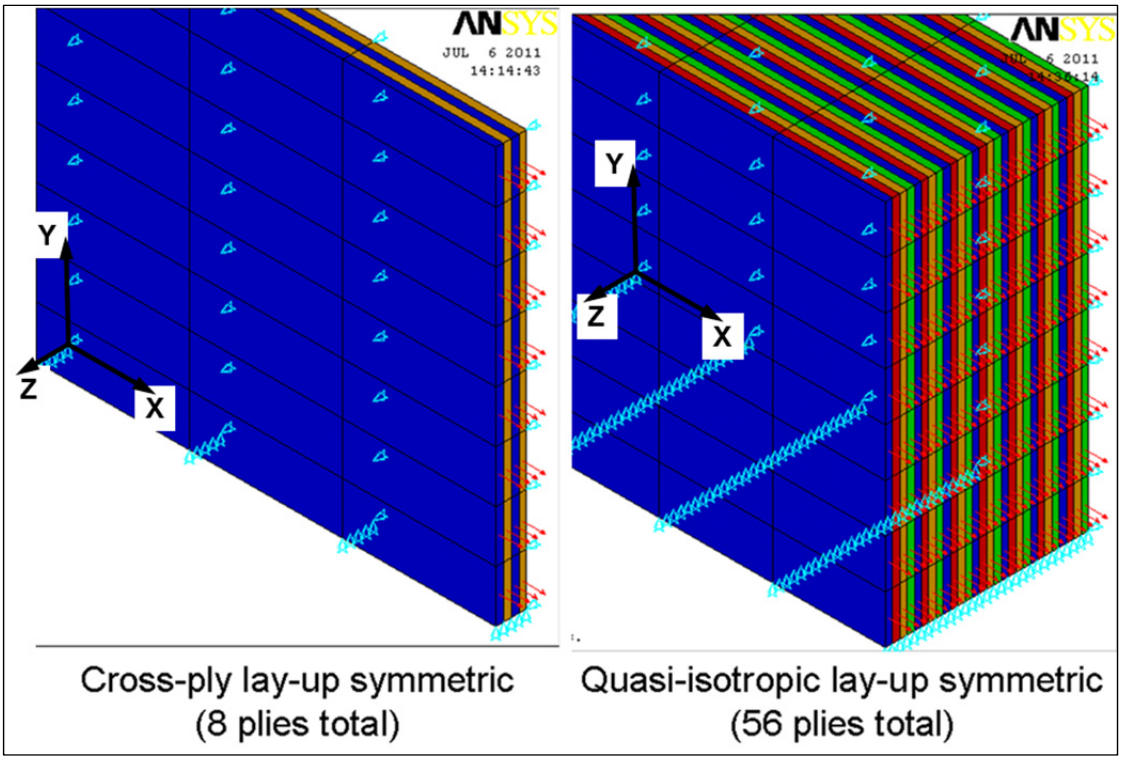

Figure 4.9 Cross-ply and quasi-isotropic lay-up models

As shown in Figure 4.9, the symmetry conditions are applied at X=0 (not shown), Y=0 and Z=0. The load is applied as a pressure at the free end. The load is gradually applied, in prevention for nonlinear analysis, until the magnitude reaches the maximum value obtained during the test.

To compute the laminate properties, displacement of 14 nodes, located at the quarter of the effective length, are recorded at every load step. The location of the 14 nodes is known and they are presented in Figure 4.10. The displacement in X is recorded for all the 14 nodes. In Y, the displacement is only recorded for nodes 10 to 14. And in Z, the displacement of the nodes on top, 5, 7, 9 and 14, is recorded. It means that nodes 1, 6, 8 and 10 are at the mid thickness of the coupons, at the symmetry.

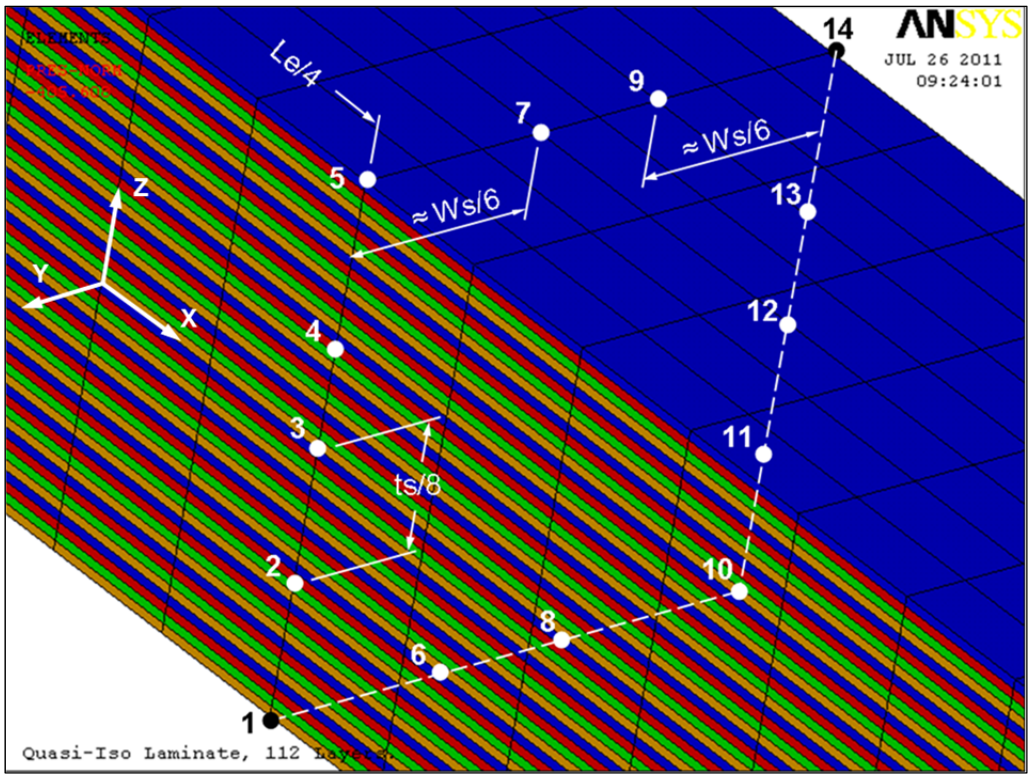

Figure 4.10 Location of the 14 nodes for displacement record

Knowing the displacement and the initial position of the 14 nodes, and the applied load, three elastic properties can be computed. The Young's modulus, E_x, is the quotient of stress over the strain, as presented in Equation 4.5. The in-plane Poisson's ratio, ν_{xy}, is the negative quotient of the transverse strain over the axial strain, Equation 4.6. The last property, the through-the-thickness Poisson's ratio, ν_{xz}, is obtained using the displacement through-the-thickness, as shown in Equation 4.7.

$$E_x = \frac{\sigma_x}{\varepsilon_x} = \frac{F/A}{\delta_x/(Le/4)} = \frac{FL_e}{4A\delta_x} \tag{4.5}$$

$$\nu_{xy} = -\frac{\varepsilon_y}{\varepsilon_x} = -\frac{\delta_y/(W_s/2)}{\delta_x/(Le/4)} = \frac{-\delta_y L_e}{2\delta_x W_s} \tag{4.6}$$

$$\nu_{xz} = -\frac{\varepsilon_z}{\varepsilon_x} = -\frac{\delta_z/(t/2)}{\delta_x/(Le/4)} = \frac{-\delta_z L_e}{2\delta_x t} \tag{4.7}$$

The influence of the fibre volume fraction and the influence of the thickness on UD properties are inspected in the same manner as for the CLT results. For a complete set of properties for the moderately thick and the thicker laminates, through-the-thickness Poisson's ratios are respectively, (ν_{13}=0.332, ν_{23}=0.291) and (ν_{13}=0.340, ν_{23}=0.312). These values are taken from Section 3.6 (see Figure 3.35). The summary tables of the elastic properties computed using FEM are presented in the following tables, Table 4.4 for the cross-ply lay-ups and Table 4.5 for the quasi-isotropic ones.

Table 4.4 Summary table of properties computed using FEM for cross-ply laminates

Cross-Ply		Test Results	FEM			
			Thin properties	Non-Linear effect	Thin with Vf factor	Thick. dep. with Vf factor
8 plies	Ex (GPa)	26.9	31.8	31.8	30.7	30.7
	νxy	0.122	0.128	0.128	0.124	0.124
	νxz	0.359	0.314	0.314	0.302	0.302
56 plies	Ex (GPa)	26.7	31.8	31.8	30.2	30.2
	νxy	0.096	0.129	0.129	0.122	0.119
	νxz	0.341	0.316	0.316	0.299	0.313
112 plies	Ex (GPa)	28.4	31.8	31.8	29.5	30.3
	νxy	0.091	0.129	0.129	0.119	0.102
	νxz	0.358	0.317	0.317	0.293	0.324

Table 4.5 Summary table of properties computed using FEM for quasi-isotropic laminates

Quasi-Isotropic		Test Results	FEM			
			Thin properties	Symmetry effect	Thin with Vf factor	Thick. dep. with Vf factor
8 plies	Ex (GPa)	20.8	25.7	25.7	24.8	24.8
	νxy	0.284	0.293	0.293	0.289	0.289
	νxz	0.269	0.256	0.256	0.247	0.247
56 plies	Ex (GPa)	20.9	25.7	25.7	24.0	23.2
	νxy	0.305	0.294	0.294	0.287	0.308
	νxz	0.302	0.257	0.257	0.239	0.242
112 plies	Ex (GPa)	23.5	25.7	25.7	24.5	23.2
	νxy	0.301	0.294	0.294	0.289	0.329
	νxz	0.291	0.257	0.257	0.244	0.249

To be sure of the FEM behaviour on symmetry boundary conditions, full thickness models are used for the quasi-isotropic configuration. Also, due to unexpected deformations at the free edges of the FEM (see Figure 4.11), geometrical nonlinear analyses are performed on the cross-ply and quasi-isotropic laminates. Results in Table 4.4 and Table 4.5 prove that the FEM for both configurations of lay-up behave properly. It is mostly shown that CLT gave same results as FEM for tensile loadings. The behaviour shown on the cross section schemes of Figure 4.11 is certainly the one that influences the strength of laminates in the so called "edge effect". For the cross-ply laminate, the difference in displacement is really not significant, only 0.001 mm. However, it is not the layer at 90° that shows the larger displacement as expected. In the case of quasi-isotropic laminate, the difference in displacement is about 0.010 mm (2%). This kind of distorsion is anticipated in a quasi-isotropic laminate due to the presence of angle plies.

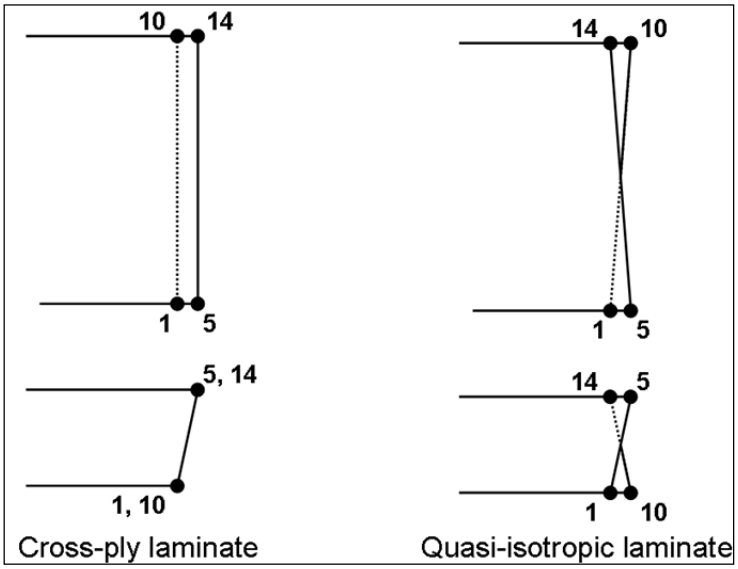

Figure 4.11 Disturbed cross sections due to axial loading

To obtain the ultimate strain using FEM, it is possible to load the model with a force corresponding to the experimental failure load and extract the element strains. Again, all the computed strains, for both configurations of lay-ups, are much lower, by about 25%, than the ones obtained in experiments. The same reason is proposed to explain this phenomenon. In using FEM, elements representing the weakest layer shall be removed from the model to

simulate a ply failure until the ultimate failure of the laminate and that should correlate experiments.

4.5 Results Comparison

Regardless of the method used, CLT or FEM, the in-plane properties are the same for tensile loading. One of the benefits of using FEM is the possibility to compute through-the-thickness properties. However, both methods compute a stiffer axial elastic modulus and larger in-plane Poisson's ratios compared to experimental values. Using FEM, the computed through-the-thickness Poisson's ratios are all lower than the recorded ones from experimental results. In addition, the computed properties are not significantly influenced by the thickness when the elastic properties of thin UD laminates are directly implemented in the analytical method.

One of the reasons the measured values are different from the computed ones is the influence of the ply angles. One of the errors on ply angles is that the specimen is not cut following the longitudinal direction of the fibres. Another is that the fibres are not perfectly aligned in the specified direction. Both reasons have been studied using FEM's of a quasi-isotropic lay-up of eight plies. The first model represents a rotation of 5° of the entire specimen, to simulate a misalignment during cutting. The second model is a misalignment of the fibres at 45° by 5°. A rotation of the specimen by 5° decreases the axial stiffness by only 0.1 GPa, the in-plane Poisson's ratio by 0.001 and increases the through-the-thickness Poisson's ratio by 0.001. For a misalignment of 5° in the plies at 45°, E_x decreases by 0.6 GPa, ν_{xy} decreases by 0.012 and ν_{xz} increases by 0.003. It is clear that the ply angle has an influence on the properties. This analysis is not sufficient to correlate experimental results and it would be difficult to find the proper combination of ply and coupon misalignments. But, the proof is that the variation of 5° in orientation may lead to a difference of about 3%. Therefore, the use of a laser projection will be beneficial to set each ply at a specified angle and particular attention shall be paid during the cutting of testing coupons.

Another possible explanation for the difference between the analytical results from both methods and the experimental values is the nonlinearity of the in-plane shear modulus, G_{12}. As shown in Figure 3.37, the in-plane shear modulus values for a thin UD laminate vary from 2.7 to 7.5 GPa. The effect of the in-plane shear modulus is only perceptible in laminates with angle plies, like the 45° in the quasi-isotropic lay-up. These two extreme values are analysed using FEM of the quasi-isotropic lay-up. When G_{12} is set equal to 2.7 GPa, the axial Young's modulus of a 8 plies quasi-isotropic laminate decreases to 22.9 GPa. It is a decrease of about 10%. However, the effect on the Poisson's ratios is in the opposite direction for the correlation; ν_{xy} increases to 0.368 and ν_{xz} decreases to 0.229. As predicted, when G_{12} is set equal to 7.5 GPa, E_x increases to 27.1 GPa, ν_{xy} decreases to 0.255 and ν_{xz} decreases to 0.269. For a cross-ply lay-up, the nonlinear effect of G_{12} will be automatically combined if a misalignment of the fibres occurs.

It is well known that the thicker the laminate, longer the gauge length should be. During the experimental study, due to the fact that the thicker specimens are stiffer than the thinner ones, a device is added to prevent an early failure in the grip. The length of this extra device reduces the effective length of the thicker specimens to 150 mm because the cutting machine available does not have the capacity to cut longer specimens. In regard to FEM, the effective length could be defined as a distance away from the boundaries, which in this case are the symmetric boundaries and the free loaded end. At this distance, the axial strain becomes stable within each layer. It is shown in Figure 4.12 to achieve stability within 5%, that 10 and 5 elements from the free end are required for the cross-ply and the quasi-isotropic lay-ups, respectively. The difference is due to the fact that it is easier to spread the load through layers when the angle between adjacent plies is not perpendicular. It is why it is recommended to never have perpendicular adjacent plies in structural lay-ups (CMH-17, 2012).

Since the laminate thickness does not seem to influence the effective length, it is may be due to the fact that the aspect ratio for the thin models (≈20) is different than the aspect ratio for the thicker ones (≈15). To study the effect of the aspect ratio, the number of elements in X and Y directions is doubled for the thinner cross-ply laminate. The effect of the aspect ratio

brings a perfect stability of the cross section in X direction compared to the one shown in Figure 4.12 and only a small difference in Y and Z directions at the sharp edge, point 14, is recorded. In terms of the effective length, the distance for a variation of 5% between elements is divided by 2. So, the effective length (loaded end effect) in FEM seems to be more related to the ply thickness and the aspect ratio than the laminate thickness itself.

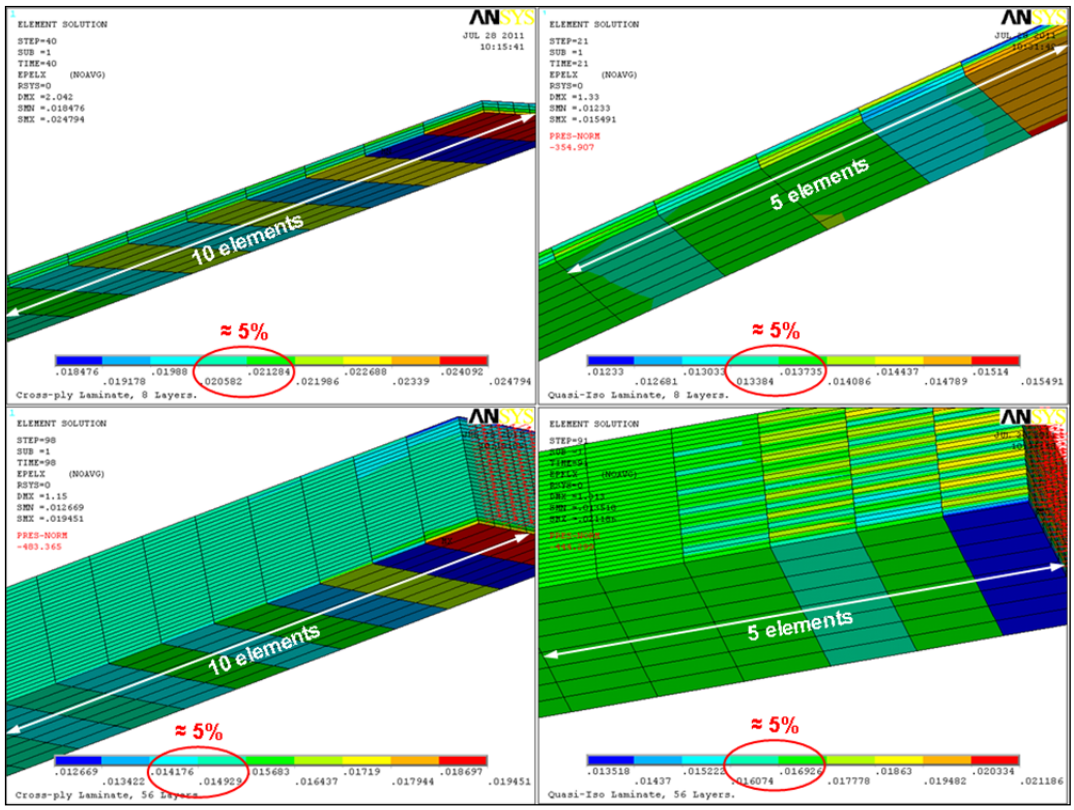

Figure 4.12 Axial strain in elements of different configurations – Loaded end effect

Comparing the ultimate loads and strains, FEA is slightly less conservative than CLT since for the same loading, the computed strain is lower by about 4% for the cross-ply lay-up and 6% for the quasi-isotropic lay-up. The conservatism in using the CLT can be directly linked to an increase of weight. A weight penalty of 6% begins to be significant in the aerospace industry since it is well known that engineers prefer the use of quasi-isotropic laminates in composite structures because of their metal-like behaviour.

4.6 Conclusion

In conclusion, cross-ply and quasi-isotropic laminated specimens made of unidirectional E-glass fibre and epoxy resin were produced with a great quality using the vacuum infusion manufacturing process. The laminates contain an average of 58% of fibre volume fraction and void content is well controlled. Both configurations were tested in tension.

For the cross-ply lay-up configuration, the effect of the thickness is not significant on the Young's modulus (E_x) with an average value of 27.3 GPa. It is difficult to conclude on the influence of the thickness on the in-plane Poisson's ratio (ν_{xy}), since a decrease of 25% is recorded from the thinner laminate at 0.122 to the thicker laminate at 0.091. The influence of the thickness is not significant on the through-the-thickness Poisson's ratio (ν_{xz}) with an average value of 0.353.

For the quasi-isotropic lay-up configuration, an increase of 13% is observed on the Young's modulus (E_x) from the thinner laminate at 20.8 GPa to the thicker laminate at 23.5 GPa. So, it is difficult to conclude on the thickness effect and extra tests shall be performed. For the in-plane and through-the-thickness Poisson's ratios (ν_{xy} and ν_{xz}), the influence of the thickness is not significant and the average values are 0.297 and 0.287, respectively.

The experimental results were also compared to elastic tensile properties (E_x, ν_{xy} and ν_{xz}) computed using the CLT and FEM. The values of both methods are very similar, within 1% for a problem representing a tensile loading experiment. In addition, as a general observation, both analytical method overestimated in-plane elastic tensile properties (E_x and ν_{xy}) even when the corresponding thickness properties and a correction factor related to the fibre volume fraction are used. For thin specimens, the Young's modulus (E_x) is overestimated by 14% and 20% for the cross-ply and the quasi-isotropic layup configuration, respectively. For the in-plane Poisson's ratio (ν_{xy}), it is an overestimation of about 10% for a thickness of 20 mm for both lay-up configurations. For the through-the-thickness Poisson's ratio, analytical values are always underestimated by at least 10%.

Some reasons are brought up to explain these differences. A difference of about 3% is computed for a misalignment of 5° for the fibres at 45° concluding that special care should be taken during specimens' preparation of different angle lay-up configurations. An opposite direction for the correlation is observed on elastic tensile properties (E_x, ν_{xy} and ν_{xz}) according to the nonlinearity of the in-plane shear modulus (G_{12}). It is found that the effective length (loading end effect) is more related to the ply thickness and element aspect ratio than the total laminate thickness. Also, the difference between effective length of cross-ply and quasi-isotropic configurations, confirms the recommendation to avoid perpendicular adjacent layers in the design of a laminate.

The benefits of using FEM instead of CLT are:

- observation of the influence of the thickness on through-the-thickness properties;
- computation of strains with more accuracy, therefore less penalty in terms of structural weight (about 4% and 6% for cross-ply and quasi-isotropic lay-up configurations, respectively);
- analysis of complex problems in term of geometry, loading, etc.

In extra testing, special care shall be taken in specimens' preparation, particularly on the fibre orientation and in cutting specimens. The use of a laser projection could be mandatory. In addition, a digital extensometer (grid of points painted on specimens with digital cameras) could be used to record the displacement to avoid noise in strain gauge values due to matrix microcracking.

On the other hand, the use of FEM necessitates particular attentions to the meshing and to the boundary and loading conditions. Solid layered elements are mandatory to accurately model thick laminated structures. Finally, engineers using FEM need to have a thorough understanding of the mechanics principles and a good idea of the behaviour of the studied structure to properly analyze the problem.

CHAPTER 5

PRELIMINARY WORKS ON NEW TEST METHODS

The objective of this chapter is to present two preliminary works in perspectives for future studies in order to address some weaknesses of standard test methods highlighted in Chapter 3. The first improvement will be the use of a digital extensometer instead of strain gauges to measure the deformation of laminated specimens. The use of strain gauges is not adequate for brittle materials like composites since matrix cracking prematurely causes the failure of the signal from the strain gauges. The second one is the development of an innovative torsion test for rectangular laminated specimens with different thicknesses. This new torsion test would allow quantifying the influence of the thickness on through-the-thickness shear properties.

5.1 Experimental Strain using a Digital Extensometer

As mentioned in Chapter 3 and Chapter 4, large scatters in the results are observed due the randomness of the failure in brittle material. A possible solution to record the deformation of the entire effective zone is to have strain gauges distributed over the entire zone and thus be certain to read the deformation at the failure location. Due to an extensive work and limited amount of strain gauges per test.

Another problem in brittle material is the premature failure of the signal from the strain gauges causes by matrix cracking. A solution to measure the displacement over the entire zone, would be the use a digital extensometer (grid of points painted on specimens with digital cameras) to record the displacements in all directions as presented in Figure 5.1. In this case, the grid is a laser printout. Using this laser application, it is possible to get a grid of points on the short transverse face to record the deformation through the thickness. An example was shown on Figure 4.6 for moderately thick and thick cross-ply laminates.

The location of each point is recorded by a system of high performance cameras. Images are recorded at a desired step of load and then the post-treatment of the data is performed to calculate the strains. This methodology could also be used in V-notched tests to avoid the failure of the strain rosette before the failure of the laminate itself. The failure or the disbond of the rosette is caused by resin cracking at the laminate surface. This application will provide more data and permit the continuity of the study on the nonlinearity of elastic shear properties. The company Trilion, specialized in optical test systems, has a common production application called “ARAMIS” for materials characterization (Trilion, 2012). An extra application, on mobile phones for example, could be developed to provide, in remote, the evolution of a fatigue test to researchers.

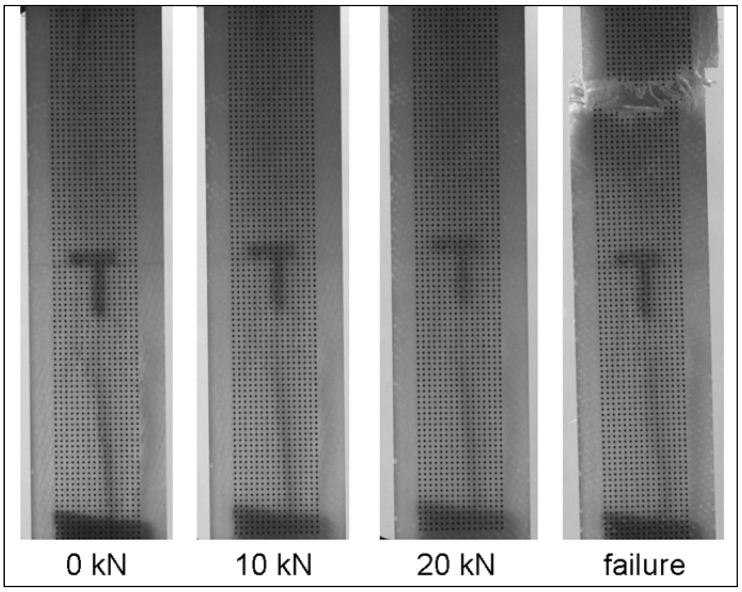

Figure 5.1 Pictures of the methodology using a grid of points

5.2 Torsion of Rectangular Bar

In order to evaluate the thickness effect on through-the-thickness elastic shear properties (G_{13} and G_{23}) for unidirectional (UD) laminates, an innovative shear test is proposed. Since the V-notched beam test does not permit the measurement of these through-the-thickness shear properties for thin laminates due to geometrical issues, a torsion test on rectangular bars is suggested. Although it is not common to load rectangular structures in torsion to get shear properties, this test is proposed in order to perform tests using the same material and the same manufacturing process as for tensile properties.

5.2.1 Test Specifications

Nothing in the literature exists for pure torsion experimental test on a rectangular laminated bar. The test is similar to the one proposed by (Ridley-Ellis *et al.*, 2003) to test rectangular hollow sections. In this case, as shown in Figure 5.2, one end of the laminated specimens is fixed. The other end is attached to a mobile circular jaw, the disk. Adjustable jaws will permit the testing of different thicknesses. The load is applied using a conventional testing machine through a rigid cable enrolled on the disk. The torsion load (T) is equal to the tensile force (F) times the distance (d) which corresponds to the disk radius.

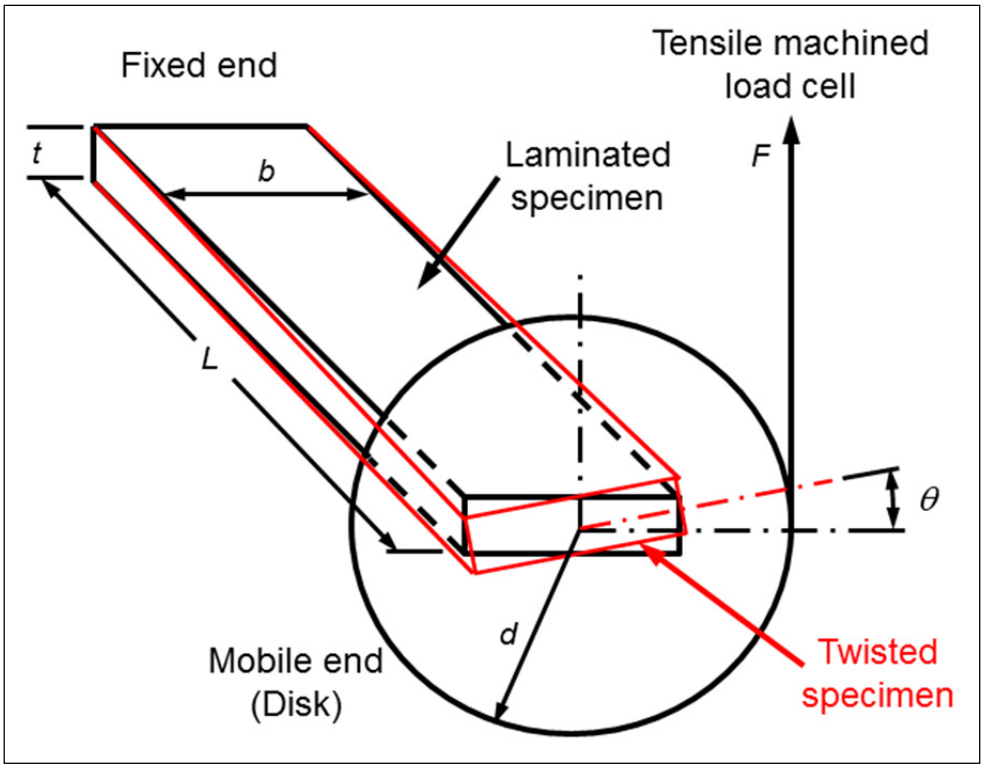

Figure 5.2 Scheme of the torsion test apparatus for rectangular laminated specimens

The angle of rotation (θ), in radians, could be measured in different manners as the displacement of the tensile machine head (u) times the disk radius (d) or angular grade marks on the disk. Knowing the angle of rotation (θ), the torsion load ($T=Fd$), the effective length of the specimen (L, between the two jaws) and the polar moment of inertia (J, developed in Section 5.2.2), the shear modulus can be computed as follow:

$$\theta = \frac{TL}{GJ} \Rightarrow G = \frac{TL}{\theta J} = \frac{FdL}{\theta J} \tag{5.1}$$

In order to get through-the-thickness shear properties, the rectangular laminated specimens are cut in particular directions as shown in Figure 5.3. For the longitudinal – through-the-thickness shear modulus (G_{13}), the width of the specimen (b) is along the fibres' direction, 1, and the effective length of the specimen (L) is in the transverse direction, 2. For the transverse – through-the-thickness shear modulus (G_{23}), the width of the specimen (b) is along the transverse direction, 2, and the effective length of the specimen (L) is in the longitudinal direction, 1, along the fibres.

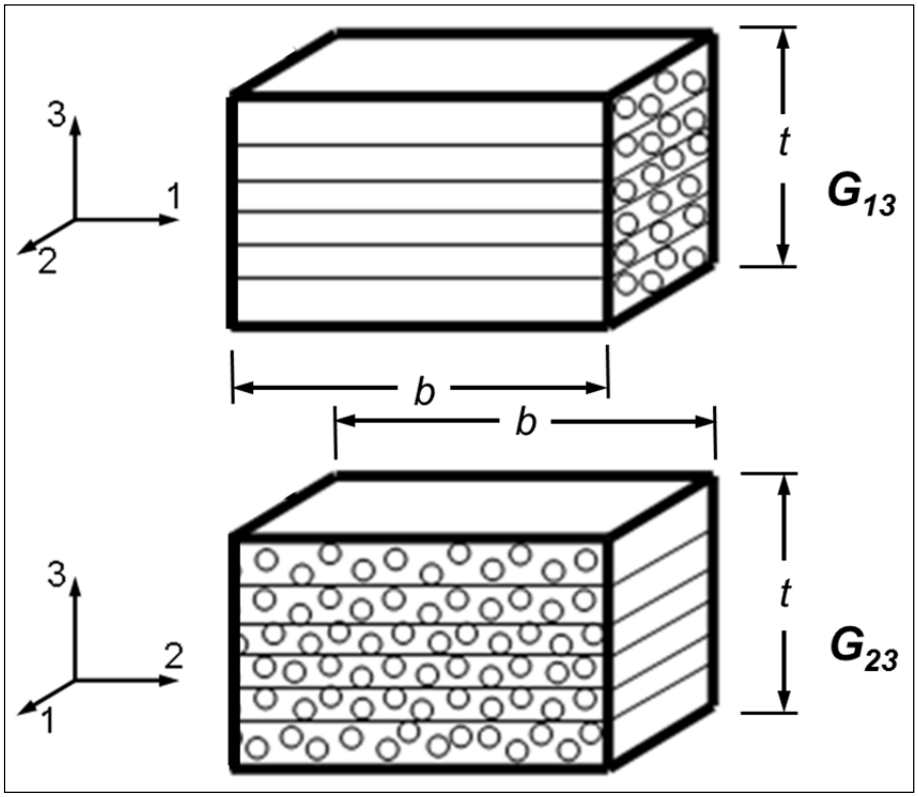

Figure 5.3 Rectangular laminated specimen cross sections to get through-the-thickness shear properties

5.2.2 Geometric Parameters

The polar moment of inertia (J) can be computed in different manners as a full Fourier analysis, a Saint-Venant's approximation or by correlation with a finite element analysis (FEA) In this section, an example with numerical specifications shown in Figure 5.4 is presented to compare the different manners of computing the polar moment of inertia (J) and the maximum shear stress.

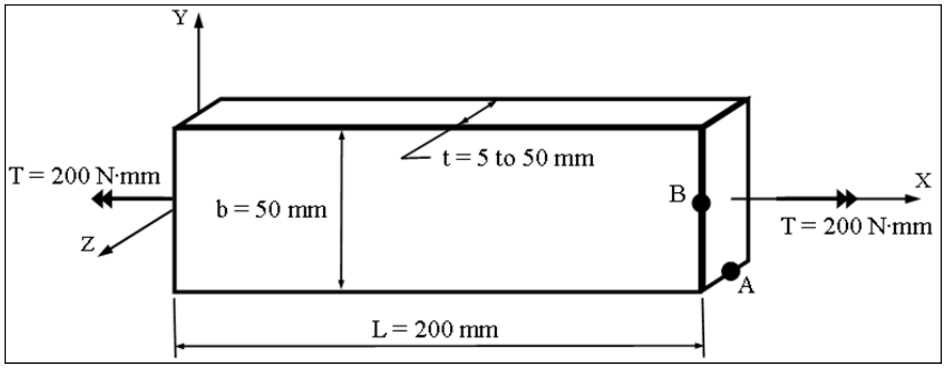

Figure 5.4 Rectangular bar in torsion

As a start, a full Fourier analysis can be used to solve geometrically a torsion problem of a rectangular bar (Soutas-Little, 1973). Theoretically, Equation 5.2 of the torsion constant J is the result of a sum to infinity (Soutas-Little, 1973):

$$J = bt^3\left[\frac{1}{3} - \frac{64}{\lambda\pi^5}\sum_{n=0}^{\infty}\frac{\tanh\left((n+½)\lambda\pi\right)}{(2n+1)^5}\right] \tag{5.2}$$

The constant λ is defined as the width to thickness ratio b over t. The maximum shear stress (τ_{max}) is on the long transverse edge, indicated by point **B**, and it is given by Equation 5.3 (Soutas-Little, 1973):

$$\tau_{\max} = \frac{Tt}{J}\left[1 - \frac{8}{\pi^2}\sum_{n=0}^{\infty}\frac{1}{(2n+1)^2\cosh\left((n+½)\lambda\pi\right)}\right] \tag{5.3}$$

Table 5.1 summarizes values for different thickness ratios that replace the sum within brackets in Equation 5.2 and Equation 5.3 to simplify the engineering calculations (Soutas-Little, 1973).

Table 5.1 Numerical values for engineering calculation from full Fourier analyses

λ	K_1	K_2	$K_3=K_2/K_1$
1.0	0.1406	0.6753	4.8038
1.25	0.1717	0.7763	4.5207
1.5	0.1958	0.8476	4.3295
2.0	0.2287	0.9301	4.0670
2.5	0.2494	0.9680	3.8821
3.0	0.2633	0.9855	3.7424
4.0	0.2808	0.9970	3.5502
5.0	0.2913	0.9993	3.4304
10.0	0.3123	1.0000	3.2018
∞	0.3333	1.0000	3.0000
$J = K_1 bt^3$,		$\tau_{max} = K_2(Tt/J) = K_3(T/bt^2)$	

As a second option, Saint-Venant's approximation formula, recalled in Equation 5.4, permits J to be written as (Soutas-Little, 1973):

$$J = \frac{0.3bt^3}{[1+(1/\lambda^2)]} = K_{1\,approx}\, bt^3 \tag{5.4}$$

$$where \quad K_{1\,approx} = \frac{0.3}{[1+(1/\lambda^2)]} \tag{5.5}$$

And if b is much larger than t, Equation 5.3 and Equation 5.4 yield to Equation 5.6 and Equation 5.7, respectively (Soutas-Little, 1973):

$$\tau_{\max} = \frac{Tt}{J} = \frac{3T}{bt^2} \tag{5.6}$$

$$J = \frac{1}{3} bt^3 \tag{5.7}$$

Another method to evaluate the shear stress due to a moment of torsion is numerical methods much as finite element analysis (FEA) using ANSYS®. This method considers the nature of the material of the bar and its geometric properties. Two element types are evaluated, shell and solid elements. The major advantage using shell elements is the ease to apply torsion load due to rotational degrees of freedom (DOF). Another advantage for shell elements is the smaller number of elements used for meshing in comparison with an equivalent mesh made of solid elements. It is difficult to apply the torsion load on a solid element model without inducing undesirable effects because solid elements have only three DOF in translation per node. In order to generate the moment of torsion on the solid model, a rigid beam must be added to the model with a force couple as shown in Figure 5.5.

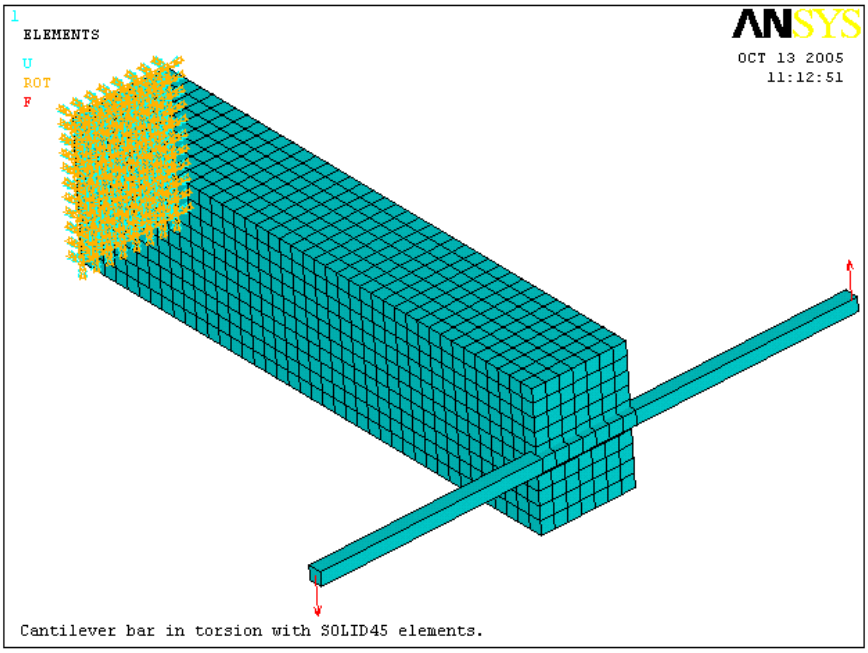

Figure 5.5 Application of torsion on a rectangular bar model with a force couple on a rigid beam

Figure 5.6 shows the shear stress at point **B** calculated using five different methods. For the comparison, the rectangular specimen is model with steel in order to validate the methodology. The methods are compared for thicknesses varying between 5 to 50 mm with an increment of 5 mm. The comparison shows that the solid element model offers a good stability regarding the relative difference with the full Fourier analysis in function of the

width to thickness ratio (λ). The shell element model gives a relative difference, compare to full Fourier analysis, just over 10% with a width to thickness ratio (λ) lower than 4, a thickness of 12.5 mm for a width of 50 mm. That is another reason why shell elements shall only be used to model thin structures. The Saint-Venant's approximation gives a maximum relative difference with the full Fourier analysis of around 6% for thick and thin bars, compared to over 10% for the thin rectangular section approximation.

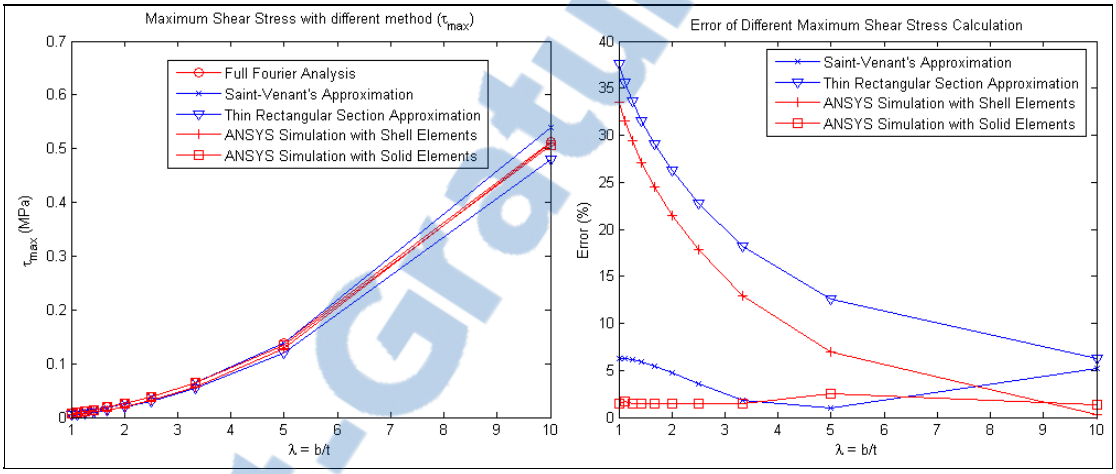

Figure 5.6 Maximum shear stress, comparison of five different methods

To obtain the shear stress in the thickness direction, indicated by the point **A** in Figure 5.4, let $t=b$ and $b=t$ in Equations 5.2 and 5.3. The results obtained with theoretical equations of a full Fourier analysis are compared with the FEM analysis with solid elements, in Figure 5.7.

In opposition to maximum shear stress behaviour on the long transverse edge, the relative difference for the shear stress on the short transverse edge increases when the thickness decreases. This is may be due to the small number of elements through the thickness of a thin bar. A study of convergence is undertaken in order to determine the influence of the number of elements through the thickness on the shear stress. The results obtained are illustrated in Figure 5.8. As expected, the number of elements through the thickness does not change anything on the reliability of maximum shear stress calculated at point **B**. On the other hand, by increasing the number of elements through the thickness it is possible to decrease the

relative difference, but never below 25%, for the through-the-thickness shear stress, at point **A**, which is unacceptable. The apparent reason of this deviation is that the analytical method proposed to calculate the shear stress through the thickness, by substituting *b* and *t* in theoretical equations of Fourier, is not valid and the FEM analysis may be closer to reality.

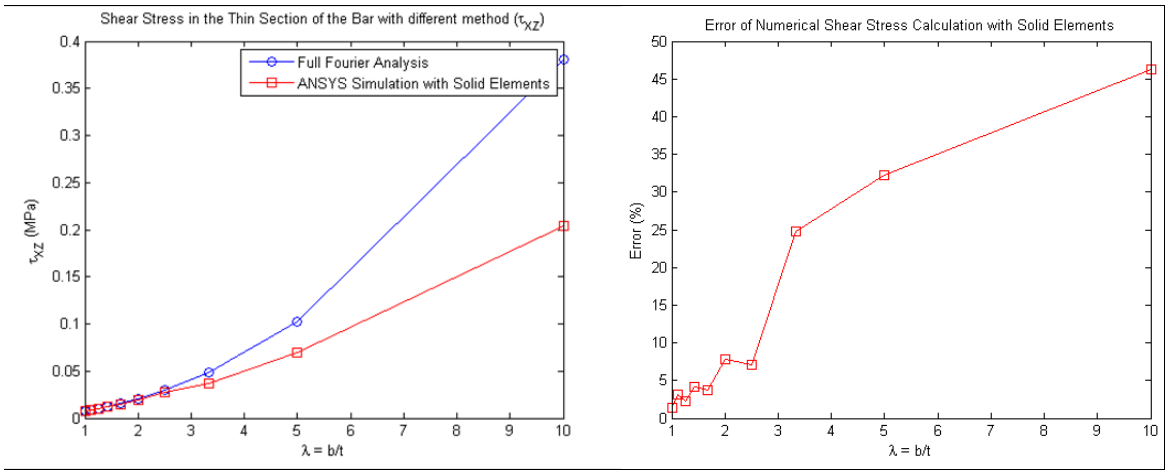

Figure 5.7 Shear stress through the thickness at point A

The conclusion is that there are several methods making possible the analysis of rectangular bars in torsion. In practice, engineers may use a linear approximation using the data in Table 5.1 from full Fourier analysis or those calculated using the Saint-Venant's Equations 5.4 to 5.6, or carry out a numerical analysis in ANSYS® with solid elements for shear stress calculations. These three methods give the most comparable results, excluding the use of these calculations for through-the-thickness shear stress which presents a relative difference with the full Fourier analysis of more than 25%. The unresolved question at this moment is: "Is this great variation due to a bad analytical interpretation (full Fourier analysis not suitable to compute the shear stress on the short edge) or a miss understanding of the finite element model?" An experimental test plan needs to be developed and the results be correlated with FEM.

Figure 5.8 Convergence on shear stress for solid elements

CONCLUSION

Since thicker composite laminates are more and more intended to be used in large primary structures, it is important to better understand the behaviour of these materials when their thickness increases. The main objective of this research was to determine the influence of the thickness, if so, on the nine orthotropic elastic mechanical properties (E_1, E_2, E_3, ν_{12}, ν_{13}, ν_{23}, G_{12}, G_{13} and G_{23}) which will be used in lamination theories or finite element analysis (FEA), in order to predict accurately the mechanical behaviour of thick laminated structures.

In order to evaluate the influence of the thickness, three categories were defined: thin laminates with thicknesses less than 6 mm (0.236"), moderately thick laminates for thickness between 6 mm (0.236") and 16 mm (0.630") and thick laminates with thicknesses greater than 16 mm (0.630"). These categories were determined by comparing the computed deflection of carbon/epoxy laminated beams in three-point bending using four different theories (CLT, TFBT with a shear factor of 5/6, TFBT with a shear factor dependent on the lay-up configuration and RHBT) and FEA. Cross-ply and quasi-isotropic lay-up configurations were studied. The results confirm that the classical lamination theory shall not be used to analyze laminated structures thicker than 6 mm. In addition, the advanced beam theories, within themselves, give similar results in term of deflection. This preliminary work indicates clearly that experiments shall be conducted to establish if a solid 3D FEA could compute accurately the deflection of laminated beams thicker than 16 mm.

For the three categories of thickness: thin laminates with a thickness of 1,5 mm (0.058"), moderately thick laminates with a thickness of 10 mm (0.408") and thick laminates with a thickness of 20 mm (0.816"), unidirectional (UD) E-glass/epoxy laminated composite plates were manufactured using vacuum infusion process. A significant difference exists between the manufacturing of thin and thick laminates. For thin laminates, the resin was infused along the fibres, whereas to manufacture thick laminates, the resin was infused through the thickness of laminates using a breather-cloth under the dried fibres. Despite this manufacturing difference, the repeatability of the process and the quality of the manufactured

laminates were indisputable with a fibre volume fraction of 60% and with almost no porosity, i.e. lower than 1%.

For the three different thicknesses of unidirectional laminates, eight of the nine orthotropic elastic mechanical properties (E_1, E_2, ν_{12}, ν_{13}, ν_{23}, G_{12}, G_{13} and G_{23}) were experimentally determined. Analyses of micrograph pictures confirmed that the through-the-thickness Young's modulus (E_3) can be considered equal to the transverse Young's modulus (E_2). Some test procedures were modified to achieve reliable results with thick laminates: lateral supports were added for longitudinal tests, long flexible tabs were inserted in between jaws and specimens for transverse tests and a modified Iosipescu jig were designed for shear tests. In addition to modifications required for properly loading UD laminates, the epoxy used as the matrix was brittle, leading to random locations of failure uneasy to catch with strain gauges. As a consequence, a lot of noise was recorded in the experimental results due to microcracking of the matrix. In order to minimize the effect of the noise on the extracted elastic properties, data recorded during the tests for the eight laminated coupons with the same thickness were interpolated linearly altogether. Also, to reduce the noise issued from microcracking and premature strain gauge failure, an inspection method using a digital extensometer was strongly recommended for composite materials in Chapter 5. In addition, because of the incompatibility between the required width for tested specimens and the thickness of thin and moderately thick laminates, it was geometrically impossible to study the thickness effect on the two through-the-thickness shear moduli (G_{13} and G_{23}) using the V-notched beam method. To address this issue, an innovative method for testing rectangular laminated specimens in pure torsion was proposed in Chapter 5. Experimental results are summarized below:

- From the longitudinal tensile tests, the longitudinal Young's modulus (E_1) was determined to be 49 GPa for the thin laminates. An increase of 7.8% on E_1 was recorded from thinner to thicker laminates. For in-plane and longitudinal – through-the-thickness Poisson's ratios (ν_{12} and ν_{13}), a value of 0.28 was measured on the thin laminates. However, ν_{12} slightly increased by 3.6% from thinner to thicker laminates, when ν_{13} significantly

increased by 12%. At failure, the ultimate longitudinal tensile strength decreased with the increase in thickness due to a 3D state of stress at the tip of the grips.

- From the transverse tensile tests, the transverse Young's modulus (E_2) was determined to be 14.3 GPa for the thin laminates. A significant decrease of 15.4% on E_2 was recorded from thinner to thicker laminates. For the transverse – through-the-thickness Poisson's ratio (ν_{23}), a value of 0.32 was measured for the thin laminates. An increase of 6.2% on ν_{23} was observed from thinner to thicker laminates. In term of failure, the ultimate transverse tensile strength was not influenced by the thickness variation.

- From the in-plane V-notched shear tests, the in-plane shear modulus (G_{12}) was determined to be 5.8 GPa for the thinner laminates. A significant decrease of 38% on G_{12} was recorded from thinner to thicker laminates. In addition, a nonlinear behaviour (nonlinearity of the stress-strain curve) was measured due to an accumulation of matrix microcracking, which modified the stiffness of the composite. Furthermore, at failure, a significant decrease of 22% was recorded on the ultimate in-plane shear strength from thinner to thicker laminates. Even though the influence of the thickness could not be verified on longitudinal – through-the-thickness and transverse – through-the-thickness shear moduli (G_{13} and G_{23}), the nonlinear behaviour due to an accumulation of matrix microcracking was observed on G_{13}. The nonlinearity was not measured for G_{23} due to a premature failure of the strain gauge.

- Furthermore, the influence of the thickness was experimentally studied on two different lay-up configurations: a cross-ply laminate and a quasi-isotropic one, under tension loading only. The laminates were manufactured using the same material and the same manufacturing process as for the characterisation of the UD laminate. The influence of the thickness was not clearly identified on the elastic tensile properties (E_x, ν_{xy} and ν_{xz}) for both lay-up configurations. Once more, it was difficult to quantify precisely the influence of the thickness on the ultimate tensile strength due to high stiffness in the loading direction, which led to an initiation of the failure at the grips.

Experimental results on elastic tensile properties were compared to values computed using CLT and FEA. Both methods gave similar results for in-plane tensile tests, within 1%, and they both overestimated in-plane elastic tensile properties. This overestimation may lead to an overdesign in term of weight of about 4% and 6% for cross-ply and quasi-isotropic lay-up configurations respectively. This overestimation remains even using the elastic mechanical properties of UD as a function of the thickness and the corresponding fibre volume fraction.

As a conclusion, this research project contributed to identify three different categories of thicknesses, to determine the nine orthotropic elastic mechanical properties (E_1, E_2, E_3, ν_{12}, ν_{13}, ν_{23}, G_{12}, G_{13} and G_{23}) and to evaluate the influence of the thickness on them. The elastic mechanical properties driven by the matrix (E_2, E_3, ν_{13} and G_{12}) are the most influenced by the thickness. Using CLT and FEA for in-plane tensile problems, similar results are obtained and both methods overestimate elastic tensile properties which may lead to overweight laminated structures by about 6%.

For future works, the comparison of Chapter 2 shall be performed using the orthotropic elastic properties found in Chapter 3. That shall be followed by the testing in three-point bending of laminated beams manufactured using the same E-glass/epoxy material and the same manufacturing process. As a recommendation, all composite materials shall be characterized using a digital extensometer to avoid noise in strain gauges signal or premature failure of them due to matrix microcracking. In addition, the influence of the thickness on in-plane shear modulus could be measured for both lay-up configurations and compared to the values computed using CLT and FEA. In FEA models, the stress-strain curves of the shear elastic moduli could be approximated by piecewise linear functions to embody the nonlinearity observed experimentally and to verify the effect on the computed properties. As another research subject, the evaluation of the depth after impact, its relation with the laminate thickness and its strength after impact shall be studied, since this aspect is of utmost importance for the aerospace industry since FAA's requirements for composite are based on damage properties which would be different for thin and thick laminates.

APPENDIX I

MATLAB ALGORITHM FOR CLT AND TIMOSHENKO USING A QUASI-ISOTROPIC K-FACTOR

```
% ********************************************************************
% * In this file the displacement of a transversely loaded beam and a   % * plate
loaded in pressure are calculated. See elsewhere for the
% * problem description. In the first part the lamina properties are
% * global axes. The second part gives the A and D matrices and their
% * inverse using the theory from Reddy. In the third part the
% * displacements are calculated whith the theory from Reddy.
% ********************************************************************

% ********************************************************************
% Part 1
% The method used is based on Daniel, pag. 63 and before.
% ********************************************************************

% Always good to start all clean.
clear all;

% Input the properties here in lamina axes.
Exlam = 148e9;            % [Pa]
Eylam = 9.65e9;           % [Pa]
Gxylam = 4.55e9;          % [Pa]
Nuxylam = 0.3;            % [-]
Nuyxlam = 0.0196;         % [-], assumed value
Nuyzlam = 0.4
% We need Gxz and Gyz material valuse as well, we assume
% that Gxz is the same as Gxy, and Gyz is per eq.3.7.
Gxzlam = Gxylam;
Gyzlam = Eylam/(2*(1+Nuyzlam));

% Here the stiffness matrix entries are calculated for the lamina in
% lamina coordinates. The stiffness matrix is called Q.
Qxxl = Exlam/(1-(Nuxylam*Nuyxlam));
Qyyl = Eylam/(1-(Nuxylam*Nuyxlam));
Qxyl = (Nuxylam*Eylam)/(1-(Nuxylam*Nuyxlam));
Qssl = Gxylam;

% Input the angle of the lamina with respect to the global axes here.
% The matrix Ang is of the format [0 45 90 -45 -45 90 45 0], all in degrees. For
other
% lay-ups, the first entry is the outside lamina. Note, the laminate has to
% be symmetric.
% ANG is the total laminates.
Ang = [0 90 0 90 0 90 0 90 0 90 0 90 0 90 0 90 0 90 0 90 0 90 0 90 0 90 0 90
90 0 90 0 90 0 90 0 90 0 90 0 90 0 90 0 90 0 90 0 90 0 90 0 90 0 90 0 90 0];
% Input of the layer thickness.
LayT = 0.000125;

% The number of loops depends on the size of Ang.
k1 = length(Ang);
% The total laminate thickness.
LamT = k1*LayT;
% Set the first h input zero here. Since it is on the midplane.
```

```
h(1,k1+1) = (LamT/2);
% Here a loop will be started. In the loop a matrix will be filled with the
% Q values needed, for the angles given in Ang. The matrix will have coloms
% whith values of Q for one angle. At the same time a vector will be filled
% with the thickness values needed to compute A and D matrices.
for i = 1:k1;
    % Here cos and sin are devined for the transformation.
    m = cos((Ang(1,i))*pi/180);
    n = sin((Ang(1,i))*pi/180);
    h(1,i) = (-(LamT/2)+(LayT*(i-1)));
    % Now using table 3.2, Engineering Mechanics of Composite Materials,
    % Daniel, the compliance matrix for the lamina in global coordinates is
    % calculated. The matrix Q has different values for all angles of Ang
    % in the coloms. In the lines we can find from top to bottom.
    % Qxx, Qyy, Qxy, Qxs, Qys, Qss, Q44, Q55, Q45. Note the numbers for Q44,
    % Q55 and Q45.
    Q(1,i) = (Qxxl*(m^4)) + (Qyyl*(n^4)) + (Qxyl*2*(m^2)*(n^2)) +
(Qssl*4*(m^2)*(n^2));
    Q(2,i) = (Qxxl*(n^4)) + (Qyyl*(m^4)) + (Qxyl*2*(m^2)*(n^2)) +
(Qssl*4*(m^2)*(n^2));
    Q(3,i) = (Qxxl*(m^2)*(n^2)) + (Qyyl*(m^2)*(n^2)) + (Qxyl*((m^4)+(n^4))) -
(Qssl*4*(m^2)*(n^2));
    Q(4,i) = (Qxxl*(m^3)*n) - (Qyyl*m*(n^3)) + (((m*(n^3))-((m^3)*n))*Qxyl) +
(((m*(n^3))-((m^3)*n))*Qssl*2);
    Q(5,i) = (Qxxl*(n^3)*m) - (Qyyl*n*(m^3)) + (((n*(m^3))-((n^3)*m))*Qxyl) +
(((n*(m^3))-((n^3)*m))*Qssl*2);
    Q(6,i) = (Qxxl*(m^2)*(n^2)) + (Qyyl*(m^2)*(n^2)) - (Qxyl*2*(m^2)*(n^2)) +
(Qssl*(((m^2)-(n^2))^2));
    % Using Reddy pag. 125 and 124, the enties for position 44 and 55 can also
    % be calculated.
    Q(7,i) = (Gyzlam*(m^2))+(Gxzlam*(n^2));
    Q(8,i) = (Gxzlam*(m^2))+(Gyzlam*(n^2));
    Q(9,i) = (Gxzlam-Gyzlam)*m*n;
end

% ********************************************************************
% Part 2
% Calculation of the A and D matrices.
% ********************************************************************

% Here the input for the A and D matrix are calculated, they should be
% inverted later. NB. for symmetric orthotropic laminates
for o=1:k1;
    D11(1,o) = (1/3)*(((h(1,o+1)^3)-(h(1,o)^3))*Q(1,o));
    D12(1,o) = (1/3)*(((h(1,o+1)^3)-(h(1,o)^3))*Q(3,o));
    D13(1,o) = (1/3)*(((h(1,o+1)^3)-(h(1,o)^3))*Q(4,o));
    D22(1,o) = (1/3)*(((h(1,o+1)^3)-(h(1,o)^3))*Q(2,o));
    D23(1,o) = (1/3)*(((h(1,o+1)^3)-(h(1,o)^3))*Q(5,o));
    D33(1,o) = (1/3)*(((h(1,o+1)^3)-(h(1,o)^3))*Q(6,o));

    A11(1,o) = ((h(1,o+1)-h(1,o))*Q(1,o));
    A12(1,o) = ((h(1,o+1)-h(1,o))*Q(3,o));
    A13(1,o) = ((h(1,o+1)-h(1,o))*Q(4,o));
    A22(1,o) = ((h(1,o+1)-h(1,o))*Q(2,o));
    A23(1,o) = ((h(1,o+1)-h(1,o))*Q(5,o));
    A33(1,o) = ((h(1,o+1)-h(1,o))*Q(6,o));
    A44(1,o) = ((h(1,o+1)-h(1,o))*Q(7,o));
    A55(1,o) = ((h(1,o+1)-h(1,o))*Q(8,o));
    A45(1,o) = ((h(1,o+1)-h(1,o))*Q(9,o));
end
```

```
D(1,1) = sum(D11);
D(1,2) = sum(D12);
D(1,3) = sum(D13);
D(2,1) = sum(D12);
D(2,2) = sum(D22);
D(2,3) = sum(D23);
D(3,1) = sum(D13);
D(3,2) = sum(D23);
D(3,3) = sum(D33);

A(1,1) = sum(A11);
A(1,2) = sum(A12);
A(1,3) = sum(A13);
A(2,1) = sum(A12);
A(2,2) = sum(A22);
A(2,3) = sum(A23);
A(3,1) = sum(A13);
A(3,2) = sum(A23);
A(3,3) = sum(A33);

Ae(1,1) = sum(A44);
Ae(1,2) = sum(A45);
Ae(2,2) = sum(A55);
Ae(2,1) = sum(A45);

% Last step is calculating the inverse matrices.
Ainv = inv(A);
Dinv = inv(D);
Aeinv = inv(Ae);

% ************************************************************************
% Part 3
% Calculation of the displacements
% ************************************************************************

% ***************************************
% Beam first with Timoshenko beam theory.
% ***************************************
% Variables.
Pbo = 3375;                    % load [N]
Gb = 0.02;                      % Width of the beam [m]
Lb = 0.1;                       % Length of the beam [m]
hb = LamT;                      % height of the beam [m]
K = 5/6;                        % Shear factor

% Calculation of constants
Pb=Pbo/Gb;                      % Load per unit width [-]
Ebxx = 12/((hb^3)*Dinv(1,1));
Gbxx = 1/(Aeinv(2,2)*hb);
Iy = Gb*(hb^3)/12;
boud = 0;
ssb = Lb/48;
% Determination of the displacement w.
for xb = 0:ssb:Lb/2;
    b = boud+1;
    wbT(b,1) = -((Pb*Gb*(Lb^3))/(48*Ebxx*Iy))*((3*xb/Lb)-(4*((xb/Lb)^3))) -
((Pb*Lb*Gb)/(2*K*Gbxx*Gb*hb))*(xb/Lb);
    posT(b,1) = xb;

    %***************   C  L  T   ****************
```

```
    wbC(b,1) = -((Pb*Gb*(Lb^3))/(48*Ebxx*Iy))*((3*xb/Lb)-(4*((xb/Lb)^3))); % CLT
calculation.
    %***************   C  L  T   *****************


    posC(b,1) = xb;
    boud = b;
end

posT=0:ssb:Lb;
wbTtemp=wbT;
k2=length(wbTtemp);
for i=1:k2-1
    wbT(k2+i)=wbTtemp(k2-i);
end;

posC=0:ssb:Lb;
wbCtemp=wbC;
k3=length(wbCtemp);
for i=1:k3-1
    wbC(k3+i)=wbCtemp(k3-i);
end;

figure(1);
plot(posT,wbT,'-r');
figure(1);
hold on
plot(posC,wbC,'-b');
```

APPENDIX II

MATLAB ALGORITHM FOR CLT AND TIMOSHENKO USING THE K-FACTOR DEVELOPED BY MADABUSHI & DAVALOS

```
% ************************************************************************
% * In this file the displacement of a transversely loaded beam is
% * calculated. In the first part the lamina properties are determined.
% * The second part gives the A, B and D matrix entries that are needed
% * to calculate the inverse stifness matrix, amongst others. In the
% * third part the k factor will be calulated based on Davalos paper.
% * In the fourth part the displacements are calculated with the
% * Timoshenko beam theory and this k-factor.
************************************************************************

% ************************************************************************
% Part 1
% The method used is based on Daniel, pag. 63 and before.
% ************************************************************************

% Always good to start all clean.
clear all;

% Input the properties here in lamina axes.
Exlam = 148e9;            % [Pa]
Eylam = 9.65e9;           % [Pa]
Gxylam = 4.55e9;          % [Pa]
Nuxylam = 0.3;            % [-]
Nuyxlam = 0.0196;         % [-], assumed value
Nuyzlam = 0.4
% We need Gxz and Gyz material valuse as well, we assume
% that Gxz is the same as Gxy, and Gyz is per eq.3.7.
Gxzlam = Gxylam;
Gyzlam = Eylam/(2*(1+Nuyzlam));

% Here the stiffness matrix entries are calculated for the lamina in
% lamina coordinates. The stiffness matrix is called Q.
Qxxl = Exlam/(1-(Nuxylam*Nuyxlam));
Qyyl = Eylam/(1-(Nuxylam*Nuyxlam));
Qxyl = (Nuxylam*Eylam)/(1-(Nuxylam*Nuyxlam));
Qssl = Gxylam;

% Input the angle of the lamina with respect to the global axes here.
% The matrix Ang is of the format [0 90 0 90], all in degrees. For other
% lay-ups, the first entry is the outside lamina.
% Ang = [0 90 0 90 0 90 0 90 0 90 0 90 0 90 0 90 0 90 0 90 0 90 0 90 0 90 0 90
0 90 0 90 0 90 0 90 0 90 0 90 0 90 0 90 0 90 0 90 0 90 0 90 0 90 0 90 0 90 0
90 0 90 0 90 0 90 0 90 90 0 90 0 90 0 90 0 90 0 90 0 90 0 90 0 90 0 90 0 90 0
90 0 90 0 90 0 90 0 90 0 90 0 90 0 90 0 90 0 90 0 90 0 90 0 90 0 90 0 90 0 90
0 90 0 90 0 90 0 90 0 90 0 90 0 90 0 90 0];
Ang = [0 45 90 -45 0 45 90 -45 0 45 90 -45 -45 90 45 0 -45 90 45 0 -45 90 45 0];
% Input of the layer thickness.
LayT = 0.000125;
% The number of loops depends on the size of Ang.
k1 = length(Ang);
% The total laminate thickness.
```

```
LamT = k1*LayT;

% Input the beam dimensions. These will be needed later.
L = 0.1;                        % L is the length.
Br = 0.02;                      % B is the width.
% Variables.
Pbo = 46656;                       % load [N]
hb = LamT;                      % height of the beam [m]

% Set the first h input zero here. Since it is on the midplane.
h(1,k1+1) = (LamT/2);
% Here a loop will be started. In the loop a matrix will be filled with the
% Q values needed, for the angles given in Ang. The matrix will have coloms
% whith values of Q for one angle. At the same time a vector will be filled
% with the thickness values needed to compute A and D matrices.
for i = 1:k1;
    % Here cos and sin are defined for the transformation.
    m = cos((Ang(1,i))*pi/180);
    n = sin((Ang(1,i))*pi/180);
    h(1,i) = (-(LamT/2)+(LayT*(i-1)));
    % Now using table 3.2, Engineering Mechanics of Composite Materials,
    % Daniel, the compliance matrix for the lamina in global coordinates is
    % calculated. The matrix Q has different values for all angles of Ang
    % in the coloms. In the lines we can find from top to bottom.
    % Qxx, Qyy, Qxy, Qxs, Qys, Qss, Q44, Q55, Q45. Note the numbers for Q44,
    % Q55 and Q45.
    Q(1,i) = (Qxxl*(m^4)) + (Qyyl*(n^4)) + (Qxyl*2*(m^2)*(n^2)) +
(Qssl*4*(m^2)*(n^2));
    Q(2,i) = (Qxxl*(n^4)) + (Qyyl*(m^4)) + (Qxyl*2*(m^2)*(n^2)) +
(Qssl*4*(m^2)*(n^2));
    Q(3,i) = (Qxxl*(m^2)*(n^2)) + (Qyyl*(m^2)*(n^2)) + (Qxyl*((m^4)+(n^4))) -
(Qssl*4*(m^2)*(n^2));
    Q(4,i) = (Qxxl*(m^3)*n) - (Qyyl*m*(n^3)) + (((m*(n^3))-((m^3)*n))*Qxyl) +
(((m*(n^3))-((m^3)*n))*Qssl*2);
    Q(5,i) = (Qxxl*(n^3)*m) - (Qyyl*n*(m^3)) + (((n*(m^3))-((n^3)*m))*Qxyl) +
(((n*(m^3))-((n^3)*m))*Qssl*2);
    Q(6,i) = (Qxxl*(m^2)*(n^2)) + (Qyyl*(m^2)*(n^2)) - (Qxyl*2*(m^2)*(n^2)) +
(Qssl*(((m^2)-(n^2))^2));
    % Using Reddy pag. 125 and 124, the enties for position 44 and 55 can also
    % be calculated.
    Q(7,i) = (Gyzlam*(m^2))+(Gxzlam*(n^2));
    Q(8,i) = (Gxzlam*(m^2))+(Gyzlam*(n^2));
    Q(9,i) = (Gxzlam-Gyzlam)*m*n;
end

% ********************************************************************
% Part 2
% Calculation of the A, B and D matrix inputs. With this, the complete
% stifness matrix is build and inverted.
% ********************************************************************

for o=1:k1;
    A11(1,o) = ((h(1,o+1)-h(1,o))*Q(1,o));
    A12(1,o) = ((h(1,o+1)-h(1,o))*Q(3,o));
    A13(1,o) = ((h(1,o+1)-h(1,o))*Q(4,o));
    A22(1,o) = ((h(1,o+1)-h(1,o))*Q(2,o));
    A23(1,o) = ((h(1,o+1)-h(1,o))*Q(5,o));
    A33(1,o) = ((h(1,o+1)-h(1,o))*Q(6,o));

    A44(1,o) = ((h(1,o+1)-h(1,o))*Q(7,o));
    A55(1,o) = ((h(1,o+1)-h(1,o))*Q(8,o));
```

```
    A45(1,o) = ((h(1,o+1)-h(1,o))*Q(9,o));

    B11(1,o) = (1/2)*(((h(1,o+1)^2)-(h(1,o)^2))*Q(1,o));
    B12(1,o) = (1/2)*(((h(1,o+1)^2)-(h(1,o)^2))*Q(3,o));
    B13(1,o) = (1/2)*(((h(1,o+1)^2)-(h(1,o)^2))*Q(4,o));
    B22(1,o) = (1/2)*(((h(1,o+1)^2)-(h(1,o)^2))*Q(2,o));
    B23(1,o) = (1/2)*(((h(1,o+1)^2)-(h(1,o)^2))*Q(5,o));
    B33(1,o) = (1/2)*(((h(1,o+1)^2)-(h(1,o)^2))*Q(6,o));

    D11(1,o) = (1/3)*(((h(1,o+1)^3)-(h(1,o)^3))*Q(1,o));
    D12(1,o) = (1/3)*(((h(1,o+1)^3)-(h(1,o)^3))*Q(3,o));
    D13(1,o) = (1/3)*(((h(1,o+1)^3)-(h(1,o)^3))*Q(4,o));
    D22(1,o) = (1/3)*(((h(1,o+1)^3)-(h(1,o)^3))*Q(2,o));
    D23(1,o) = (1/3)*(((h(1,o+1)^3)-(h(1,o)^3))*Q(5,o));
    D33(1,o) = (1/3)*(((h(1,o+1)^3)-(h(1,o)^3))*Q(6,o));
end

A(1,1) = sum(A11);
A(1,2) = sum(A12);
A(2,1) = sum(A12);
A(1,3) = sum(A13);
A(3,1) = sum(A13);
A(2,2) = sum(A22);
A(2,3) = sum(A23);
A(3,2) = sum(A23);
A(3,3) = sum(A33);

Ae(1,1) = sum(A44);
Ae(1,2) = sum(A45);
Ae(2,1) = sum(A45);
Ae(2,2) = sum(A55);

B(1,1) = sum(B11);
B(1,2) = sum(B12);
B(2,1) = sum(B12);
B(1,3) = sum(B13);
B(3,1) = sum(B13);
B(2,2) = sum(B22);
B(2,3) = sum(B23);
B(3,2) = sum(B23);
B(3,3) = sum(B33);

D(1,1) = sum(D11);
D(1,2) = sum(D12);
D(2,1) = sum(D12);
D(1,3) = sum(D13);
D(3,1) = sum(D13);
D(2,2) = sum(D22);
D(2,3) = sum(D23);
D(3,2) = sum(D23);
D(3,3) = sum(D33);

StMat = [A B;B D];
StMatinv = inv(StMat);

% Here an alternative way to calculate the inverse stifness matrix is used.
% It's the method based on Barbero.
a = inv(A);
d = inv(D);
ae = inv(Ae);
alpha = inv(A-(B*d*B));
```

```
delta = inv(D-(B*a*B));
betha = -(a*B*delta);
bethaT = -(d*B*alpha);
StMatinvalt = [alpha betha;bethaT delta];

% ********************************************************************
% Part 3
% Calculation of the k factor, based on Davalos.
% ********************************************************************

% First Hk and Jk are calculated.
Hk = ((Q(1,:)*StMatinv(1,4))+(Q(3,:)*StMatinv(1,5))+(Q(4,:)*StMatinv(1,6)));
Jk = ((Q(1,:)*StMatinv(4,4))+(Q(3,:)*StMatinv(4,5))+(Q(4,:)*StMatinv(4,6)));

% In this loop, Uk and Tk will be calculated.
Uk(1,1) = 0;
Tk(1,1) = 0;
for p = 2:k1;
    for q=1:p-1
        Uki(1,q)=(Jk(1,q)/2)*(((h(1,q+1))^2)-((h(1,q))^2));
        Tki(1,q)=(Hk(1,q))*((h(1,q+1))-(h(1,q)));
    end
    Uk(1,p) = sum(Uki);
    Tk(1,p) = sum(Tki);
end

% In the next loop, the rest of the variables are calculated.
for r=1:k1;
    Wk(1,r) = Hk(1,r)*Jk(1,r);
    Xk(1,r) = ((Jk(1,r))^2)/4;
    Vk(1,r) = ((Hk(1,r))^2) - ((((Jk(1,r))^2)*((h(1,r))^2))/2) + (Uk(1,r)*Jk(1,r))
+ (Tk(1,r)*Jk(1,r)) - (h(1,r)*Hk(1,r)*Jk(1,r));
    Rk(1,r) = (2*Tk(1,r)*Hk(1,r)) - (2*(Hk(1,r)^2)*h(1,r)) + (2*Hk(1,r)*Uk(1,r)) -
(Hk(1,r)*Jk(1,r)*(h(1,r)^2));
    Pk(1,r) = (Tk(1,r)^2) + ((Hk(1,r)^2)*(h(1,r)^2)) - (2*Tk(1,r)*Hk(1,r)*h(1,r)) +
(Uk(1,r)^2) + (((Jk(1,r)^2)*(h(1,r)^4))/4) - (Uk(1,r)*Jk(1,r)*(h(1,r)^2)) +
(2*Tk(1,r)*Uk(1,r)) - (Tk(1,r)*Jk(1,r)*(h(1,r)^2)) - (2*Hk(1,r)*Uk(1,r)*h(1,r))
+(Hk(1,r)*Jk(1,r)*(h(1,r)^3));
    kn(1,r) = (1/(Q(7,r)-((Q(9,r)^2)/Q(8,r))))*((Pk(1,r)*(h(1,r+1)-
h(1,r)))+((Rk(1,r)/2)*((h(1,r+1)^2)-(h(1,r)^2)))+((Vk(1,r)/3)*((h(1,r+1)^3)-
(h(1,r)^3)))+((Wk(1,r)/4)*((h(1,r+1)^4)-(h(1,r)^4)))+((Xk(1,r)/5)*((h(1,r+1)^5)-
(h(1,r)^5))));
end

% So finaly we get.

K = ((Ae(1,1)-((Ae(1,2)^2)/Ae(2,2)))^(-1))/(sum(kn));

% ********************************************************************
% Part 4
% Calculation of the displacements.
% ********************************************************************

% Calculation of constants
Pb=Pbo/Br;                          % Load per unit width [-]
Ebxx = 12/((hb^3)*d(1,1));
Gbxx = 1/(ae(2,2)*hb);
Iy = Br*(hb^3)/12;
boud = 0;
ssb = L/48;
% Determination of the displacement w.
```

```
for xb = 0:ssb:L/2;
    b = boud+1;
    wbT(b,1) = -((Pb*Br*(L^3))/(48*Ebxx*Iy))*((3*xb/L)-(4*((xb/L)^3))) -
((Pb*L*Br)/(2*K*Gbxx*Br*hb))*(xb/L);
    posT(b,1) = xb;
    wbC(b,1) = -((Pb*Br*(L^3))/(48*Ebxx*Iy))*((3*xb/L)-(4*((xb/L)^3)));
    posC(b,1) = xb;
    boud = b;
end

posT=0:ssb:L;
wbTtemp=wbT;
k2=length(wbTtemp);
for s=1:k2-1
    wbT(k2+s)=wbTtemp(k2-s);
end;

posC=0:ssb:L;
wbCtemp=wbC;
k3=length(wbCtemp);
for i=1:k3-1
    wbC(k3+i)=wbCtemp(k3-i);
end;

figure(1);
plot(posT,wbT,'-r');

figure(1);
hold on
plot(posC,wbC,'-b');
```

APPENDIX III

MATLAB ALGORITHM FOR RHBT OF ZENKOUR

```
% ************************************************************************
% * In this file the displacement of a transversely loaded beam is
% * calculated. In the first part the lamina properties are determined.
% * The second part gives the A, B, D, E, F, G, H matrix entries that
% * are needed in accordance with the article of Zenkour.
% * In the third part the vector lambda will be calulated in a loop. In
% * same loop the matrix [C], see article, and the vector {f} should be
% * calulated. It is a series approximation. In the fourth part the
% * displacements are calculated with this theory.
% ************************************************************************

% ************************************************************************
% Part 1
% The method used is based on Daniel, pag. 63 and before.
% ************************************************************************

% Always good to start all clean.
clear all;

% Input the properties here in lamina axes.
Exlam = 148e9;            % [Pa]
Eylam = 9.65e9;           % [Pa]
Gxylam = 4.55e9;          % [Pa]
Nuxylam = 0.3;            % [-]
Nuyxlam = 0.0196;         % [-], assumed value
Nuyzlam = 0.4
% We need Gxz and Gyz material valuse as well, we assume
% that Gxz is the same as Gxy, and Gyz is per eq.3.7.
Gxzlam = Gxylam;
Gyzlam = Eylam/(2*(1+Nuyzlam));

% Here the stiffness matrix entries are calculated for the lamina in
% lamina coordinates. The stiffness matrix is called Q.
Qxxl = Exlam/(1-(Nuxylam*Nuyxlam));
Qyyl = Eylam/(1-(Nuxylam*Nuyxlam));
Qxyl = (Nuxylam*Eylam)/(1-(Nuxylam*Nuyxlam));
Qssl = Gxylam;

% Input the angle of the lamina with respect to the global axes here.
% The matrix Ang is of the format [0 90 0 90], all in degrees. For other
% lay-ups, the first entry is the outside lamina. (Only cross ply lay-up)
Ang = [0 90 0 90 0 90 0 90 0 90 0 90 0 90 0 90 0 90 0 90 0 90 0 90 0 90 0
90 0 90 0 90 0 90 0 90 0 90 0 90 0 90 0 90 0 90 0 90 0 90 0 90 0 90 0 90
0 90 0 90 0 90 0 90 90 0 90 0 90 0 90 0 90 0 90 0 90 0 90 0 90 0 90 0 90
0 90 0 90 0 90 0 90 0 90 0 90 0 90 0 90 0 90 0 90 0 90 0 90 0 90 0 90 0
90 0 90 0 90 0 90 0 90 0 90 0 90 0];
% Input of the layer thickness.
LayT = 0.000125;
% Input the beam dimensions. These will be needed later.
L = 0.1;                  % L is the length.
b = 0.02;                 % b is the width.
% Input the loading q0. See the article for the right value. According to
% the article it is in [N], along a line on the centre of the beam along
```

```
% the x-axis.
q0 = 46656; %(Total load in N)

% The number of loops depends on the size of Ang.
k1 = length(Ang);
% The total laminate thickness.
LamT = k1*LayT;

% Input the values for the third order theory. Alfa, Betha, Gamma and
% Lambda are needed.
Alfa = 0;
Betha = 1;
Gamma = -4/(3*(LamT^2));
Lambda = 1;

% Set the first h input zero here. Since it is on the midplane.
h(1,k1+1) = (LamT/2);
% Here a loop will be started. In the loop a matrix will be filled with the
% Q values needed, for the angles given in Ang. The matrix will have coloms
% whith values of Q for one angle. At the same time a vector will be filled
% with the thickness values needed to compute A and D matrices.
for i = 1:k1;
    % Here cos and sin are defined for the transformation.
    m = cos((Ang(1,i))*pi/180);
    n = sin((Ang(1,i))*pi/180);
    h(1,i) = (-(LamT/2)+(LayT*(i-1)));
    % Now using table 3.2, Engineering Mechanics of Composite Materials,
    % Daniel, the compliance matrix for the lamina in global coordinates is
    % calculated. The matrix Q has different values for all angles of Ang
    % in the coloms. In the lines we can find from top to bottom.
    % Qxx, Qxs, Qss, Q55.
    Q(1,i) = (Qxxl*(m^4)) + (Qyyl*(n^4)) + (Qxyl*2*(m^2)*(n^2)) +
(Qssl*4*(m^2)*(n^2));
    Q(2,i) = (Qxxl*(m^3)*n) - (Qyyl*m*(n^3)) + (((m*(n^3))-((m^3)*n))*Qxyl) +
(((m*(n^3))-((m^3)*n))*Qssl*2);
    Q(3,i) = (Qxxl*(m^2)*(n^2)) + (Qyyl*(m^2)*(n^2)) - (Qxyl*2*(m^2)*(n^2)) +
(Qssl*(((m^2)-(n^2))^2));
    % Using Reddy pag. 125 and 124, the enties for position 44 and 55 can also
    % be calculated.
    Q(4,i) = (Gxzlam*(m^2))+(Gyzlam*(n^2));
end

% ********************************************************************
% Part 2
% Calculation of the A, B, D, E, F, G and H matrix inputs. Only the entries
% needed are calcutlated. (See the article by Zenkour.)
% ********************************************************************

for o=1:k1;
    A11(1,o) = ((h(1,o+1)-h(1,o))*Q(1,o)*b);
    A13(1,o) = ((h(1,o+1)-h(1,o))*Q(2,o)*b);
    A33(1,o) = ((h(1,o+1)-h(1,o))*Q(3,o)*b);
    A55(1,o) = ((h(1,o+1)-h(1,o))*Q(4,o)*b);

    B11(1,o) = (1/2)*(((h(1,o+1)^2)-(h(1,o)^2))*Q(1,o)*b);
    B13(1,o) = (1/2)*(((h(1,o+1)^2)-(h(1,o)^2))*Q(2,o)*b);
    B33(1,o) = (1/2)*(((h(1,o+1)^2)-(h(1,o)^2))*Q(3,o)*b);

    D11(1,o) = (1/3)*(((h(1,o+1)^3)-(h(1,o)^3))*Q(1,o)*b);
    D13(1,o) = (1/3)*(((h(1,o+1)^3)-(h(1,o)^3))*Q(2,o)*b);
    D33(1,o) = (1/3)*(((h(1,o+1)^3)-(h(1,o)^3))*Q(3,o)*b);
```

```
    D55(1,o) = (1/3)*(((h(1,o+1)^3)-(h(1,o)^3))*Q(4,o)*b);

    E11(1,o) = (1/4)*(((h(1,o+1)^4)-(h(1,o)^4))*Q(1,o)*b);
    E13(1,o) = (1/4)*(((h(1,o+1)^4)-(h(1,o)^4))*Q(2,o)*b);

    F11(1,o) = (1/5)*(((h(1,o+1)^5)-(h(1,o)^5))*Q(1,o)*b);
    F13(1,o) = (1/5)*(((h(1,o+1)^5)-(h(1,o)^5))*Q(2,o)*b);
    F55(1,o) = (1/5)*(((h(1,o+1)^5)-(h(1,o)^5))*Q(4,o)*b);

    G11(1,o) = (1/6)*(((h(1,o+1)^6)-(h(1,o)^6))*Q(1,o)*b);

    H11(1,o) = (1/7)*(((h(1,o+1)^7)-(h(1,o)^7))*Q(1,o)*b);
end

A(1,1) = sum(A11);
A(1,3) = sum(A13);
A(3,3) = sum(A33);
A(5,5) = sum(A55);

B(1,1) = sum(B11);
B(1,3) = sum(B13);
B(3,3) = sum(B33);

D(1,1) = sum(D11);
D(1,3) = sum(D13);
D(3,3) = sum(D33);
D(5,5) = sum(D55);

E(1,1) = sum(E11);
E(1,3) = sum(E13);

F(1,1) = sum(F11);
F(1,3) = sum(F13);
F(5,5) = sum(F55);

G(1,1) = sum(G11);

H(1,1) = sum(H11);

% ********************************************************************
% Part 3
% Calculation of the series approximation.
% ********************************************************************

% First determine some constants that can be used for the [C] matrix
% in the Zenkour Appendix. The extra b stands for bar, the h for hat.
Ab55 = A(5,5) + (3*Gamma*D(5,5));
Db55 = D(5,5) + (3*Gamma*F(5,5));

Bb11 = (Alfa*B(1,1)) + ((1+Alfa)*Gamma*E(1,1));
Bb13 = (Alfa*B(1,3)) + ((1+Alfa)*Gamma*E(1,3));
Db11 = (Alfa*D(1,1)) + ((1+Alfa)*Gamma*F(1,1));
Db13 = (Alfa*D(1,3)) + ((1+Alfa)*Gamma*F(1,3));
Eb11 = (Alfa*E(1,1)) + ((1+Alfa)*Gamma*G(1,1));
Fb11 = (Alfa*F(1,1)) + ((1+Alfa)*Gamma*H(1,1));

Bh11 = Betha*(B(1,1)+(Gamma*E(1,1)));
Bh13 = Betha*(B(1,3)+(Gamma*E(1,3)));
Dh11 = Betha*(D(1,1)+(Gamma*F(1,1)));
Dh13 = Betha*(D(1,3)+(Gamma*F(1,3)));
Eh11 = Betha*(E(1,1)+(Gamma*G(1,1)));
```

```
Fh11 = Betha*(F(1,1)+(Gamma*H(1,1)));

Ct1 = zeros(5);
c = 12;                  % Number of steps in this and the next loop.
        % Number of terms in the Single-Fourier Series
for a = 1:c;
    Num = (a*pi/L);
    Qm =(2*q0/L)*(sin(Num*(L/2)));
    C(1,1) = (Num^2)*A(1,1);
    C(1,2) = (Num^3)*Bb11;
    C(2,1) = C(1,2);
    C(1,3) = (Num^2)*Bh11;
    C(3,1) = C(1,3);
    C(1,4) = -Lambda*Num*(A(1,3)+((1/2)*(Num^2)*D(1,1)));
    C(4,1) = C(1,4);
    C(1,5) = -Lambda*Num*((2*B(1,3))+((1/3)*(Num^2)*E(1,1)));
    C(5,1) = C(1,5);

    C(2,2) = (Num^2)*((((1+Alfa)^2)*(Ab55 + (3*Gamma*Db55))) +
((Num^2)*((Alfa*Db11) + ((1+Alfa)*Gamma*Fb11))));
    C(2,3) = Num*(((Betha*(1+Alfa))*(Ab55 + (3*Gamma*Db55))) +
((Num^2)*((Alfa*Dh11) + ((1+Alfa)*Gamma*Fh11))));
    C(3,2) = C(2,3);
    C(2,4) = -Lambda*(Num^2)*(Bb13 + ((1/2)*(Num^2)*Eb11));
    C(4,2) = C(2,4);
    C(2,5) = -Lambda*(Num^2)*((2*Db13) + ((1/3)*(Num^2)*Fb11));
    C(5,2) = C(2,5);

    C(3,3) = ((Betha^2)*(Ab55 + (3*Gamma*Db55))) + (Betha*(Num^2)*(Dh11 +
(Gamma*Fh11)));
    C(3,4) = -Lambda*Num*(Bh13 + ((1/2)*(Num^2)*Eh11));
    C(4,3) = C(3,4);
    C(3,5) = -Lambda*Num*((2*Dh13) + ((1/3)*(Num^2)*Fh11));
    C(5,3) = C(3,5);

    C(4,4) = (Lambda^2)*(A(3,3) + ((Num^2)*D(1,3)) + ((1/4)*(Num^4)*F(1,1)));
    C(4,5) = (Lambda^2)*((2*B(3,3)) + ((4/3)*(Num^2)*E(1,3)) +
((1/6)*(Num^4)*G(1,1)));
    C(5,4) = C(4,5);

    C(5,5) = (Lambda^2)*((4*D(3,3)) + ((4/3)*(Num^2)*F(1,3)) +
((1/9)*(Num^4)*H(1,1)));

    % Here the values for {delta} will be calculated.
    Cinv = inv(C);
    Fvectorh = [0; 1; 0; (-(LamT/2)*Lambda); (((LamT^2)/4)*Lambda)];
    Fvector = Qm*Fvectorh;
    Delta(:,a)=Cinv*Fvector;
end

% ********************************************************************
% Part 4
% Calculation of the displacements.
% ********************************************************************

ss=L/48;
d=0;
for x=0:ss:L;
    d=d+1;
    for e=1:c;
       Num2 = (e*pi/L);
```

```
        W0t(1,e) = Delta(2,e)*(sin(Num2*x));
        W1t(1,e) = Delta(4,e)*(sin(Num2*x));
        W2t(1,e) = Delta(5,e)*(sin(Num2*x));
    end

    W0=sum(W0t);
    W1=sum(W1t);
    W2=sum(W2t);

    z=LamT;
    w(d,1) = W0 + (Lambda*((z*W1)+((z^2)*W2)));
end

wmin = -w;

figure(1);
hold on;
plot([0:ss:L],wmin,'-r');
```

APPENDIX IV

ANSYS® ALGORITHM FOR A COMPOSITE BEAM IN THREE-POINT BENDING

```
! Finite element analysis on thickness effects for a
! compostite beam build with solid46 elements.
! The lay-up is ([0, +45, 90, -45]n)s.
FINISH ! Always start with finish and clear commands.
/CLEAR

! Set the parameters (N, m).
! Dimensions.
L=0.1         ! One side, say length. (X).
W=0.02        ! One side, say width. (Y).
lt=0.000125   ! Layer thickness.
n=2           ! Number of repetition for each orientation.
nb_plies=8*n  ! Number of layers.
Tlt=lt*nb_plies     ! Total laminate thickness.

! The loading can be set here.
! (NB, this is half of that for shell99, due to number of nodes at load location.)
F=40          ! F is the force, 1000 assumed.

! Specify the mesh parameters here.
nx=40         ! Number of elements in x-direction.
ny=8          ! Number of elements in y-direction.
nz=8          ! Number of elements in z-direction.

! Apply title.
/TITLE, Beam, modeled with solid 46
/STITLE,1,05-11-15 (yy-mm-dd.) SOLID46, %nb_plies% layers, %Tlt% m. thick.
/STITLE,2, %nz% elements in thickness


! Finish the parameter module.
FINISH

! Go to the preparation module.
/PREP7

! Define the element types.
! Keyopt (9) is about were the things of interest are evaluated.
! In this case the option is 0, evaluate at top and bottom of each layer.
! Keyopt (8) now doesn't store data for all layers (option is 0).
! Keyopt (10) gives material propertiy matrices.
ET,1,Solid46
KEYOPT,1,8,0
KEYOPT,1,9,0
KEYOPT,1,10,1

! Define Real constants
! 0 degree ply real constant
R,1,nb_plies/nz,0
RMORE               ! Real constants 7 to 12 are zero.
RMORE,1,0,lt,1,-45,lt            ! Mat. nb, deg., thick.

! 45 degree ply real constant
```

```
R,2,nb_plies/nz,0
RMORE               ! Real constants 7 to 12 are zero.
RMORE,1,90,lt,1,45,lt            ! Mat. nb, deg., thick.

! 90 degree ply real constant
R,3,nb_plies/nz,0
RMORE               ! Real constants 7 to 12 are zero.
RMORE,1,45,lt,1,90,lt            ! Mat. nb, deg., thick.

! -45 degree ply real constant
R,4,nb_plies/nz,0
RMORE               ! Real constants 7 to 12 are zero.
RMORE,1,-45,lt,1,0,lt            ! Mat. nb, deg., thick.

! Material properties (T300/N5208) required for solid46, mat 1.
! Values were taken from Larry Lessard course notes and Bersee mail.
MP,Ex,1,148e9       ! Longitudinal Young's Modulus in Pa.
MP,Ey,1,9.65e9            ! Transverse Young's Modulus in Pa.
MP,Ez,1,9.65e9            ! Young's modulus in Pa in z-direction, assumed
identical to Ey.
MP,Gxy,1,4.55e9           ! Longitudinal Shear Modulus in Pa.
MP,Gyz,1,3.45e9           ! Shear modulus in Pa, check for better figures.
MP,Gxz,1,4.55e9           ! Shear modulus in Pa, check for better figures.
MP,PRxy,1,0.3       ! Major poissons ratio, check for better.
MP,PRyz,1,0.4       ! Major poissons ratio, check for better.
MP,PRxz,1,0.3       ! Major poissons ratio, check for better.


! Create the model geometrie.
! First determine the keypoints.
BLOCK,0,L,0,W,0,Tlt

! Create mesh
LSEL,S,LOC,Z,0.0,0.0
LSEL,R,LOC,Y,0.0,0.0
LESIZE,ALL,,,nx
LSEL,S,LOC,Z,0.0,0.0
LSEL,R,LOC,X,0.0,0.0
LESIZE,ALL,,,ny
LSEL,S,LOC,X,0.0,0.0
LSEL,R,LOC,Y,0.0,0.0
LESIZE,ALL,,,nz
ALLS
MSHKEY,1
VMESH,ALL

! Modify the element real constant properties
! Constant 2
NSEL,S,LOC,Z,n*4*lt,n*5*lt
ESLN,S,1,ALL
NSEL,S,LOC,Z,n*6*lt,n*7*lt
ESLN,A,1,ALL
EMODIF,ALL,REAL,2

! Constant 3
NSEL,S,LOC,Z,n*lt,n*2*lt
ESLN,S,1,ALL
NSEL,S,LOC,Z,n*3*lt,n*4*lt
ESLN,A,1,ALL
EMODIF,ALL,REAL,3
```

```
! Constant 4
NSEL,S,LOC,Z,0.0,n*lt
ESLN,S,1,ALL
NSEL,S,LOC,Z,n*2*lt,n*3*lt
ESLN,A,1,ALL
EMODIF,ALL,REAL,4

! Reselect all nodes and elements.
ALLS
! Finish the preparation module.
FINISH


! Go to the solution module.
/SOLU

! Define the analyses type. Static if none specified.
ANTYPE, STATIC

! Define boundary conditions.

! Left hand side.
! First select the right nodes.
NSEL,S,LOC,X,0
NSEL,R,LOC,Z,0
! No displacements in x-direction and in z-direction.
D,ALL,UX,0.0
D,ALL,UZ,0.0
! Restrain first displacement in y-direction.
NSEL,R,LOC,Y,0
D,ALL,UY,0.0

ALLS

! Right hand side.
! First select the right nodes.
NSEL,S,LOC,X,L
NSEL,R,LOC,Z,0
! No displacement in z-direction.
D,ALL,UZ,0.0
! Restrain second displacement in y-direction.
NSEL,R,LOC,Y,0
D,ALL,UY,0.0

ALLS

! Loading of nodes in the model of the beam.
NSEL,S,LOC,X,L/2
NSEL,R,LOC,Z,Tlt
NSEL,R,LOC,Y,0
F,ALL,FZ,-F/(2*ny)

NSEL,S,LOC,X,L/2
NSEL,R,LOC,Z,Tlt
NSEL,R,LOC,Y,W
F,ALL,FZ,-F/(2*ny)

NSEL,S,LOC,X,L/2
NSEL,R,LOC,Z,Tlt
NSEL,R,LOC,Y,W/ny,(ny-1)*W/ny
F,ALL,FZ,-F/ny
```

```
! Solve this case, don't forget the alls command.
ALLS
SOLVE
! Finish the solution module.
FINISH

! Go to the result analysis module.
/POST1

! Here some nice commands can be added to show what you like.
! Here the element will be plotted with thickness. (Only for SHELL Elements)
/ESHAPE,1

! Plot the results. Here the displaced shape and the original shape as countour are
plotted.
/VIEW,1,,-1
PLNS,U,Z,2

! Path definition
node1=NODE(0,W/2,Tlt/2)
node2=NODE(L,W/2,Tlt/2)

LPATH,node1,node2
PDEF,z_displacement,U,Z
PLPATH,z_displacement
PRPATH,z_displacement
```

REFERENCES

Aghdam, M. M., and S. R. Falahatgar. 2003. "Bending analysis of thick laminated plates using extended Kantorovich method". *Composite Structures,* vol. 62, n° Compendex, p. 279-283.

ANSYS. *Release 9.0 Documentation for ANSYS.*

ASM International. 2002. *ASM handbooks online*. Coll. "ASM materials information". Materials Park, OH: ASM International.

ASTM. 2000. *Standard Test Method for Density and Specific Gravity (Relative Density) of Plastics by Displacement*. ASTM D792-00. 6 p.

ASTM. 2003. *Standard Test Methods for Flexural Properties of Unreinforced and Reinforced Plastics and Electrical Insulating Materials*. ASTM D790-03. 11 p.

ASTM. 2004. *Standard Test Methods for Constituent Content of Composite Materials*. ASTM D3171-99 (Reapproved 2004). 10 p.

ASTM. 2005. *Standard Test Method for Shear Properties of Composite Materials by the V-Notched Beam Method*. ASTM D5379/D5379M-05. 13 p.

ASTM. 2006. *Standard Test Method for Tensile Properties of Polymer Matrix Composite Materials*. ASTM D3039/D3039M-00(reapproved 2006). 13 p.

Bathe, Klaus-Jürgen. 1996. *Finite element procedures*. Englewood Cliffs, N.J.: Prentice Hall, xiv, 1037 p.

Bernasconi, A., S. Beretta, F. Moroni and A. Pirondi. 2010. "Local stress analysis of the fatigue behaviour of adhesively bonded thick composite laminates". In *Durability of Adhesive Joints*, 5-6. Vol. 86, p. 480-500. Coll. "Journal of Adhesion". Philadelphia, USA: Taylor and Francis Inc.

Berthelot, Jean-Marie. 2005. *Matériaux composites : comportement mécanique and analyse des structures*, 4e éd. Paris: Éditions Tec & Doc, xxi, 645 p.

Bogetti, Travis A., Christopher P.R. Hoppel, Vasyl M. Harik, James F. Newill and Bruce P. Burns. 2004. "Predicting the nonlinear response and progressive failure of composite laminates". *Composites Science and Technology,* vol. 64, n° Compendex, p. 329-342.

Bogetti, Travis A., Christopher P.R. Hoppel, Vasyl M. Harik, James F. Newill and Bruce P. Burns. 2004. "Predicting the nonlinear response and failure of composite laminates: correlation with experimental results". *Composites Science and Technology,* vol. 64, n° Compendex, p. 477-485.

Broughton, W. R., M. R. L. Gower, M. J. Lodeiro and R. M. Shaw. 2001. *Through-Thickness Testing of Polymer Matrix Composites*. MATC(MN)06. Teddington (Middlesex): National Physical Laboratory, 16 p.

Broughton, W. R., and G. D. Sims. 1994. *An Overview of Through-Thickness Test Methods for Polymer Matrix Composites*. DMM(A)148. Teddington (Middlesex): National Physical Laboratory, 52 p.

Chan, A., W. K. Chiu and X. L. Liu. 2007. "Determining the elastic interlaminar shear modulus of composite laminates". *Composite Structures,* vol. 80, n° Compendex, p. 396-408.

Cinquin, Jacques, and Bruno Medda. 2009. "Influence of laminate thickness on composite durability for long term utilisation at intermediate temperature (100-150 C)". *Composites Science and Technology,* vol. 69, n° Compendex, p. 1432-1436.

Coguill, Ronda J., and Donald F. Adams. 2000. "Tabbed axial tensile specimen configurations for unidirectional composites". *International SAMPE Symposium and Exhibition (Proceedings),* vol. 45, n° Compendex, p. I/.

Composite Material Handbook (CMH-17) Volume 3. 2012. "Polymer matrix composites: Material usage, design and analysis". *SAE International*.

Daghia, Federica, Stefano de Miranda, Francesco Ubertini and Erasmo Viola. 2007. "Estimation of elastic constants of thick laminated plates within a Bayesian framework". *Composite Structures,* vol. 80, n° Compendex, p. 461-473.

Daniel, Isaac M., and Ori Ishai. 1994. *Engineering mechanics of composite materials*. New York: Oxford University Press.

Daniel, Isaac M., Jyi-Jiin Luo and Patrick M. Schubel. 2008. "Three-dimensional characterization of textile composites". *Composites: Part B,* vol. 39, n° Compendex, p. 13-19

Duchaine, François. 2004. "Génération de maillage structuré par krigeage avec raffinement elliptique local". Montréal, École de technologie supérieure.

Duchaine, François, Eelco M. Baten, Henri Champliaud and Harald E.N. Bersee. 2006. "Comparison of Beam Theories with Finite Element Analysis in Three-Point Bending of Thick Composites", in Proceedings of the Eighth International Conference on Computational Structures Technology, B.H.V. Topping, G. Montero and R. Montenegro, (Editors), Civil-Comp Press, Stirlingshire, United Kingdom, paper 268.

Duchaine, François, Harald E.N. Bersee and Henri Champliaud. 2007. "The influence of the thickness on 3D elastic material properties of unidirectional E-glass/epoxy laminated composites", in Proceedings of the Sixth Canadian-International Composites Conference on Defelopment and Commercialization of Composite Materials and Technologies, Winnipeg (Manitoba), Canada, paper MCT-3.

ÉireComposites, Expert in Composites. 2006. Online. http://www.EIREComposites.com/services/... .html. Consulted on June 18th, 2014.

Gibson, Ronald F. 2007. *Principles of composite material mechanics*, 2nd. Boca Raton: CRC Press, xxvii, 579 p.

Gunnion, Andrew J., Murray L. Scott, Rodney S. Thomson and Dieter Hachenberg. 2004. "Thickness effects on the compressive stiffness and strength of stitched composite laminates". *Composite Structures,* vol. 66, n° Compendex, p. 479-486.

Gurvich, Mark R. and R. Byron Pipes. 1995. "Strength size effect of laminated composites". *Composites Science and Technology,* vol. 55, n° Compendex, p. 93-105.

Hodgkinson, J. M. 2000. *Mechanical testing of advanced fibre composites*. Boca Raton, Flor.: CRC Press., xv, 362 p.

Holmes, Stanley. 2005. "A Plastic Dream Machine". *BusinessWeek*, (June 20), p. 32-35.

Hufenbach, W., M. Gude, B. Zhou and L. Kroll. 2004. "Stress and failure analysis of thick-walled conical composite rotors". *Proceedings of the Institution of Mechanical Engineers, Part L: Journal of Materials: Design and Applications,* vol. 218, n° Compendex, p. 1-8.

Jackson, Karen E. 1992. "Scaling effects in the flexural response and failure of composite beams". *AIAA journal,* vol. 30, n° Compendex, p. 2099-2105.

Jiang, Yijun, and Suong V. Hoa. 2006. "A novel method for the manufacturing of thick composites". *Journal of Composite Materials,* vol. 40, n° Compendex, p. 433-453.

Johnson, David P., John Morton, Sotiris Kellas and Karen E. Jackson. 2000. "Size effects in scaled fiber composites under four-point flexure loading". *AIAA journal,* vol. 38, n° Compendex, p. 1047-1054.

Kaddour, A.S., and M.J. Hinton. 2005. "The launch of WWFE-II: Benchmarking of 3D strength and damage theories for polymer fibre". In *15th international conference on composite materials*. Durban, South Africa.

Kellas, Sortiris, and John Morton. 1992. "Strength scaling in fiber composites". *AIAA journal,* vol. 30, n° Compendex, p. 1074-1080.

Kellas, Sotiris, David P. Johnson, John Morton and Karen E. Jackson. 1993. "Scaling effects in sublaminate-scaled composite laminates". In *34th AIAA/ASME/ASCE/AHS/ASC Structures, Structural Dynamics, and Materials Conference, April 19, 1993 - April 22, 1993*, pt 6. p. 3715-3725. Coll. "Collection of Technical Papers - AIAA/ASME Structures, Structural Dynamics and Materials Conference". La Jolla, CA, USA: Publ by AIAA.

Kim, Byung Chul, Dong Chang Park, Byoung Jung Kim and Dai Gil Lee. 2010. "Through-thickness compressive strength of a carbon/epoxy composite laminate". *Composite Structures,* vol. 92, n° Compendex, p. 480-487.

Kulakov, V. L., Yu M. Tarnopol'skii, A. K. Arnautov and J. Rytter. 2004. "Stress-Strain State in the Zone of Load Transfer in a Composite Specimen under Uniaxial Tension". *Mechanics of Composite Materials,* vol. 40, n° 2, p. 91-100.

Lavoie, J. Andre, Costas Soutis and John Morton. 2000. "Apparent strength scaling in continuous fiber composite laminates". *Composites Science and Technology,* vol. 60, n° Compendex, p. 283-299.

Lee, J., and C. Soutis. 2005. "Thickness effect on the compressive strength of T800/924C carbon fibre-epoxy laminates". In, 2 SPEC. ISS. Vol. 36, p. 213-227. Coll. "Composites Part A: Applied Science and Manufacturing". Elsevier Ltd.

Lee, J., and C. Soutis. 2007. "A study on the compressive strength of thick carbon fibre-epoxy laminates". *Composites Science and Technology,* vol. 67, n° Compendex, p. 2015-2026.

Lessard, Larry. 2004. *Mechanics of Composite Materials (course notes - MECH 530)*. Montreal: McGill University.

Liu, Zhuofeng, Jingcheng Zeng, Jiayu Xiao, Dazhi Jiang and Xiaoqing Dai. 2010. "Distribution of the cure degree for the thick GFRP laminates". *Fuhe Cailiao Xuebao/Acta Materiae Compositae Sinica,* vol. 27, n° Compendex, p. 92-98.

Luedtke, Benjamin M., and Dale Brosius. 2009. "Active exotherm management in out-of-autoclave curing of thick laminates using fluid heating and cooling". In *SAMPE '09 Spring Symposium Conference Proceedings, May 18, 2009 - May 21, 2009*. Vol. 54, p. SAMPE's Baltimore/Washington Chapter; SAMPE's Midwest and Northern Ohio Chapters. Coll. "International SAMPE Symposium and Exhibition (Proceedings)". Baltimore, MD, United states: Soc. for the Advancement of Material and Process Engineering.

Madabhusi-Raman, Prabhu, and Julio F. Davalos. 1996. "Static shear correction factor for laminated rectangular beams". *Composites Part B: Engineering,* vol. 27, n° Compendex, p. 285-293.

Mazumdar, Sanjay K. 2002. *Composites manufacturing materials, product, and process engineering Sanjay K. Mazumdar*. Boca Raton, Fla.: CRC Press.

Melin, L. Niklas, and Jonas M. Neumeister. 2006. "Measuring constitutive shear behavior of orthotropic composites and evaluation of the modified Iosipescu test". *Composite Structures,* vol. 76, n° Compendex, p. 106-115.

Narayana Naik, G., A. V. Krishna Murty and S. Gopalakrishnan. 2005. "A failure mechanism based failure theory for laminated composites including the effect of shear stress". *Composite Structures,* vol. 69, n° Compendex, p. 219-227.

Nguyen, Viet-Tung, Jean-Francois Caron and Karam Sab. 2005. "A model for thick laminates and sandwich plates". *Composites Science and Technology,* vol. 65, n° Compendex, p. 475-489.

Nilsson, S., A. Bredberg and L. E. Asp. 2009. "Effects of CFRP laminate thickness on bending after impact strength". In *13th European Conference on Composite Materials*, 2-4. Vol. 38, p. 61-66. Coll. "Plastics, Rubber and Composites". Suite 1C, Joseph's Well, Hanover Walk, Leeds, LS3 1AB, United Kingdom: Maney Publishing.

Pervez, T., A.C. Seibi and F.K.S. Al-Jahwari. 2005. "Analysis of thick orthotropic laminated composite plates based on higher order shear deformation theory". *Composite Structures,* vol. 71, n° Compendex, p. 414-422.

Reddy, J. N. 1997. *Mechanics of laminated composite plates : theory and analysis*. Boca Raton, Flor.: CRC Press, 782 p.

Ridley-Ellis, D.J., J.S. Owen and G. Davies. 2003. "Torsional behaviour of rectangular hollow sections". *Journal of Constructional Steel Research,* vol. 59, n° Compendex, p. 641-663.

Schlimbach, J., A. Ogale and S. Schimmel. 2009. "Quickstep processing to control exothermic reaction during the manufacture of thick laminates". In, 9-10. Vol. 38, p. 374-378. Coll. "Plastics, Rubber and Composites". Suite 1C, Joseph's Well, Hanover Walk, Leeds, LS3 1AB, United Kingdom: Maney Publishing.

Schmitt, D. F. Jr. 1974. "Materials Parameters that Govern the Erosion Behavior of Polymeric Composites in Subsonic Rain Environments". *Composite Materials: Testing and Design (Third Conference)*. ASTM STP 546. American Society for Testing and Materials. p. 303-323.

Schubel, P. M., J. J. Luo and I. M. Daniel. 2006. "Through-thickness characterization of thick composite laminates". In *SEM Annual Conference and Exposition on Experimental and Applied Mechanics 2006, June 4, 2006 - June 7, 2006*. Vol. 4, p. 1793-1800. Coll. "Proceedings of the 2006 SEM Annual Conference and Exposition on Experimental and Applied Mechanics 2006". Saint Louis, MO, United states: Society for Experimental Mechanics Inc.

Shepheard, Barry, Dan Jackson, Mark Dixon and Graham Sims. 2004. "Testing of thick carbon fibre laminate composites: Comparison of thick with thin coupons, current standards and product case study". In *36th International SAMPE Technical Conference - Materials and Processing:Sailing into the Future, November 15, 2004 - November 18, 2004*. p. 965-975. Coll. "International SAMPE Technical Conference". San Diego, CA, United states: Soc. for the Advancement of Material and Process Engineering.

Soden, P. D., M. J. Hinton and A. S. Kaddour. 1998. "Lamina properties, lay-up configurations and loading conditions for a range of fibre-reinforced composite laminates". *Composites Science and Technology,* vol. 58, n^{o} Compendex, p. 1011-1022.

Soden, P. D., A. S. Kaddour and M. J. Hinton. 2004. "Recommendation for designers and researchers resulting from the world-wide failure exercise". *Composites Science and Technology,* vol. 64, n^{o} Compendex, p. 589-604.

Soutas-Little, Robert William. 1973. *Elasticity*. New York: Dover Publications, Inc.

Stevanovic, M. M., A. A. Elhisnavi and D. R. Peikan. 2002. "Size effect in carbon fiber/epoxy resin composite". In *Proceedings of the fourth Yugoslav Materials Research Society Conference (YUCOMAT IV), September 10, 2001 - September 14, 2001*. Vol. 413, p. 207-212. Coll. "Materials Science Forum". Herceg-Novi, Yugoslavia: Trans Tech Publications Ltd.

Sutherland, L. S., and C. Guedes Soares. 2004. "Effect of laminate thickness and of matrix resin on the impact of low fibre-volume, woven roving E-glass composites". *Composites Science and Technology,* vol. 64, n^{o} Compendex, p. 1691-1700.

Sutherland, L. S., R. A. Shenoi and S. M. Lewis. 1999a. "Size and scale effects in composites. I. Literature review". *Composites Science and Technology,* vol. 59, n° Copyright 1999, IEE, p. 209-20.

Sutherland, L. S., R. A. Shenoi and S. M. Lewis. 1999b. "Size and scale effects in composites: II. Unidirectional laminates". *Composites Science and Technology,* vol. 59, n° Copyright 1999, IEE, p. 221-33.

Sutherland, L. S., R. A. Shenoi and S. M. Lewis. 1999c. "Size and scale effects in composites: III. Woven-roving laminates". *Composites Science and Technology,* vol. 59, n° Copyright 1999, IEE, p. 235-52.

Tabiei, Ala, and Jianmin Sun. 2000. "Analytical simulation of strength size effect in composite materials". *Composites Part B: Engineering,* vol. 31, n° Compendex, p. 133-139.

Trilion, Optical Test System. 2012. Online. http://www.trilion.com/Applications/. Consulted on April 18th, 2012.

Viens, François. 2004. "Implantation d'une loi de matériau des alliages à mémoire de forme dans un logiciel d'éléments finis commercial". Montréal, École de technologie supérieure.

White, S.R. and H.T. Hahn. 1992. "Process modeling of composite materials: Residual stress development during curing. Part I. Model formulation". *Journal of Composite Materials,* vol. 26, n° Compendex, p. 2423-2453.

Whitney, J.M. 1973. "Shear correction factors for orthotropic laminates under static load". *Journal of applied mechanics,* vol. 40, n° Compendex, p. 302-304.

Yildiz, Hasan, and Mehmet Sarikanat. 2001. "Finite-element analysis of thick composite beams and plates". *Composites Science and Technology,* vol. 61, n° Compendex, p. 1723-1727.

Zenkour, Ashraf M. 1999. "Transverse shear and normal deformation theory for bending analysis of laminated and sandwich elastic beams". *Mechanics of Composite Materials and Structures,* vol. 6, n° Compendex, p. 267-283.

Zhou, G., and G. A. O. Davies. 1995. "Characterization of thick glass woven roving/polyester laminates: 1. Tension, compression and shear". *Composites,* vol. 26, n° Compendex, p. 579-586.

Zhou, G., and G. A. O. Davies. 1995. "Characterization of thick glass woven roving/polyester laminates: 2. Flexure and statistical considerations". *Composites,* vol. 26, n° Compendex, p. 587-596.

Zimmermann, Kristian, and Markus Siemetzki. 2008. "Ultra thick laminates for highly loaded main landing gear fittings". *VDI Berichte*, n^{o} Compendex, p. 47-61.